
THE INFLUENCE OF PAVEMENT STIFFNESS ON VEHICLE FUEL CONSUMPTION

Tao Lu, MSc.

*Thesis submitted to the University of Nottingham for the
degree of Doctor of Philosophy*

September 2010

Abstract

This thesis estimates the effect of pavement stiffness on energy dissipation of a rolling vehicle tyre. One objective of this study is to compare the relative amount of energy dissipated in pavement by the rolling depending on the pavement stiffness, speed and load. The study also assesses the effect of the vertical deflection, induced by the tyre, on overall energy dissipation in pavement.

A comprehensive literature was carried out to prove a wide background for the study. Field measures and laboratory tests were discussed to provide basis for analyses. Theories from vehicle engineering have been used for tyre/pavement contact area calculation.

Results indicate that energy dissipated in pavement significantly depend on the stiffness of pavement. Flexible pavements absorb more energy than rigid pavements. An obvious influence of speed on energy dissipation can be found only when the stiffness is at a low level.

Acknowledgements

First, I would like to thank Dr. Nick Thom, who is my tutor and friend. Thanks for his excellent guidance and patience supervision throughout the course of this research project

I would like to thank Dr. Tony Parry, co-supervisors, for his advices, suggestions and encouragement.

I am also grateful to Dr. Yuan Yang, my wife, for her great supports and selfless helps.

I would also like to thank my parents for their continuous encouragements and supports.

Finally, I would like to thank my friends and class mates: Wang Juan, Geng Yan, Geng Xue Yu, Li Xia, Jia Yu Dan, Di Yu for the many fascinating discussions in the research room.

Contents

Contents	III
List of Figures	IX
List of Tables	XVII
List of Notations	XIX
List of Abbreviations	XXI
Chapter 1 Introduction	1
1.1 Background	2
1.2 Aims, objectives and benefits of study	3
1.3 Research methodology.....	5
1.4 Structure of thesis.....	7
Chapter 2 Literature Review.....	9
2.1 Vehicle fuel economy	9
2.2 Factors influencing fuel consumption	11
2.2.1 Engine.....	11
2.2.2 Vehicle type.....	12
2.2.3 Fuel type.....	13
2.2.4 Vehicle weight.....	15
2.2.5 Vehicle speed	17
2.2.6 Aerodynamic characteristics.....	19
2.2.7 Road system.....	21
2.2.8 Skid resistance.....	22
2.2.9 Pavement surface.....	22
2.2.10 Pavement stiffness.....	24

2.3	Essential pavement engineering background.....	25
2.3.1	Structure of pavement.....	25
2.3.2	Materials of pavement.....	26
2.4	Rolling resistance	29
2.4.1	Interpretation of rolling resistance	29
2.4.2	Factors influencing rolling resistance.....	33
2.4.3	Rolling resistance influencing fuel consumption	38
2.5	Tyre-Pavement interaction	41
2.5.1	Tyre structure.....	41
2.5.2	Tyre load distribution.....	42
2.5.3	Type/pavement contact area.....	46
2.6	Falling Weight Deflectometer Test	48
2.7	Case Study	52
2.7.1	TRL Laboratory testing	52
2.7.2	Truck fuel consumption measurements in Canada	56
2.7.3	Van fuel consumption measurements in US.....	59
2.8	Embedded Energy	63
2.9	Finite element analysis and ABAQUS.....	64
2.9.1	Elements.....	65
2.9.2	Material Damping	68
2.9.3	Step and increment.....	71
2.9.4	Half-step residual tolerance	72
2.9.5	Boundary Condition	73
2.10	Summary	77
Chapter 3	Preliminary Study	79
3.1	Principals of analysis.....	79
3.1.1	Dimensions and boundary conditions	80
3.1.2	Material properties	84
3.1.3	Tyre-pavement contact area.....	86

3.1.4	Load levels.....	86
3.2	Physical models	87
3.2.1	Dimensions.....	87
3.2.2	Materials	90
3.3	Finite Element Models	90
3.3.1	Axisymmetric model	91
3.3.2	3D model.....	93
3.4	Summary	108
	Chapter 4 Confirmation Tests.....	110
4.1	Model definition.....	111
4.2	Materials	111
4.3	Loading.....	114
4.4	Results.....	116
4.5	Summary	119
	Chapter 5 Case Study –TRL Measurements	122
5.1	Problem description	122
5.2	Model Definition	122
5.2.1	Background of TRL measurements	122
5.2.2	Material properties	125
5.2.3	3D model.....	127
5.3	Results.....	131
5.4	Summary	136
	Chapter 6 Asphalt Pavements	137
6.1	Problem description	137
6.2	Model Definition	137

6.3	Boundary Conditions.....	142
6.4	Loading.....	144
6.5	Solution Controls.....	144
6.6	Results.....	145
6.6.1	Vertical deflection	145
6.6.2	Speed influencing energy dissipation	147
6.6.3	Stiffness influencing energy dissipation.....	151
6.6.4	Load influencing energy dissipation.....	152
6.7	Summary	154
	Chapter 7 Low Quality Pavements	155
7.1	Introduction	155
7.2	Model Definition	156
7.3	Results.....	159
7.3.1	Vertical deflections	159
7.3.2	Stiffness influencing energy dissipation.....	162
7.3.3	Speed influencing energy dissipation	163
7.3.4	Load influencing energy dissipation.....	165
7.4	Summary	166
	Chapter 8 Concrete Pavements	168
8.1	Problem description	168
8.2	Model Definition	168
8.3	Loading.....	169
8.4	Boundary Conditions.....	170
8.5	Parameters.....	170
8.6	Results.....	170

8.7 Summary	173
Chapter 9 Discussion of Results.....	175
9.1 Discussion of TRL measurements	175
9.2 Discussion of pavement stiffness	177
9.3 Discussion of vehicle speed	180
9.4 Discussion of embedded energy	182
Chapter 10 Conclusions and Recommendation	185
Reference.....	187
Appendix A. Plotted data of FE analyses.....	197
A.1 Static pressure on axisymmetric model	197
A.2 Dynamic pressure on axisymmetric model	200
A.3 Deflection-time traces of FWD-FE confirmation tests.....	203
A.4 Hysteresis curves of FWD-FE confirmation tests	204
Appendix B. Plotted data of FE analyses.....	206
B.1 Speed influencing pavement resistance	206
B.2 Speed influencing maximum deflection	208
B.3 Vertical load influencing pavement resistance	209
B.4 Stiffness influencing pavement resistance.....	211
Appendix C. Model dimensions.....	212
C.1 Cross section	212
C.2 Dimension of the 3D models	214
Appendix D. Infinite Element Boundary	215

Appendix E. Contour Plots.....	221
--------------------------------	-----

List of Figures

Figure 1-1: Procedure of research	7
Figure 2-1 Energy flow of a midsize passenger car (FuelEconomy.gov, 2009)	12
Figure 2-2 Fuel economy improvement vs. weight reduction (Casadei & Broda, 2007)	16
Figure 2-3 Volkswagen Golf fuel consumption at steady speeds (Week, 1981)	17
Figure 2-4 Volkswagen Golf fuel consumption in traffic (Week, 1981)	18
Figure 2-5 Power required to overcome aerodynamic drag and rolling resistance (McCallen et al, 1998)	20
Figure 2-6 Sketch figure of texture of pavement surface	23
Figure 2-7 A typical pavement structure	26
Figure 2-8 Tyre rolling resistance (Miege & Popov, 2005)	30
Figure 2-9 Hysteresis loop and energy dissipation	31
Figure 2-10 Rolling resistance coefficient vs. Tyre temperature (Descornet, 1990)	35
Figure 2-11 Measurements during tyre warm-up (Popov, Cole, Cebon, & Winkler, 2002)	36
Figure 2-12 Pavement surface influence on tyre rolling resistance (DeRaad, 1977)	37
Figure 2-13 Rolling resistance coefficient vs. texture depth (Descornet, 1990)	38
Figure 2-14 Distribution of fuel consumption of a uneven driving test (Nokian Tyres plc., 1999).....	39

Figure 2-15 Effect on total energy consumption as a function of different changes in rolling resistance (Nokian Tyres plc., 1999)	40
Figure 2-16 Rolling resistance coefficient and the fuel consumption for a passenger car at 60km/h (Descornet, 1990)	41
Figure 2-17 Profile of a typical pneumatic tyre (Nokian Tyres plc., 1999)	42
Figure 2-18 Behaviour of a tyre under the action of a driving torque (Clark, 1971)	43
Figure 2-19 Typical vertical wheel force at 80km/h for medium roughness road and Walking Beam Suspension (Sweatman, 1983).....	44
Figure 2-20 Tyre compressions with load changing (a) Case 1: 720kPa, 20kN, n-shape; (b) Case 2: 720kPa, 35kN, m-shape; (c) Case 3: 720kPa, 50kN, m-shape (De Beer, Fisher, C., & Kannemeyer, 2004)....	45
Figure 2-21 Tyre/pavement contact areas (a) from (PCA, 1966) (b) from (PCA, 1984)	47
Figure 2-22 FWD equipment in use (FPMS, 2008)	49
Figure 2-23 Layered pavement structure and FWD testing instrument (Kim & Kim, 2008).....	50
Figure 2-24 Load and deflection histories of FWD testing	51
Figure 2-25 Energy dissipation of FWD testing	51
Figure 2-26 TRL 's Pavement Test Facility (Benbow, Iaquinta, Lodge, & Wright, 2007).....	53
Figure 2-27 Relationship between rolling resistance and tyre temperature	55
Figure 2-28 Coefficient of rolling resistance for flexible and rigid pavements.....	56
Figure 2-29 Side view of tractor trailer (Taylor & Patten, 2006)	57

Figure 2-30 Instrumented 2000 Chevy Astro Van (Ardekani & Sumitsawan, 2010)	62
Figure 2-31 Pole node location for an infinite element (ABAQUS Theory Manual, 2001)	68
Figure 2-32 Influence of the alpha damping on deflection	70
Figure 2-33 Influence of the beta damping on deflection.....	71
Figure 2-34 VDB and energy wave (Ross, 2004)	74
Figure 2-35 VDB dashpots in the axisymmetric model	75
Figure 2-36 Conventional Boundary.....	76
Figure 2-37 VDB vs. Rigid Boundary vs. Conventional Boundary	77
Figure 3-1 Solid model of the pavement	84
Figure 3-2 Dimensions of Axisymmetric model.....	88
Figure 3-3 ½ view of the 3D model	89
Figure 3-4 Load pulse of axisymmetric model	92
Figure 3-5 Mesh of the Axisymmetric model	92
Figure 3-6 Stress on contact patch.....	94
Figure 3-7 Pressures located on contact patch (local coordinates system)	96
Figure 3-8 Vertical stress distribution of the TIML in the contact zone....	97
Figure 3-9 Amplitudes of pressures on contact area	98
Figure 3-10 The mesh of the 3D model.....	100
Figure 3-11 the mesh of the contact zone	100
Figure 3-12 Distribution of boundary conditions	103
Figure 3-13 VDB in cylindrical coordinate system	104
Figure 3-14 VDB vs. rigid boundary (3D model, 30km/h)	105
Figure 3-15 Load and Deflection histories of a node at contact zone	106

Figure 3-16 Load vs. Deflection of the node	108
Figure 4-1 Process of confirmation tests	111
Figure 4-2 Mesh of axisymmetric model used for confirmation test.....	113
Figure 4-3 3D model used for dynamic analyses	114
Figure 4-4 FWD load and deflection histories	115
Figure 4-5 Load used for the 3D model.....	116
Figure 4-6 Deflection-time traces when A1=100	117
Figure 4-7 Load vs. deflection when A1=100	117
Figure 4-8 Energy dissipation retrieved from FWD-FE model (E _{FWD} is the energy calculated by using FWD results).....	118
Figure 4-9 Deflection load traces retrieved from 3D model and FWD test	119
Figure 4-10 Load vs. deflection, 3D model vs. FWD	119
Figure 5-1 Locations of the pavements used for measurement (McKeown, 2002)	123
Figure 5-2 Dimensions of the FE model used to simulate TRL investigation	127
Figure 5-3 Profile of the model used for flexible composite pavement ...	128
Figure 5-4 FE mesh of 3D model analyses, flexible composite pavement	129
Figure 5-5 Mesh at cross setion (a) flexible composite pavment (b) rigid pavment (c) fully flexible pavment.....	130
Figure 5-6 Deflections at D1, D4 and D6, flexible composite pavement.	132
Figure 5-7 Deflections at D1, D4 and D6, rigid pavement.....	132
Figure 5-8 Deflections at D1, D4 and D6, fully flexible pavment	133
Figure 5-9 Deflections of observation points, offset is 5.61m	134

Figure 5-10 Stiffness influencing fuel economy (McKeown, 2002).....	136
Figure 6-1 Parts and dimensions of asphalt pavement model.....	138
Figure 6-2 Profile of asphalt concrete model	139
Figure 6-3 Mesh of asphalt concrete pavement model.....	141
Figure 6-4 Mesh on Area 1 of asphalt concrete pavement model	141
Figure 6-5 Mesh on Area 3 of asphalt concrete pavement model	142
Figure 6-6 Mesh on Area 2 of asphalt concrete pavement model	142
Figure 6-7 Mesh on Area 4 of asphalt concrete pavement model	144
Figure 6-8 Deflection at P1, asphalt concrete pavement.....	146
Figure 6-9 Deflection vs. stiffness, $Lv=40kN$, asphalt concrete	146
Figure 6-10 PR vs. speed, $Lv= 40kN$, asphalt concrete	148
Figure 6-11 PRs with speed-influenced stiffnesses, $Lv =40kN$, asphalt concrete	149
Figure 6-12 PRs with speed-influenced stiffnesses, $Lv =50kN$, asphalt concrete	150
Figure 6-13 PRs with speed-influenced stiffnesses, $Lv =60kN$, asphalt concrete	150
Figure 6-14 PR vs. stiffness, $Lv=40kN$, asphalt concrete	151
Figure 6-15 PR vs. stiffness, $Lv=50kN$, asphalt concrete	152
Figure 6-16 PR vs. stiffness, $Lv=60kN$, asphalt concrete	152
Figure 6-17 PR vs. Load, stiffness=1000MPa, asphalt concrete	153
Figure 6-18 PR vs. Load, stiffness=5000MPa, asphalt concrete	153
Figure 6-19 PR vs. Load, stiffness=11000MPa, asphalt concrete	154
Figure 7-1 VDBs on pavement boundary	158
Figure 7-2 Deflection vs. upper layer stiffness, BISAR.....	160

Figure 7-3 Maximum deflection vs. upper layer stiffness, 30km/h, FE analyses	161
Figure 7-4 Maximum deflection vs. upper layer stiffness, 160km/h, FE analyses	162
Figure 7-5 PR vs. E1 when $Lv = 40kN$	163
Figure 7-6 PR vs. speed when $Lv = 40kN$	164
Figure 7-7 PRs with speed-influenced stiffnesses, $Lv=40kN$	164
Figure 7-8 PR vs. Lv when $E1=500MPa$	165
Figure 8-1 Pavement resistance vs. top layer stiffness, concrete pavement	171
Figure 8-2 PR increment vs. E1 increment.....	172
Figure 8-3 Pavement resistance vs. speed, concrete pavement.....	173
Figure 9-1 Pavement stiffness vs. pavement resistance	177
Figure 9-2 Pavement resistance vs. speed, typical pavement stiffness ..	180
Figure 9-3 Pavement stiffness related fuel consumption.....	181
Figure 9-4 Pavement-related energy of pavements during 40-year life .	184
Figure A-1 Vertical Deflection of static simulation	198
Figure A-2 Load pulse.....	198
Figure A-3 Deflections magnitudes of collected nodes	199
Figure A-4 Velocity magnitudes of collected nodes	200
Figure A-5 FWD pressure, peak=850kPa	200
Figure A-6 Vertical deflection against time	202
Figure A-7 Deflection-time traces when $A1=0$	203
Figure A-8 Deflection-time traces when $A1=60$	203
Figure A-9 Deflection-time traces when $A1=70$	203
Figure A-10 Deflection-time traces when $A1=90$	204

Figure A-11 Load vs. deflection when A1=0.....	204
Figure A-12 Load vs. deflection when A1=60	205
Figure A-13 Load vs. deflection when A1=70	205
Figure A-14 Load vs. deflection when A1=90	205
Figure B-1 PR vs. speed when $Lv = 50kN$, low quality pavement.....	206
Figure B-2 PR vs. speed when $Lv = 60kN$, low quality pavement.....	206
Figure B-3 Calibrated PR vs. speed when $Lv = 50kN$, low quality pavement	207
Figure B-4 Calibrated PR vs. speed when $Lv = 60kN$, low quality pavement	207
Figure B-5 Deflection vs. stiffness, $Lv=50kN$, asphalt concrete	208
Figure B-6 Deflection vs. stiffness, $Lv=60kN$, asphalt concrete	208
Figure B-7 PR vs. Lv when $E1=1000MPa$, low quality pavement.....	209
Figure B-8 PR vs. Lv when $E1=1500MPa$, low quality pavement.....	209
Figure B-9 PR vs. Lv when $E1=2000MPa$, low quality pavement.....	210
Figure B-10 PR vs. Lv when $E1=2500MPa$, low quality pavement	210
Figure B-11 PR vs. $E1$ when $Lv = 50kN$, low quality pavement	211
Figure B-12 PR vs. $E1$ when $Lv=60kN$, low quality pavement.....	211
Figure C-1 Profile of the model used for the rigid pavement	212
Figure C-2 Profile of the model used for the fully flexible pavement.....	212
Figure C-3 Profile of the mode used for the low quality pavement	213
Figure C-4 Profile of the mode used for the concrete pavement	213
Figure C-5 Dimensions of the model for low quality pavement	214
Figure D-1 View of the 3D model with a boundary of infinite element ..	216
Figure D-2 Contact area and symmetrical boundary	218
Figure D-3 Boundary of infinite element.....	219

Figure D-4 Vertical Deflection (free boundary nodes).....	220
Figure D-5 Vertical deflections (fixed boundary nodes)	220
Figure E-1 Contour plots of the asphalt pavement.....	222
Figure E-2 Contour plots of the low quality pavement.....	223
Figure E-3 Contour plots of the concrete pavement	224
Figure E-4 Contour plots of the TRL rigid pavement.....	225

List of Tables

Table 2-1 Conversion table of mpg and km/L.....	10
Table 2-2 Volkswagen Golf fuel consumption on different types of road (TRRL, 1980).....	14
Table 2-3 Young's modulus of typical soils (Herndon, 1990)	27
Table 2-4 Rolling resistance coefficient due to effects of pavement surface	33
Table 2-5 Flexible pavement construction (Benbow, Iaquinta, Lodge, & Wright, 2007).....	53
Table 2-6 Rigid pavement construction (Benbow, Iaquinta, Lodge, & Wright, 2007).....	54
Table 2-7 Summary of test sites and initial test conditions	58
Table 2-8 Summary of results	59
Table 2-9 Road section characteristics (Ardekani & Sumitsawan, 2010) .	61
Table 2-10 Fuel economy of vehicle (Ardekani & Sumitsawan, 2010)....	63
Table 3-1 Average volume of an element and number of elements.....	82
Table 3-2 Load levels and dimensions of contact area.....	86
Table 3-3 Single amplitude table.....	98
Table 4-1 Thicknesses of the layers of the pavement.....	111
Table 4-2 Material properties of the layers of the pavement	112
Table 4-3 Dashpot coefficients of VDBs used for axisymmetric model ...	113
Table 4-4 Dashpot coefficients of VDB used for 3D model	114
Table 4-5 Material properties of the layers of the pavement (result).....	120
Table 5-1 Composite pavement	124
Table 5-2 Rigid pavement	124

Table 5-3 Fully flexible pavement.....	124
Table 5-4 Mean FWD deflections of the three pavements	125
Table 5-5 Axle loading of TRL test vehicle	125
Table 5-6 Composite pavement	126
Table 5-7 Rigid pavement	126
Table 5-8 Fully Flexible pavement	127
Table 5-9 Dimension of tyre/pavement contact area.....	131
Table 5-10 Mean pavement resistance and maximum deflection	134
Table 6-1 Material properties of each pavement layer.....	140
Table 6-2 Illustrations of boundary conditions as shown in Figure 6-3...143	143
Table 6-3 VDB configuration of asphalt concrete pavement model.....	143
Table 6-4 Parameters has been varied for the asphalt pavement	145
Table 7-1 Material properties for low quality pavements	156
Table 7-2 Parameters have been varied for the low quality pavement...157	157
Table 7-3 VDB configuration for low quality pavement	159
Table 8-1 Material configurations of the concrete pavement model.....	169
Table 8-2 Parameters have been varied for the concrete pavement.....	170
Table 9-1 Comparison of FE and fuel economy.....	175
Table 9-2 Comparison of Young's modulus and layer thickness	178
Table 9-3 Pavement resistance and fuel economy	179
Table 9-4 Embedded energy of asphalt pavement	183
Table 9-5 Embedded energy of concrete pavement	183
Table D-1 Locations of nodes.....	216
Table D-2 Material prosperities of pavement layers and surrounding ground	217
Table E-1 Parameters of models	221

List of Notations

A_c	Tyre/pavement contact area
C_{rr}	Rolling resistance coefficient
E_1	Yong's modulus of layer 1
E_n	Constants of vehicle fuel consumption calculation
E_h	Energy dissipation by hysteresis
f_c	Counterforce
f_r	Horizontal force caused by rolling resistance
f_x	Drag force generated by engine
f_z	Vertical force subjected to a tyre
F	Fuel consumption
F_r	Rolling resistance
L	Total length of the tyre/pavement contact area with a conventional shape
L_c	Length of the contact zone
L_j	Length of contact zone
L_m	Length of 3D model
L_s	The length of non-contact area
L_t	Length of tyre/pavement contact area
L_v	Vertical load on a tyre
N_n	Number of nodes
P	Load applied on a FE model
P_t	Tyre inflation pressure
r	Radius of the 3D model
r_f	Radius of FWD contact plate
t_t	Time used by tyre passing contact zone
$R_{t+\Delta t/2}$	Half-step residual tolerance
S_n	Area of selected region on boundary

t	Time
u	Deflection
v_t	Velocity of tyre
V_a	Average speed of a vehicle
V_x	Horizontal velocity of a rolling tyre
W_h	$\frac{1}{2}$ width of pavement
W_t	Width of tyre/pavement contact area
ε	Strain
σ	Stress
δ	Deflection

List of Abbreviations

3D	Three Dimension
CBR	California Bearing Ratio
CRCP	Continuously Reinforced Concrete Pavement
CRCP	Continuously Reinforced Concrete Pavement
DBM	Dense Bitumen Macadam
FE	Finite Element
FWD	Falling Weight Deflectometer
FEM	Finite Element Method
HDM	Heavy Duty Macadam
HGV	Heavy Goods Vehicle
HMA	Hot Mix Asphalt
HRA	Hot Rolled Asphalt
IRI	International Roughness Index
JPCP	Jointed Plain Concrete Pavement
NRC	The National Research Council (US)
PCC	Portland Cement Concrete
PIARC	World Road Association
PQC	Pavement Quality Concrete
PR	Pavement Resistance
PTF	Pavement Test Facility
RRC	Rolling Resistance Coefficient
SMA	Stone Mastic Asphalt
SMTD	Sensor Measured Texture Depth
TIML	Time-Interval-Moving Load
TRL	Transport Research Laboratory
TRRL	Transport and Road Research Laboratory
VDB	Viscous Damping Boundary

Chapter 1

Introduction

Fossil fuels on this planet are finite and limited. Unfortunately, modern vehicles are still inefficient in fuel consumption; only a small amount of the total fuel which is input into the fuel tank gets used to drive the vehicle. The rest of the fuel is converted to heat and consumed. The ever-increasing requirement for fossil fuel results in a consequence of pollution and global climate change. Recently, sustainable development strategies and reduction of fuel consumption has been assigned a higher priority by governments.

It is well known that rolling resistance generated by tyres affects vehicle fuel economy. Therefore, most of the research carried out previously has focused on the energy dissipation caused by rubber tyres. The energy loss in the pavement due to stiffness is ignored since it is much smaller than that caused by tyres.

Recently, however, it has been realised that pavement stiffness should also influence rolling resistance and vehicle fuel consumption, because pavements as well as tyres have a nonlinear deformation-recovery characteristic.

This PhD project demonstrates an approach by employing a numerical method using finite element software to predict energy dissipation of a section of pavement under a rolling tyre.

1.1 Background

Works carried out previously show that the principal reasons influencing vehicle fuel consumption are engine efficiency and air resistance. For vehicles, most of the fuel is lost in internal combustion engine (ICE). ICE engines are inefficient at converting chemical energy in fuel into mechanical energy. The lost energy is converted to wasted heat, engine friction, and pumping air into and out of engine.

Both pavement and vehicle engineers have found that rolling resistance generated by the tyre-road interaction, other than engine and air effects, has a significant influence on vehicle fuel economy (Meyer, Watson, & Skinner, 2006). Schuring and Redfield (1982) stated that the rolling resistance contributes one-third of the energy consumption of a heavy vehicle engine.

Pavement engineers also suggest that pavement stiffness has a significant effect on rolling resistance. This is based on the fact that stiffer pavements deliver lower rolling resistance; therefore they also deliver lower vehicle fuel consumption. The UK's Transport Research Laboratory (TRL) stated that the rolling resistance of rigid pavements is 5.6% lower than flexible pavements, and TRL also suggested that increases in pavement deflection of 60-100 microns could increase fuel consumption by up to 28% (Benbow, Iaquinta, Lodge, & Wright, 2007).

It is easy to visualise the energy dissipated in a pavement in the form of an energy wave which is a function of density and stiffness.

The energy waves generated by rolling tyre radiate into the pavement layers from the tyre/pavement contact area and will be damped by pavement and subgrade.

However, the relationship between pavement stiffness and fuel consumption is not fully understood. In spite of some field observations and measurements estimating vehicle fuel consumption, with corresponding pavement stiffness properties measured as well, the results retrieved from the measurements do not show the relationship clearly. This is because ambient factors (temperature, humidity and so on), pavement conditions (surface texture, gradient and so on) and vehicle conditions affect fuel consumption and interaction of the factors occurs as well. Thus, various uncertainties can be observed with the results carried out from field tests or measurements. Therefore, more studies of the influence of pavement stiffness on fuel consumption are required.

1.2 Aims, objectives and benefits of study

The principal aim of this research is to study and understand the energy consumption of a rolling tyre with different pavements. The research is to implement numerical model simulations by using the Finite Element (FE) method to identify and quantify the influence of pavement stiffness on fuel consumption. The specific objectives of this research study are outlined as follows:

- To investigate mechanics of tyre rolling resistance caused by tyre-road interaction.

- To realize the background and previous evaluation methods about rolling resistance.
- To identify the factors influencing tyre/road interaction.
- To simplify factors influencing fuel consumption and find the major factors for analytical analyses.
- To develop a constitutive FE model for the prediction of energy consumption. The constitutive FE model is a three-dimensional (3D) model and the rolling tyre load can be simplified to be a series of time interval vertical pressures.
- To verify and validate the constitutive model by comparing experimental results which can be retrieved and derived from referenced literature.
- To predict detailed influences on energy consumption using the FE model with varied factors.

This research using the FE method attempts to quantify the levels of fuel consumption and energy dissipation caused by pavement stiffness. It is anticipated that from analysis of the results carried out from the FE model, it can be determined how a variation of the material properties of a pavement affects vehicle energy loss, due to a change in pavement stiffness and surface deflection. It is hoped that once an evaluation of the energy dissipation related to pavement stiffness has been carried out, recommendations can be made to improve vehicle fuel economy.

1.3 Research methodology

It is worthwhile to consider a numerical approach to solve many problems in research. One of the main advantages of a numerical simulation, for the vehicle fuel consumption problem, is that it requires fewer resources than laboratory tests. As a matter of fact, the typical laboratory test requires a section of pavement built in a laboratory, an apparatus to control a rolling tyre and a data collection system to record the test results. Meanwhile, a numerical approach only requires a suitable computer and related software packages. Besides, a numerical simulation costs less time and much less money than in-situ observation. This is because in order to reduce inaccuracy and retrieve acceptable results, a typical in-situ observation requires a large amount of tests and every test requires a vehicle to perform a journey on the pavement. However, analyses with varied parameter levels are not difficult in numerical analysis. Therefore, a numerical approach is used for this PhD project to achieve the purpose.

In order to achieve overall aims, a research plan has been made, as shown in Figure 1-1. The details of the plan are listed as follows:

- The first step of the research starts from a comprehensive literature review of all the factors affecting vehicle fuel consumption. Major factors will be studied for the FE analyses.
- The background of pavement stiffness measurement, Falling Weight Deflectometer (FWD) testing, will be reviewed. This

includes the process of the measurement, results analysis and related calculations.

- In order to assess the FE method used to calculate the energy consumed in the pavement, an axisymmetric finite element model will be built and assessed by using the results retrieved from FWD tests.
- Confirmed configurations used in the axisymmetric model, such as boundary conditions, material damping and so on will be used in another FE model for dynamic rolling analyses. Varied factors such as pavement materials, structure and tyre load will be used for this model to investigate the influence on energy dissipation.
- Finally, a discussion based on the results carried out from the FE analyses will be given and conclusions of the research will be drawn.

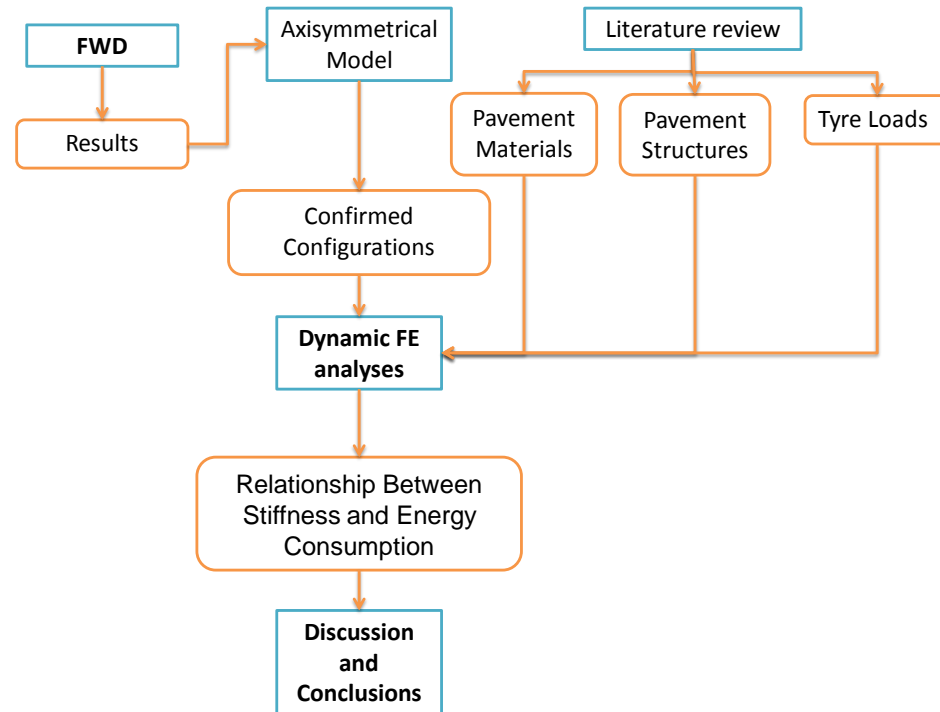


Figure 1-1: Procedure of research

1.4 Structure of thesis

Chapter 2 gives background information of vehicle fuel consumption, factors affecting the fuel consumption, tyre rolling resistance, field measurements of vehicle fuel consumption and laboratory tests to assess the pavement stiffness effects.

Chapter 3 will discuss principles of the FE analyses, tyre load calculation, design of model dimensions and details of FE model building involving dynamic load, boundary conditions and material configurations.

Chapter 4 will introduce an assessment process of the FE method on energy dissipation calculations; confirmation using FWD results will be given as well.

Chapter 5 provides a case study using data provided by TRL to calculate energy dissipated in 3 sorts of pavement induced by a Heavy Goods Vehicle (HGV). Comparison of energy consumption with relative stiffness is given to investigate the relationship between energy dissipation and pavement stiffness.

Chapter 6 estimates the stiffness effects on energy consumption by an asphalt concrete pavement with varied stiffness and speed of the tyre travelling.

Chapter 7 will assess the influence of varied stiffness of the top layer on energy consumption by using a concrete pavement structure.

Chapter 8 gives detailed information on energy dissipation of a low quality pavement under a rolling tyre load.

Chapter 9 summarises the key results carried out and identifies any limitations during the analyses.

Chapter 10 will give final conclusions and recommendations.

Chapter 2

Literature Review

In order to understand the subject of this PhD project, the influence of pavement stiffness on vehicle fuel consumption, it is necessary to consider in more detail the actual mechanisms of fuel consumption involved and the effects of the pavement. Therefore, the literature review covers the following areas: vehicle fuel economy, rolling resistance, pavement characteristics.

The purpose of this literature review is to identify and understand details of the background information and answer the subsequent questions as follows:

- Which factors influence the fuel consumption?
- How do these factors affect the fuel consumption?
- How does the pavement affect the fuel consumption?
- How to test the fuel consumption?

Furthermore, a background study of pavement engineering, measurement of stiffness, tyre/pavement interaction and finite element analysis will be given in the chapter.

2.1 Vehicle fuel economy

The term 'fuel consumption' or 'fuel economy' has been used to explain the relationship between the distance of a vehicle's journey and the amount of fuel consumption. Fuel consumption is the amount of fuel

consumed per unit distance that a vehicle has travelled. The definition of fuel economy is the distance travelled per unit of fuel used (Wikipedia, Fuel economy in automobiles, 2006). It is not difficult to understand that fuel consumption is the multiplicative inverse of fuel economy. Fuel economy is mainly used in a wide range of vehicle fuel usage tests.

Normally, the unit of fuel economy can be expressed as miles per gallon (mpg) or kilometres per litre (km/L). In most cases, the unit relating to fuel, in UK, is litre and the unit of distance is mile. Hence, the unit of fuel economy, normally, could be expressed as miles per litre and the unit of fuel consumption may be expressed as litres per mile (L/mile). Furthermore, the unit litres per 100 kilometres (L/100km) has been widely used in the literature. Fortunately, these units are not difficult to convert. A conversion table is listed as follows.

Table 2-1 Conversion table of mpg and km/L

Fuel economy	
1 mpg = 0.425 km/L	1 km/L=2.352mpg
Fuel consumption	
1L/mile=62.15 L/100km	1L/100km=0.016 L/mile

By nature, fuel consumption is a consequence of many factors. These factors come from 5 main sources: vehicles, road system, environment, traffic and driver. No single factor is an isolated item for the fuel economy of a vehicle. Factors causing fuel consumption may affect each other. For instance, a reduction in weight of a vehicle will not only yield a decrease in fuel consumption but also result a smaller rolling resistance. A smaller

rolling resistance will also reduce the fuel consumption. Fuel economy research is therefore complicated and it is very important to understand details of the factors that cause fuel economy.

2.2 Factors influencing fuel consumption

Vehicle engineers have performed extensive research relating to fuel economy. This research has not only focused on the effects of vehicle factors but also of pavements. This section will list the factors causing vehicle fuel consumption and give results obtained in previous research.

2.2.1 Engine

Figure 2-1 shows the typical energy used by a midsize vehicle. Over 62% of the fuel is lost in the internal combustion engine. The engine needs this part of the fuel to overcome the internal friction, pump air and in generating waste heat. It is also noted that over 17% of the energy is wasted by idling in urban driving. This significant proportion of energy is lost during stop-start conditions. Only about 18.2% of the energy generated from the fuel tank is transferred to the drive line, and energy is also lost in transmission and other drive line parts. Hence, only 12.6% of the fuel is used to generate the force to overcome the resistance from aerodynamic drag, rolling resistance and inertia, which is represented by braking.

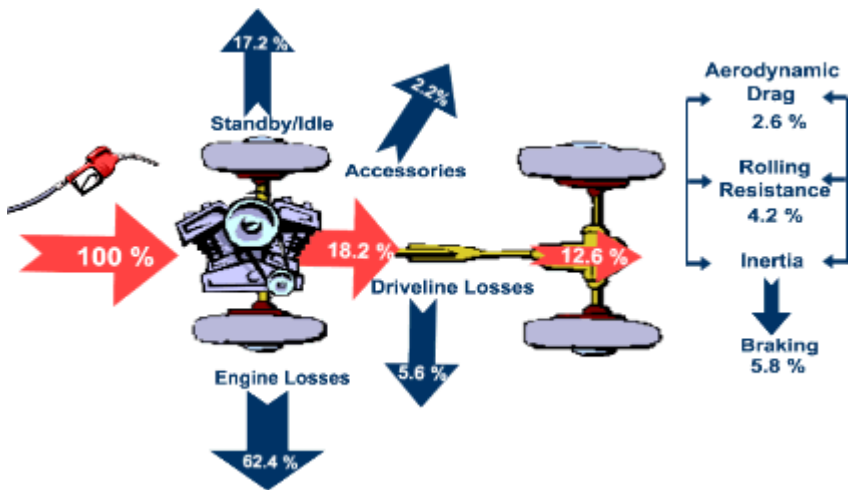


Figure 2-1 Energy flow of a midsize passenger car (FuelEconomy.gov, 2009)

Ang-Olson and Schroeer (2002) also stated that a typical modern diesel truck consumes 53% of total fuel as engine heat and another 5% is dissipated through engine friction and pumping losses. Therefore, only 42% of the total fuel is used for engine output.

2.2.2 Vehicle type

A modern vehicle is a complicated machine. In every important respect, the performance of today's vehicles is much better than that of their predecessors. In particular, the performance in terms of fuel consumption has seen a significant improvement. During the mid-1970s, a new car, which was sold in the USA, had an average fuel economy of 16mpg (Meyer, Watson, & Skinner, 2006). The National Research Council (NRC) of US (1992) indicated that the average fuel economy had been improved by up to 50% during the 1980s. Nowadays, some new vehicles already have much higher mpg than before. The US corporate average fuel economy standard was 27.5mpg for passenger vehicle in 2005 and 20.7 for light truck (Bamberger, 2005).

Unfortunately, the improvements in fuel consumption are far from enough to let customers or governments feel satisfied, due to rapidly increased amounts of fuel usage and fuel price rises. This is because the modern vehicle is still fuel inefficient. For instance, the most fuel efficient vehicle on the market nowadays is the 2010 Toyota Prius 1.8 with estimated fuel economy of 50mpg (21km per Litre), which compares to an average fuel economy about 25mpg (11km per Litre) (Fueleconomy.gov, 2010). According to widely recognised data (Wikipedia, Gasoline, 2010), the energy content of petrol is 32MJ/L. On this basis, the vehicle needs, theoretically, 152MJ of energy for a 100km journey. If the total weight of the car including one driver and luggage is 2000kg, based on the gross weight of the Prius, 1800kg (Toyota, 2010), and the mean rolling resistance coefficient of a tyre is 0.0102 based on observations of 154 replacement tyres estimated by Rubber Manufacturers Association (2005), then the resistance force that is applied to the car is 200N. Therefore, the work done during the 100km journey (at constant velocity) is around 20MJ. The ratio of the energy consumed by rolling resistance (20MJ) and the theoretical chemical energy in the petrol (152MJ) is therefore only 13%; the other 87% of the fuel is transformed to heat and other sorts of energy, and used to overcome air resistance.

2.2.3 Fuel type

It has long been known that diesel engines are more efficient than petrol engines. Normally, diesel engines save about 30-35% more energy than petrol engines (FuelEconomy.gov, 2009).

In 1978, two Volkswagen Golf cars were used to test the difference in fuel consumption between petrol and diesel. The petrol engine was 1100cc and diesel engine was 1500cc (Week, 1981). A route from Crowthorne to London was used followed by driving around in the central urban area. Each test covered over a 6000km journey. Table 2-2 shows the fuel economy results and comparative ratio between diesel and petrol engines. Obviously, the diesel engine took, at least, a 24% advantage in fuel saving over the petrol engine. In particular, in densely trafficked urban areas the saving was up to 40%. The results of fuel usage of the two different cars were calculated as a weighted average 50% fuel economy from central London, 40% from rural areas and 10% on motorways, showing that with the same amount (by volume) of fuel, the petrol engine vehicle only covered 63.4% of the journey covered by the diesel vehicle.

Table 2-2 Volkswagen Golf fuel consumption on different types of road (TRRL, 1980)

Route	Diesel (mpg)	Petrol (mpg)	Ratio Petrol /Diesel (%)
Central London	27.72	16.48	59.4
Crowthorne to London	38.00	26.40	69.5
Rural	39.14	27.07	69.2
Motorway	37.40	27.64	73.9
Average Mixed 50%40%10%	32.35	20.52	63.4

However, the significant advantage of fuel saving of diesel engines might change. Redsell et al (1988) tested Cavalier cars at the University of

Loughborough. The diesel car had a 1600cc engine and the petrol had a 1300cc engine. The fuel saving of the diesel Cavalier was 22%, 17% and 4% in urban, suburban and motorway driving compared to the petrol Cavalier. The average mixed fuel consumption, which is a sum of fuel consumption of 40% urban driving, 50% suburban driving and 10% motorway driving, showed that the diesel engine saved 18% fuel compare to its counterpart.

Because of fuel efficiency and rising fuel prices, the demand for diesel and diesel vehicles increased. Martin and Shock (1980) stated that diesel engines were used over in 50% of the heavy goods vehicle (HGV) population, over 90% of two axle rigid trucks and 90% of all other rigid and articulated lorries.

2.2.4 Vehicle weight

A greater drag force is required by a heavier vehicle to drive it at the same speed as a lighter vehicle. This also means heavier vehicles consume a greater amount of fuel. Reducing vehicle weight results in less traction required to accelerate the vehicle and less rolling resistance. Results measured from tests using various cars with different weights over all driving conditions indicated that each 10% decrease of vehicle weight leads to a 3-5% reduction of fuel usage (Maddock, 1979). Casadei and Broda (2007) also stated that a reduction in vehicle weight leads to a significant increase of fuel economy. Figure 2-2 shows the results of fuel economy improvement with vehicle weight reduction retrieved from 4 kinds of vehicles.

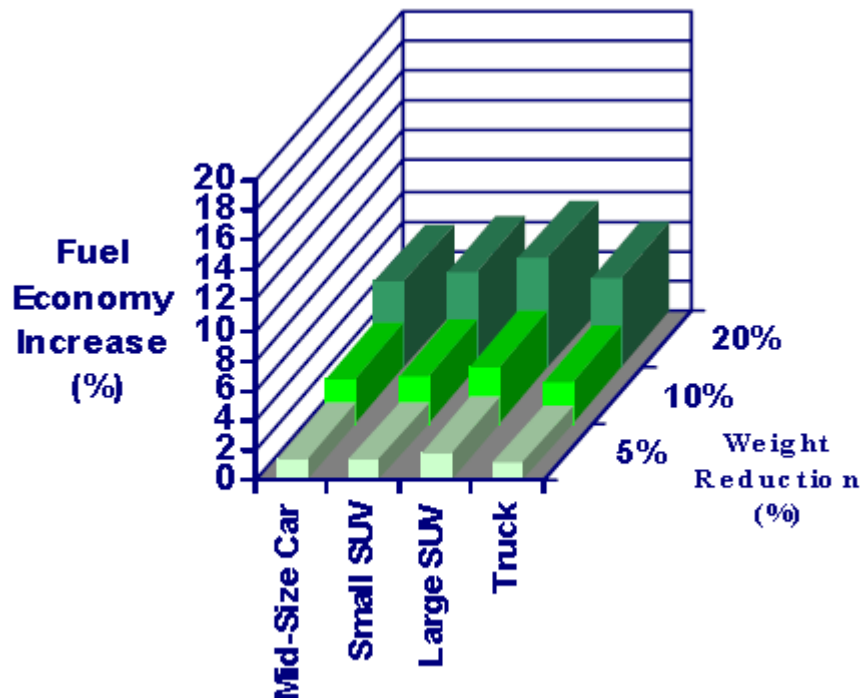


**Figure 2-2 Fuel economy improvement vs. weight reduction
(Casadei & Broda, 2007)**

Figure 2-3 shows a comparison of fuel consumption tests when the cars were driven at steady speeds. Both diesel and petrol cars show a higher fuel consumption with increasing weight of the cars. For the petrol Golf, the fuel consumption was around 5.2L/100km (45.23 mpg in fuel economy) when driven at 50 km/h and taking 2 passengers. With 5 passengers, the fuel consumption was around 5.5L/100km (42.77mpg in fuel economy). The difference in fuel consumption between the 5-passenger test and 2-passenger test at 50km/h is about 0.3L/100km (2.46mpg). It is noted that a similar value of the difference (0.3L/100km) was also found when the car was driven at other speeds (50 to 100km/h). The same picture was also found in the tests which used the diesel car. Therefore, this indicates that the extra weight significantly affects the fuel consumption, and this influence is not affected by the velocity changing.

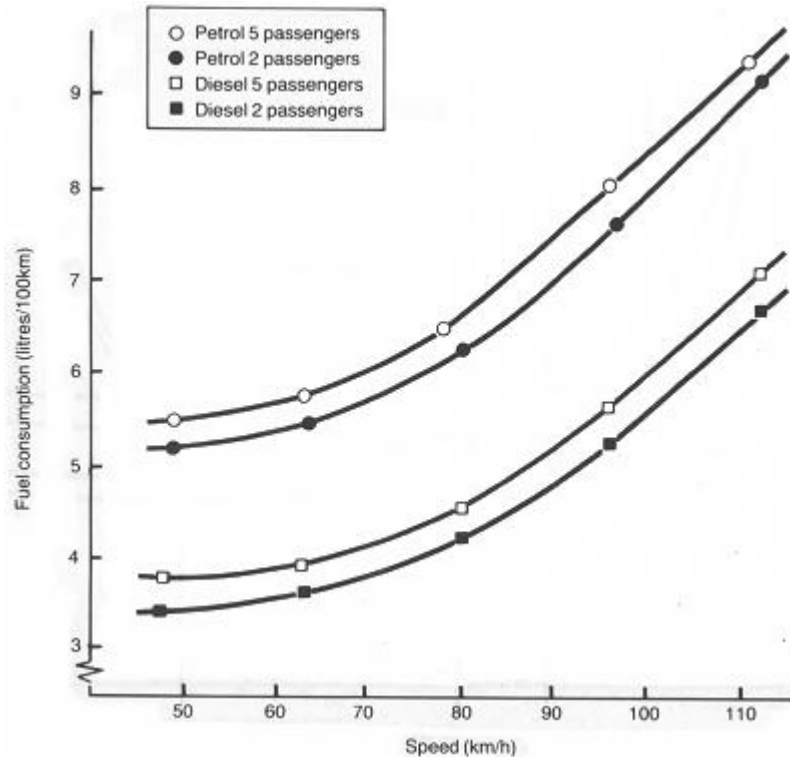


Figure 2-3 Volkswagen Golf fuel consumption at steady speeds (Week, 1981)

2.2.5 Vehicle speed

Additional energy is required when vehicles are driven at a higher speed as compared to a lower speed. The additional energy is used to compensate for the energy loss caused by resistance force to keep vehicle driving at a constant speed. Therefore, fuel consumption increases as vehicle speed increases when vehicles are driven at steady speeds. This is proved by the results plotted in Figure 2-3.

However, sometimes low speed driving demands high fuel consumption. Figure 2-4 shows the comparative fuel consumption of the two Golf cars in urban traffic. The results of fuel consumption were retrieved when vehicles were driven at average speeds in an urban area. It shows that the fuel consumption decreases as the speed increases when speeds are smaller than 70km/h. The fuel consumption increase can be observed in the 4

tested cases, a petrol vehicle with 2 or 5 passengers and a diesel vehicle with 2 or 5 passengers.

This might be explained by more start/stop processes occurring for vehicles with a low average speed in traffic-influenced (urban) driving. Vehicles have to consume fuel to generate energy for acceleration. Then, the kinetic energy transforms to heat when the vehicles have to decelerate (brake). With increasing average speed, start/stop is less frequently observed. This smooth driving will give a higher performance on fuel economy. Therefore, the curves of fuel consumption show a sharp fall between 0km/h and 20km/h and the best fuel economy can be achieved at 70km/h for the diesel vehicle and 80km/h for the petrol vehicle. After 70km/h, vehicles are likely to be driving on a motorway or trunk road and the fuel consumption represents steady speed driving.

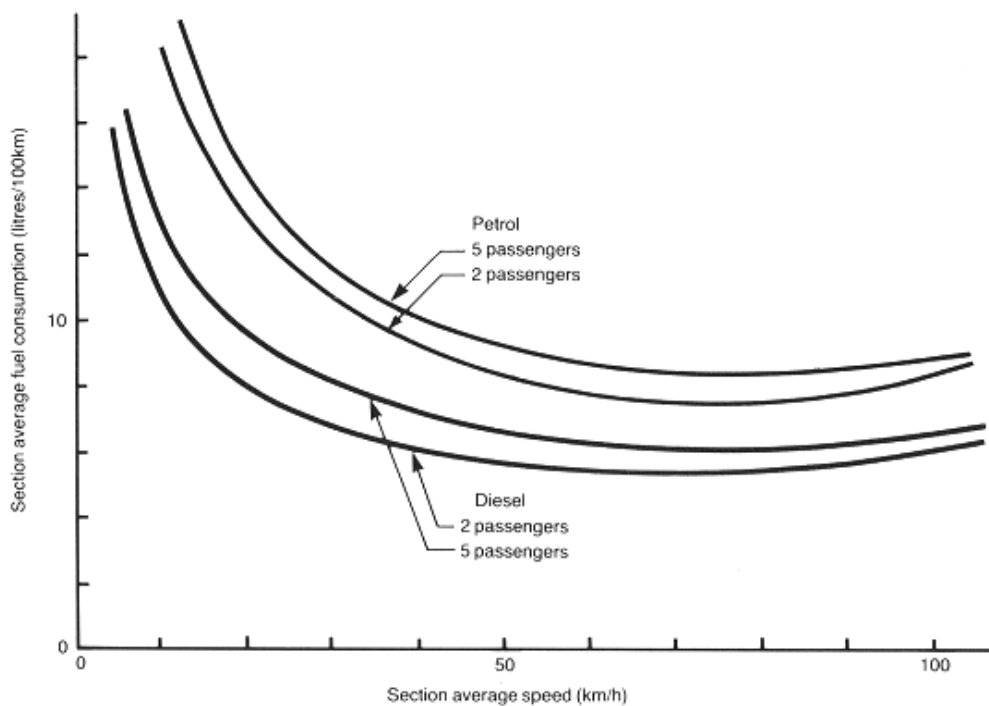


Figure 2-4 Volkswagen Golf fuel consumption in traffic (Week, 1981)

Figure 2-3 and Figure 2-4 indicate that fuel consumption in traffic-influenced driving is totally different from the isolated fuel consumption of a vehicle. High fuel consumption can also be observed when vehicles are driven at high speed. This is because more aerodynamic drag and rolling resistance are generated. Therefore, the engine needs more fuel to produce energy to balance the resistance forces.

The influence of vehicle speed on fuel consumption varies for different vehicles. A Ford Box, 1980, pickup truck, has its best fuel economy at 20 mph (32.20km/h). The fuel economy decreases with increasing speed by about -1.4 mpg with every 10 mph (16.09km/h) increase (Zaniewski & Jhon, 1989). A 2-axle single unit truck, GMC van, has its best fuel economy at 30mph (48.28km/h), 9.6 mpg. It also has a reduction in fuel economy with increasing speed by about -0.85 mpg per 10 mph increase (Zaniewski & Jhon, 1989). A 28 ton semitrailer truck, Freightliner, flat bed, shows a very small decrement of fuel economy with speed, 0.1 mpg per 10 mph increase. This result applies both on concrete pavement and asphalt pavement (Zaniewski & Jhon, 1989).

2.2.6 Aerodynamic characteristics

Aerodynamic drag is a resistance force caused by the airflow that impacts on the vehicle. Vehicle speed, vehicle frontal area, and vehicle shape are the major factors influencing the aerodynamic drag. Basically, at a constant speed, aerodynamic drag is proportional to the product of drag coefficient and projected frontal area of a vehicle (Plotkin, 1991).

The fuel consumption of a vehicle is significantly influenced by its aerodynamic characteristics. Hucho (1987) indicated that aerodynamic

drag accounts for about 80% of total drag at 100km/h for a medium size Volkswagen Golf. It was also noticed that about 21% of the fuel used for driving a medium size car is required to overcome the aerodynamic drag. McCallen et al (1998) indicated that at a speed of about 50mph, for a modern Class 8 tractor-trailer, the energy contribution required to overcome rolling resistance equals the contribution required to overcome aerodynamic drag. When the vehicle was driven at 70mph, aerodynamic drag accounted for 65% of the total energy consumption, as shown in Figure 2-5.

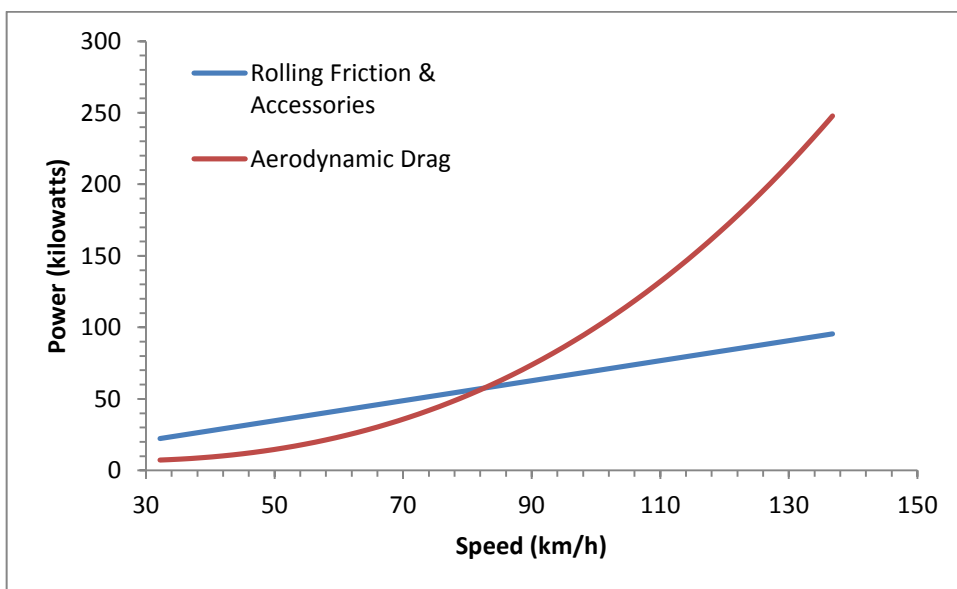


Figure 2-5 Power required to overcome aerodynamic drag and rolling resistance (McCallen et al, 1998)

The greater the aerodynamic drag, the more power is required, i.e. the more fuel is consumed. Conversely, a reduction in the drag leads to a higher fuel economy. It is noted that reducing the drag coefficient of a vehicle by 10% leads to 2.3% to 2.4% improvement in fuel economy. The Euromix fuel consumption method also stated that a 10% reduction of aerodynamic drag saves 3-5% fuel consumption (Bang, 1990).

2.2.7 Road system

As mentioned in section 2.2.5, vehicle speed has a significant influence on fuel consumption and this influence varies with driving style. The fuel consumed by a car driving at a steady speed (motorway driving) is not equivalent to the fuel used by the same car passing a section of journey with a similar average speed level (urban driving).

Researchers have developed models to simulate the fuel consumption of traffic-influenced driving. A widely published model was developed by Everall (1968), who stated that the relationship between fuel consumption and average speed can be represented as an "Everall curve", which can be derived as an equation as follows:

$$F = E_1 + \frac{E_2}{V_a} + E_3 V_a^2 \quad 2-1$$

where: F is fuel consumption,

E_1 , E_2 and E_3 are constants, and

V_a is the average speed of a vehicle.

Langdon (1984) also developed a numerical model to calculate vehicle fuel consumption in which additional factors were used in the calculation. Not only vehicle speed, but also factors related to vehicle acceleration or deceleration, road gradient and road design were applied. The model indicated that vehicle speed only accounted for about 35% of variability of the total fuel consumption. Waston et al (1980) and Akcelik et al (1983) also developed improved models based on Everall's model. But, Everall's model is still widely used, especially for laboratory tests.

It is clear that acceleration and deceleration are the major factors influencing the fuel consumption of traffic-influenced driving. Therefore, in terms of fuel consumption it is of benefit to improve traffic capacity and smooth the traffic stream to reduce the acceleration/deceleration process.

2.2.8 Skid resistance

Skid resistance is “the force developed when a tyre that is prevented from rotating slides along the pavement surface” (HRB, 1972). The skid resistance is dependent on the surface properties of road and tyre. The skid resistance can be lower when road surface is wet than the same surface when dry. Adequate skid resistance is necessary, since the level of skid resistance is a significant contributory factor enabling vehicles to achieve adequate acceleration or deceleration.

The mechanism of skid resistance is the interaction between pavement texture and tyre tread. Weather affects the pavement surface most of the time; moisture on the pavement surface due to rain or snow would increase the skidding greatly. The decreased skid resistance will affect driving style and this also leads to a fuel consumption change.

2.2.9 Pavement surface

Obviously, the pavement surface is an important issue that should not be overlooked, since vehicles have to contact the pavement surface to gain traction force. Therefore, it is necessary to understand the influence of the surface characteristics on fuel consumption.

In terms of pavement engineering, texture is used to describe the very short wavelengths applying on the pavement surface. It also takes the

form of "roughness" of larger rocks found in asphalt or concrete mixtures. The World Road Association (PIARC, 2009) define the categories of these wavelengths (textures) as megatexture (50-500mm), macrotexture (0.5-50mm) and microtexture (<0.5mm). Figure 2-6 illustrates textures of some typical pavement surfaces.

	TEXTURE	
	MACRO	MICRO
1. POLISHED CONCRETE	SMOOTH	SMOOTH
2. NEW CONCRETE	SMOOTH	HARSH
3. ROLLED ASPHALT MIXED AGGREGATE-ROUNDED	MEDIUM	MEDIUM SMOOTH
4. ROLLED ASPHALT MIXED AGGREGATE	MEDIUM	MEDIUM
5. ROLLED ASPHALT MIXED AGGREGATE	MEDIUM COARSE	MEDIUM
6. ASPHALT WITH COARSE SEAL COAT	COARSE	HARSH

Figure 2-6 Sketch figure of texture of pavement surface

It is noted that the characteristics of a pavement surface have a significant influence on vehicle fuel consumption. It is easy to image that repeated vibrations of a vehicle caused by road unevenness or macrotexture can result in energy loss. The vibrations can be absorbed by vehicle suspension systems and transformed into heat. Sandberg (1990) indicated that fuel consumption varies over a range of 11% if the wavelengths of texture are in the range 0.6 to 3.5 m. The fuel consumption also varies over a range of 7% if the wavelength is in the range 2 to 50mm. These results are based on an experiment which was

conducted by using a Volvo 242 car driven at 50, 60 and 70km/h over various roads. A set of coast-down tests were applied to identify the influence of fuel consumption on pavement surface factors in South Africa. One passenger car, two trucks and two buses were driven at steady speeds on different road surfaces to measure fuel consumptions. A numerical model was derived and predicted that surface characteristics have an influence on fuel consumption of up to 7% for passenger cars and 20% for trucks and buses (Plessis, Viser, & Curtayne, 1990). Laganier and Lucas (1990) state that fuel consumption is influenced by unevenness and macrotexture and varies by up to 7%. Gyenes and Mitchell (1994) indicated that fuel consumption of a goods vehicle can be increased up to 10% by road unevenness.

2.2.10 Pavement stiffness

That stiffer pavements save energy can be explained by the fact that a lower deflection equates to a reduced inertial resistance from pavement materials, and the pressure waves induced, both in the pavement and its subgrade, are therefore of smaller magnitude. These waves represent the mechanism by which energy is carried away from the wheel-surface contact and into the surrounding ground.

Recently, it has been suggested that pavement stiffness has a quantifiable influence on rolling resistance (Cenek, Jamieson, & Ball, 1996) and vehicle fuel consumption (Taylor 2002), i.e. stiffer pavements save energy. For example, a 20% reduction in fuel consumption was found for a 25 ton truck running on concrete pavements compared with running on an asphalt surface (Zaniewski & Jhon, 1989). The UK's Transport Research

Laboratory (TRL) stated that an increase from 60 microns to 98 microns of pavement surface deflection led to 28% more fuel consumption (McKeown, 2002). TRL also suggested that a 5.6% reduction in the rolling resistance was found on a rigid pavement when compared with a flexible pavement in laboratory tests (Benbow, Iaquinta, Lodge, & Wright, 2007).

2.3 Essential pavement engineering background

One of the purposes of the FE analysis is to build a model to calculate energy consumption. Furthermore, the model has to be flexible. This means that the model can be used to simulate different cases involving varied characteristics of tyre and pavement. Based on this point, the fundamental elements of pavement design have to be understood.

2.3.1 Structure of pavement

Clearly, a typical pavement has a layered structure, as shown in Figure 2-7, which includes surface course, binder course, base, subbase, capping and subgrade. The surface course is a layer on the top of a pavement. It directly withstands loads and transmits them to lower layers. For this reason, the surface course needs to be tough, and this requires the use of high quality materials, which also means expensive materials. The binder course can be explained as a layer to connect the surface course and the base layer. The base layer is designed to give strength to the pavement, so large aggregates tend to be used. A subbase is required to give firm support in order to limit flexure. The materials used in the capping are, normally, cheap and can be regarded as a subgrade improvement. Naturally, the materials of the subgrade are soil. The thickness of the subgrade can be assumed to be infinite in numerical analysis.

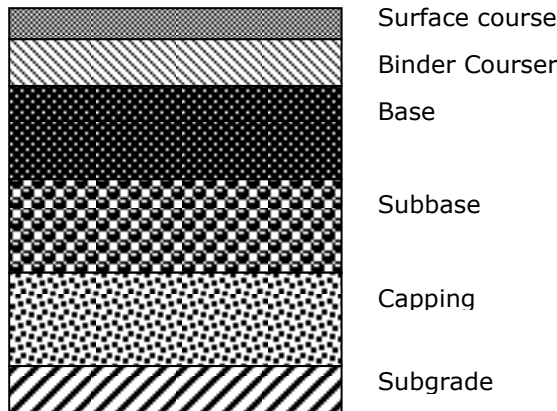


Figure 2-7 A typical pavement structure

2.3.2 Materials of pavement

It is not be possible to avoid the influence of materials used in pavements in pavement designing. One of the key points for materials which are to be used in FE analysis is how to retrieve accurate properties. Therefore, characteristics of materials should be understood in this preliminary study.

The most basic material found in a pavement is the subgrade soil. In fact, soil is a combination of various constituents, covering a wide spectrum of granular materials; such as clays, sands, rocky materials and so on. Thus, the uncertainty of the soil constituents leads to a problem that it is difficult to completely understand the mechanical properties.

For elastic analysis of soil, Young's modulus and Poisson's ratio are used to describe the elastic properties. A typical range of Young's modulus is between 0.5 and 200 MPa. Table 2-3 shows ranges of typical soils. The range of Poisson's ratio is between 0.3 and 0.45.

Laboratory tests indicate that hysteresis can be found in soil (Rahnama & Krawinkler, 1993). This is because friction due to the interaction of soil

particles absorbs a part of the energy when load is applied on the soil. Therefore, damping is used in analyses to simulate the energy dissipation.

Table 2-3 Young's modulus of typical soils (Herndon, 1990)

Soil		Young's Modulus (MPa)
Clay	Very soft clay	0.5 - 5
	Soft clay	5 -20
	Medium clay	20-50
	Stiff clay	50-100
	Sandy Clay	25-200
	Clay shale	100-200
Sand	Loose sand	10-25
	Dense sand	25-100
	Dense sand and gravel	100-200
	Silty sand	25-200

A widely used material in pavement engineering is bitumen bound material, commonly known as asphalt. It is a mixture of aggregate and bitumen. The bitumen is used as a binder or glue for the aggregate particles. Naturally, the bitumen is a highly viscous material, and aggregates used in asphalt represent elastic behaviour.

Concrete is also a widely used material in pavements; it is a kind of hydraulically bound material where the binder is Portland cement. For numerical analysis, concrete can be categorised as an elastic material and can be used in base and subbase as well as a surface layer. Cement can also be used for stabilisation of subgrade.

Nowadays, pavements of various types are composed of many different materials and have various layers. In general, 3 main types can be described (Huang, 2004; Papagiannakis & Masad, 2008):

- Flexible pavements,
- Rigid pavement, and
- Composite pavements.

For flexible pavements, the top layer is a surface course composed of bitumen bound materials, i.e. asphalts. Dense Bitumen Macadam (DBM), Stone Mastic Asphalt (SMA) and Hot Rolled Asphalt (HRA) are typical materials which are extensively used in the surface course to give a tough support resisting the distortion generated by traffic loads. The thickness of the surface course is between 20 and 50mm. Materials used in the layers beneath, binder course and base, could be composed of bitumen bound materials or hydraulically bound materials. The thickness of the base would typically be in the range 100 to 400mm depending on road category (Design Manual for Roads and Bridges HD 26/06, 2006).

Rigid pavements are so named due to the rigid nature of concrete. The surface course is, typically, composed of Portland Cement Concrete (PCC). An asphalt layer may be laid on top to improve certain characteristics, such as smoothness, friction and noise. Normally, the thickness of the PCC slab is in the range 150 to 300mm (Huang, 2004).

Composite pavements are composed of both asphalt and PCC. PCC forms the bottom layer providing a strong base. Asphalt forms the top layer and provides a smooth surface.

Normally, there is a subbase of 150 to 250mm composed of unbound or hydraulically-bound material under all types of pavement to reduce the influence of flexure in the base under traffic load (Thom, 2008).

2.4 Rolling resistance

Rolling resistance is the force acting on a vehicle over a full journey. It is generated by the hysteresis of tyre and pavement. As mentioned before, only a small fraction of the total fuel is consumed by rolling resistance during normal driving. However, rolling resistance has a significant influence on fuel economy during constant speed driving, and this will be described in this section.

2.4.1 Interpretation of rolling resistance

Figure 2-8 shows a single tyre rolling on a pavement surface with a constant velocity V_x . The radius of the tyre is r . f_z is a vertical load generated by the weight of a vehicle. f_x is a drag force generated by the engine to push the tyre forward. As can be shown, the sequence under the drag force f_x ends up as a rotation of the tyre, and this rotation pushes the tread into a tyre/pavement interface, which has been named as the contact zone. Tread and pavement compress each other into a contact zone. The deformation is found to occur in both tyre and pavement. Meanwhile, the rotation pushes another part of the tread out of the trailing edge of the contact zone. Then, both pavement and tyre are decompressed after the tread goes out of the contact zone. The stress applied on the contact zone is uneven. Normally, the front edge experiences a bigger pressure compared to the trailing edge. Due to the uneven distribution of stresses on the contact zone, the counterforce f_c , which is generated by the pavement, is not in the centre of the contact zone, but, shifts forward by a short distance e . When multiplied by the distance e of the counterforce f_c it represents a resistance moment, which

has been named as the rolling resistance moment. To keep the balance of the moment, another moment needs to act on the tyre and it is a product of the tyre radius r and a horizontal force f_r . The horizontal force f_r is the rolling resistance of the tyre (Wong, 2001).

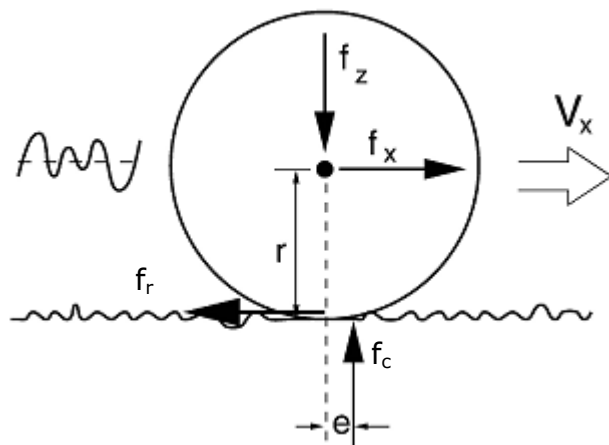


Figure 2-8 Tyre rolling resistance (Miege & Popov, 2005)

It is well known that a pure elastic substance does not consume energy when undergoing deformation. A viscoelastic substance exhibits both viscous and elastic characteristics, and the viscous component consumes energy when a load is applied then removed.

A hysteresis phenomenon can be observed when viscoelastic materials undergo a load-then-unload process. A typical hysteresis curve of viscoelastic material can be found in Figure 2-9. The shadow area enclosed by the hysteresis loop represents energy loss. The dissipated energy can be calculated by using the following equation:

$$E_h = \int \sigma d\varepsilon \quad 2-2$$

where: E_h is the dissipated energy,

σ is the stress and ε is the strain.

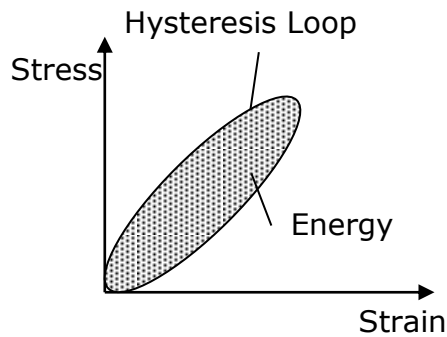


Figure 2-9 Hysteresis loop and energy dissipation

Rubber compounds of a tyre, at a regular temperature, display viscoelastic characteristics (Nokian Tyres plc., 1999), i.e. the hysteresis phenomena can be observed when a rubber compound undergoes repeated strain. A rolling tyre deforms when it contacts the pavement surface and recovers when it leaves the contact area. Therefore, rubber compounds of the tyre rapidly repeat the process of straining when the tyre is rolling on pavement. This process consumes energy which ends up as heat.

Rolling resistance is not only caused by the deformation of the tyre. Bendtsen (2004) summarized three main mechanisms influencing rolling resistance:

1. The macro deformation of tyre
2. The micro deformation in the contact area between tyre and pavement
3. The slippage friction in the contact area between tyre and pavement

Sandberg (1997) also indicated that road surface texture needs to be considered in the rolling resistance calculation or simulation. Benbow et al (2007) stated that stiffness, texture and temperature have a quantifiable influence on rolling resistance.

Generally, rolling resistance linearly relates to the vertical load of the tyre and can be expressed as a near-constant coefficient (NRC, 1992). The rolling resistance coefficient (RRC) can be derived as follows:

$$C_{rr} = \frac{F_r}{L_v} \quad 2-3$$

where: C_{rr} is rolling resistance coefficient,

F_r is rolling resistance force,

L_v is the vertical load applied on the tyre.

The RRC value of a new tyre is between 0.007 and 0.014 (NRC, 1992). Hence, a 60kN vertical load applied to a tyre delivers 0.42 to 0.84kN rolling resistance and 1.68 to 3.36kN rolling resistance for a 4-tyre vehicle. Therefore, at 100km/h, a 24-tonne vehicle consumes 47 to 93kW to overcome the rolling resistance.

For an isolated tyre, the RRC value is only affected by tyre structure and vehicle speed. Clark (1971) built two numerical models, which were based on a large amount of measurement, to describe the relationship between RRC and velocity. Equation 2-4 is used to describe the relationship between velocity and fuel consumption for radial-ply tyres and Equation 2-5 is used for bias-ply tyres calculation.

$$F_r = 0.006 + 0.23 \times 10^{-6} v_t^2 \quad 2-4$$

Where: v_t is the velocity of the tyre

$$F_r = 0.007 + 0.45 \times 10^{-6} v_t^2 \quad 2-5$$

The carcass, the inner layer of a tyre, as shown in Figure 2-17, is fabricated by plies of cord. With cords crossed over each other at an angle

about +60 and -60 degrees to the direction of travel, the tyre is called cross-ply or bias-ply. In radial-ply tyres all of the cord plies are at 90 degrees to the direction of travel.

The characteristics of the pavement surface also influence RRC value when tyres roll on different surfaces. Wong (2001) summarised the RRC values related to pavement surface characteristics, as shown in Table 2-4.

Table 2-4 Rolling resistance coefficient due to effects of pavement surface

Road surface	Rolling resistance coefficient
Car tyre	
Concrete, asphalt	0.013
Rolled gravel	0.02
Tarmacadam	0.025
Unpaved Road	0.05
Field	0.1-0.35
Truck tyres	
Concrete, asphalt	0.006-0.01

2.4.2 Factors influencing rolling resistance

Vehicle Velocity

Like the fuel consumption, rolling resistance also has a significant relationship with velocity. An experiment has shown that, for a 32-tonne goods vehicle, rolling resistance contributes about 70% of total drag when driven at 50km/h and about 37% at 100km/h, aerodynamic drag contributing the remainder (Gyenes & Mitchell, 1994).

The results from the experiment indicate that the main factor determining vehicle fuel consumption is speed. Ejsmont (1990) stated that the relationship between rolling resistance and velocity could be described as Equation 2-6.

$$F_r = C_1 + C_2 v$$

2-6

Where: C_1 and C_2 are constants,

v is the velocity of the vehicle.

As mentioned in Section 2.4.1, hysteresis is a major factor causing rolling resistance. As a tire rotates under load, it experiences repeated cycles of deformation and recovery of rubber compounds, i.e. the tyre exhibits hysteresis. Meanwhile, the hysteresis energy loss is dissipated as heat. This energy loss is considered to be the work contributed by tyre rolling resistance. Therefore, it is not difficult to explain Ejsmont's model. There is more deformation-rebound process in the tyre as vehicle speed increases. Thus, a high-speed rotating tyre exhibits more hysteresis energy loss than a low-speed rotating tyre in the same time period. Hence, the associated rolling resistance of the high-speed rotating tyre is bigger than the low-speed one. Therefore, a higher rolling resistance can be measured.

Temperature

Rolling resistance is affected by both tyre and ambient temperature. The temperature of tyre will be presented first then followed up by ambient temperature.

Descornet (1990) measured rolling resistance by using a "quarter-car" trailer which had been designed and tested at the Belgian Road Research Centre. A mutual dependency between RRC and temperature can be found, i.e. RRC values reduced if the tyre had a higher temperature, as shown in Figure 2-10. This is logical since a warmed tyre becomes soft and thus, less energy is needed to deform the tyre, which means less

energy is consumed in the rolling process. There would also be reduced stress concentration at tyre-pavement contacts and therefore less pavement deformation.

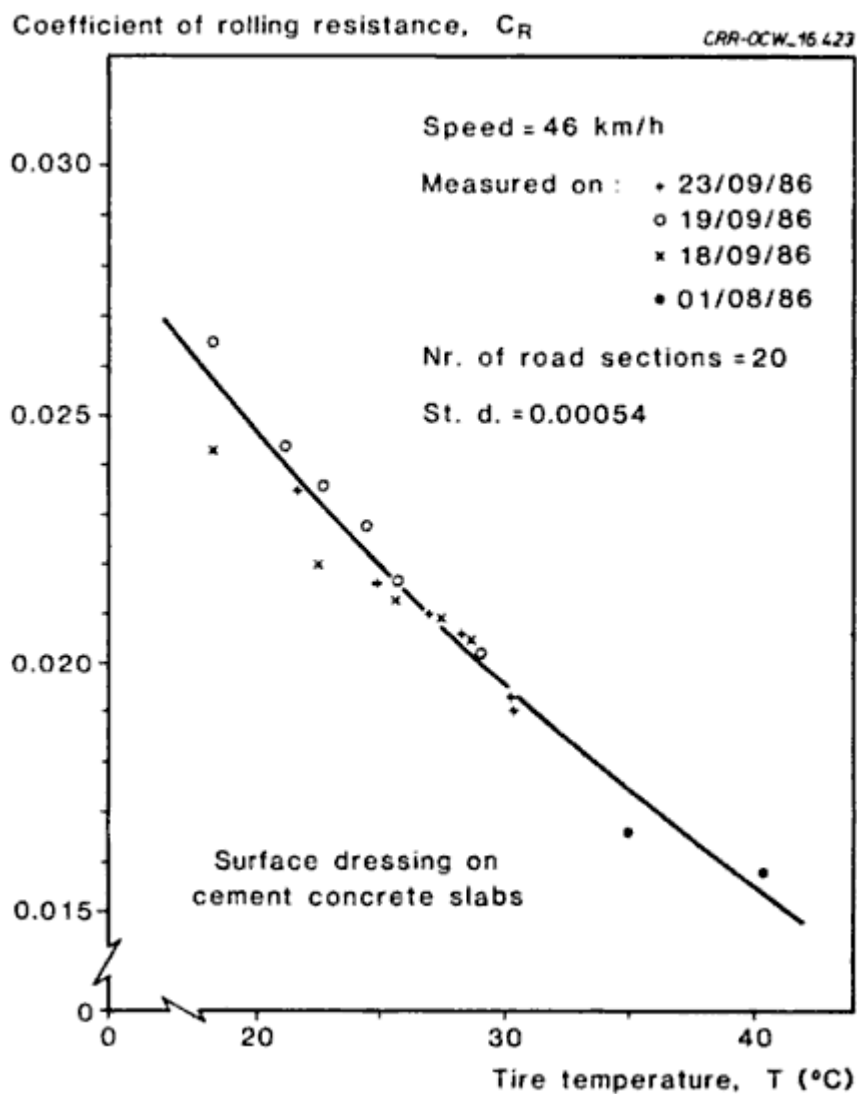


Figure 2-10 Rolling resistance coefficient vs. Tyre temperature (Descornet, 1990)

Results of field measurements conducted by the National Research Council of Canada (2000) indicate that fuel consumption will be raised by 2 to 5% if ambient temperature drops 10°C . This is because as temperature increases, the inflation pressure of the tyre increases as well. This brings a reduction of tyre/pavement contact area. Thus increased temperature

reduces tyre rolling resistance. Figure 2-11 shows measured results of rolling loss and corresponding tyre pressure by laboratory tests.

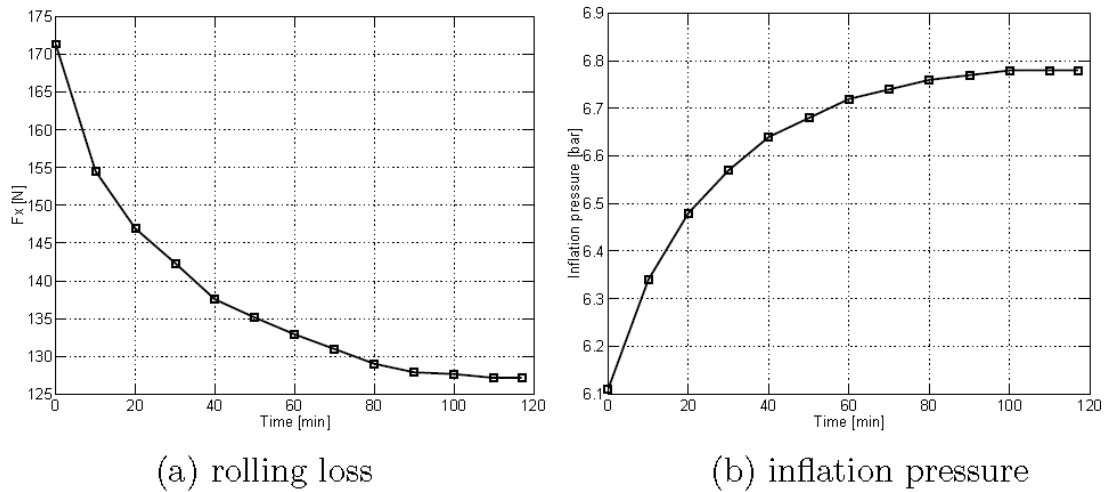


Figure 2-11 Measurements during tyre warm-up (Popov, Cole, Cebon, & Winkler, 2002)

Pavement Surface

An important issue which should not be overlooked is that rolling resistance is affected by the characteristics of the pavement surface. Rolling resistance varies between different pavement surfaces. Hard and smooth surfaces produce lower rolling resistance than soft and rough surfaces. The materials and surface characteristics also affect the rolling resistance (DeRaad, 1977). Figure 2-12 shows a comparison of relative rolling resistance over a range of pavement surface types. The rolling resistance generated by a new concrete pavement has been defined as a standard value; 100%. The polished concrete pavement achieves the lowest rolling resistance; 88% of new concrete. The polished asphalt is a little higher than the standard, at 101%. The rolled asphalt pavements, number 4 and number 5, are 104% and 108%. The seal coated asphalt has the highest value, 133%.

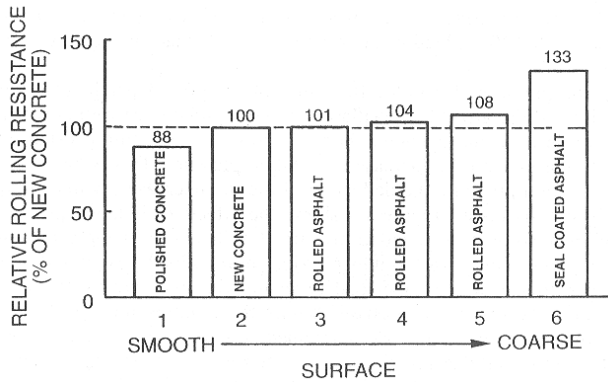


Figure 2-12 Pavement surface influence on tyre rolling resistance (DeRaad, 1977)

There are two main approaches that can be used to minimise the rolling resistance. Since the tyre is the major source generating rolling resistance, therefore, a properly inflated and aligned tyre provides a smaller rolling resistance (Meyer, Watson, & Skinner, 2006).

Since the frictional characteristics of a pavement surface are influenced by pavement texture (Thom, 2008), pavement texture influences rolling resistance as well. Descornet (1990) stated a linear relationship between rolling resistance coefficient and texture depth by measuring a reference tyre of a trailer, as shown in Figure 2-13. The results show that the rolling resistance coefficient increases by 0.002 as the depth of pavement texture increases by 1mm.

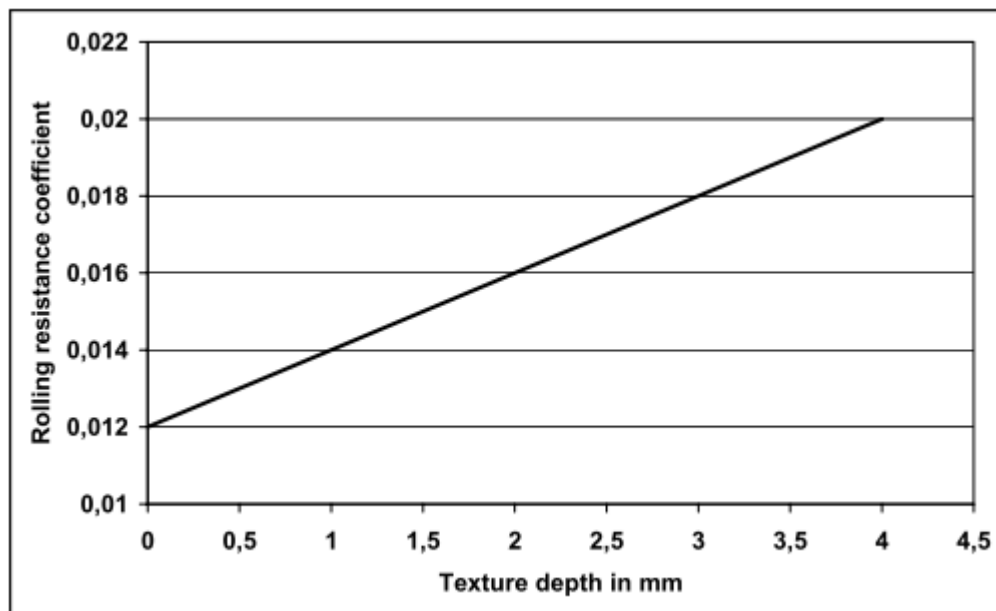


Figure 2-13 Rolling resistance coefficient vs. texture depth (Descornet, 1990)

2.4.3 Rolling resistance influencing fuel consumption

It is often estimated that a change in rolling resistance of 10% leads to 2-3% more fuel consumption (Sandberg & Ejsmont, 2002).

A research based on using ten different driving modes including acceleration and declaration shows that the rolling resistance counts for 14% of the total fuel consumption (Nokian Tyres plc., 1999), as shown in Figure 2-14.

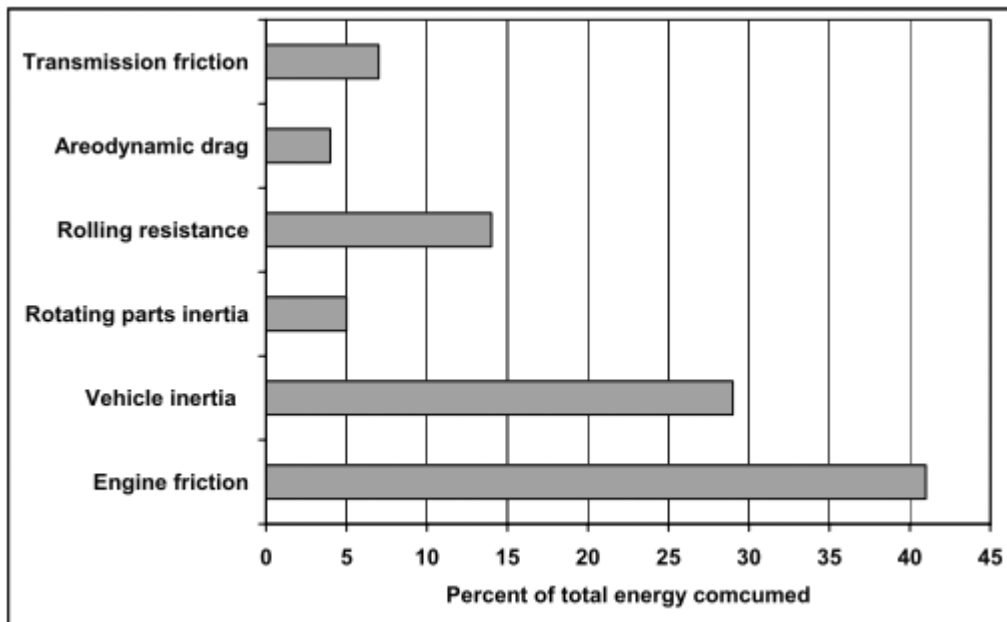


Figure 2-14 Distribution of fuel consumption of a uneven driving test (Nokian Tyres plc., 1999)

Figure 2-15 shows the relationship between rolling resistance and vehicle fuel consumption, derived from the driving tests. It indicates that the relationship between the change in rolling resistance and the change in total energy consumption is approximately linear. Thus, a 10% increase in rolling resistance coefficient will bring an additional 2% fuel consumption.

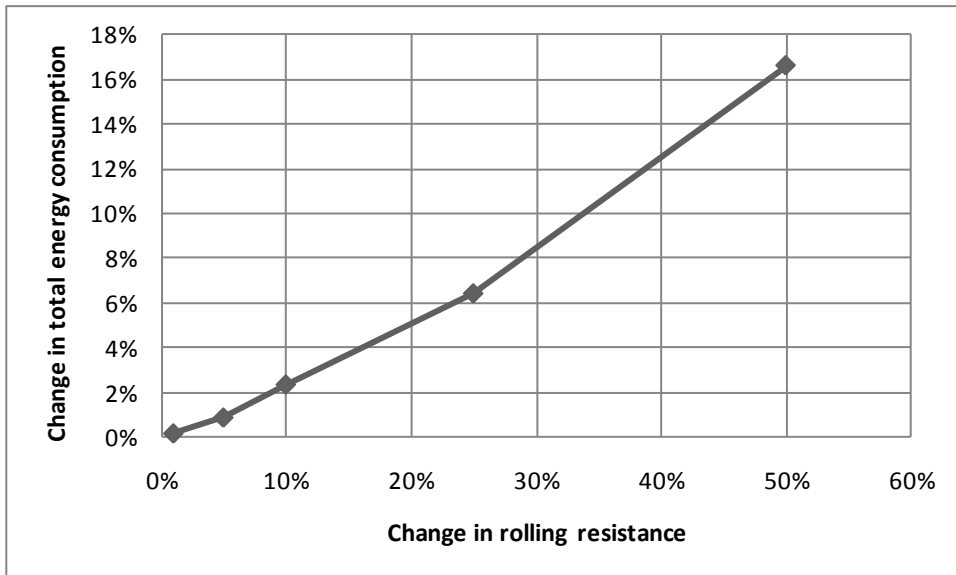


Figure 2-15 Effect on total energy consumption as a function of different changes in rolling resistance (Nokian Tyres plc., 1999)

Schuring and Redfield (1982) measured the fuel consumption and rolling resistance by using a five-axle tractor-trailer. The results show a linear relationship between fuel consumption and the total rolling resistance of all tyres. A 2.7% reduction in rolling resistance for crossply tyres or a 3.7% for radials will decrease fuel consumption by 1%. Descorent (1990) stated that fuel consumption changes linearly with rolling resistance coefficient. Figure 2-16 shows a linear relationship between fuel consumption and rolling resistance coefficient.

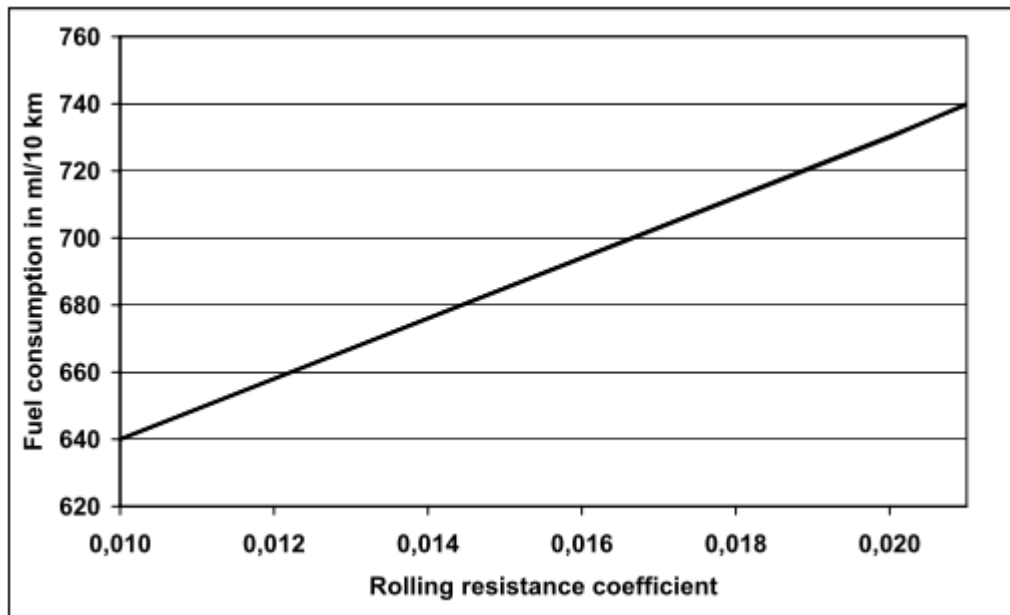


Figure 2-16 Rolling resistance coefficient and the fuel consumption for a passenger car at 60km/h (Descornet, 1990)

2.5 Tyre-Pavement interaction

Vehicle engineers believe that each part of a tyre has an influence on rolling resistance and fuel consumption. Therefore, it is necessary to understand the interaction of tyre and pavement. The following subsections present a review of the structure of pneumatic rubber tyres and the expected load distribution onto a pavement from a rolling tyre. A numerical method to calculate tyre/pavement contact area will also be included.

2.5.1 Tyre structure

A pneumatic rubber tyre consists of a lot of parts. Figure 2-17 shows the profile of a pneumatic tyre which includes 9 parts; tread, carcass, belt etc. The tread, which is made up of rubber compounds, is required to be tough and give a high resistance against abrasion tearing and crack growth. With material technology development, the rubber compounds used in tyre

manufacture have a low hysteresis to reduce the energy dissipation. The carcass is made up of a cords matrix embedded in rubber compounds. Basically, the cords comprise fabrics of synthetic or metallic wires, which are used as reinforcement, to give a resistance against tension. The bead is made up of rubber compounds and is used to anchor the tyre on the rim. The sidewall is also made up of rubber compounds and is used to resist against scuffing. It allows some compression when the tyre has a low pressure (Wong, 2001).

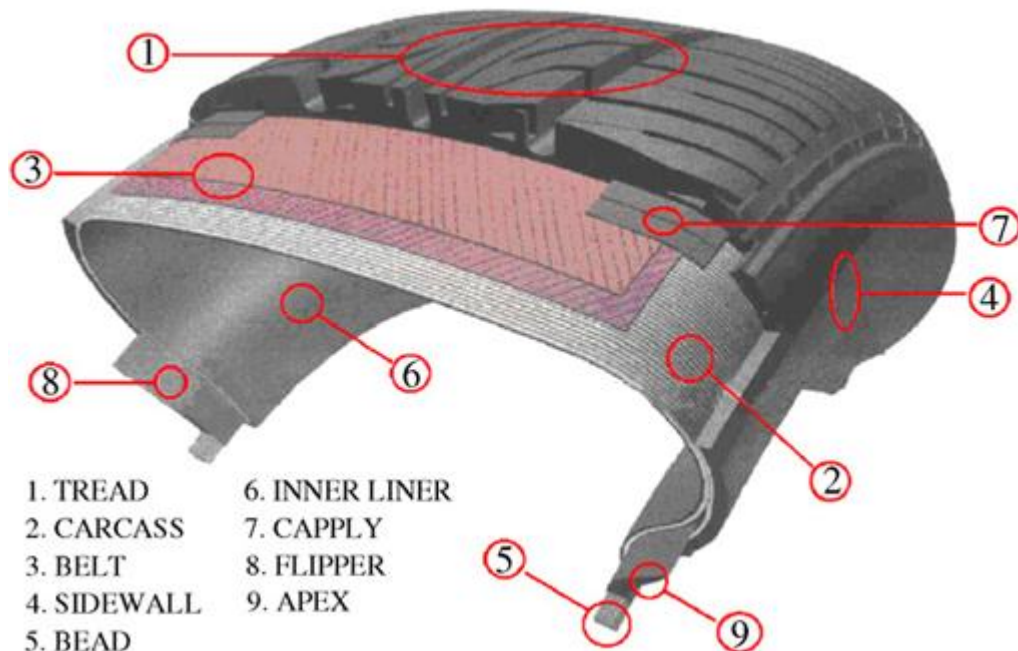


Figure 2-17 Profile of a typical pneumatic tyre (Nokian Tyres plc., 1999)

2.5.2 Tyre load distribution

Both vertical and horizontal pressures have been observed at the tyre/pavement contact area when a driving torque is applied to a tyre. Figure 2-18 shows the normal pressure and longitudinal stress at the contact area. It is worth noting that the distribution of the normal (vertical) pressure is non-uniform due to the rolling resistance. At the

same time, a shear force is generated at the contact area due to the corresponding force of the sidewall.

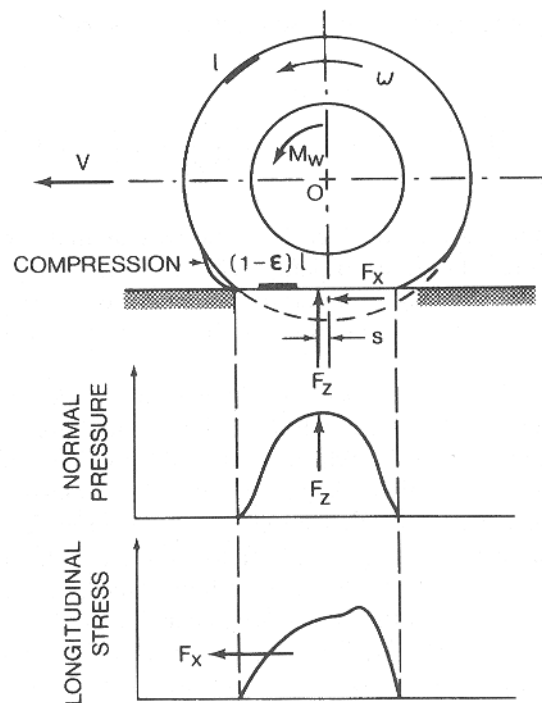


Figure 2-18 Behaviour of a tyre under the action of a driving torque (Clark, 1971)

Most numerical studies of pavements have been static analyses e.g. Kou & Chou (2004). However, the real load applied to pavements is dynamic. A rolling tyre under the weight of a vehicle implements a pressure onto a tyre/pavement contact area, and the pressure also moves forward with the vehicle. The vertical forces applied by tyres vary instantaneously above or below the static weight of vehicle due to the tyre/pavement interaction effects. The variation is influenced by pavement profile, vehicle suspension and vehicle speed. Figure 2-19 shows a typical instantaneous vertical force measured using a sensor mounted on the truck axle. The truck is driving at 80km/h on a medium roughness pavement.

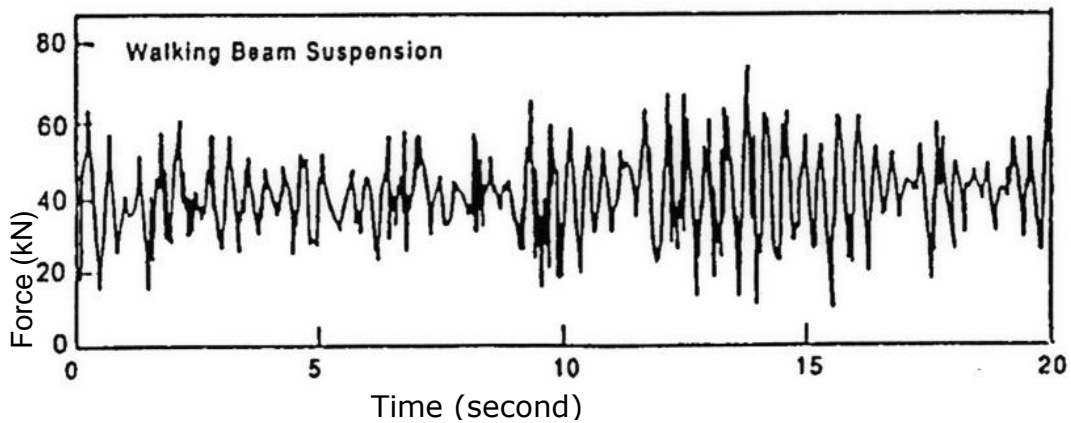


Figure 2-19 Typical vertical wheel force at 80km/h for medium roughness road and Walking Beam Suspension (Sweatman, 1983)

De Beer et al (2004) measured the tyre/pavement contact pressure using a Stress-In-Motion (SIM) facility. Figure 2-20 shows a stress matrix generated by a single tyre with three vertical loads. The 1st row of the matrix shows the vertical stresses, the second row of the matrix shows the longitudinal stresses and the third row of the matrix shows the lateral stresses. Column a, case 1, shows the case where the vertical load applied on the tyre is 20kN. Column b, case 2, shows the case where the vertical load is 35kN. Column c, case 3, shows the case where the vertical load is 50kN. The inflation pressure is 720kPa in all cases.

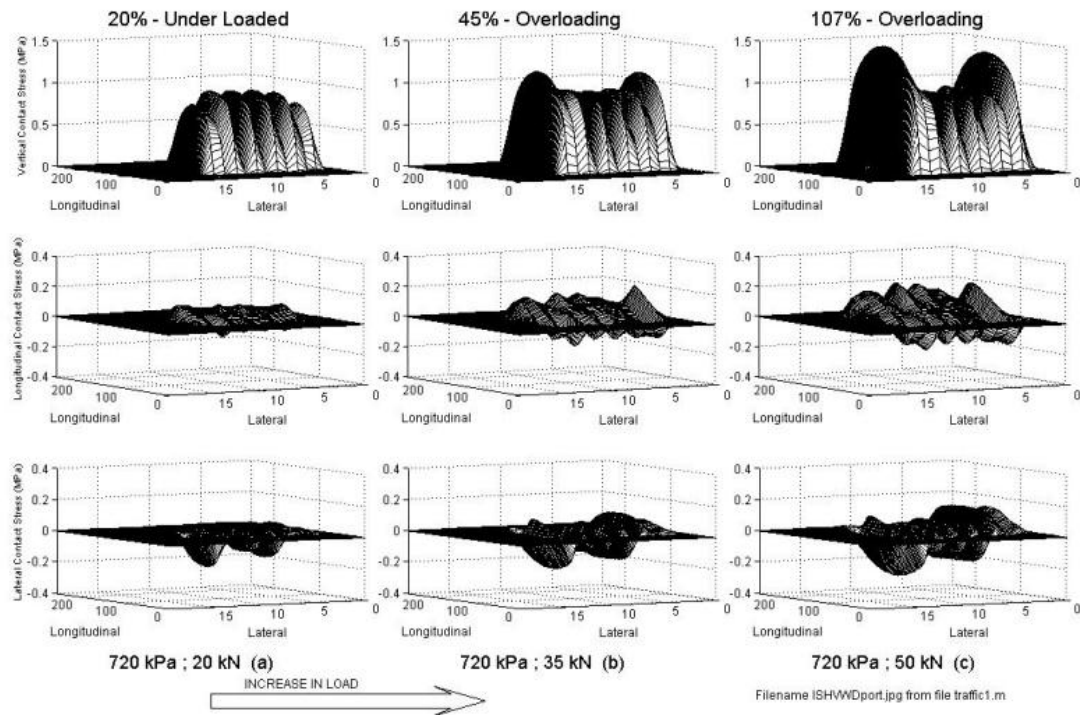


Figure 2-20 Tyre compressions with load changing

(a) Case 1: 720kPa, 20kN, n-shape;

(b) Case 2: 720kPa, 35kN, m-shape;

(c) Case 3: 720kPa, 50kN, m-shape (De Beer, Fisher, C., & Kannemeyer, 2004)

Each case shows that the distribution of vertical stress is non-uniform. Case 1 shows that the vertical stress uniformly distributes on the centre of the tyre/pavement contact area and the peak value is approximately equivalent to the tyre inflation pressure. The distribution of the vertical stresses at the longitudinal edges is similar to the shape of the normal pressure which is shown in Figure 2-20. The vertical stress falls sharply to 0 at the adjacent domains at the lateral edges. The shape of vertical stress distribution in case 1 is termed an n-shape. It represents incomplete tyre/pavement contact when the tyre is under loaded. At this stage, the sidewalls have no contact with the pavement, so, sharp reductions of the vertical stress can be found at the lateral edges of the contact area. With increasing load the tyre fully contacts the pavement, a

part of the vertical load acts directly on the sidewalls of the tyre, and it increases with increasing vertical load. Thus, it is common to find the peak value of the vertical stress near the longitudinal edges, as in case 2 and 3, when the tyre is overloaded. The shape of vertical stress distribution in case 2 and 3 is termed m-shape.

It is worth noting that the longitudinal and lateral stresses are much smaller than the vertical stress. Based on this point, only the vertical stress has been considered in this project. Furthermore, overloading cases have been neglected since most tyres obey the tyre pressure regulations, which avoid tyre overloading.

Fortunately, it is not necessary to include non-uniformly distributed vertical stresses in the FE analyses. Instead, a uniform distribution is used in this project. The method widely used in pavement and vehicle practice is an assumption that the load under a tyre is uniform and that the vertical pressure is equivalent to the inflation pressure of the tyre. The error related to pavement stress, which is caused by this assumption, is relatively small. (Thom 2008, Wong 2001).

2.5.3 Type/pavement contact area

The most popular approach used to calculate the tyre/pavement contact area has been given by the Portland Cement Association (PCA, 1966), as shown in Figure 2-21 (a). It is clear that, the shape of this contact area is fairly similar to a tyre footprint. Basically, the contact area consists of two semicircles and a rectangle. The contact area (A_c) can be calculated as follows:

$$A_c = \frac{L_v}{P_t}, \quad 2-7$$

where L_v is the vertical load on the tyre,

P_t is the pressure of the tyre.

The relationship between the total length of the contact area (L) and A_c is:

$$A_c = \pi(0.3L)^2 + (0.4L)(0.6L) = 0.5227L^2.$$

Thus,

$$L = \sqrt{\frac{A_c}{0.5227}} \quad 2-8$$

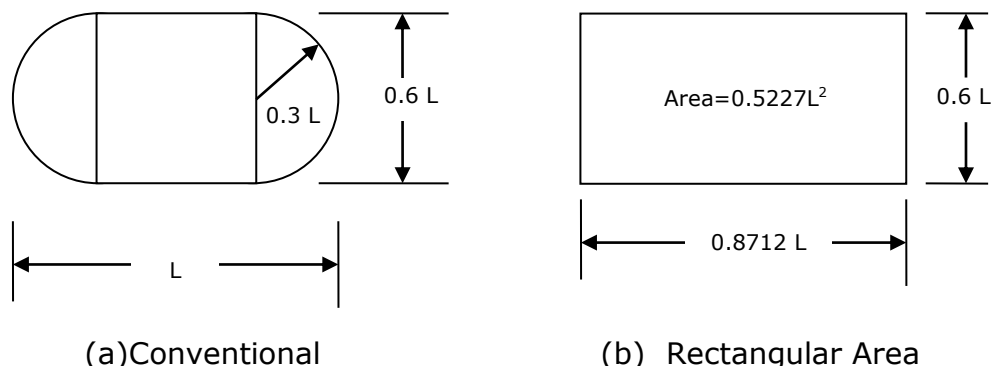


Figure 2-21 Tyre/pavement contact areas (a) from (PCA, 1966) (b) from (PCA, 1984)

With the development of FEM, a rectangular contact area has been widely used in pavement engineering practice. Figure 2-21 (b) shows the rectangular contact area proposed by PCA (1984). The area is equivalent to the conventional shape, as shown in Figure 2-21 (a), and can be calculated by Equation 2-9. The rectangular shape can easily be

implemented in FE models. Therefore, the rectangular contact area will be used in the 3D analysis here.

For example, the contact area of a tyre with an inflation pressure of 552kPa and a vertical load of 40kN is 725cm². L is equivalent to 37cm; the length of the equivalent rectangular contact area is therefore 32cm and the width is 22cm.

With the development of layered elastic theory for pavement engineering, the contact area has often been assumed to be a circle with an area of A_c . Despite the assumed contact shape not matching reality, the error is believed to be small in practice (Huang, 2004). Therefore, the contact area which will be used in axisymmetric FE models can be described as having a radius (r_L) as follows:

$$r_L = \sqrt{\frac{A_c}{\pi}} = \sqrt{\frac{L_v}{P_t \pi}} \quad 2-9$$

2.6 Falling Weight Deflectometer Test

Basically, there are two kinds of method to measure pavement properties, such as pavement stiffness. The first is conducted in the laboratory using either laboratory specimens or undisturbed samples retrieved from a pavement. The second is by means of non-destructive testing. The measurements of non-destructive testing are conducted on a pavement. This form of testing can avoid damage to the pavement structure and better evaluate load conditions than laboratory testing.

The Falling Weight Deflectometer (FWD) is a device used to evaluate the mechanical properties of a pavement, as shown in Figure 2-22. The testing conducted using a FWD device is non-destructive and consists of the application of a load pulse of similar magnitude and duration to that induced by a vehicle moving at normal traffic speed.



Figure 2-22 FWD equipment in use (FPMS, 2008)

Figure 2-23 shows the FWD concept and a section of pavement. A pulse is generated by the weight falling onto a buffer system which is mounted on a circular plate. The buffer system smoothes the load on the plate and generates a pulse. The height and weight can be adjusted to generate different amplitudes of pulse. Deflection sensors or geophones distributed radially from the centre of the loading plate collect deflection information against time. The load, deflections and the corresponding times can be used to plot load and deflection histories.

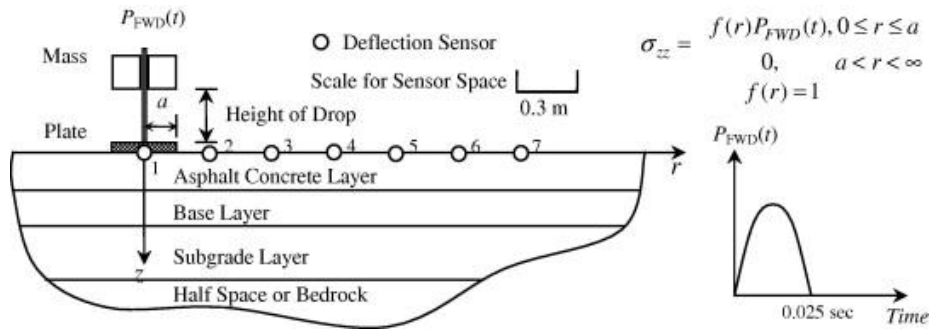


Figure 2-23 Layered pavement structure and FWD testing instrument (Kim & Kim, 2008)

Some typical parameters of the FWD are listed below:

- The radius of the loading plate (mm): 150;
- Offsets of geophones (cm): 0, 30, 60, 90, 120, 150 and 210;
- Load levels for flexible pavement (kN): 50, 75;
- Load levels for rigid pavement (kN): 75, 100.

Basically, the central deflection (D_1) at the centre of the plate indicates the overall stiffness. The outer deflection (D_6 or D_7) reflects the stiffness properties of subgrade. The difference between the centre and points next to the centre (e.g. D_1-D_4) is related to the stiffness of the upper layers. The term “deflection bowl” refers to the full shape of the deflection radial distance characteristics.

Figure 2-24 shows a deflection history collected from D_1 which is located at the centre of the loading plate. The maximum load is around 54kN at 25millisecond (ms). The maximum deflection is 81 microns at 29ms. Retardation by about 4ms can be found between the two peaks (maximum load and maximum deflection). The retardation is due to the inertial forces acting on the observation point and keeping it moving downward even after the load has reached a peak value.

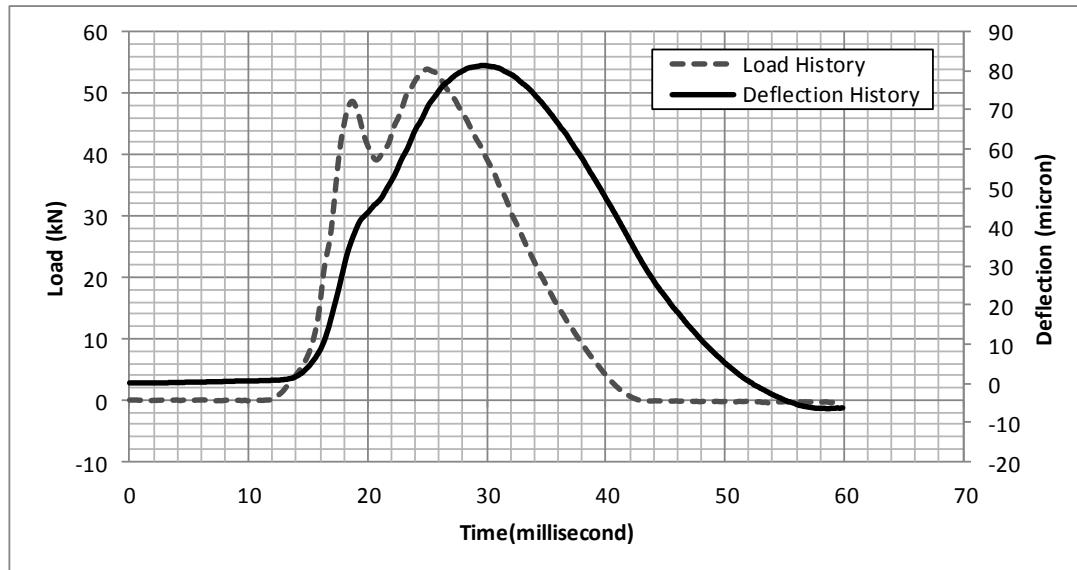


Figure 2-24 Load and deflection histories of FWD testing

The energy dissipation can be calculated by using the hysteresis curve (load vs. deflection) as shown in Figure 2-25. The result shows that the dissipated energy is 2.661J, which is equivalent to the enclosed area. The 4ms retardation caused by inertia results in a nonlinear relationship between the load and deflection. The absorbed energy, 2.661J, generated by the falling weight, is absorbed and transmitted into the subgrade.

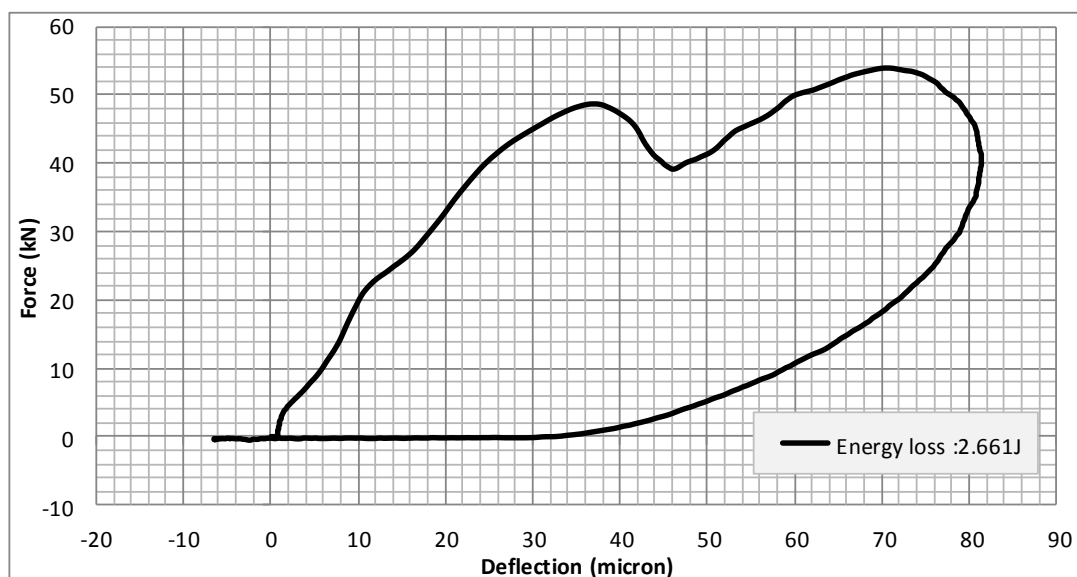


Figure 2-25 Energy dissipation of FWD testing

2.7 Case Study

Until recently many researchers have shown interest in the relationship between fuel consumption and pavement stiffness. A number of laboratory experiments and field observations have been conducted to investigate quantifiable and meaningful influences of pavement stiffness on vehicle fuel consumption. Literature related to the observations and experiments provide a large amount of background information to this research.

2.7.1 TRL Laboratory testing

In order to determine the advantage of stiffer pavement on fuel consumption, 2 pavement sections have been constructed and tested by TRL. In the research carried out by TRL and others, it is worth noting that, not all factors can be controlled in road network measurement. Therefore, a laboratory test which provides a more stable and repeatable environment was carried out using TRL's Pavement Test Facility (PTF) (Benbow, Iaquinta, Lodge, & Wright, 2007).

TRL's Pavement Test Facility is a laboratory facility which allows measurement of the rolling resistance between a single tyre and a pavement, as shown in Figure 2-26. It consists of a carriage and a gantry. The carriage is suspended from a pair of rails which is mounted on the gantry. A tyre is mounted in the carriage above the pavement surface. The carriage, which is attached to a motor via cables, drives the tyre in both directions on the test strip. The tyre can be accelerated to 20km/h over the first 1.5m of the total 10m journey and maintains this velocity over the next 7m before decelerating in the final 1.5m. A ram is mounted in the carriage, so that the vertical load on the tyre can be up to 8000kg.

Sensors have been mounted in different parts of the facility. The loads, accelerations and temperatures can be measured by these sensors and transported to a computer for data analysis.



Figure 2-26 TRL's Pavement Test Facility (Benbow, Iaquinta, Lodge, & Wright, 2007)

Two pavements were constructed in the PTF test bed; a flexible construction and a rigid construction. Table 2-5 shows the construction of the flexible pavement section which has a 30mm thin surface course, a 60mm Dense Bitumen Macadam (DBM) 125 (long term elastic stiffness of 2500MPa), a 120mm DBM125 base, a 260mm subbase and a subgrade which has a 4% California Bearing Ratio (CBR). Table 2-6 shows the rigid pavement construction which has 30mm thin surface course, a 230mm Continuously Reinforced Concrete Pavement (CRCP) base (6.0MPa flexural strength), a 260mm subbase and the same subgrade as used for the flexible pavement.

Table 2-5 Flexible pavement construction (Benbow, Iaquinta, Lodge, & Wright, 2007)

ID	Layer	Thickness (mm)	Material
1	Thin surface Course	30	Asphalt concrete
2	Binder Course	60	DBM125
3	Base	120	DBM125
4	Subbase	260	Soil
5	Subgrade	-	Soil

Table 2-6 Rigid pavement construction (Benbow, Iaquinta, Lodge, & Wright, 2007)

ID	Layer	Thickness (mm)	Material
1	Thin surface Course	30	Asphalt concrete
2	Base	230	CRCP
3	Subbase	260	Soil
4	Subgrade	-	Soil

The texture of the pavements was measured using a circular texture meter. The sensor measured texture depth (SMTD) of the rigid pavement was 1.10mm and the flexible pavement was 1.25mm.

The stiffness of both pavements was measured using a Falling Weight Deflectometer (FWD); two load levels were used, 50kN and 75kN. The deflection of the rigid pavement at 50kN was 245microns and at 75kN was 390microns. The deflection of the flexible pavement at 50kN was 273microns and at 75kN was 438microns.

A long trial has been carried out in the PTF, using a tyre pressure of 827kPa, speed of 15km/h and vertical load of 25kN. Figure 2-27 shows the relationship between RRC and tyre temperature. As can be seen, a linear relationship was found during the trials. For rigid pavement, the slope of the line is 0.00017 per °C. For flexible pavement, the slope of the line is 0.00019 per °C.

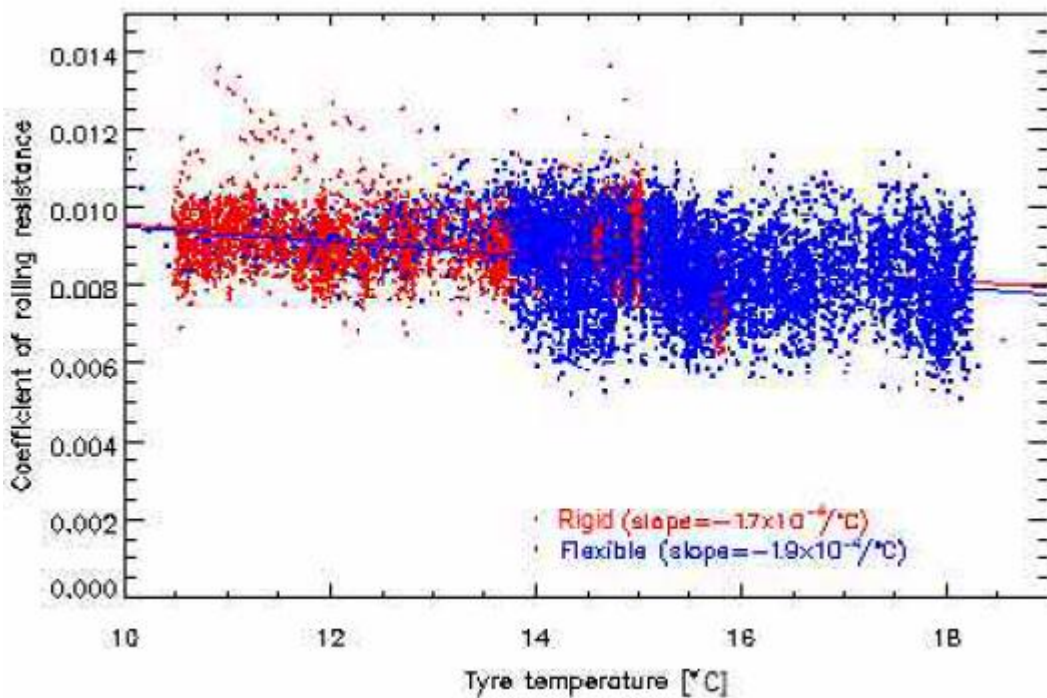


Figure 2-27 Relationship between rolling resistance and tyre temperature

The RRCs were also collected during conditions of common temperature, with the tyre at 11°C, the pavement at 10.0 to 11.3°C and an ambient temperature of 7.1 to 7.4°C. On this basis, a load of $29.0 \pm 0.1\text{kN}$ was applied to the rigid pavement, and $29.3 \pm 0.1\text{kN}$ applied to the flexible pavement. The average RRC for the rigid pavement was 0.008326 and for the flexible pavement was 0.008822. These RRC results were adjusted for the effects of texture.

The results from the PTF long trials show a linear relationship between RRC and temperature. Descomet (1990) also found a similar relationship and this can be confirmed by Figure 2-28.

The results also show that the difference of RRC between the two pavements is 0.0005. Considering the vertical load to the pavements, the rolling resistance for the rigid pavement is 0.24kN and for the flexible pavement is 0.26kN, i.e. the difference is 0.02kN. Thus, in terms of rolling

resistance, the rigid pavement has an 8% advantage over the flexible pavement.

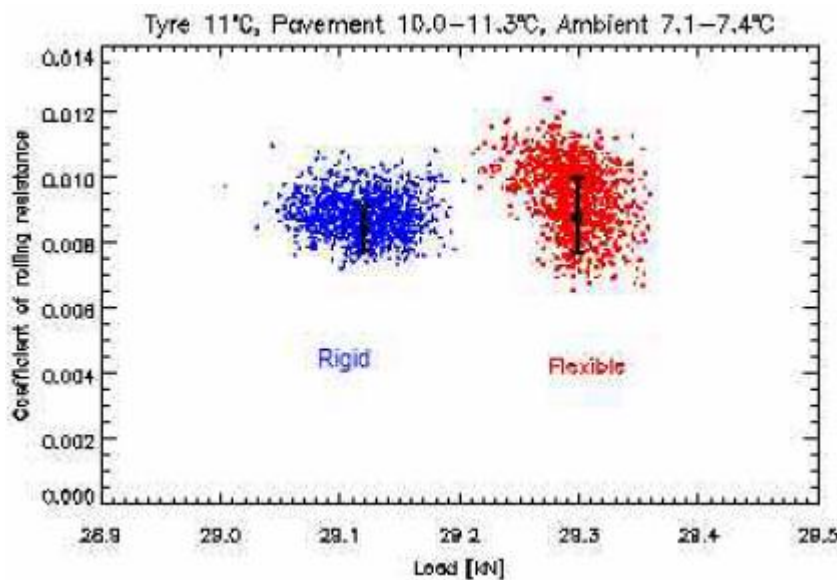


Figure 2-28 Coefficient of rolling resistance for flexible and rigid pavements

2.7.2 Truck fuel consumption measurements in Canada

In order to quantify potential fuel consumption differences, a set of systematic tests using a highway tractor pulling a loaded van semi-trailer (Figure 2-29) were conducted between fall 2002 and fall 2003 by the Canadian National Research Council's (NRC) Centre for Surface Transportation Technology (CSTT) (Taylor & Patten, 2006).

A wide range of test conditions was covered during the research. The tractor trailer was tested in five ambient temperature ranges. Three kinds of load condition were also applied to the tractor trailer; 16000kg (empty), 43660kg (typical full load) and 49400kg (maximum legal load). A summary of test conditions can be found in Table 2-7.

The research was conducted on 10 pavement sections which include concrete, asphalt and composite. The factors of each pavement section

have been measured and observed. This includes pavement length, average IRI, gradient and curvature.



Figure 2-29 Side view of tractor trailer (Taylor & Patten, 2006)

FWD tests were conducted to identify the strength of the pavement sections. However the effect of road strength was not an important variable in the mathematical analysis as shown in the research. According to the report of the research, the reason is that the road beds have similar construction and quality.

Table 2-7 Summary of test sites and initial test conditions

Variable	Number of conditions	Locations or Test conditions
Pavement types	3	Concrete Asphalt Composite(Asphalt/Concrete)
Pavement Roughness	Variable	IRI<2 (m/km)
Vehicle Types	1	3 axle tractor with tridem van semi-trailer
Load	3	Empty – 16,000 kg Typical Full – 43,660 kg Maximum Legal – 49,400 kg
Speed	3	100, 80, 60 km/h
Seasons	5	Spring, Summer Night, Summer Day, Fall and Winter
Temperatures Ranges	4	Less than -10°C -5 to 10 °C 10 to 25 °C Greater than 25 °C
Ambient Wind	Variable	Less than 10km/h average
Grade	Variable	Less than 0.5%
Road conditions		Bare and dry

The main findings achieved from the research are follows:

Fuel consumption reductions were realised on most of the concrete pavements when compared to asphalt or composite pavements. Table 2-8 lists the details of results.

According to the fuel economy models derived from the results, pavement roughness, pavement grade, pavement temperature, vehicle mass, vehicle speed and air speed all have significant influence on fuel consumption.

Table 2-8 Summary of results

Speed (km/h)	Road A	Road B	Loading	Seasons	Road A Savings (L/100km)
100	Concrete	Asphalt	Full or Empty	5 seasons	0.4 to 0.7
100	Concrete	Asphalt	Full or Empty	Summer Night	0.25
100	Concrete	Composite	-	Except Summer Day and Spring	0.2 to 1.5
100	Composite	Concrete	-	Summer Day	0.5
100	Composite	Concrete	-	Spring	Insignificant
60	Concrete	Asphalt	Empty	Except summer Night	0.4 to 0.5
60	Concrete	Asphalt	Empty	Summer Nigh	0.1
60	Concrete	Asphalt	Full	Except summer Night	0.2 to 0.4
60	Concrete	Asphalt	Full	Summer Night	0.1
60	Concrete	Composite	Empty	Except Summer day	1.1 to 1.9
60	Composite	Concrete	Empty	Summer day	0.2
60	Concrete	Composite	Full	Except Summer day	0.6 to 1.4
60	Composite	Concrete	Full	Summer day	0.2

2.7.3 Van fuel consumption measurements in US

In order to identify any differences in fuel consumption and CO₂ emission when driving a vehicle on an asphalt concrete pavement (flexible pavement) versus a Portland cement concrete pavement (rigid pavement) under city driving conditions, research was conducted by the University of Texas at Arlington in USA (Ardekani & Sumitsawan, 2010).

The factors influencing vehicle fuel consumption have been controlled in the measurements included:

- Weigh of vehicle
- Tyre pressure
- Fuel type
- Ambient temperature
- Humidity
- Wind speed and direction

Two driving modes were used in the research; cruise and acceleration. The cruise mode consisted of the vehicle driving at 30mph throughout every test run. In acceleration mode, the vehicle was accelerated from 0 to 30mph in 10 seconds, which means the average acceleration rate equals 3mph/second.

Two test sites were selected for the research; each of them had two pavement sections. In order to investigate the roughness characteristics of the pavements, average values of International Roughness Index (IRI) were measured. Furthermore, the average values of longitudinal gradient of the pavement were measured as well. The details of road section characteristics can be found in Table 2-9.

Table 2-9 Road section characteristics (Ardekani & Sumitsawan, 2010)

Test Sites	Pavement	Type	Structure	Average IRI (mm/m)	Longitudinal Slope in Data Collection Direction (%)
First	Rigid	CRCP	203mm CRCP, 51mm HMA type D on 203mm lime stabilized subgrade	2.8	+1.2
	Flexible	HMA	178mm HMA (38mm Type D, 140mm Type B) on 152mm lime stabilized subgrade	2.9	+1.2
Second	Rigid	JPCP	178mm JRCP on 152mm lime stabilized subgrade 6m transverse joint spacing	5.1	+0.4
	Flexible	HMA	203mm HMA (51mm Type D, 152mm Type A) on 152mm lime stabilized subgrade	4.4	+0.6

The vehicle used for the research was an instrumented model 2000 Chevy Astro van, as shown in Figure 2-30. The fuel sensor, temperature sensors and data acquisition system were mounted in the vehicle.

A typical record included following items:

- Date of observation
- Time of observation
- Ambient air temperature
- Atmospheric pressure
- Relative humidity
- Wind speed and direction
- Temperature of fuel flowing into and out of the tank
- Vehicle weight
- Tyre pressure

- Status of auxiliary devices (A/C, radio, headlights, windows, wipers, etc.)



Figure 2-30 Instrumented 2000 Chevy Astro Van (Ardekani & Sumitsawan, 2010)

The results of the research can be found in Table 2-10. It was found that the fuel economy (distance travelled per unit fuel consumed) was lower on the flexible pavement sections. The results indicate that depending on the driving mode and pavement surface condition rigid pavements save fuel by 3% to 17%.

Table 2-10 Fuel economy of vehicle (Ardekani & Sumitsawan, 2010)

Road	Speed Mode	Surface Condition	
		Dry	Wet
		Average Fuel Economy (kilometres per litre)	Average Fuel Economy (kilometres per litre)
Rigid Pavement 1	Cruise mode	10.0	9.3
Flexible Pavement 1	Cruise mode	8.3	7.7
Rigid Pavement 1	Acceleration mode	1.8	1.9
Flexible Pavement 1	Acceleration mode	1.6	1.6
Rigid Pavement 2	Cruise mode	9.3	7.9
Flexible Pavement 2	Cruise mode	8.6	7.6
Rigid Pavement 2	Acceleration mode	1.8	1.6
Flexible Pavement 2	Acceleration mode	1.7	1.6

2.8 Embedded Energy

Embedded energy and carbon life cycle analysis are acknowledged as being of paramount interest in ensuring that engineering construction is as environmentally friendly as possible. In the case of a highway the bulk usage of materials is considerable, resulting in high costs, high embedded energy – particularly where bitumen or cement is involved – and consequently large carbon footprints. This is well understood and there is pressure from governments across the world to reach increased levels of sustainability in terms of material usage.

Embedded energy is not easy to estimate with confidence over the full life cycle of a highway, including demand for materials during maintenance and rehabilitation and the potential for re-use of existing materials either on site or elsewhere. The requirements of life cycle analysis are well

established (BSI, 2006a, 2006b, 2008) but there are few studies of pavement construction that meet them (e.g. Stripple, 2001; Huang et al, 2009; Waymen et al, 2009). Estimates will be sensitive to assumptions, notably the extent of future maintenance, which is hard to justify for the excellent reason that this is something which varies greatly from site to site. Concrete roads can last for 40 years or more when they are properly constructed, with no need for any replacement materials other than very minor repairs, while asphalt surfaces on major highways typically need replacement every 10-15 years, but the problem is that this level of performance for concrete is far from guaranteed and the consequences of underperformance can be very expensive, both in direct monetary terms and in associated energy and carbon.

2.9 Finite element analysis and ABAQUS

The ABAQUS theory manual (ABAQUS Theory Manual, 2001) shows that the ABAQUS FE system includes:

- ABAQUS/Standard, a general-purpose FE programme
- ABAQUS/Explicit, an explicit dynamics finite element program
- ABAQUS/CAE, an interactive environment used to create finite element models, submit ABAQUS analyses, monitor and diagnose jobs, and evaluate results
- ABAQUS/Viewer, a subset of ABAQUS/CAE that contains only the postprocessing capabilities of the Visualization module

Three of these are used in this study: ABAQUS/Standard, ABAQUS/CAE and ABAQUS/Viewer.

In order to control the load distribution and dynamic simulation, ABAQUS scripting has been used for the research. It is an extension of Python object-oriented programming language. Therefore Python scripts are used in the ABAQUS scripting interface to do the following:

- Create and modify FE models which include dimensions, materials, meshing and so on.
- Create and modify calculation steps, loads and boundary conditions.
- Retrieve and calculate results from ABAQUS output database.

2.9.1 Elements

An extensive element library has been provided by ABAQUS which includes (ABAQUS Theory Manual, 2001):

- continuum elements, such as solid elements and infinite elements;
- structural elements, such as membrane elements, truss elements;
- beam elements, frame elements and elbow elements;
- rigid elements, such as point masses;
- connector elements, such as springs and dashpots;
- special-purpose elements, such as cohesive elements and hydrostatic fluid elements;
- contact elements, such as gap contact elements, tube-to-tube contact elements.

The types of elements used for this research are listed as follows:

- Continuum elements, which are used to model the pavement and subgrade

- Special-purpose elements (spring elements and dashpot elements), which are used to model the boundary condition

Continuum elements

Continuum elements can be classified into first-order (linear) elements and second-order (quadratic) elements. Models built by first-order elements require less calculation time than second-order elements. Second-order elements provide a higher accuracy solution in ABAQUS/standard than first-order elements. Results carried out from the model using second-order elements show a “smoother” distribution than first-order elements, because more nodes are built into a single element.

ABAQUS uses Gaussian quadrature for most elements and evaluates the material response at each integration point in each element. Some elements in ABAQUS can use full or reduced integration. Reduced integration reduces calculation time, especially in 3D simulations. Generally, second-order reduced-integration elements give more accurate solutions than corresponding fully integrated methods (ABAQUS Theory Manual, 2001).

Spring elements

Spring elements are used to model actual physical springs and represent structural dampers by special purpose. According to the element type, there are 3 sorts of springs; SPRING1, SPRING2 AND SPRINGA. SPRING1 can be used to connect a node and the ground, acting in a fixed direction. SPRING2 can be used to connect two nodes, acting in a fixed direction.

SPRINGA can be used to specify a spring element between two nodes with its line of action being the line joining the two nodes.

Dashpot elements

Dashpots are used to model relative velocity-dependent force or torsional resistance. Energy can be absorbed by dashpots elements. DASHPOT1 and DASHPOT2 elements are available in ABAQUS/Standard. DASHPOT1 can be used to connect a node and the ground in a specified degree of freedom. DASHPOT2 can be used to specify a dashpot element between two degrees of freedom.

Infinite elements

The infinite element can be described as an element with a special shape function for the side of an infinite boundary. Figure 2-31 shows a one-dimensional example of the infinite element. The reference coordinate system is r . Based on node 1 at the interface between the finite and infinite elements, the distance $r_1 = a$ from the pole and the distance between node 1 and 2 is a , so, $r_2 = 2a$. Node 3 is located at an infinite side. These nodes can be mapped in a new system (s) using a mapping function, Equation 2-10.

$$r = -\frac{2s}{1-s}r_1 + \frac{1+s}{1-s}r_2 \quad 2-10$$

So that

$$r = \frac{2a}{1-s}$$

This yields an infinite distance when $s=1$.

$$r = \lim_{s \rightarrow 1} \frac{2a}{1-s} = \infty \quad \text{2-11}$$

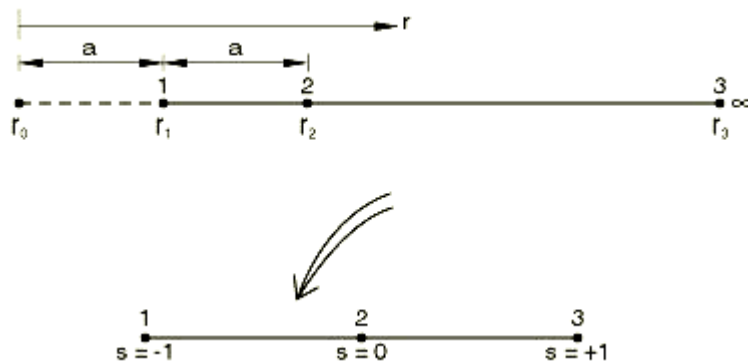


Figure 2-31 Pole node location for an infinite element
 (ABAQUS Theory Manual, 2001)

2.9.2 Material Damping

For FE analysis, the damping is not only a parameter but a matrix. Normally, there are four variables that can be used to build the damping matrix in ABAQUS: alpha, beta, composite and structural damping. Alpha damping is a factor to create a mass proportional damping; the unit is 1/second. Beta is a factor to create a stiffness-proportional damping; the unit is second. The composite factor is a value to create a fraction of critical damping. Structural damping factor is a value to create imaginary stiffness-proportional damping. Alpha and beta were used for this analysis because they are independent of the frequency issues.

Material damping can be defined for dynamic analysis in ABAQUS/Standard. Two sorts of material damping have been used; mass

proportional damping and stiffness proportional damping. Mass proportional damping (alpha damping) generates damping forces caused by the velocities of the model. The factor α_R defining mass proportional damping gives a damping contribution proportional to the mass matrix for an element. The factor β_R is used to define stiffness proportional damping. β_R defines damping proportional to the elastic material stiffness. According to the β_R , ABAQUS creates a damping stress (σ_d) proportional to the total strain rate:

$$\sigma_d = \beta_R D^{el} \dot{\varepsilon}$$

where: σ_d is damping stress,

D^{el} is elastic stiffness,

$\dot{\varepsilon}$ is the strain rate.

By way of illustration, Figure 2-32 shows the deflection histories retrieved from the axisymmetric model, which will be fully described in Chapter 3, with different alpha damping factors. It is worth noting that each case has the same properties except for the damping value. VDB has been applied in these models. The sinusoidal loading pulse acts on the models between 0.01 and 0.05s. Four damping values have been used: 0, 10, 100, and 1000. It can readily be seen that the curves with alpha equal to 0 and 10 are quite similar. This means that alpha damping has a very limited influence on energy absorption when the damping value is relatively small. Therefore, a test using alpha=10⁴ has been applied. An obvious change of amplitude can be seen at this stage. The maximum deflection reduces to approximately half, from 50 microns (when alpha=0) to 28 microns (when

$\alpha=10\ 000$). The deflection rebounds more slowly than previous cases after the loading period. The last case, $\alpha=100$, shows that most of the oscillations are damped quickly. The maximum deflection is 48 microns; only a 4% reduction compared to the case where α is 0.

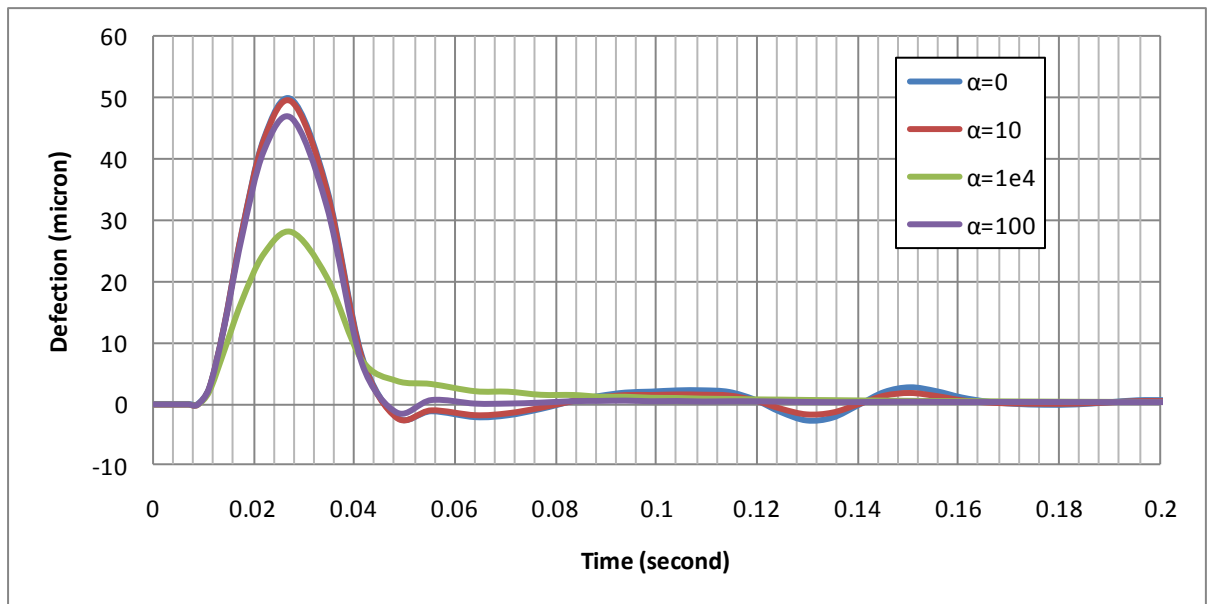


Figure 2-32 Influence of the alpha damping on deflection

Figure 2-33 shows similar cases when beta damping is applied; $\beta=0$, 0.001, 0.01 and 0.005. The similarity compared to the alpha damping cases is that deflection is reduced as beta damping increases. However, phase lags can be found in all cases with beta damping.

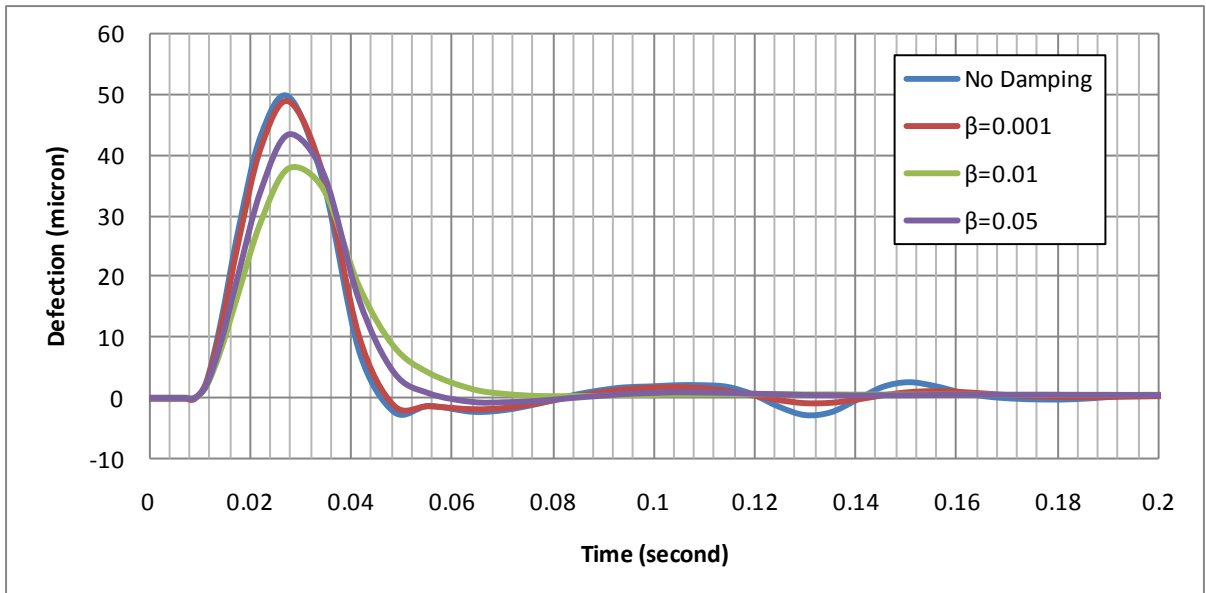


Figure 2-33 Influence of the beta damping on deflection

Results retrieved from the models indicate that most of the oscillations can be damped by using alpha or beta damping. Due to the influence of beta damping on phase lag, only alpha damping has been used in the rest of the analysis. The damping value is not a constant number for different pavement constructions. It has to be verified for each set of stiffness properties used in the model.

2.9.3 Step and increment

The term step or analysis step is used to describe a specific procedure of a simulation that defines the type of analysis to be performed during the step. The increment is used to divide the total time period of an analysis step. Depending on the time incrementation type, increment can be defined by fixed time incrementation or calculated by ABAQUS automatically.

In order to control the accuracy of time dependable simulation, factors of time incrementation have to be controlled. The maximum number of

increments is used to limit the number of total increments in an analysis step. The initial increment size is used to define the time of first increment in a step. The minimum increment size is used to limit the smallest value of each increment when ABAQUS generates increments automatically. The maximum increment size is used to define the maximum value of each increment when ABAQUS generates increments automatically.

2.9.4 Half-step residual tolerance

The parameter to be considered for step setting is the half-step residual tolerance ($R_{t+\Delta t/2}$). "The half-step residual tolerance has dimensions of force and is usually chosen by comparison with typical actual force values, P , such as applied forces or expected reaction forces." (ABAQUS Theory Manual, 2001). The relationship between the half-step residual tolerance and load (P) can be found as follows:

- If $R_{t+\Delta t/2} \approx 0.1P$, the solution will generally be highly accurate for elastic cases with little damping. In problems where considerable plasticity or other dissipation is expected to damp out the high frequency response, a tolerance this restrictive is not necessary.
- If $R_{t+\Delta t/2} \approx P$, the solution is moderately accurate for elastic cases with little damping and highly accurate for problems including plasticity or other damping mechanisms.
- If $R_{t+\Delta t/2} \approx 10P$, the solution is coarse for elastic problems with little damping but still quite good for problems with dissipative effects.
- Even values of $R_{t+\Delta t/2} \approx 100P$ will give useful results for primary effects such as overall deformation.

2.9.5 Boundary Condition

Lysmer & Kuhlemeyer (1969) stated that, the boundary conditions of infinite media could be expressed as follows:

$$\sigma_{zz} = a\rho V_p \dot{u}_z$$

$$\tau_{zx} = b\rho V_s \dot{u}_x$$

$$\tau_{yz} = b\rho V_s \dot{u}_y$$

where: σ_{zz} is the normal stress,

τ_{zx} and τ_{yz} are the shear stresses,

a and b are dimensionless parameters,

$\dot{u}_x, \dot{u}_y, \dot{u}_z$ represent the velocities in the x,y,z-direction,

V_p, V_s are the velocities of primary and secondary waves.

Figure 2-34 shows the concept of the energy wave and the Viscous Damping Boundary (VDB) element. An incident wave consisting of primary wave and secondary wave acts on the boundary and has an angle θ from the z-axis. Lysmer & Kuhlemeyer (1969) also indicated that if θ is smaller than 30 degrees, a and b are equivalent to 1.

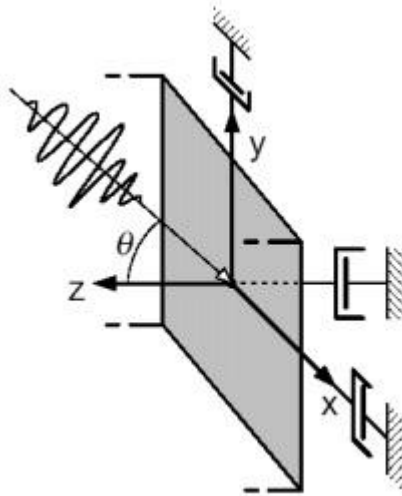


Figure 2-34 VDB and energy wave (Ross, 2004)

The velocity of the primary wave can be calculated using Equation 2-12.

$$V_p = \sqrt{\frac{(1-\nu)E}{(1-2\nu)(1+\nu)\rho}} \quad 2-12$$

where: E is the Young's modulus,

ν is the Poisson's ratio.

The velocity of the secondary wave can be calculated using Equation 2-13.

$$V_s = \sqrt{\frac{E}{2(1+\nu)\rho}} \quad 2-13$$

Thus, the damping coefficient, normal to the boundary surface, can be calculated by using Equation 2-14.

$$c_p = \int_{\Gamma} a\rho V_p d\Gamma \quad 2-14$$

where: Γ is the surface area of the boundary element,

c_p is the damping coefficient of the boundary, normal to the boundary surface.

The damping matrix, in x and y directions, can be calculated by using Equation 2-15.

$$c_s = \int_{\Gamma} b\rho V_s d\Gamma \quad 2-15$$

where: c_s is the damping coefficient of the boundary, parallel to the boundary surface.

A dashpot can be defined by using special-purpose elements named as engineering features in ABAQUS/CAE, which is mentioned in Chapter 2.9.1. Therefore, engineering features have been applied to the boundary nodes, i.e. every node is connected to two dashpots. Figure 2-35 shows the connection between the boundary node and dashpots. Dashpot A normal to the boundary surface is used to absorb the primary wave. Dashpot B parallel to the boundary surface is used to absorb the secondary wave.

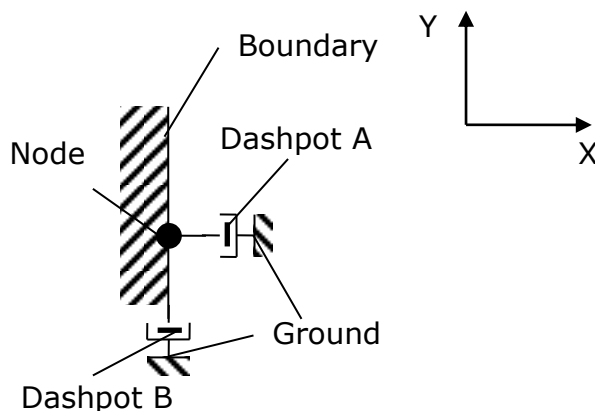


Figure 2-35 VDB dashpots in the axisymmetric model

It is worth introducing two additional boundary conditions which are widely used in FE analysis; conventional and rigid boundary. A conventional boundary is shown in Figure 2-36. Every node at the boundary is horizontally restricted. The definition of a rigid boundary is that nodes at the boundary are fixed in every direction.

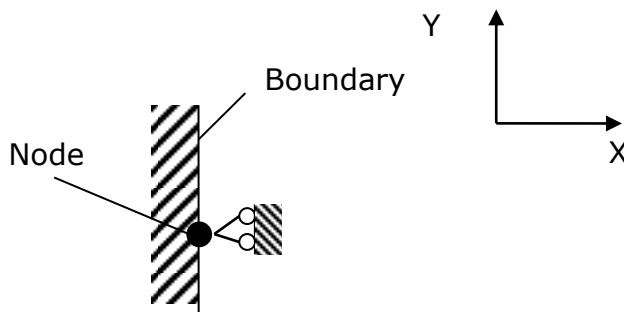


Figure 2-36 Conventional Boundary

To examine the influence of VDB on deflection, 3 types of boundary conditions (VDB, rigid, and conventional) were implemented. It is worth noting that material damping has not been applied in these tests. Figure 2-37 shows the deflection histories of the node at the centre of the contact area. The input load is a sinusoidal pulse which lasts 0.05s. It may be seen that curves of the deflection of the three different types of boundary condition in the first 0.05s are exactly the same. The explanation for this phenomenon is that the loads and stiffness properties are exactly the same. Oscillations can be found in all cases after the loading period. However, models with rigid and conventional boundaries have more oscillations. Despite oscillations being damped in all cases by the numerical damping control parameter (default setting of ABAQUS) the case with VDB shows that oscillations had disappeared within 0.2s. This 0.2s duration is much shorter than for other cases. This issue shows that

the VDB has absorbed most of the energy wave propagated at the boundary. It also shows that the energy wave cannot be absorbed completely in a short period. In order to reduce the oscillations, material damping has also been used in the subgrade, regarding the hysteresis of all soils.

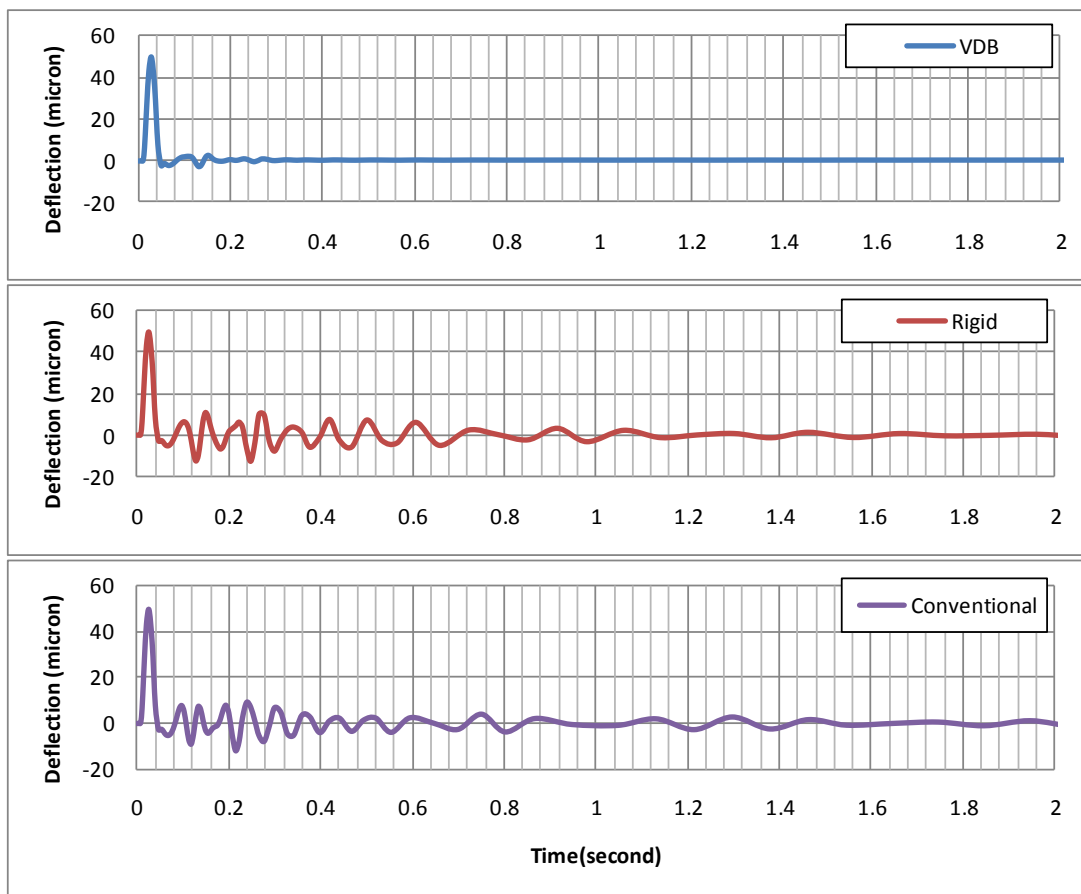


Figure 2-37 VDB vs. Rigid Boundary vs. Conventional Boundary

2.10 Summary

Depending on the type of vehicle, the values of fuel consumption caused by the engine are different. But, results consistently show that the engine is the major factor affecting vehicle fuel consumption.

A lot of factors affect vehicle fuel usage. Generally, these factors come from vehicle, pavement, environment and driver. Different combinations of factors result in varied fuel usage. Therefore, the major factors influencing fuel consumption have been studied.

The laboratory measurements of TRL showed that the difference of rolling resistance between the rigid pavement and flexible pavement was 0.02kN per wheel, while the FWD results, tested under a 50kN load level, were 245 microns for the rigid pavement and 273 microns for the flexible pavement. The result rolling resistance can be converted to a form of energy dissipation, which is about 2MJ/100km per wheel. However, the effects related to pavement texture on the results were not identified clearly.

The measurements conducted in Canada show that the rigid (concrete) pavement saves more fuel than flexible (asphalt) pavement. The fuel savings were affected by season, speed and loading condition.

A similar conclusion can be made using the results carried out by the measurements in US, which is vehicle consumes less fuel when it is driven on a rigid pavement comparing to a flexible pavement. But, all of the results from the measurements have not clearly identify the influence of pavement stiffness on fuel consumption clearly qualify.

Chapter 3

Preliminary Study

In order to build a computationally efficient and accurate model using FEM, it is necessary to optimise the dimensions of the model and to retrieve accurate material properties. Therefore, based on the literature review, a systematic preliminary study has been conducted. The study includes the physical dimensions required for the finite element analysis, boundary conditions, material properties and solution control.

3.1 Principles of analysis

For FE analysis, in the first stage, it is necessary to design a basic process and recognise essential elements of the research, concerning components assumed in the FE model, the interaction between the model components and the required solution. In this case, it is permissible to assume that a single tyre under a vertical weight is rolling with a constant speed upon a section of straight pavement. The aim is to investigate the influence of pavement stiffness on energy dissipation. On the basis of this point, there are two objects that have to be built into a FE model; a tyre and a section of layered pavement.

In general, for a FE model, a rolling tyre can be built directly as a 3D object, imparting a moving load upon the pavement surface. However, it is not necessary to do so. Firstly, the dynamic simulation of a rolling object on a pavement calculated using FEM consumes significant computer resources; thus, it requires a powerful computer system. Furthermore,

even if a powerful computer system were used, it would also need a long time for the calculation due to the 3D issues. Furthermore, it also has to include a contact analysis under rolling, requiring even more time for calculation and complicated parameter adjustment, and it is not easy to avoid convergence errors at that stage.

Instead of the 3D-tyre object, a time-interval-moving load which is a combination of a series of pressures has been designed. Each pressure acts on the pavement during one time interval, which depends on tyre velocity. This method is more computationally efficient compared with the 3D object approach. It also represents the tyre/pavement interaction well. More details will be described in this chapter.

The International System of Units (SI) has been used to build the FE model in ABAQUS. The units used are listed as follows:

- Length: meter (m)
- Force: Newton (N)
- Mass: kilogram (kg)
- Time: second (s)
- Stress: Pascal (N/m²)
- Energy: Joule (Ns)
- Density: kg/m³

3.1.1 Dimensions and boundary conditions

To build a FE model, it is necessary to understand the parameters used in analysis which involves dimensions, material properties, and loads. Furthermore, understanding of the physical parameters is not enough; it is

also necessary to neglect less important factors, simplify complicated situations and make sensible assumptions.

Technically, it is not necessary to build a FE model to simulate a whole pavement. First of all, the subgrade is considered as semi-infinite for numerical analysis, i.e. the thickness of the subgrade layer is assumed to be infinite. However, every FE model needs finite dimensions and the model is constrained within boundaries. Therefore, only a part of the pavement and subgrade can be built into a FE model. Secondly, the purpose of the project is to retrieve the energy dissipation in the pavement. A section of pavement with finite length can achieve this purpose, so long as an approximate steady energy dissipation per unit length can be determined.

A key issue here is that any boundaries of the model must allow the energy waves which are generated by the rolling tyre to pass through and not reflect. On account of this issue, a conventional approach is that the FE model can be built with sufficiently large dimensions such that there is therefore enough space for the wave propagation without reflection. This approach is computationally inefficient and difficult to satisfy in this research.

To illustrate the difficulty, if it is assumed that:

- the speed of the energy wave is 300m/s,
- the speed of the rolling tyre is 130km/h (36m/s),
- the journey of the tyre is 10m.

Then, a 10m journey of the tyre requires 278ms. To avoid the effect of reflected waves, the shortest distance between the tyre/pavement contact area and the boundary is 42m, which represents the journey of wave with 300m/s propagation in 277ms. If the FE model of this case has a 10m length and a ¼ circular profile with a radius of 42m, then, the volume is 13854m^3 . Table 3-1 shows 4 assumptions of average element volume and corresponding number of elements. Since the maximum number of elements in a FE model that can be calculated using current equipment is 10^6 , the average volume of an element has to be smaller than 0.01m^3 . However, for a FE simulation with a rolling load, the average volume of an element would have to be bigger than 0.01m^3 . It is worth noting that the real speed of an energy wave in soil is usually higher than 300m/s, which means that more elements have to be generated. Therefore, a FE model with large dimensions (far boundary) is not acceptable for this research.

Table 3-1 Average volume of an element and number of elements

Average volume (m^3)	Number of Elements
0.001	1.4×10^7
0.01	1.4×10^6
0.1	1.4×10^5
1	1.4×10^4

Basically, there are three methods that can be used to simulate infinite media using FEM in ABAQUS:

- far boundary,
- Viscous Damping Boundary (VDB),
- and infinite element.

The first one, far boundary, has just been mentioned in the example. The boundary is moved a great distance away from the finite structure until the influence of the boundary becomes negligible. The distance depends on the size of the model.

The VDB is a boundary condition in terms of FEM. The basic concept of VDB is to apply a set of viscous dampers on the outside of the boundary. This allows the radiating wave energy to be absorbed by the dampers (Jiang & Zhang, 2004; Lei & Wei, 2005).

The last one, infinite element, has already been introduced in Chapter 2.8. An infinite element has a special shape function for the side of an infinite boundary. The simulation of FE models with infinite elements is efficient.

Ross (2004) indicated that a model built with infinite elements only represents the situation of an object fully enclosed in an infinite medium, such as a submarine analysis. A trial using infinite elements in the boundary has been conducted (Appendix D) but results collected from the trial indicated that significant residual vertical deflections were predicted even after the load had been removed. It was therefore impossible to calculate a realistic energy dissipation, and VDB elements were therefore used to build the boundary.

With respect to the boundary condition, the physical model has been designed as shown in Figure 3-1. A layered pavement with length L is laid on a subgrade with radius R . The semi-circular shape of the profile is applied in this model with regard to the influence of the primary wave in the VDB. This design needs fewer elements in comparison to a conventional rectangular shape. The FE model used for the project is

asymmetrical about the pavement centre line and so only one half has been built to take advantage of computational efficiency. Details can be found in Section 3.2.

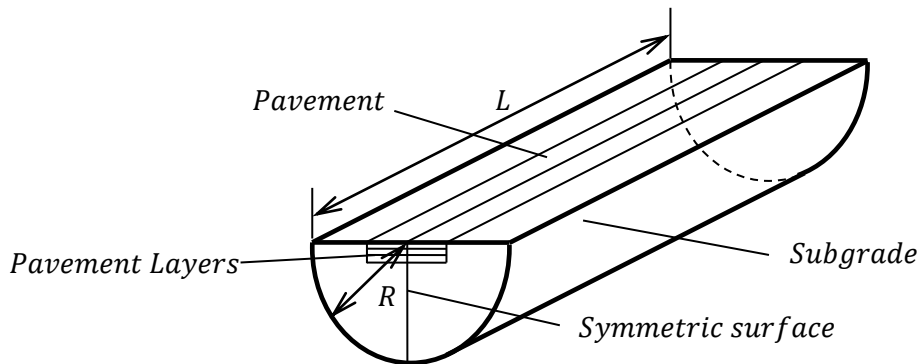


Figure 3-1 Solid model of the pavement

3.1.2 Material properties

Normally, material properties used in a FE model involve density, relationship between load and deformation, and damping. In most cases, there are two kinds of material constitutive laws that can be used to describe the mechanical behaviour of a pavement; linear elastic and nonlinear. Materials with linear elastic behaviour can be represented by just using Young's modulus and Poisson's ratio. PCC is a typical material which can be modelled to be linear elastic. Nonlinear materials are complicated and cover a wide range of behaviours, such as viscoelasticity. Researchers in pavement engineering often use viscoelasticity to model the mechanical properties of pavement materials. Bitumen bound materials are often modelled as viscoelastic.

Materials used in this project have been considered to be linear elastic. Only Young's modulus and Poisson's ratio have been used to describe the relationship between load and deformation. This is because the duration of

the load on the pavement is relatively short. For example, if the speed of the rolling tyre is 30km/h (8.33m/s), which is the slowest speed used in this project, and if the length of the tyre footprint is 397.3mm, the largest size used in this project, the duration of the load acting on a node that is located at the tyre/pavement contact zone is only 47.7 milliseconds. An asphalt should exhibit an approximately linear elastic behaviour during 47.7 milliseconds. The influence of creep (the deformation of a structure under sustained load) can be neglected as well, since every simulation just includes one wheel pass.

In addition to Young's modulus and Poisson's ratio, density and damping have been used. The governing equation (Equation 3-1) of dynamic analysis is as follows.

$$M\ddot{u} + C\dot{u} + Ku = f \quad 3-1$$

where: M is the mass,

C is the damping,

K is the stiffness,

f is the force,

u is the displacement,

\dot{u} is the velocity,

\ddot{u} is the acceleration.

Density is clearly involved since it governs inertia and wave energy. For this project, material damping is used as a convenient means of inducing hysteresis. Thus, soil (subgrade) is modelled with an amount of damping using damping coefficients in ABAQUS to absorb the oscillation and wave energy.

3.1.3 Tyre-pavement contact area

In order to efficiently control the dynamic load generated by a rolling tyre, a rectangular tyre/pavement contact area has been chosen for the research. The rectangular contact area allows the load to be distributed uniformly on the pavement surface, since the shape of the pavement mesh is rectangular. The method to calculate the rectangular tyre/pavement contact area has been given in Chapter 2.5.3.

3.1.4 Load levels

This project will consider a “typical” 40-tonne 5-axle HGV driving over a section of pavement. Three load levels will be used for the analysis, reflecting the typical range of loaded axle weights. The vertical loads considered are 40, 50 or 60kN.

Based on the Equations 2-7, 2-8 and the method shown in Figure 2-21, the corresponding dimensions of tyre/pavement contact area can be calculated using the three load levels, assuming the inflation pressure of tyre has been kept as a constant of 552kPa for each level, as shown in Table 3-2. The 1/2 width is used for each simulation since the model has a symmetrical structure.

Table 3-2 Load levels and dimensions of contact area

Load (kN)	Pressure (kPa)	Length (m)	Width(m)	1/2width(m)
40	552	0.3244	0.2234	0.1117
50	552	0.3627	0.2498	0.1249
60	552	0.3973	0.2736	0.1368

3.2 Physical models

According to the plan of the project mentioned in Chapter 1.3, two models have been built, an axisymmetric model and a 3D model. The data collected from FWD tests has been compared to simulations using the axisymmetric model. These simulations numerically represent the process of FWD testing and have been used to calibrate material properties including subgrade damping parameters. These properties have then been used in a 3D FE model. This section gives detailed dimensions of both the axisymmetric model and the 3D model. Rational selection of dimensions is introduced as well. The material properties used in the FE simulation will be given at the end of this section.

3.2.1 Dimensions

The model dimension not only influences consideration of the boundary but also the issues of meshing. A large model results in excessive elements and slows down the analysis. In contrast, a small model cannot completely absorb the energy wave and the solution therefore is inaccurate. The dimensions and method to build the boundary are varied with the volume of model. The detailed discussion will be given in Section 3.3. To reduce the number of elements in an FE model, achieving computational efficiency and an accurate solution, it is necessary to optimise the dimensions of the model.

Axisymmetric model

The physical model used to simulate the process of FWD testing is axisymmetric, since the load generated by an FWD concentrates on a fixed

location and the distribution is symmetrical. Figure 3-2 shows the geometry of the axisymmetric model. It is a combination of a multi layered pavement and surrounding ground which represents subgrade and surrounding soil. Since the model is axisymmetric a cylindrical coordinate system is used.

Two dimensions need to be selected for the axisymmetric model; the depth and the radius. A set of tests with different dimensions was applied to determine optimised dimensions. Confirmation tests show that a 10m depth and a 10m radius represent optimised dimensions for the model. The details of the confirmation test can be found in Appendix A.

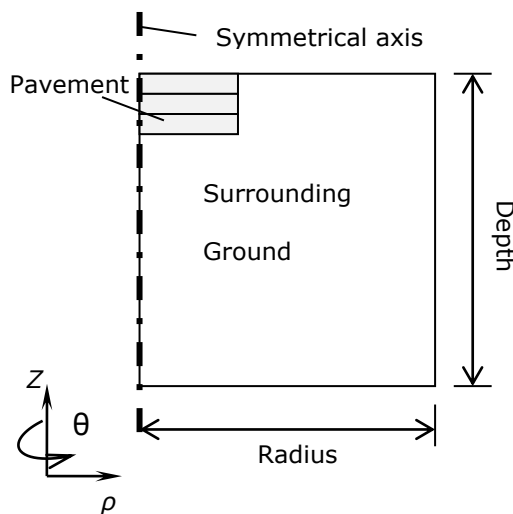


Figure 3-2 Dimensions of Axisymmetric model

3D Model

With respect to the energy calculation of a tyre rolling on a section pavement, the 3D model has been built as a combination of pavement layers and surrounding ground. Since the distribution of the load is symmetrical as well, the model has been built to be symmetrical. Figure 3-3 shows a 1/2 view of the 3D model consisting of a combination of a

layered pavement and surrounding ground with a radius of 10m. The length of the radius is based on consideration of the optimised dimensions, derived from confirmation tests of the axisymmetric model. Therefore, a 10m radius gives enough space for the model to absorb wave energy. In consideration of the influence of the boundaries and at each end the length of the contact zone, the length of the pavement has been designed to be 26m; a 6m pavement to take the load and two 10m-pavement sections to absorb wave energy. This length is also confirmed by tests which can be found in Appendix A. This dimension allows enough space to transport and damp the energy wave when loads are applied onto the contact zone. Thus, the minimum distance between the contact zone and the fan boundary is not less than 10 meters, a distance determined as suitable during design of the axisymmetric model. The width of the pavement has been designed to be 4m and 2m for the half model.

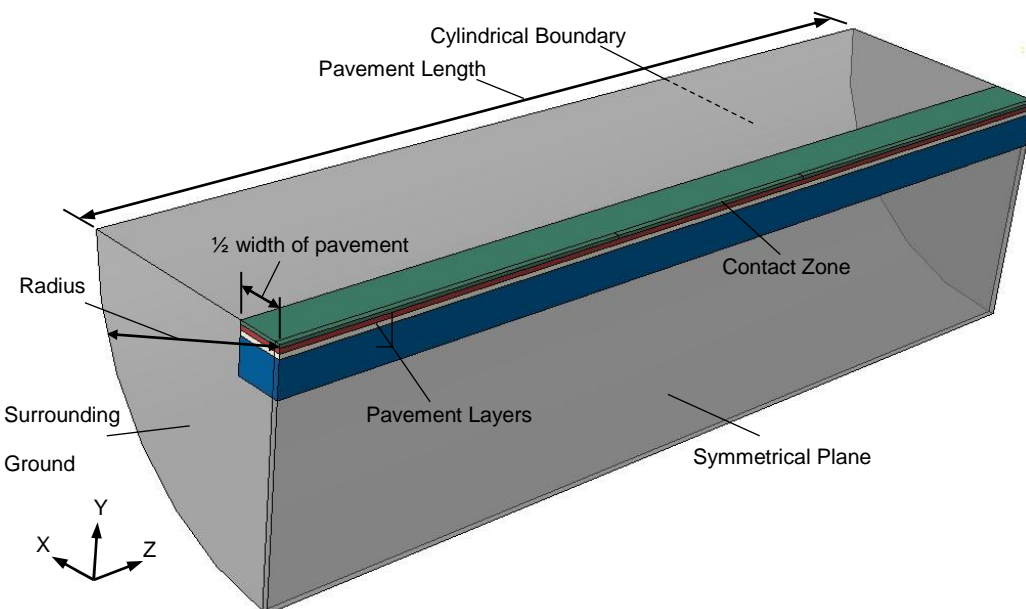


Figure 3-3 ½ view of the 3D model

3.2.2 Materials

Pavement layers are composed of materials which are considered to be linear elastic. Therefore, Young's modulus and Poisson's ratio are used to define the elastic characteristics. Typical values of Young's modulus and Poisson's ratio of pavement and soil materials are used. Density has also been used for every material due to the influence of dynamic effects. Material damping is only used in the subgrade to simulate the hysteresis inherent in soil behaviour. A set of confirmation tests has been conducted to predict damping values. Details will be given in Chapter 4.

The material properties of boundaries have to be determined as well. The details of boundary conditions and calculation of material properties has been given in Section 2.9.5.

3.3 Finite Element Models

The FE models used for the research have been designed and built using ABAQUS. Since the structure of the axisymmetric model is relatively simple, the model has been generated using ABAQUS CAE. In order to build a 3D model with varied layer thickness, material properties and calculation steps, Python script has been used. The mesh of the 3D model has been generated and tested in ABAQUS CAE to control the quality of the mesh. The VDB boundary elements for both the axisymmetric and 3D models have been generated by Python script, since a large number of VDB elements are involved. In order to retrieve the data from the results of ABAQUS calculations, Python script has also been used for data collection and the data have been saved as EXCEL files. This section will give the detailed approach used to design the FE models.

3.3.1 Axisymmetric model

Step

Since the load history from FWD testing is a pulse, an implicit dynamic load step approach has been used in the axisymmetric model. The type of incrementation is automatic. The time period of the step is 10s, which is longer than the pulse duration. Normally, the pulse duration is no more than 50ms. This ensures that enough results can be collected. The maximum increment size is 1/10 of the time period, 0.1s. The initial increment size is 1×10^{-7} s. The minimum increment size is 1/10 of the initial increment size. To retrieve highly accurate results, the half-step residual tolerance has been designed to be equivalent to 0.1P (P is the load).

Load

The load applied onto the axisymmetric model is in the form of a stress pulse, as shown in Figure 3-4 (a). The stress has been applied vertically to the centre of the model. The radius of the contact area equals the radius of the contact plate of the FWD. In terms of ABAQUS, a time dependent pressure can be built as a combination of 'Distribution', 'Magnitude', and 'Amplitude'. The 'Amplitude' of the load has been taken straight from the FWD load history. Figure 3-4 (b) shows a typical load pulse (load history) collected from a FWD test.

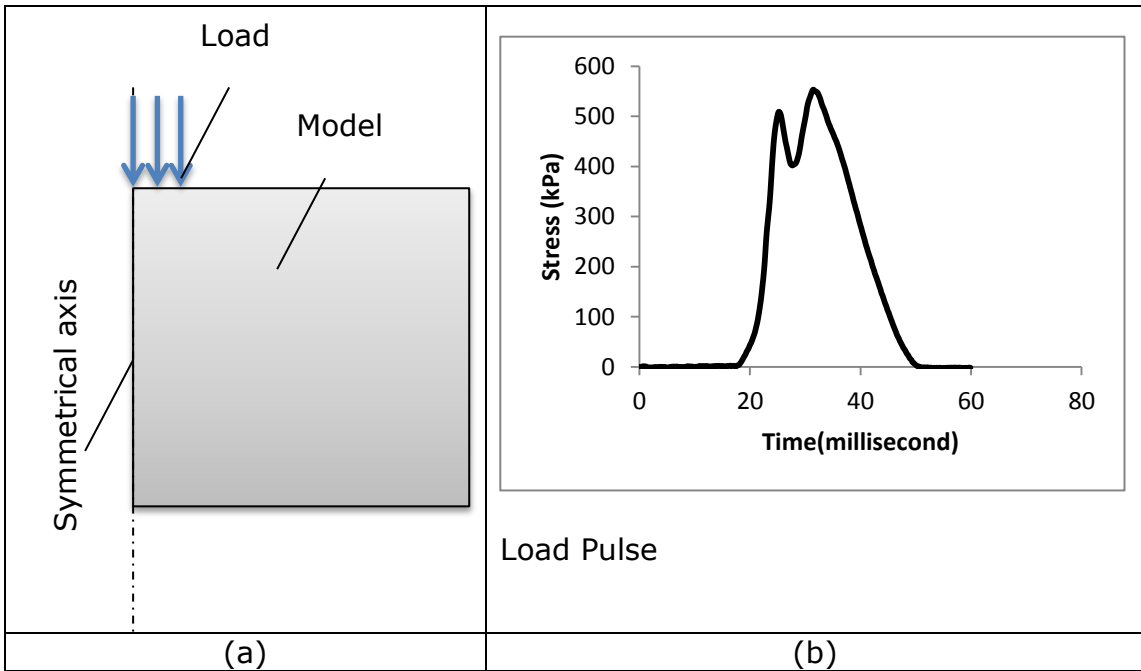


Figure 3-4 Load pulse of axisymmetric model

Mesh

Figure 3-5 shows the mesh of the model. To achieve an accurate solution, element size at the top of the pavement is smaller than at the boundary. This allows more detail to be found at/near the pavement. The element type used in this model is 8-node biquadratic axisymmetric quadrilateral; CAX8R. The quadratic element makes the solution more accurate.

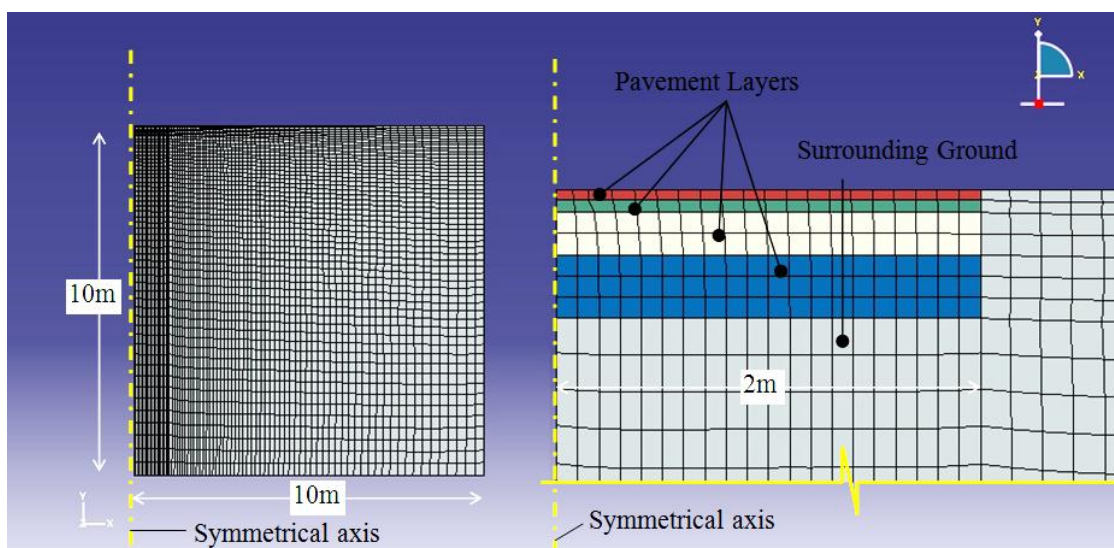


Figure 3-5 Mesh of the Axisymmetric model

Boundary conditions

VDB elements have been used as the boundary of the model. A detailed description of the VDB elements was presented in Section 2.9.5.

Material damping

VDB damping is an efficient method to absorb the energy waves propagated in FE models. However, oscillations can still be observed in the deflection histories output from analyses of axisymmetric models with VDB. Although the amplitudes of the oscillations are smaller than models without VDB, they can still be observed. So, this means that the influence of reflected energy waves still exists in the analysis, and this influence needs to be avoided.

At this stage, material damping is used to represent hysteresis. The results collected from simulations that used material damping show that the oscillation could be significantly reduced. However, till now, it is difficult to mathematically determine the material damping in linear FE analyses. Therefore, the material damping needs to be assigned by using computer modelling. The details of the determination of material damping will be given in Chapter 4.

3.3.2 3D model

Motion of tyre

Figure 3-6 shows the rolling tyre and the contact zone. L_T is the length of the tyre/road contact area. L_J is the distance of the journey. L_C is the total loaded length of the contact area. L_e is the length of a 20-node-brick element which is laid along the contact zone.

Each simulation includes two stages. The first stage is that, the tyre load is applied in the starting zone, the length of which is equivalent to the length of the tyre/pavement area. The duration of this step is 10s. This leads to a deflected state without oscillation. The second stage allows the tyre to travel on the contact zone through a journey with a length of L_J . The horizontal speed of the tyre is v_t .

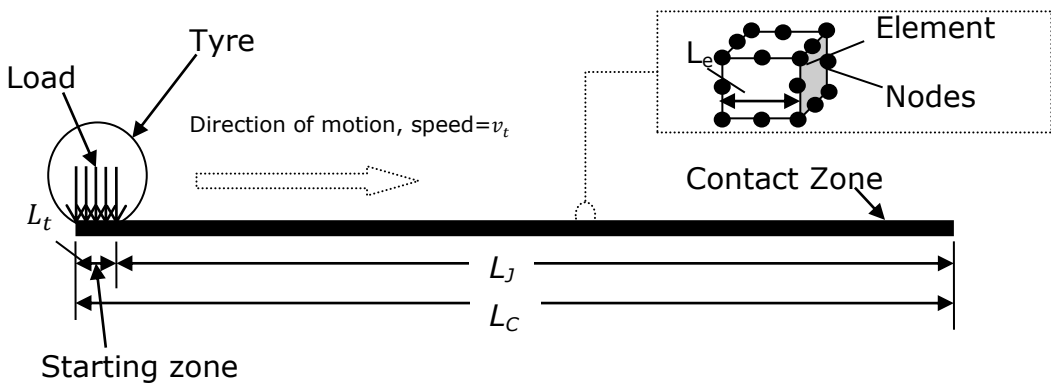


Figure 3-6 Stress on contact patch

Steps

In order to generate two stages in ABAQUS simulation, two analysis steps have been created. The first step is static to avoid the influence of oscillation and energy waves. This allows a vertical pressure to act upon the starting zone for 10s. Then an implicit dynamic analysis (second analysis step) is used. This is because the boundary dashpots (connected to the ground) cannot be used in explicit analysis. The total travel period (t_t) can be calculated as follows:

$$t_t = \frac{L_c - L_t}{v_t} = \frac{L_J}{v_t}$$

The incrementation of the second step is automatic. The maximum number of increments is 10^8 . This is an artificial number to allow enough increments in the analysis. The maximum increment size is equivalent to the initial increment size and can be calculated as follows:

$$t_{imax} = t_{ii} = \frac{L_e}{v_t}$$

where: t_{ii} is the initial increment size,

t_{imax} is the maximum increment size,

L_e is the length of element.

The minimum increment size is a fraction of the initial increment size and has been set as 10^{-7} seconds to reach a convergent solution.

Load

A Time-Interval-Moving Load (TIML) is applied onto the model. It is a combination of a series of vertical pressures. The pressures are distributed side by side along the contact zone. Each pressure has a duration which is equivalent to the maximum time increment, t_{imax} , i.e. the time taken by the tyre passing the length of an element located at the contact zone. Figure 3-7 shows two pressures located on a contact zone. According to the direction of tyre movement, Pressure A acts firstly. With time increasing, Pressure B acts on the contact zone subsequently.

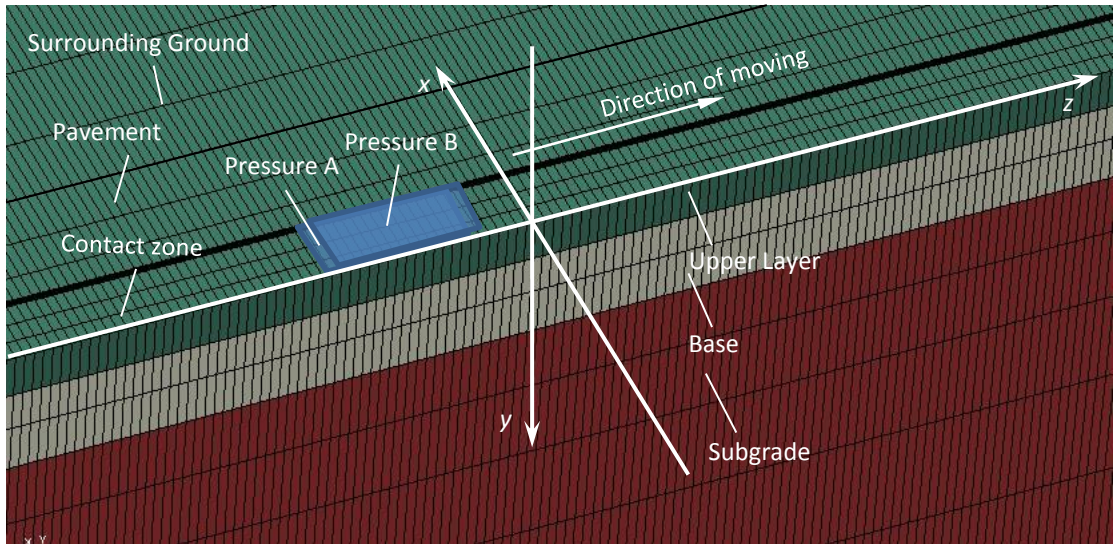


Figure 3-7 Pressures located on contact patch (local coordinates system)

Every pressure used in the TIML also consists of 3 parameters: Distribution, Magnitude and Amplitude. The Distribution is defined as an 'Analytical Field' function, Equation 3-2.

$$f(x, z, t) = P_t k \left(\frac{2(z - L_t - t v_t)}{L_t} \right)^{100} k \left(\frac{2x}{W_t} \right)^{100} \quad 3-2$$

where k is a constant and is equivalent to 0.01,

W_t is the width of the tyre/pavement contact area,

P_t is the inflation pressure of the tyre,

t is the time with respect to the origin of the calculation step of loading.

Figure 3-8 shows a typical vertical stress of the TIML which is derived by using Equation 3-2.

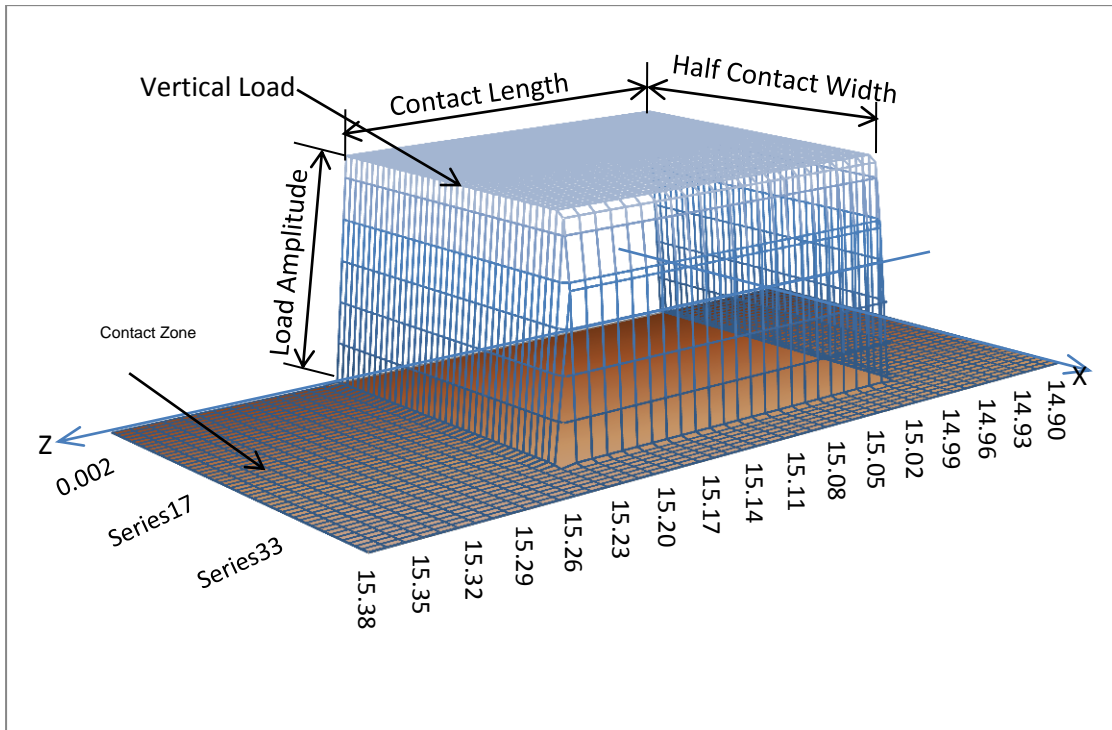


Figure 3-8 Vertical stress distribution of the TIML in the contact zone

The Amplitude is generated by a table describing the relationship between time and pressure. Table 3-3 shows a typical amplitude table, in which T_b is the time the pressure starts to act upon a contact area, T_e is the time when the pressure is removed, and k is a constant to avoid convergence errors and is equivalent to $\frac{t_{ii}}{100}$.

Table 3-3 Single amplitude table

Time	Amplitude
0	0
T_b	0
$T_b + k$	1
$T_e - k$	1
T_e	0
t_t	0

Figure 3-9 shows two typical amplitude-time curves used for TIML applicable to two consecutive load areas (e.g. Pressure A and Pressure B in Figure 3-7). With respect to the consideration of convergence, each has been built as a trapezoid. An overlap time T_e has been assigned to allow the total load applied onto the model to be constant in each calculation step. The duration of Amplitude A is $T_e - T_b$. The duration of average increment is equal to $T_e - T_b - k$. Amplitude A and Amplitude B both exist from $T_e - k$ to T_e . At this period, the total amplitude is equal to the maximum value of Amplitude A or B. Therefore, the vertical pressure applied on the contact zone has not been changed between $T_e - k$ and T_e .

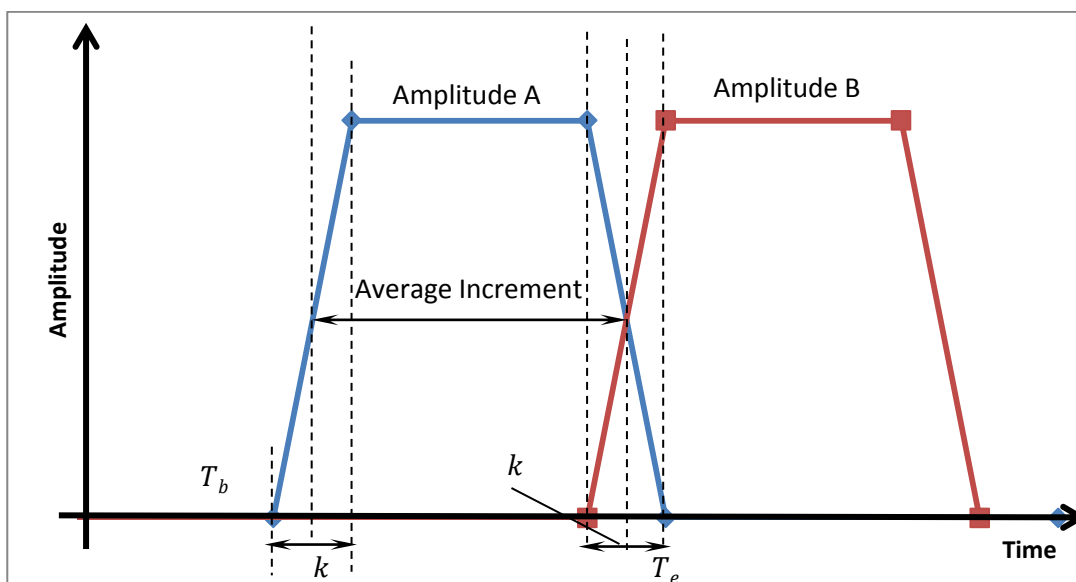


Figure 3-9 Amplitudes of pressures on contact area

The Magnitude of pressure is equivalent to 1. The number (N_L) of pressures can be determined by the equation below:

$$N_L = \frac{L_J}{L_e}$$

Take for example, a tyre rolling on the contact zone with a speed of 100km/h (27.8m/s); the inflation pressure is 552kPa and vertical load is 40kN. The length of the contact zone is 10m. The length of the contact area is 324.4mm and the width is 223.4mm. So, the time (t_t) during which the tyre travels along the contact zone is 348ms. If the length of every element in the contact zone is 3cm, the time used by the tyre passing an element is 1.1ms. The TIML consists 323 pressure applications.

The analytical field function is:

$$f(x, z, t) = 552 \times 10^3 \times 0.01 \left(\frac{2(z - 0.3244 - t27.77)}{0.3244} \right)^{100} 0.01 \left(\frac{2x}{0.2234} \right)^{100}$$

Mesh

Figure 3-10 shows the mesh of a typical 3D model which consists 63960 C3D20R elements. Each C3D20R element is a 20-node quadratic brick. With regard to the computational capability of the computers used in this project, every FE model can contain up to 100000 C3D20R elements. Therefore, to reduce the element numbers, it is worth using large elements in surrounding ground and smaller element in pavement layers and the contact zone to obtain accurate solutions.

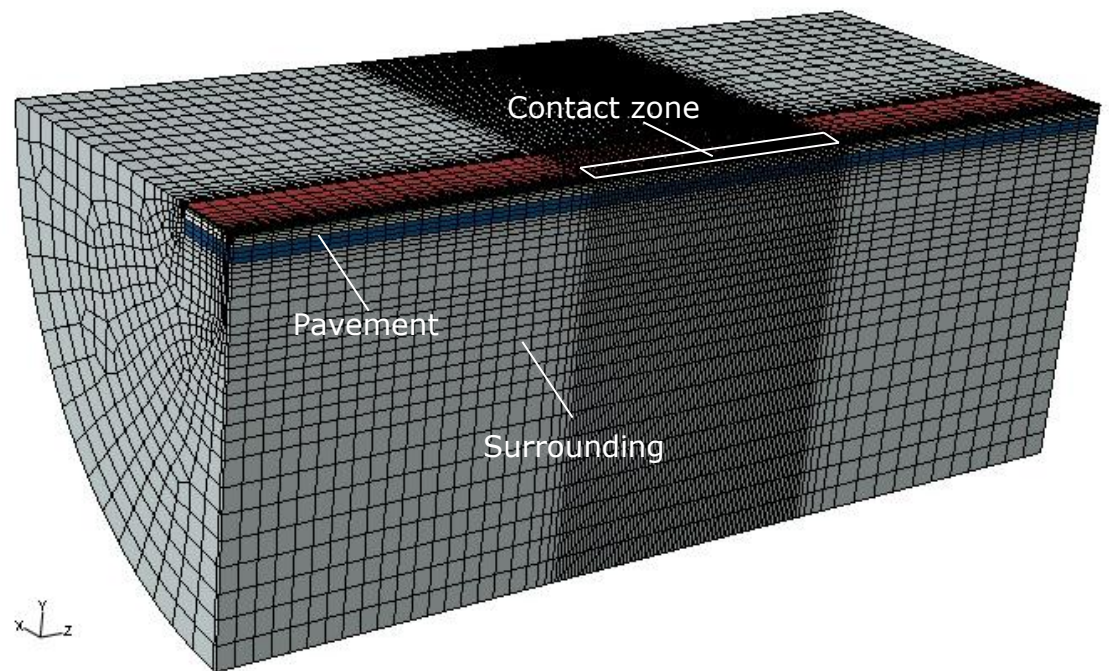


Figure 3-10 The mesh of the 3D model

Figure 3-11 shows the mesh used in the contact zone. Every element in the contact zone has the same size and this allows each pressure application of the TIML to have the same contact area, i.e. this allows the load to move smoothly along the contact zone.

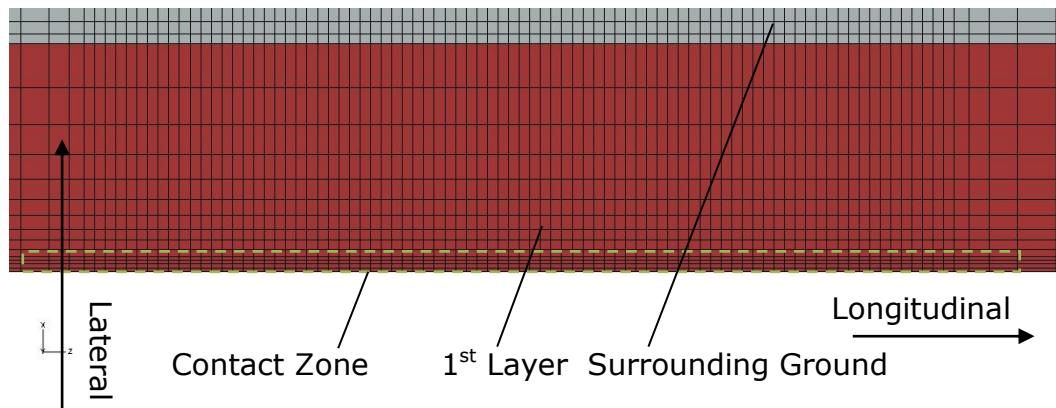


Figure 3-11 the mesh of the contact zone

Mesh verification has been applied to the models to check the geometrical issues. The check list is shown below:

- Face corner angle less than 10° ,
- Face corner angle greater than 160° ,
- Aspect ratio greater than 10,
- Edge shorter than 0.01,
- Edge longer than 1,
- Stable time increment less than 0.0001,
- Warning elements.

With regard to the limitation on element numbers and size, it is impossible for every element to match the conditions. Fortunately, the models used in this project do not include any warning element or error element. Only a fraction of the elements have an aspect ratio greater than 10 and they are distributed in the surrounding ground. Therefore, the solutions carried out are acceptable and sufficiently accurate.

Boundary conditions

VDB damping is also used in the 3D models. Figure 3-12 shows the boundary faces defined in the 3D model. Faces 1, 2 and 3 are boundary faces, VDB dashpots are only applied to Face 2. Each node on boundary face 2 connects to a dashpot element DASHPOT 1. In order to reduce the total amount of VDB elements of each model, conventional boundaries have been applied to Faces 1 and 3. In order to reduce the reflection angle (θ), which can be found in Figure 2-34, a cylindrical coordinate system is used for Face 2. The origin of the cylindrical coordinate system has been located at the center of the model where global x and y are equal to zero, and global z equals half its length. The z of the cylindrical system is parallel to global x-axis. As shown in Figure 3-13, Dashpot A in

the VDB system can be controlled to face the oncoming waves, resulting in a very small reflection angle θ , so, a in Equation 2-14 and b in Equation 2-15 are equal to 1. A symmetrical boundary condition has been used for Face 4.

By using Equations 2-14 and 2-15, the dashpot coefficients of VDBs can be calculated. It is worth noting that the equations have been simplified as follows:

$$c_p = \rho V_p \Gamma$$

$$c_s = \rho V_s \Gamma$$

This is because ρV_s or ρV_p is a constant for each boundary element. Γ has been determined according to using the area of the selected region of the boundary (S_n) and the number of nodes located in that region (N_n), as follows:

$$\Gamma = \frac{S_n}{N_n}$$

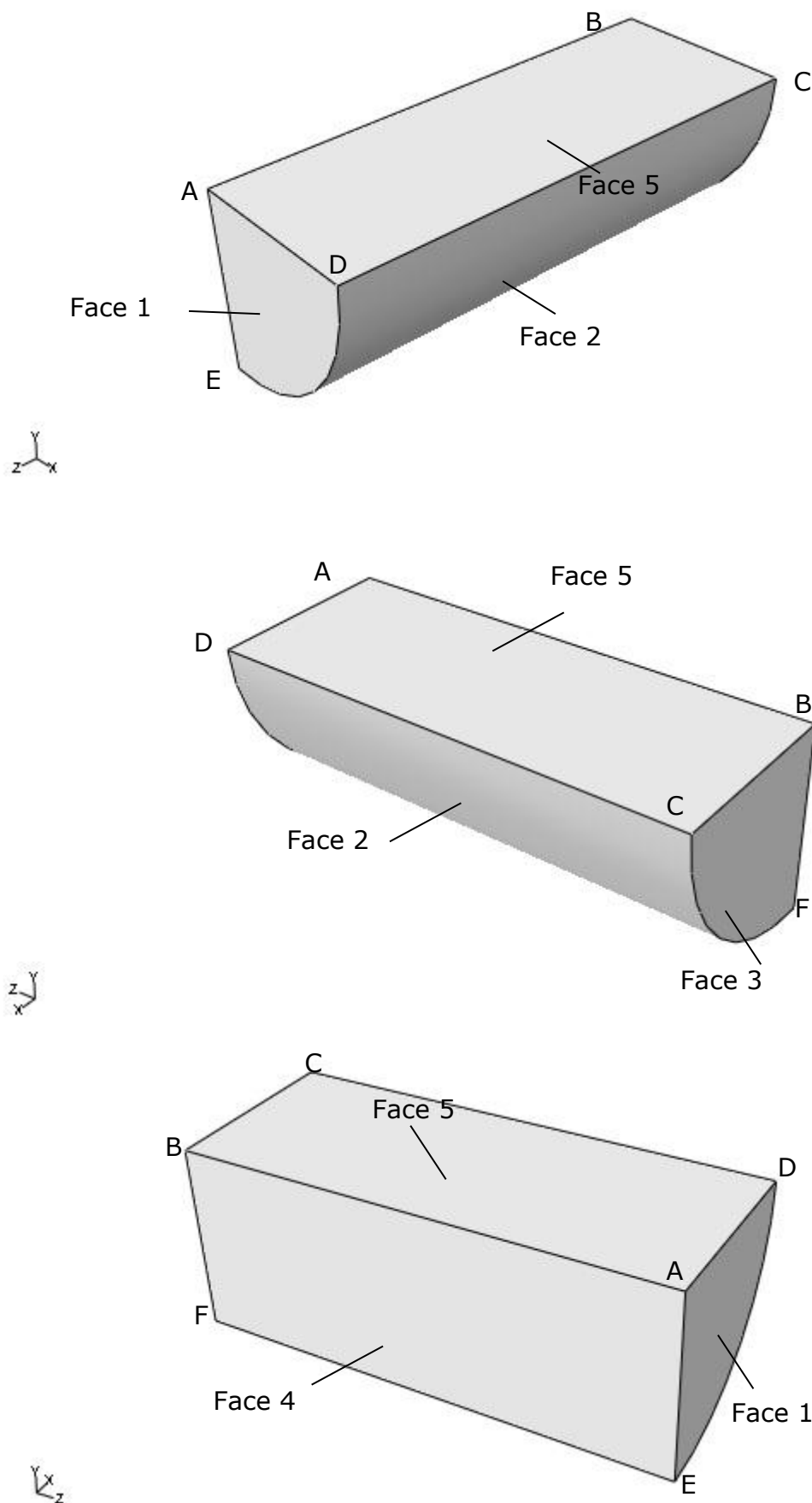


Figure 3-12 Distribution of boundary conditions

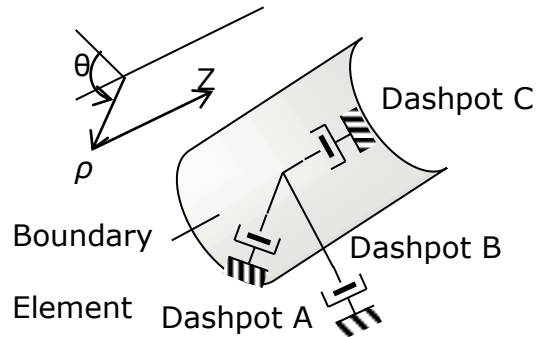


Figure 3-13 VDB in cylindrical coordinate system

Figure 3-14 shows the deflections computed using the 3D model at an observation node which is located on the contact zone with 2 different boundary conditions (VDB and rigid boundary). Material damping has not been applied in this case. The rigid boundary means that all degrees of freedom at the boundary nodes are equal to 0. Thus, a rigid boundary will reflect energy waves completely. Obviously, oscillation due to reflected waves can be seen in the case of the rigid boundary, the frequency of which is about 20Hz and the amplitude about 10 microns. The case with VDB has a relatively smooth curve compared to the case with a rigid boundary. Comparing the curves, it is quite clear that the oscillations at 20Hz have been removed by using VDB. Nevertheless, an oscillation with a frequency of about 200Hz can still be observed, especially when the deflection approaches its peak value. The explanation for this oscillation is not straightforward but it has been found that when material damping of the subgrade is included (e.g. Figure 3-15) this effect disappears.

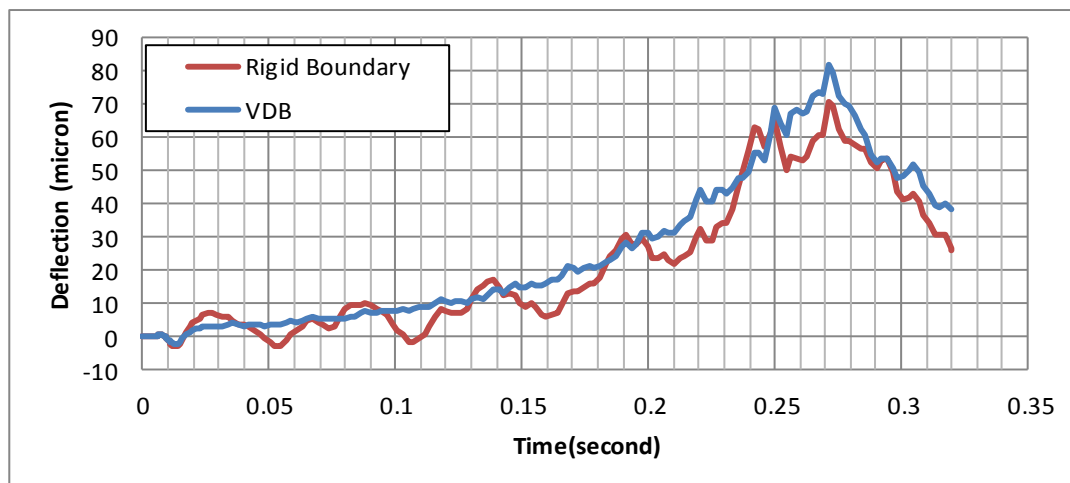


Figure 3-14 VDB vs. rigid boundary (3D model, 30km/h)

Solution Control

Due to an enormous amount of elements have been built for the 3D model, the simulation takes a long time for calculation. According to ABAQUS Theory Manual (2001), the quasi-Newton method is an efficient method for 3D FE calculation. In order to reduce the calculation time, a technique of quasi-Newton method has been used in the calculation step.

Energy dissipation

For this project, an energy balance equation for the entire model can be written as follows:

$$E_k + E_s + E_v = E_w \quad 3-3$$

where: E_w is the external work,

E_k is the kinetic energy,

E_s is the strain energy,

E_v is the energy dissipated by viscosity effects.

Since only the pavement has been modelled the energy related to the tyre is not discussed here. The kinetic energy and strain energy can be

observed when the tyre rolls on the pavement and will be transformed to E_v , which is the energy absorbed by the VDB and material damping. Therefore, the energy dissipation of the entire model is equal to E_v , under one condition, when the kinetic energy and strain energy are completely transformed.

Figure 3-15 shows a deflection curve and a related load curve observed from a node located in the contact zone. The curves are terminated at 861ms, at which point the simulation was stopped. At this time (816ms), the load (vertical pressure) equals 0, but the deflection is still about 352 microns. Therefore, strain energy still exists in the model. Kinetic energy also exists, since the node will rebound and the deflection will reduce to 0. At this stage, E_v is not the entire dissipated energy because the kinetic energy and strain energy have not been entirely transformed.

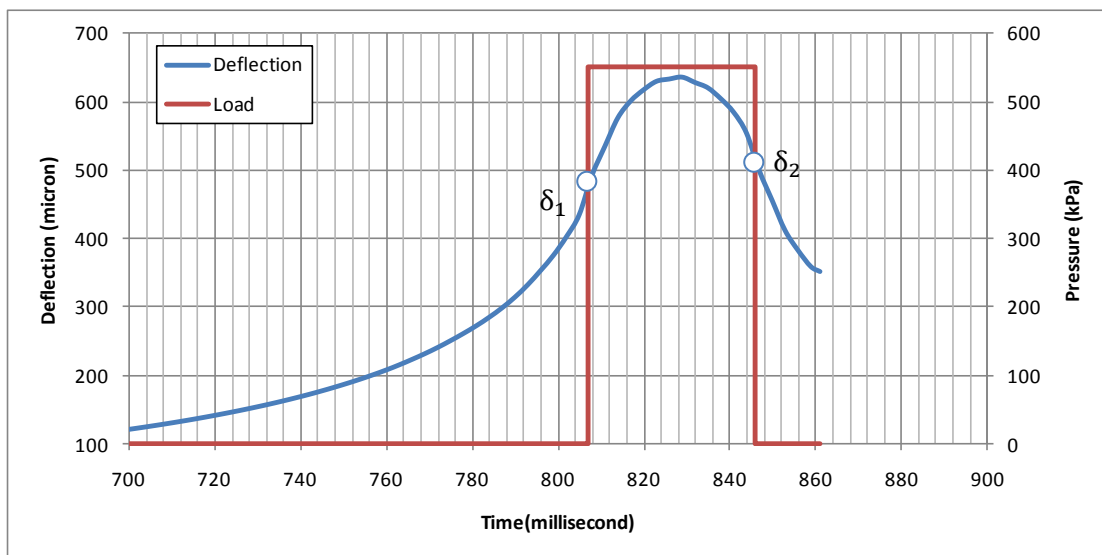


Figure 3-15 Load and Deflection histories of a node at contact zone

Alternatively, the external work can be calculated using the load and deflection curves. Figure 3-16 shows the resulting hysteresis diagram, stress vs. deflection, which is based on the results plotted in Figure 3-15.

The seven arrows indicate the trend of the curve and the meaning is as follows:

Arrow 1. The vertical stress has yet reached the node but deflection increases as the load approaches.

Arrow 2. The vertical stress reaches the node.

Arrow 3. The vertical stress is applied to the node but maximum deflection has not yet occurred.

Arrow 4. Same as Arrow 3

Arrow 5. The vertical stress is still applied to the node, but the deflection is now reducing.

Arrow 6. The stress leaves the node.

Arrow 7. There is no stress applied on the node. The deflection reduces as the load departs.

The shaded area indicates the energy imparted by the load and not recovered, and can be calculated using the equation below:

$$E_d = \sigma(\delta_2 - \delta_1) \quad 3-4$$

where: E_d is the energy density,

σ is the stress,

δ_1 is the deflection when the load starts to act on the node,

δ_2 is the deflection when the load leaves the node.

It is worth noting that E_d is the energy in the tyre/pavement contact area, the unit is J/m^2 and σ equals the pressure applied by the tyre. When E_d is multiplied by the width of the tyre/pavement contact area (W_t), it represents the energy dissipation per meter travel of the rolling tyre. The equation becomes:

$$R_p = E_d W_t = \sigma(\delta_2 - \delta_1)W_t \quad 3-5$$

The unit of R_p is Joules per metre or Newtons. Therefore, R_p is termed 'Pavement Resistance' (PR). It is a resistance force and comprises part of the rolling resistance. The value of PR is controlled by both tyre load and pavement stiffness.

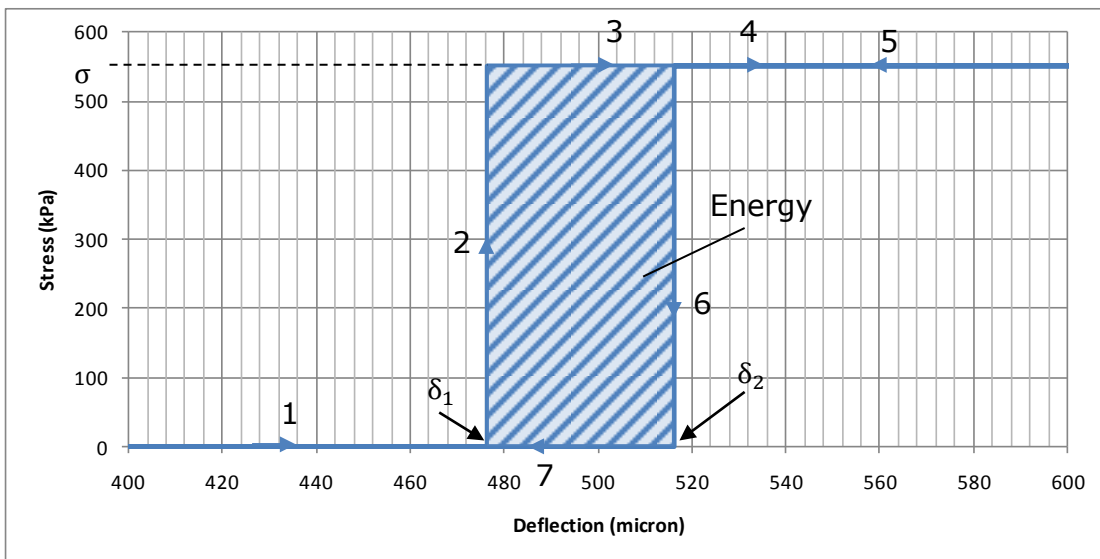


Figure 3-16 Load vs. Deflection of the node

3.4 Summary

This chapter has introduced the process of FE analysis and discussed three aspects of the modelling: materials, physical dimensions and FE modelling.

Two FE models, an axisymmetric model and a 3D model, have been designed. The axisymmetric model is used to identify the material properties and to simulate FWD tests. The 3D model is used to simulate a single tyre rolling on a section of pavement. In order to build computational efficiency, dimensions of the models have been determined

by a series of confirmation tests. This allows the models to have enough volume to damp the energy waves; meanwhile, the number of elements does not exceed the computational limitations.

To achieve accurate solutions, some unique modelling methods are used. A time-interval-moving load approach is used to impart a smoothly moving load onto the pavement surface. A viscous damping boundary (VDB) is used to absorb the energy waves; in this way, the subgrade, an infinite medium, can be simulated by using FEM. The oscillations that would otherwise be caused by reflected energy waves in the pavement can be significantly reduced by the combination of VDB boundary and material damping in the subgrade.

The external work caused by the time-interval moving load can be calculated by using a load-deflection hysteresis plot.

The Pavement Resistance has been derived. This indicates the influence of the pavement stiffness and the tyre load on energy dissipation.

Chapter 4

Confirmation Tests

In order to assess the viability of the FE method in estimating energy dissipated as a function of pavement stiffness, confirmation tests simulating FWD measurements have been conducted.

Figure 4-1 shows the detailed process. The first step is to evaluate the material moduli of the pavement layers subjected to the FWD test. Calculations using the multi-layer linear elastic analysis program BISAR will be used to achieve this purpose. Secondly, the load history recorded during the FWD tests, material moduli determined from the BISAR calculations, assumed values of dimensions (pavement layer thicknesses) and estimated material damping parameters will be input into the axisymmetric model for dynamic simulations. The results of the simulations are deflection-time traces of nodes located on the pavement surface. The result from simulation is termed "Deflection History B". By using the comparison between the "Deflection History A" measured by the FWD and "Deflection History B", the values of damping used in the simulations can be adjusted. Then, all the materials parameters confirmed by using the axisymmetric model and FWD load history will be input into a 3D FE model to calculate the deflection history again. This will then be compared to the measured deflection once more to determine the applicability of the configurations used by the 3D FE model.

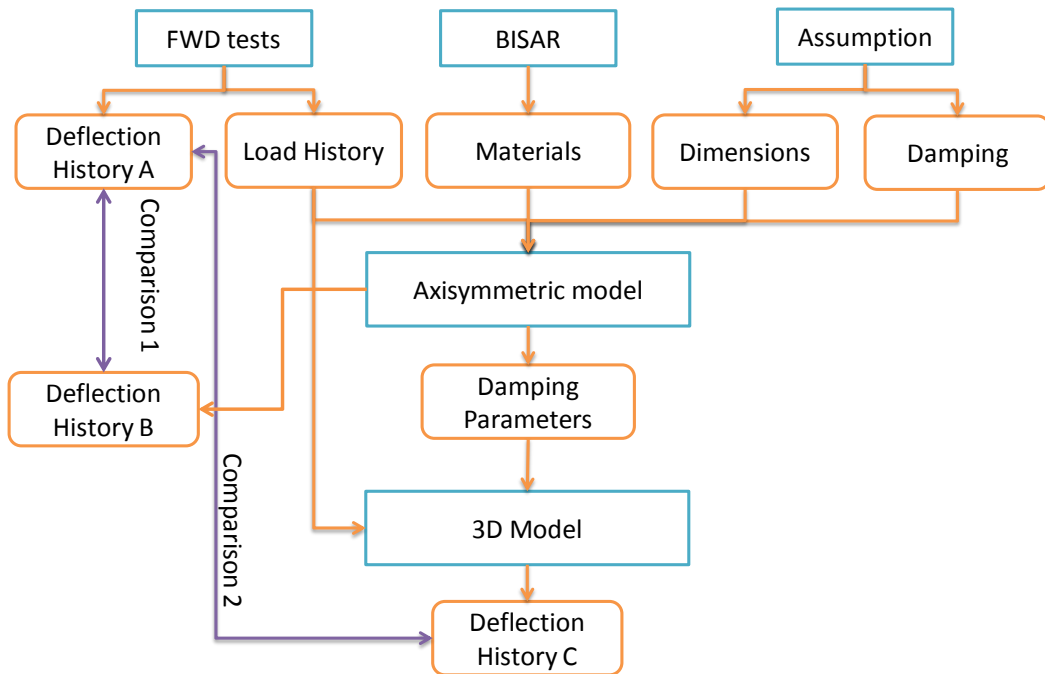


Figure 4-1 Process of confirmation tests

4.1 Model definition

4.2 Materials

Results of FWD tests on a composite (asphalt over concrete) pavement were kindly provided by Scott Wilson Ltd. However, the detailed pavement structure and corresponding material properties were not provided with the results. Based on the core information available, a reasonable estimate of the structure is assumed as shown in Table 4-1. These thicknesses will be used for all calculations mentioned in this section.

Table 4-1 Thicknesses of the layers of the pavement

Layer	Layer 1	Layer 2	Layer 3	Layer 4
Material	Asphalt	Concrete	Cemented Base	Soil
Thickness (mm)	140	200	300	unlimited

The results of the BISAR calculations give estimates of the material properties of the pavement, as shown in Table 4-2. Since BISAR is a static analysis, the calculation only involves Young's modulus and Poisson' Ratio. The values of density shown in Table 4-2 are simply typical values for the material present.

Table 4-2 Material properties of the layers of the pavement

	Name	Young's Modulus (MPa)	Poisson's Ratio	Density (kg/m ³)	Damping	
					Alpha (s)	Beta (1/s)
Layer 1	Asphalt	7000	0.35	2400	0	0
Layer 2	Concrete	7000	0.35	2400	0	0
Layer 3	CB*	2400	0.25	2000	0	0
Subgrade	Soil	90	0.3	1800	A1	B1

Note*: Cemented Base

Damping Parameters, A1 for alpha damping, B1 for beta damping, were varied as shown below:

- Alpha: 0, 60, 70, 90 and 100
- Beta: 0.01, 0.012, 0.015, 0.02 and 0.021

The combination of alpha and beta damping is used to control the detailed shape of the deflection history trace. A well fitted deflection history will indicate an appropriate combination of parameters.

Figure 4-2 shows the axisymmetric which is composed of 557 CAX8R (an 8-node biquadratic axisymmetric quadrilateral, reduced integration) elements and 164 Dashpot1 elements which are used as VDBs.

The width and height of the model are both 20m. Pavement layers have been included at the top of the model with a radius of 2m. The Γ value can be determined from the average area occupied by boundary nodes, giving VDB coefficients as shown in Table 4-3. The values for VDB1 and VDB2 differ because of the difference in node density.

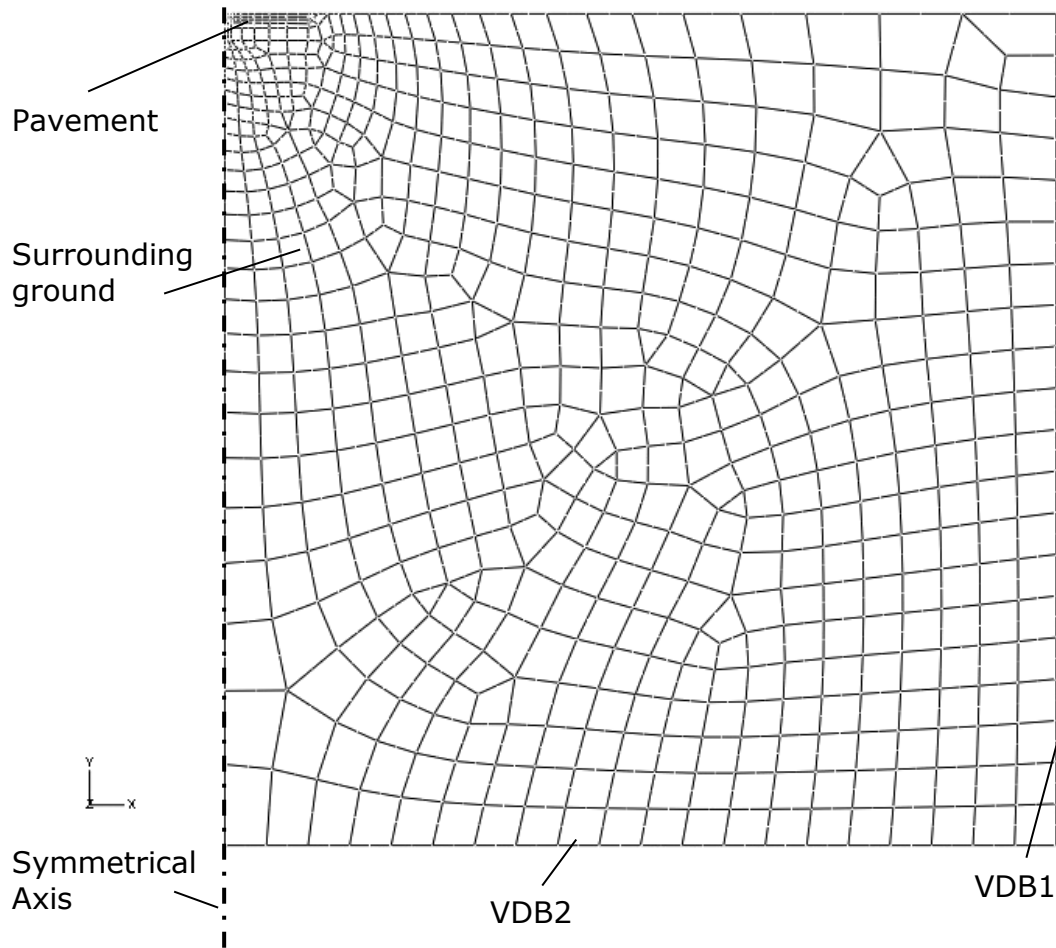


Figure 4-2 Mesh of axisymmetric model used for confirmation test

Table 4-3 Dashpot coefficients of VDBs used for axisymmetric model

	Dashpot Coefficient (N·s/m)	
	Primary (c_p)	Secondary (c_s)
VDB1	2.86×10^7	1.53×10^7
VDB2	1.47×10^7	7.84×10^6

The model used for the 3D dynamic analyses is shown Figure 4-3. It is built by using 34928 C3D20R elements with 22959 Dashpot1 elements. The dimensions of the model have been introduced in Chapter 3.2.1. The dashpot coefficients of VDBs can be found in Table 4-4. These values were calculated by using Equations 2-14 and 2-15. Since the amount of boundary nodes in the 3D model is more than in the axisymmetric model, the average area occupied by every node of the 3D model is smaller than in the axisymmetric model. Therefore, the dashpot coefficient values of the 3D model are smaller than those of the axisymmetric model.

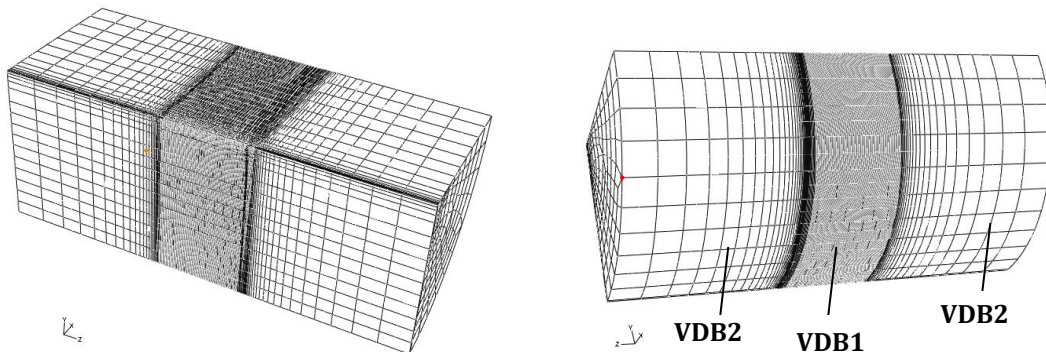


Figure 4-3 3D model used for dynamic analyses

Table 4-4 Dashpot coefficients of VDB used for 3D model

	Dashpot Coefficient (N·s/m)	
	Primary (c_p)	Secondary (c_s)
VDB1	1.16×10^5	6.22×10^4
VDB2	6.27×10^3	3.35×10^3

4.3 Loading

A typical FWD load history has been used for each simulation, with a maximum load level of 40kN (570kPa) and a duration of about 30ms. For the 3D model, the load is applied as a pressure of 570kP. It is exerted on

the contact zone by using an analytical field. The analytical field can be derived using Equation 4-1. The load and analytical field can be plotted as shown in Figure 4-5. Figure 4-4 shows the load history and a deflection history measured by deflection transducer at D1 located in the centre of the loading plate. In order that the deflection and load can be more easily compared on the graphs, load and deflection downward into pavement have been given positive values.

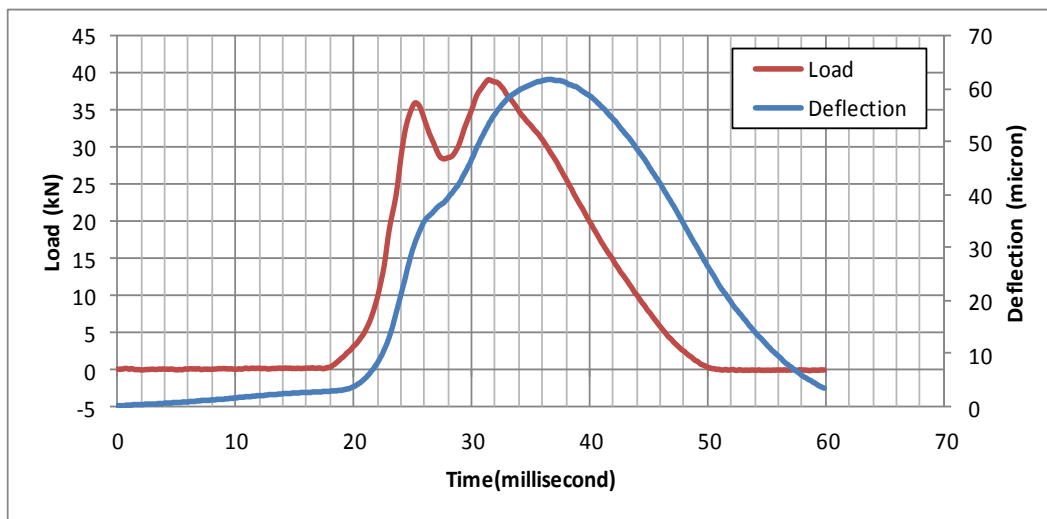


Figure 4-4 FWD load and deflection histories

$$f(x, z) = P_t k \left(\frac{\sqrt{x^2 + (z - \frac{L_m}{2})}}{r_f} \right)^{100} \quad 4-1$$

where k is a constant and is equivalent to 0.01,

x and z are the coordinates,

P_t is the pressure of the load,

L_m is the length of the model.

r_f is the radius of the FWD load plate

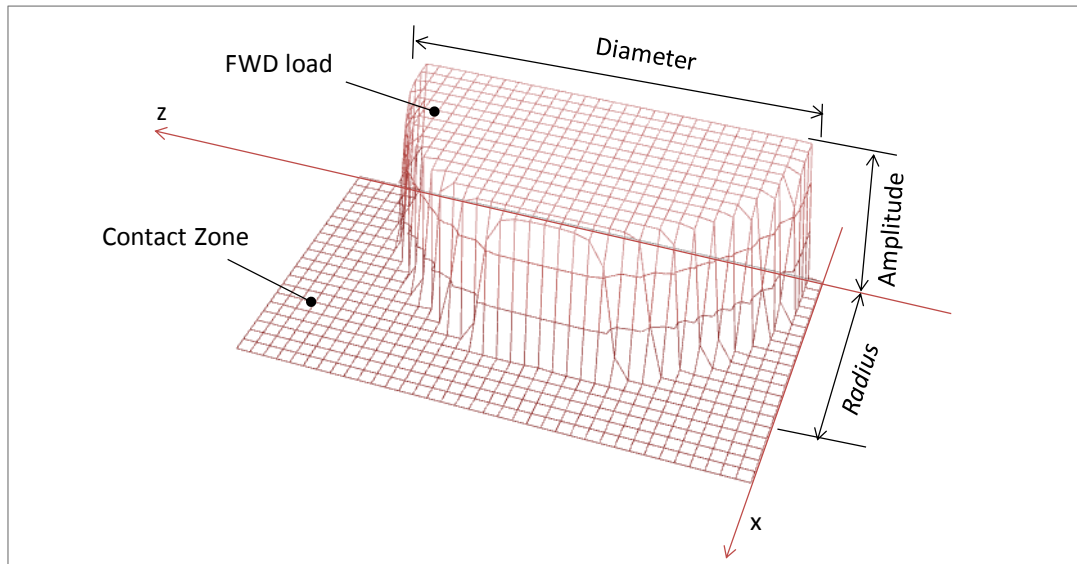


Figure 4-5 Load used for the 3D model

4.4 Results

The result retrieved from the each simulation using the axisymmetric model is a deflection-time trace. Figure 4-6 show the results carried out when alpha damping (A_1) equals 100 against the measured deflection history retrieved from the FWD test. Results indicate that the deflection-time trace with $A_1=100$ and $B_1=0.02$ is approximately the same as the FWD deflection history, in spite of differences that can be observed in Phases A and D. The deflection recorded by the FWD in Phase A is ignored, since the load exerted from 0 to 18ms is zero. Results in Phase B and Phase C indicate that the FE model gives a well fitted curve when $A_1=100$ and $B_1=0.02$. The result from FE analyses in Phase D is larger than the FWD result in each case due to damping resistance to the motion. Thus, the deflection reduces more slowly than in the FWD test. Nevertheless, the influence of this difference on energy dissipation is limited, since no load is being exerted at the time.

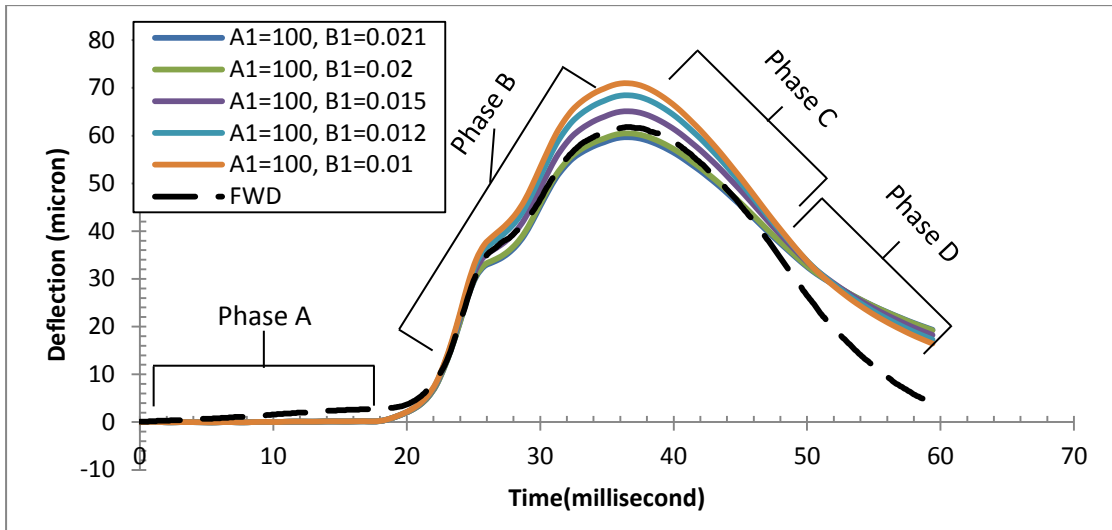


Figure 4-6 Deflection-time traces when A1=100

Figure 4-7 shows the corresponding hysteresis curves. The energy dissipated in the FWD test is 1.37J. The curve when A1=100 and B1=0.02 gives similar results: 1.38J.

The plotted data of deflection-time traces and hysteresis curves with all the different damping combinations are show in Appendix A.3.

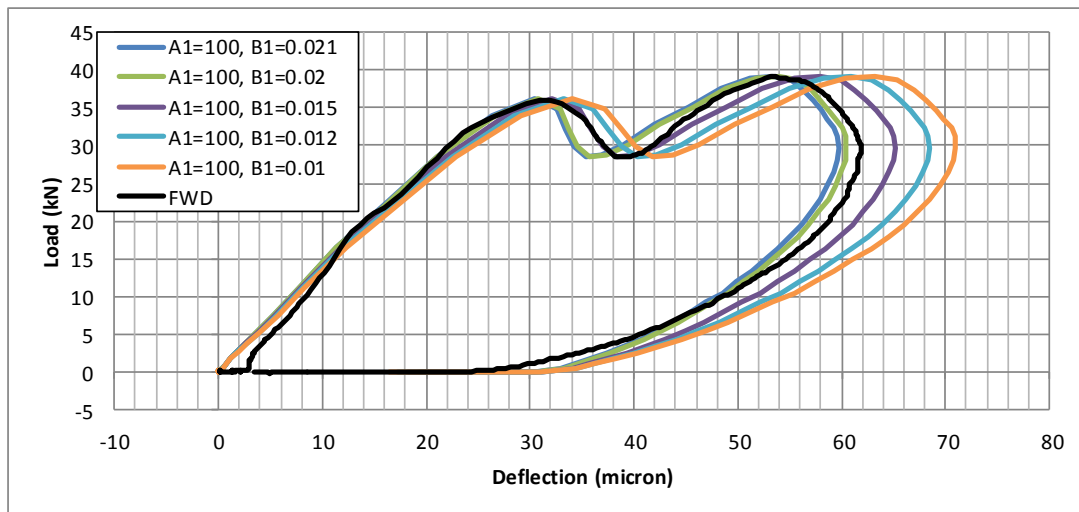
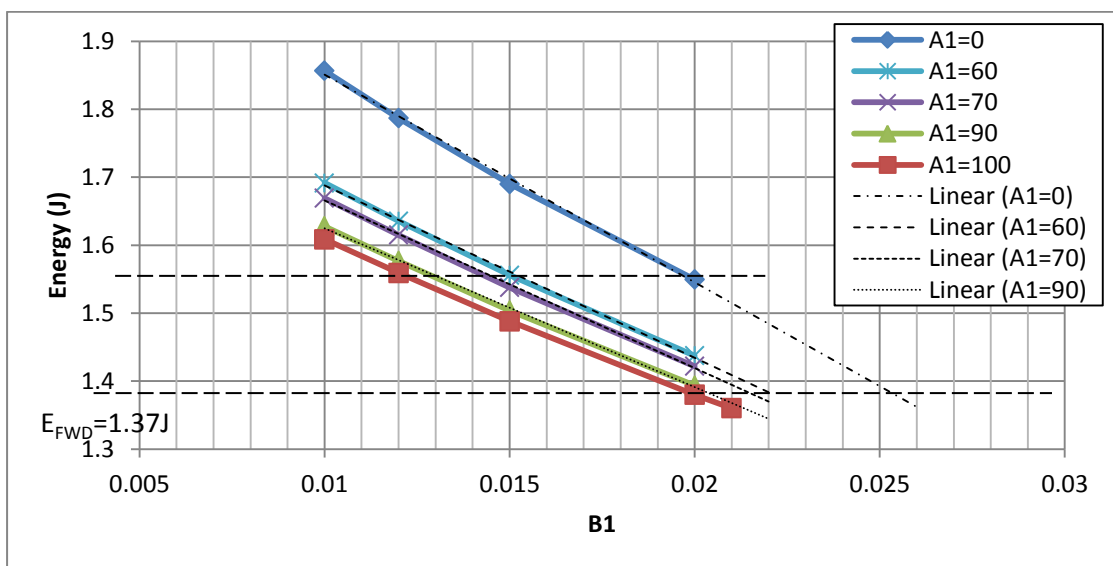


Figure 4-7 Load vs. deflection when A1=100

In order to assess the influence of damping on energy dissipation, energy dissipated in each simulation is plotted against the beta damping

parameter, as shown in Figure 4-8. Results indicate that the relationship between dissipated energy and beta damping is linear. Combinations with different alpha and beta damping values may result in the same energy dissipation. The case when $A_1=60$ and $B_1=0.015$ gives an energy dissipation of 1.54J, this is same as the case when $A_1=0$ and $B_1=0.02$. Trend lines predict that the same amount of dissipated energy as the FWD result can be achieved when $A_1=0$, $B_1=0.0255$ or $A_1=60$, $B_1=0.022$ and so on. This prediction has been verified by FE tests, which show that the energy is 1.37J when $A_1=0$, $B_1=0.0255$ or $A_1=60$, $B_1=0.022$.



**Figure 4-8 Energy dissipation retrieved from FWD-FE model
(E_{FWD} is the energy calculated by using FWD results)**

The same FWD load history has been exerted on the 3D model with the damping values of $A_1=100$ and $B_1=0.02$. The deflection-time trace retrieved from the simulation has been plotted, as shown in Figure 4-9. The 3D model gives a similar trace to that of the axisymmetric model.

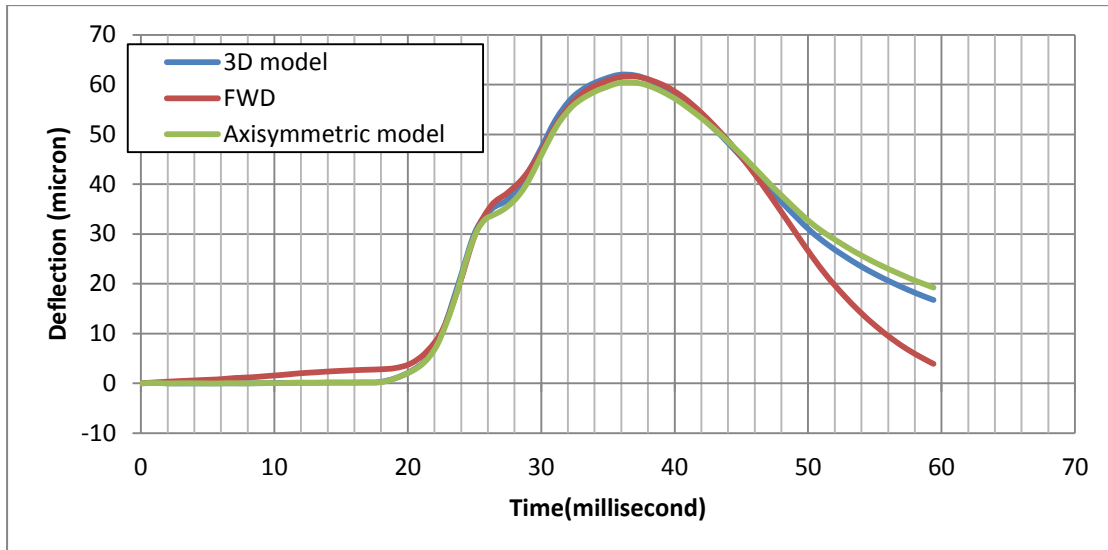


Figure 4-9 Deflection load traces retrieved from 3D model and FWD test

The hysteresis curve plotted by using the deflection-time trace and corresponding load history, as shown in Figure 4-10, gives a dissipated energy of 1.38J. This is similar to the FWD result.

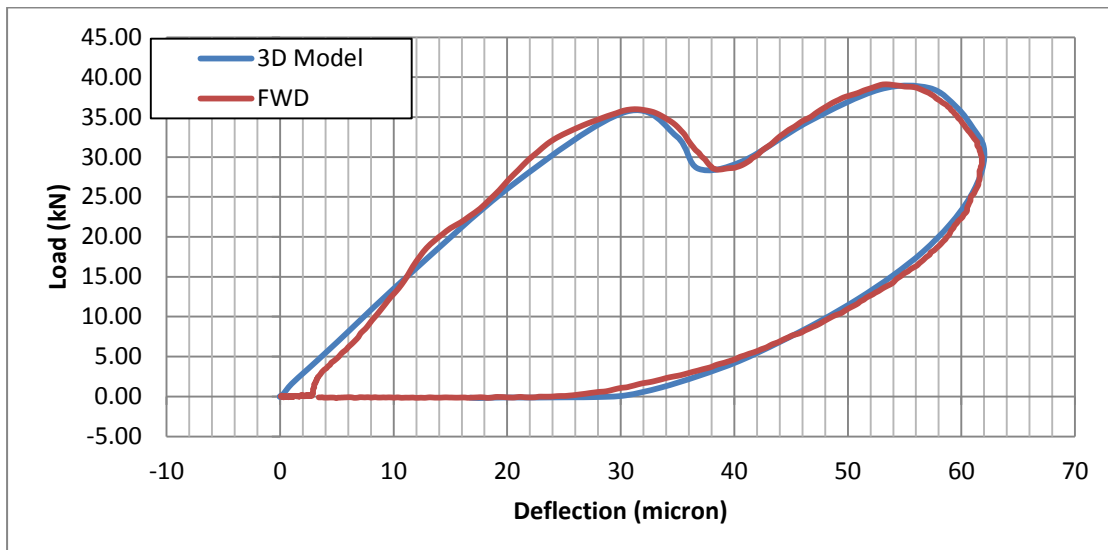


Figure 4-10 Load vs. deflection, 3D model vs. FWD

4.5 Summary

Table 4-5 shows the material properties and damping values selected for use in the FE analyses. By using these properties both the axisymmetric

model and the 3D model can give similar results for energy dissipation as the FWD measurements. Although the value of Poisson's ratio is relatively low for the subgrade (suggesting a highly granular material) it is nevertheless within limits.

Table 4-5 Material properties of the layers of the pavement (result)

	Name	Young's Modulus (MPa)	Poisson's Ratio	Density (kg/m ³)	Damping	
					Alpha (s)	Beta (1/s)
Layer 1	Asphalt	7000	0.35	2400	0	0
Layer 2	Concrete	7000	0.35	2400	0	0
Layer 3	CB	2400	0.25	2000	0	0
Subgrade	Soil	90	0.3	1800	100	0.02

Deflection-time traces determined from the FE models indicate that material damping resists motion of elements and nodes in the model. This resistance causes energy to be dissipated.

The results imply that the relationship between damping and dissipated energy is linear. For a linear elastic model, the damping values are artificial parameters acting in place of the real non-linearity and hysteresis exhibited by soil. Thus, the combination of damping values (alpha or beta damping) can be varied to control energy dissipation.

Since the deflections collected from D1 represent the overall stiffness of a pavement and this research only focuses on the relationship between the overall stiffness of pavement and energy consumption, the results of D2 to D6, which are affected by preferentially by the stiffnesses of different layers of pavement, have been omitted.

These confirmation tests have effectively validated the FE models as a realistic method of simulating dynamic behaviour and estimating energy dissipation.

Chapter 5

Case Study –TRL Measurements

5.1 Problem description

In order to identify and quantify the influence of pavement stiffness on truck fuel consumption on the highway network, the UK's Transport Research Laboratory (TRL) carried out research to assess fuel dissipation on two pavements with varying pavement stiffness (McKeown, 2002).

The fuel consumption was measured for two pavement constructions: a continuously reinforced concrete pavement (CRCP) (i.e. a rigid pavement with low deflection) and a fully flexible pavement (i.e. a flexible pavement with high deflection). Additionally, a composite pavement was included as well. However, for this pavement section it has been noted that the details of the construction varied along its length, and the information obtained was very limited.

This chapter will report a set of FE analyses based on the TRL measurements using stiffness moduli derived from FWD results to investigate the energy dissipated in the pavements. The findings from FE analysis will then be compared with the measurement made by TRL

5.2 Model Definition

5.2.1 Background of TRL measurements

The locations of the three pavement structures can be found in Figure 5-1.

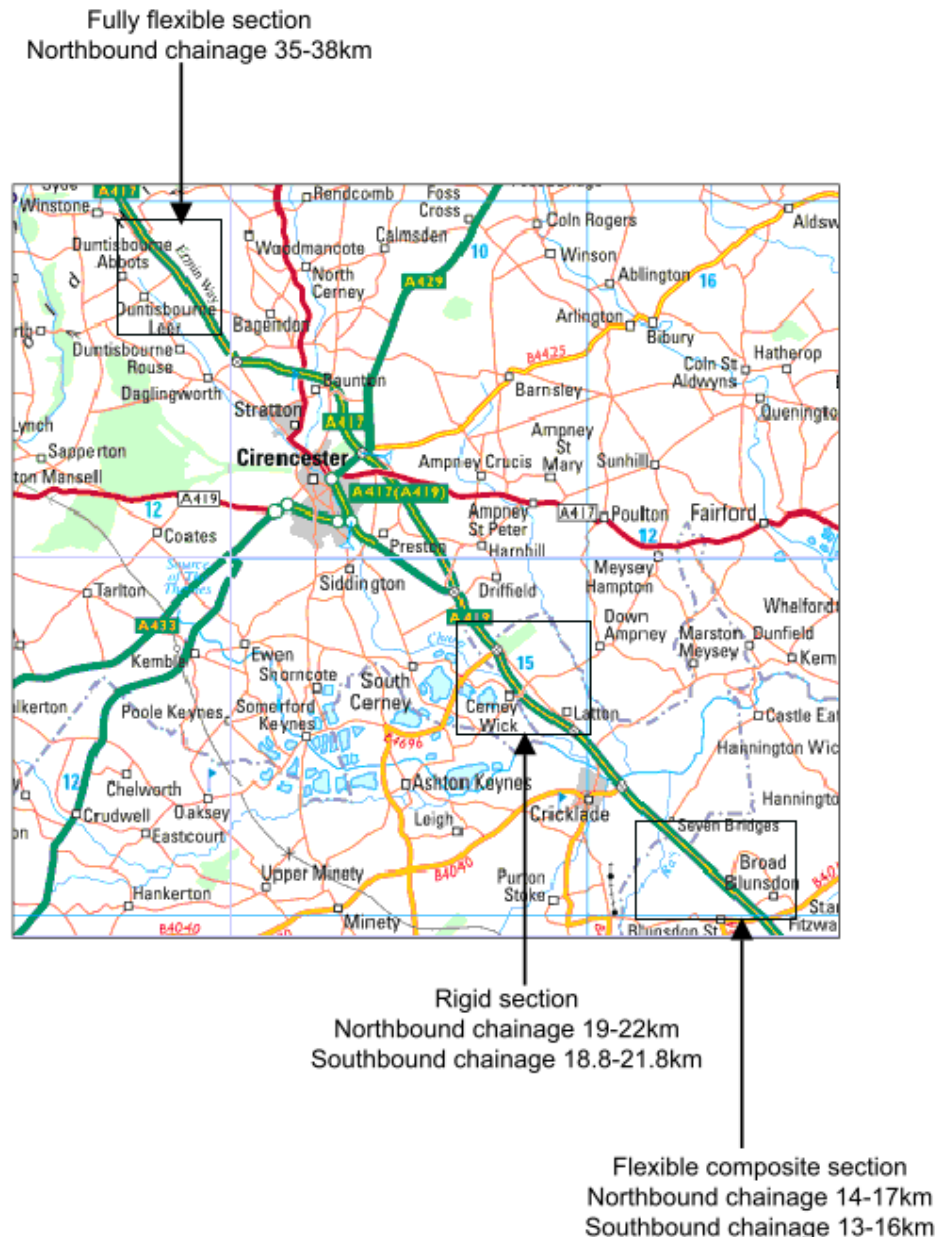


Figure 5-1 Locations of the pavements used for measurement (McKeown, 2002)

Table 5-1, Table 5-2 and Table 5-3 show the thicknesses used for each pavement model. It is worth noting that a 300mm subbase was built into the composite pavement, since the stiffness values determined by using the given structure and the FWD results are much larger than ordinary values.

Chapter 5 Case Study – TRL Measurements

Table 5-1 Composite pavement

Layer	Name	Thickness (mm)
1	HRA	45
2	Binder Course	60
3	Concrete Roadbase	200
4	Subbase	300
5	Subgrade	infinite

Note: HRA is Hot Rolled Asphalt

Table 5-2 Rigid pavement

Layer	Name	Thickness (mm)
1	CRCR	210
2	CBB	300
3	Subgrade	infinite

Note: CRCR is Continually Reinforced Concrete Pavement, CBB is Cement Bound Base

Table 5-3 Fully flexible pavement

Layer	Name	Thickness (mm)
1	SMA	49
2	HDM	323
3	Granular	300
4	Subgrade	infinite

Note: SMA is Stone Mastic Asphalt, HDM is Heavy Duty Macadam

In order to assess pavement stiffness, measurements using FWD were made on each pavement. Table 5-4 shows the mean deflection measured by the FWD at d1 (offset 0m), d4 (offset 0.9m) and d6 (offset 1.5m).

Table 5-4 Mean FWD deflections of the three pavements

Pavement	d1(micron)	d4(micron)	d6(micron)
Fully Flexible	69	25	9
Rigid	50	25	20
Flexible Composite	95	60	37

The vehicle used in the TRL measurements was a DAF 95 350Ati, 4 by 2 tractor unit. The tractor-trailer combination was chosen to be a typical 28 tonne haulage vehicle. The tyres of the tractor unit were Michelin XZA 295/80R22.5 in single configuration on the steer axle and in twin configuration on the drive axle. The speed of the vehicle is 80km/h. The tyres of the semi-trailer were Michelin XZE 385/65R22.4 wide-single tyres on all axles. The axle loads and tyre pressure can be found in Table 5-5.

Table 5-5 Axle loading of TRL test vehicle

	Axle	Type	Pressure	Load	Contact Area
Tractor Unit	1	Steer	816kPa	61.7kN	7.56 cm ²
	2	Drive	612kPa	79.4kN	12.97 cm ²
Semi-Trailer	3	Trailing	816kPa	78.6kN	9.63 cm ²
	4	Trailing	816kPa	76.5kN	9.38 cm ²
	5	Trailing	816kPa	76.6kN	9.39 cm ²

5.2.2 Material properties

The model used in the analyses is composed of linear elastic materials. In order to identify the properties of the materials, BISAR calculations were conducted to match the FWD deflections and thereby to determine the stiffness properties of the pavements. Table 5-6, Table 5-7 and Table 5-8

Chapter 5 Case Study – TRL Measurements

show the results confirmed by BISAR. It is worth noting that BISAR can only confirm Young's moduli and Poisson's ratios. The densities are assumed typical values and material damping factors are those derived in Chapter 4 and assumed to be typical of soil behaviour. Regarding the values shown, the asphaltic and granular layers are within the ranges for sand materials, as the CRCP and CBB materials in Table 5-7. The concrete road base in Table 5-6 implies that this is actually a Pavement Quality Concrete (PQC) that has been overlaid at some stage. The subgrade moduli are all relatively high and that in Table 5-7 almost certainly includes the effect of one or more granular foundation layers.

Table 5-6 Composite pavement

Layer	Name	Young's Modulus (MPa)	Poisson's Ratio	Density (kg/m ³)	Damping	
					Alpha (s)	Beta (1/2)
1	HRA	8000	0.35	2400	0	0
2	Binder Course	8000	0.35	2400	0	0
3	Concrete Road Base	45000	0.2	2400	0	0
4	Subbase	80	0.35	2200	0	0
5	Subgrade	320	0.35	1800	100	0.02

Table 5-7 Rigid pavement

Layer	Name	Young's Modulus (MPa)	Poisson's Ratio	Density (kg/m ³)	Damping	
					Alpha (s)	Beta (1/s)
1	CRCP	25000	0.15	2500	0	0
2	CBB	6000	0.2	2200	0	0
3	Subgrade	500	0.35	1800	100	0.02

Table 5-8 Fully Flexible pavement

Layer	Name	Young's Modulus (MPa)	Poisson's Ratio	Density (kg/m ³)	Damping	
					Alpha (s)	Beta (1/s)
1	SMA	4000	0.35	2400	0	0
2	HDM	10000	0.35	2400	0	0
3	Granular	150	0.35	2200	0	0
4	Subgrade	120	0.35	1800	100	0.02

5.2.3 3D model

Regarding the different pavement structures, different models have been used for the analyses; 3D models have been designed. Each model has a total length of 26m and a radius of 10m as shown in Figure 5-2. The wheel contact zone of each model has the same dimensions; the width is 0.1288m and the length is 6m. This is because the vertical loads and tyre pressures used for each model are the same.

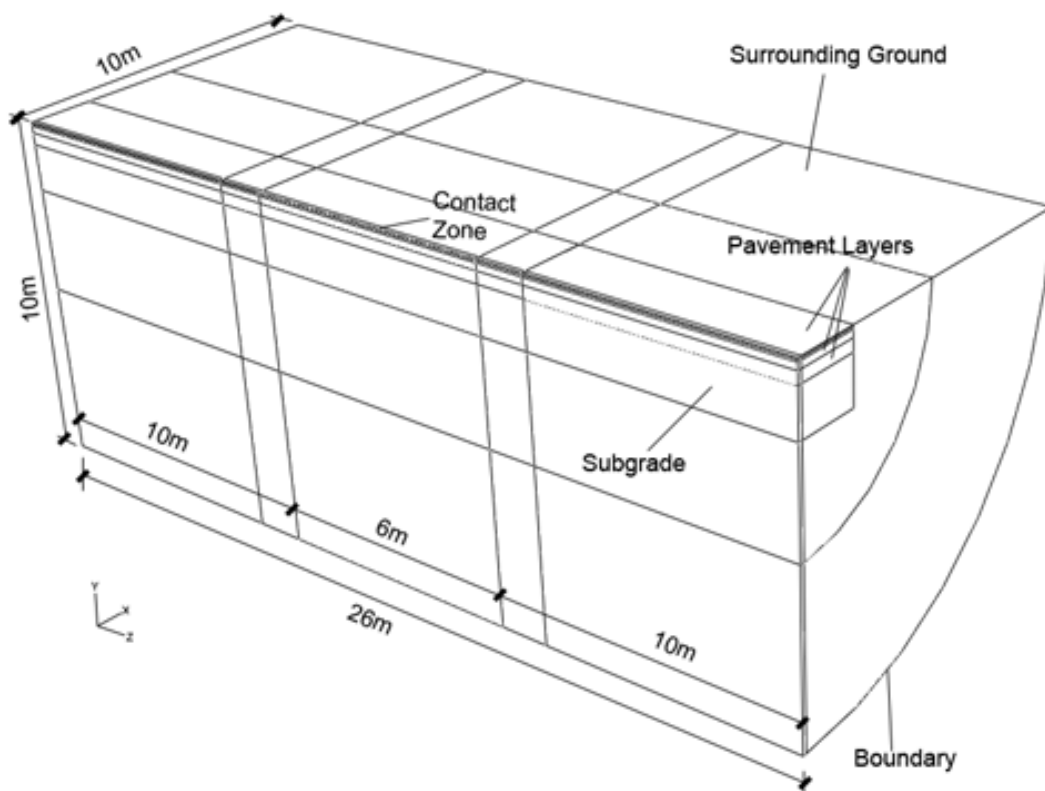


Figure 5-2 Dimensions of the FE model used to simulate TRL investigation

Chapter 5 Case Study – TRL Measurements

The first step of model building was to create a cross-section with a 2m by 2m pavement part and surrounding ground with a radius of 10m. Secondly, according to the structure of each pavement, the pavement part was divided into several layers. The surrounding ground has also been divided into two parts. The purpose of this step is to control the number of nodes and the element distribution in the surrounding ground. In order to exert the loading pressure accurately on the pavement, according to the ½ width of the tyre footprint, a partition of the contact zone has been built. The last step is to sweep the cross-section along the longitudinal direction over the total length of the model to create a 3D object. The cross section of the composite pavement model is plotted in Figure 5-3. The cross section of rigid and fully flexible pavements can be found in Appendix C.1.

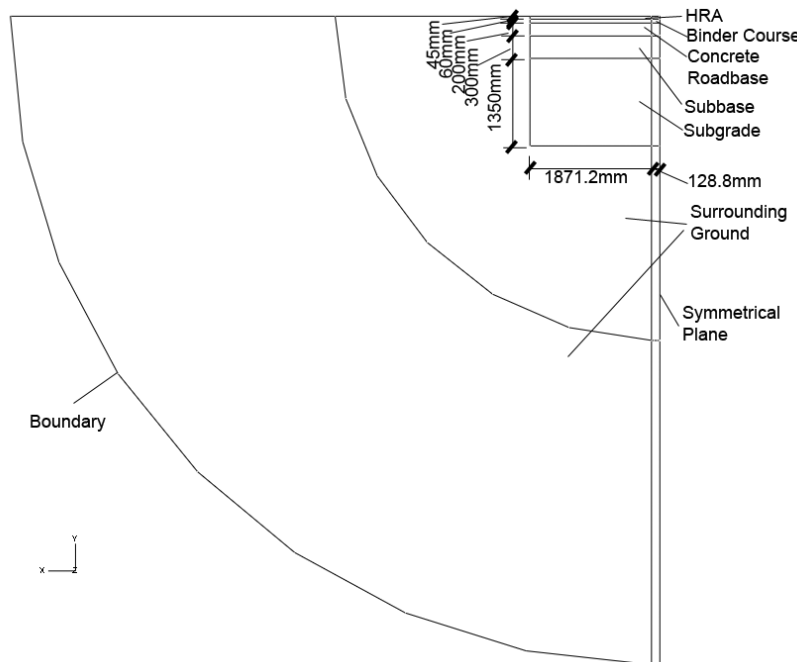


Figure 5-3 Profile of the model used for flexible composite pavement

A twenty-node quadratic element, C3D20R, was used to mesh the 3D models. In order to control the total amount of elements used for the

analyses, a dense mesh was applied in the central region of each model. This allows enough elements to be located in the contact zone. The mesh used for the composite pavement is plotted as Figure 5-4. Since the rigid and fully flexible pavements were meshed with the same C3D20R elements using the same method, the 3D mesh figures of the pavements are omitted. Nevertheless, it is still worth showing the mesh of each pavement in cross section, as shown in Figure 5-5.

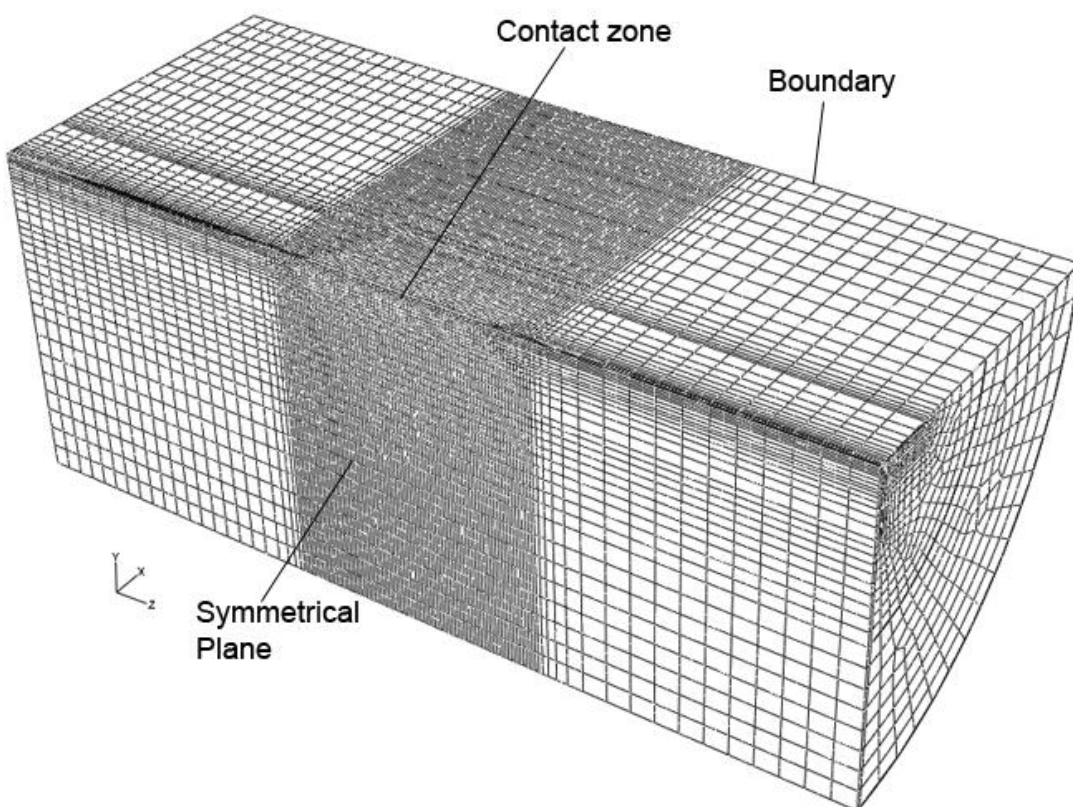


Figure 5-4 FE mesh of 3D model analyses, flexible composite pavement

To allow the time interval to be distributed uniformly along the contact zone and to control the accuracy of the FE analysis solution, the mesh at the contact zone has been built with uniform element dimensions; length 3cm, width 6.44cm. Thus, the contact zone of each 3D model presents as a 2-by-200 array.

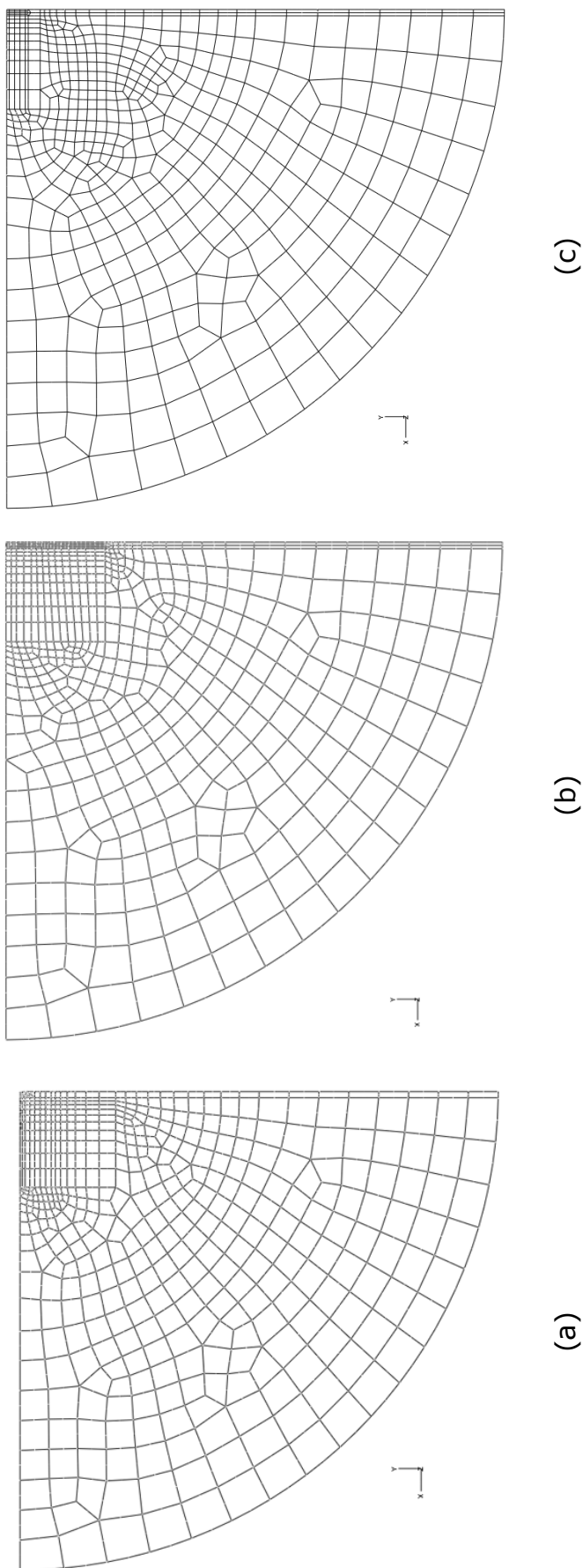


Figure 5-5 Mesh at cross section (a) flexible composite pavement (b) rigid pavement (c) fully flexible pavement

The TIML applied to each model has the same properties, containing 375 vertical pressures exerted at the contact zone. The journey of each analysis is 5.6250m. Thus, every pressure acts for 0.68 milliseconds since the velocity of the truck is 80km/h, and the total journey time is 253 milliseconds. Table 5-9 shows the dimensions used for the loaded area. Since the model is symmetrical, the length of the load contact area is 374.0mm which is equal to the length of the tyre footprint, and the width of the load contact area equals half of the width of the tyre footprint which is 128.8m.

Table 5-9 Dimension of tyre/pavement contact area

Load (kN)	Pressure (kPa)	Area (m ²)	Length (m)	Width (m)	½ Width (m)
78.6	816	0.0963	0.3740	0.2576	0.1288

VDBs have been used for the study. Depending on the area occupied by each boundary node, several sets of VDBs have been built. VDBs with high dashpot coefficient are located at the centre ($16m \leq z \leq 10m$) of the model, and VDBs with low dashpot coefficient are located at either end ($z < 10m$ and $z > 16m$).

5.3 Results

In order to check the capability of the FE models, 3 static FE analyses have been conducted. A static pressure 707kPa has been applied onto the models with a circular contact area of radius 0.15m.

Figure 5-6 shows vertical deflections calculated by BISAR and ABAQUS similarity and TRL's FWD test on their flexible composite pavement; Figure 5-7 shows these deflections for the rigid pavement and Figure 5-8 shows

these deflections for the fully flexible pavement. The results indicate that the deflections retrieved from the FE analysis are very close to these given by BISAR.

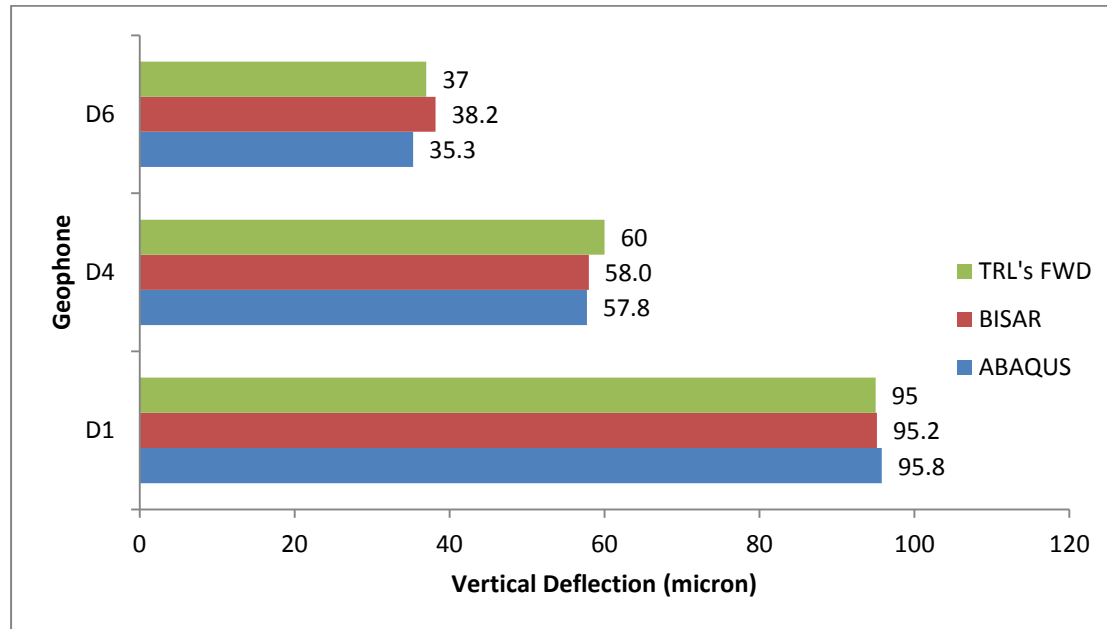


Figure 5-6 Deflections at D1, D4 and D6, flexible composite pavement

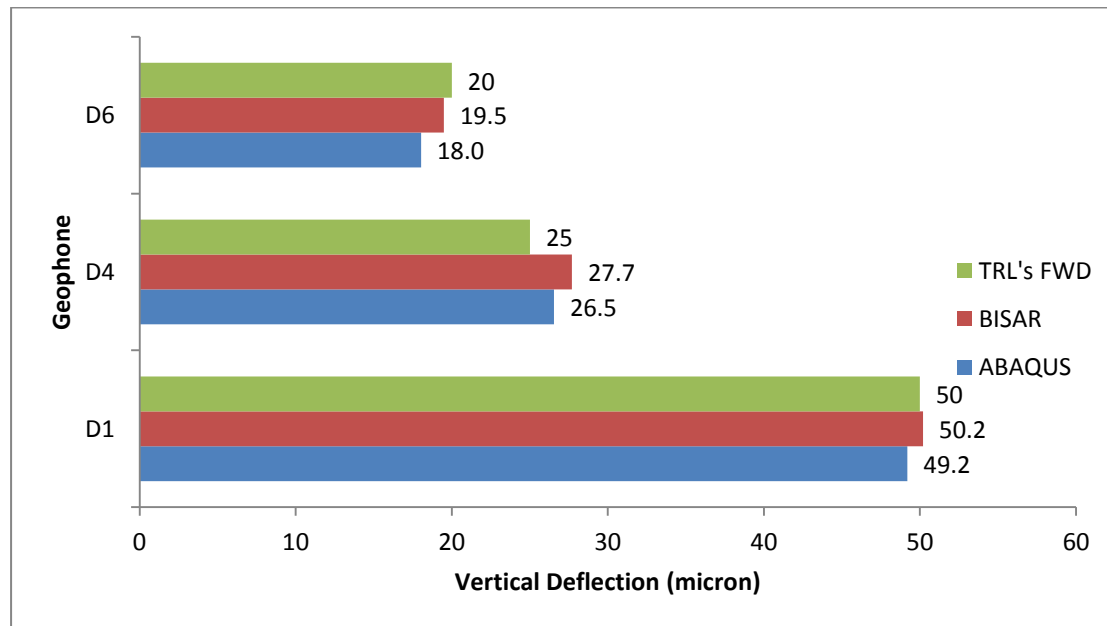


Figure 5-7 Deflections at D1, D4 and D6, rigid pavement

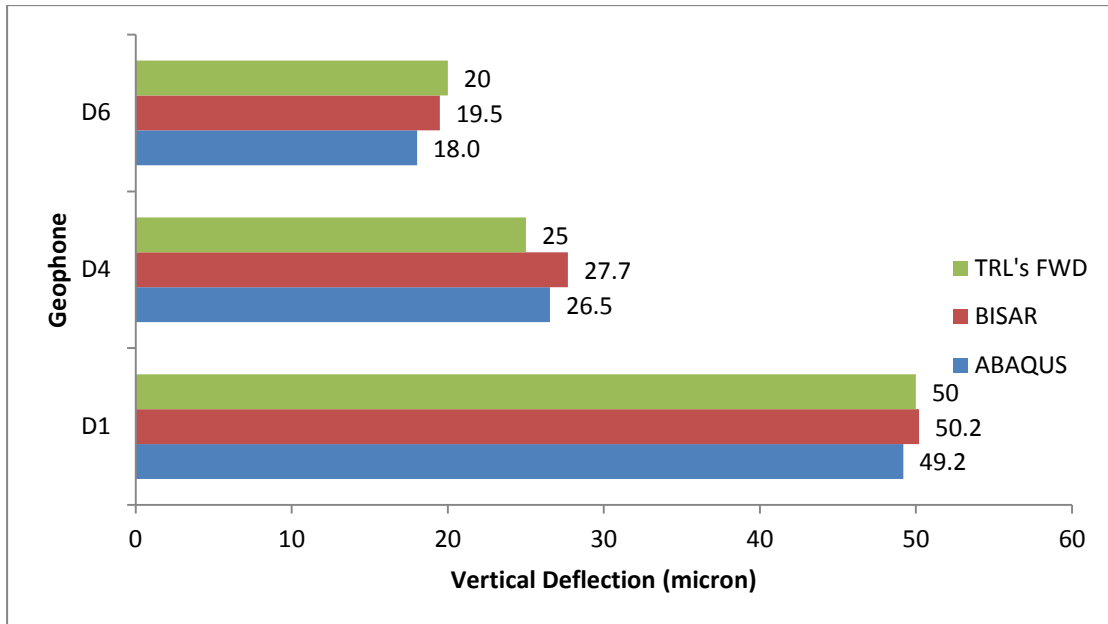


Figure 5-8 Deflections at D1, D4 and D6, fully flexible pavement

Appendix E shows example computed vertical deflections in the form of contour plots for 3 wheel positions for the case of rigid pavement. However, the parameter required in this study is the energy dissipated along the pavement (pavement resistance) and the unit is N or J/m. The pavement resistance can be calculated by using Equation 3-5 and corresponding deflection-time traces.

Figure 5-9 shows a deflection-time trace diagram retrieved from the three pavements at an observation points 5.61m from the start point. Thus, at a speed of 80km/h, this means that the tyre load reaches the observation point at 235.62 milliseconds and leaves at 252.45ms, as the length of tyre footprint is 0.374m. Using the deflection readings at these two points and the corresponding loading pressure of 816kPa and the width of the tyre footprint 0.2576m, the calculated values of pavement resistance are: 0.689N for the composite pavement, 0.639N for the rigid pavement and 0.948N for the fully flexible pavement.

Chapter 5 Case Study – TRL Measurements

For each pavement model, 10 observation points were used to collect deflection information. Table 5-10 shows the mean pavement resistance and maximum deflection for each model using the 10 sets of data.

In comparison with the mean deflections measured at D1 from TRL's FWD tests, each FE model shows a large value of deflection. This is because the vertical load applied by the FWD was 50kN and the corresponding pressure was 708kPa; however the load used for 3D model analyses was 78.6kN and the pressure was 816kP, which are significantly larger than the values used for the FWD test.

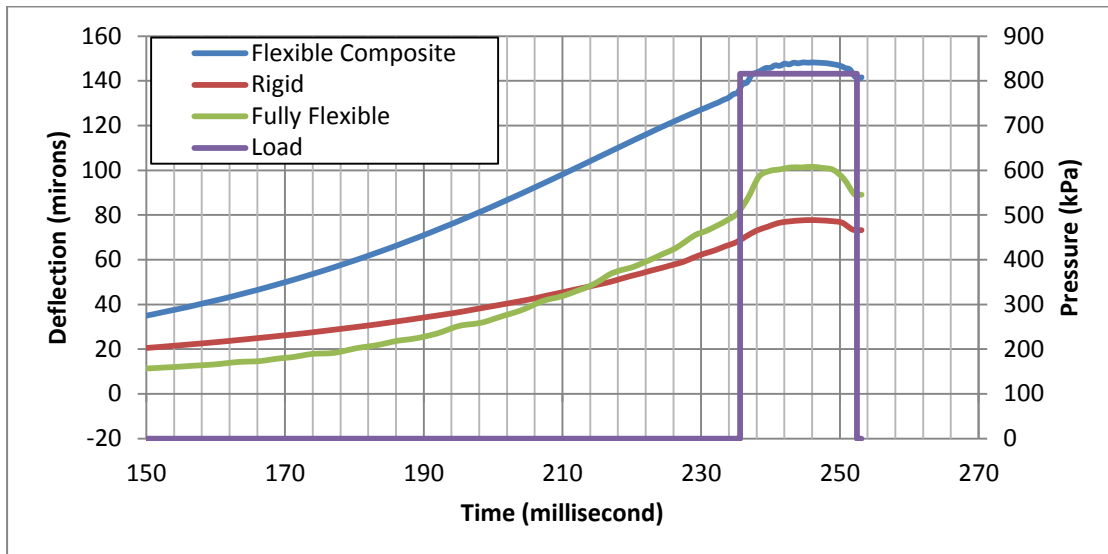


Figure 5-9 Deflections of observation points, offset is 5.61m

Table 5-10 Mean pavement resistance and maximum deflection

Model	Pavement Resistance (N)	Maximum deflection (micron)
Composite	0.796	148
Rigid	0.606	78
Fully flexible	0.791	102

The results also indicate that pavement stiffness affects energy dissipation although it is evident that there is no unique relationship between pavement resistance and maximum deflection. For example, comparing the rigid and fully flexible pavements, the results indicate that an increase of 24 microns in vertical deflection correspond to an increase of 30% in the energy dissipated in the pavement.

Since the details of the structural information along the length of the composite pavement are limited and an additional subbase layer has been added in the 3D FE model, the results from the composite pavement have been neglected in this comparison.

Figure 5-10 shows the data for fuel economy actually obtained by TRL and corresponding deflection at D1. The dashed trend line shows that there is no relationship between the stiffness and fuel consumption, considering the data retrieved from all pavement types. However, if the composite pavement section is discarded, a possible relationship can be found, although it must be recognized that other influences such as surface texture and pavement geometry will also have affected the results.

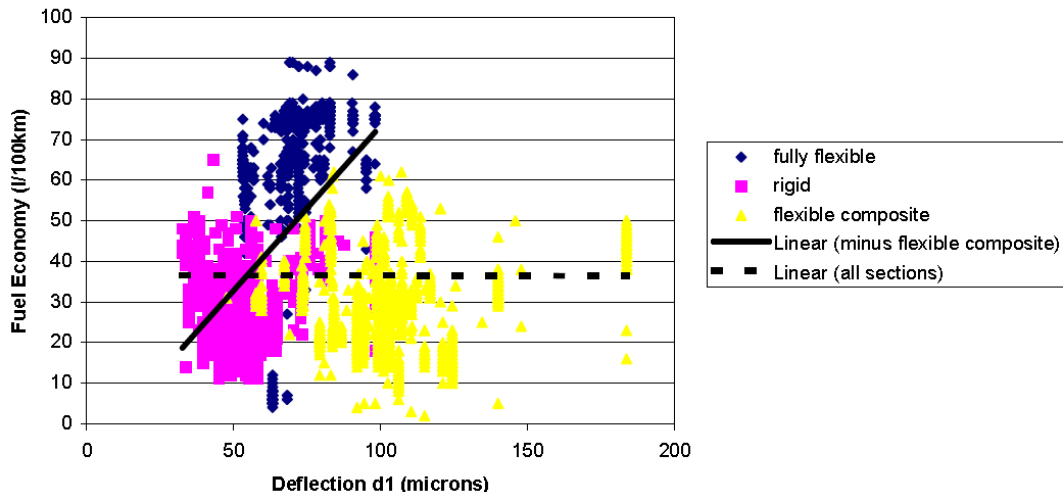


Figure 5-10 Stiffness influencing fuel economy (McKeown, 2002)

5.4 Summary

This chapter has introduced a case study using FE analysis to predict the energy dissipated in a pavement. Results of pavement resistance retrieved from the analyses indicate that pavement stiffness has a significant influence on energy dissipation; an increment of vertical deflection of 24 microns results in an additional energy consumption of 30%. The results from the TRL's measurements also gave a similar indication; with the level of deflection increased from 50 microns to 100 microns, the fuel economy increased by 112%.

Chapter 6

Asphalt Pavements

6.1 Problem description

To investigate the energy dissipated in the pavement layers and the subgrade, a 3D model has been built in ABAQUS 6.9. It assumes a typical 40-tonne 5-axle HGV driving at a constant speed on a section of asphalt pavement. A set of analyses has been applied by using the 3D model with varying factors: vehicle speed, vertical load and pavement stiffness.

The analyses focus on the energy lost per unit distance in each simulation, which is computed from deflection-time traces and tyre pressure.

The results retrieved from the analyses include the maximum deflection on the pavement surface and the influences of various factors on energy loss. Furthermore, a set of static calculations of vertical deflection using BISAR is also described in the results section.

6.2 Model Definition

The analyses presented here were undertaken in 3D using ABAQUS version 6.9. Figure 6-1 shows the model used in the analyses. The model is a combination of pavement layers and surrounding ground. A typical heavy duty asphalt structure has been modelled composed of an asphalt layer, a cement bound base, a cement-bound sub base and a subgrade.

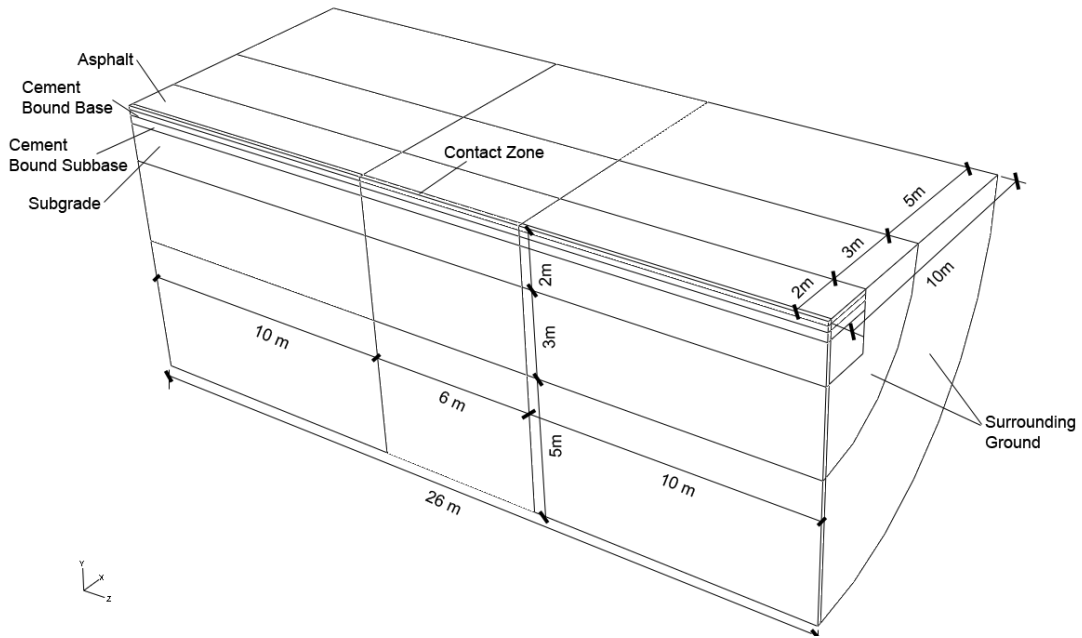


Figure 6-1 Parts and dimensions of asphalt pavement model

The total length of the model is 26m. A contact zone is located at the centre of the model with 6m length and 0.16m width. Since the model is symmetrical, the width of each pavement layer in the model is 2m. Thus, the real width of each pavement layer is 4m. The surrounding ground has been built around the pavement, and consists of two parts, controlling the location of meshing seeds. The boundary is located 10m away from the centre of the model.

For convenience the same pavement structure has been adopted as was assumed in Chapter 4 for FWD analysis. The thickness of each layer can be found in Figure 6-2. The asphalt layer thickness is 0.14m. The cement bound base layer has a thickness of 0.2m. For the cement bound subbase layer, the thickness is 0.3m. The thickness of subgrade is 1.36m. Thus the thickness of pavement layers is 2m. By using the partitioning method in ABAQUS, the contact zone has been built, with a width of 0.16m.

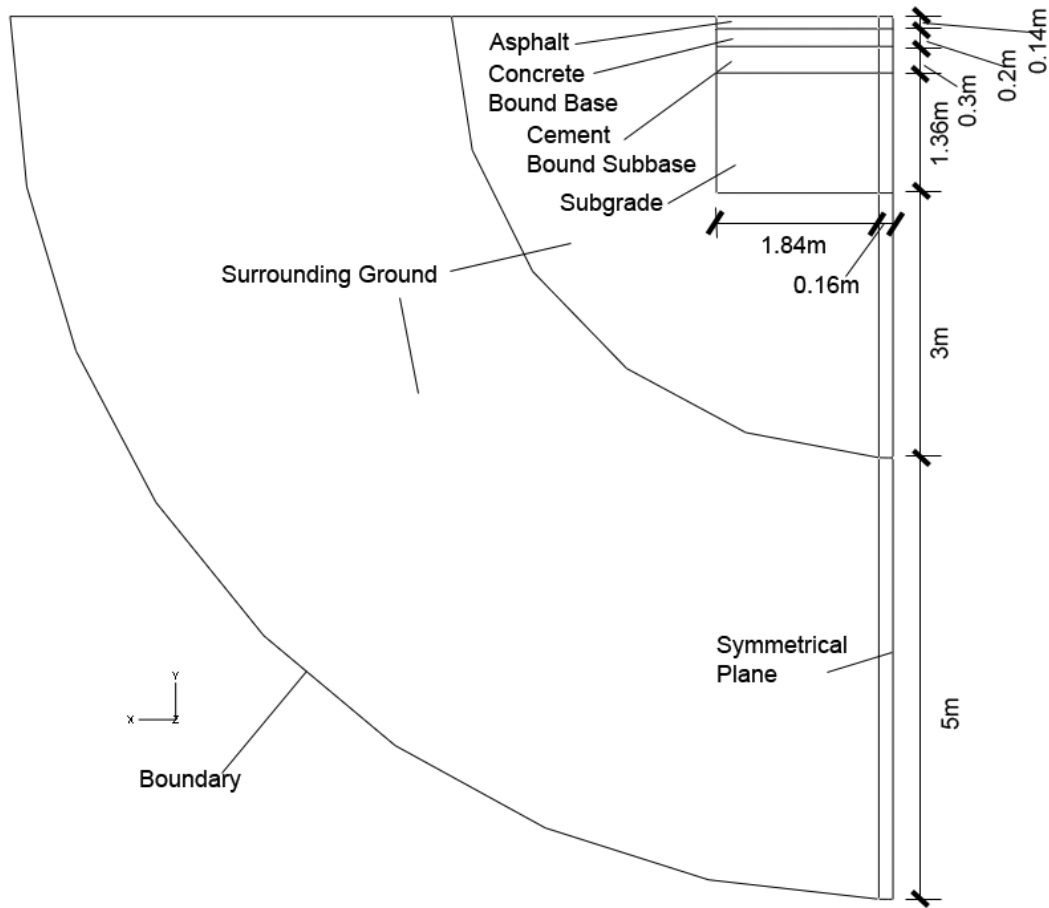


Figure 6-2 Profile of asphalt concrete model

Table 6-1 shows the material properties of the pavement layers and the surrounding ground. Other than the asphalt layer properties are as used in Chapter 4. The subgrade and surrounding ground have same material properties since they are both composed of soil. Typical material properties of the base and subbase layers have been used. The Young's modulus of the asphalt layer (E_1) has been varied to 6 levels: 1000, 3000, 5000, 7000, 9000 and 11000MPa. The lower modulus represents a low quality or a high ambient temperature, and the high modulus represents a good quality or a low ambient temperature. Furthermore variation in vehicle speed and therefore loading ratio would also lead to variation in asphalt modulus. Material damping has been applied in layers which are

composed of soil (subgrade and surrounding ground) to represent hysteresis.

Table 6-1 Material properties of each pavement layer

Layer	Young's Modulus (MPa)	Poisson's Ratio	Density (kg/m ³)	Damping	
				Alpha(s)	Beta(1/s)
Asphalt	E1	0.35	2400	0	0
Base	7000	0.35	2400	0	0
Subbase	2400	0.25	2000	0	0
Subgrade	90	0.3	1800	100	0.02
Surrounding ground	90	0.3	1800	100	0.02

Figure 6-3 shows the mesh for the whole model, which is composed of 68060 elements. It includes 34928 C3D20R (20-node quadratic brick solid element) and 33132 dashpots (Dashpot1). In order to achieve an accurate solution, it has to include enough elements at the contact zone. Thus, every element located at the contact zone was controlled to a 30mm×32mm×140mm (width × length × height) cuboid and the longitudinal distance between two neighbouring nodes at the contact zone is 15mm. This allows enough elements and nodes to capture the dynamic motion of the pavement and give an accurate solution.

A very fine mesh has been created in the x-z plane and the mesh in the z-y plane has not been refined due to the limitation of total element numbers and the computational ability of the hardware.

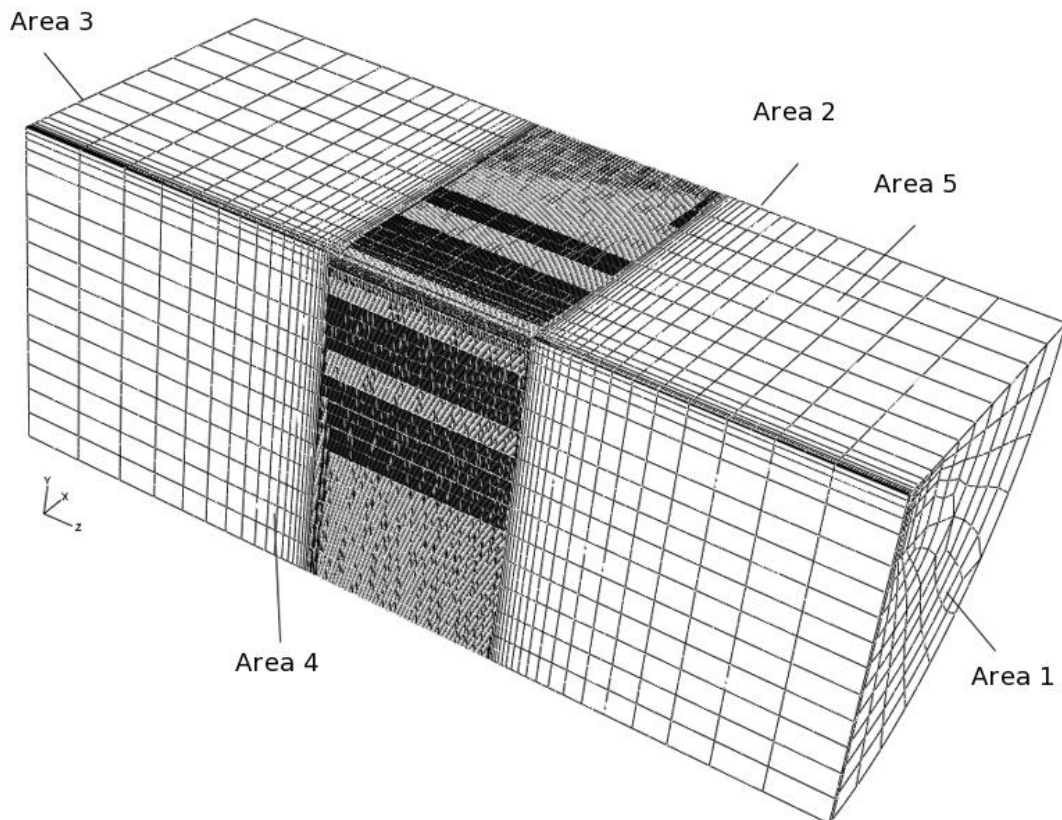


Figure 6-3 Mesh of asphalt concrete pavement model

Figure 6-4 shows mesh at the symmetrical plane.

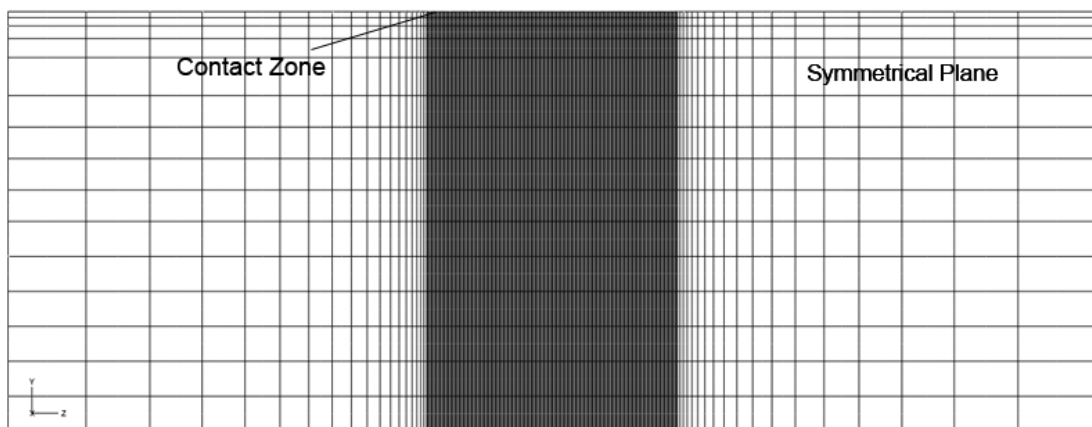


Figure 6-4 Mesh on Area 1 of asphalt concrete pavement model

Figure 6-5 shows the mesh at the top surface.

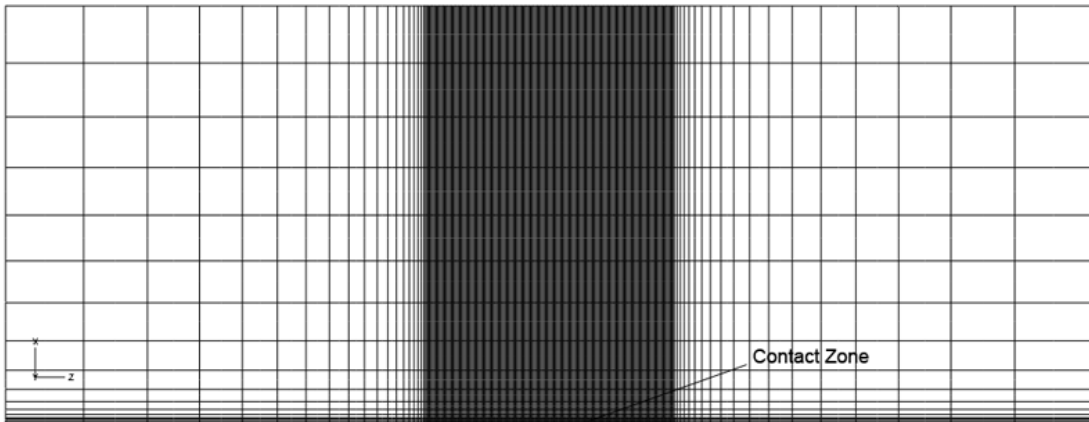


Figure 6-5 Mesh on Area 3 of asphalt concrete pavement model

Figure 6-6 shows the mesh in cross section.

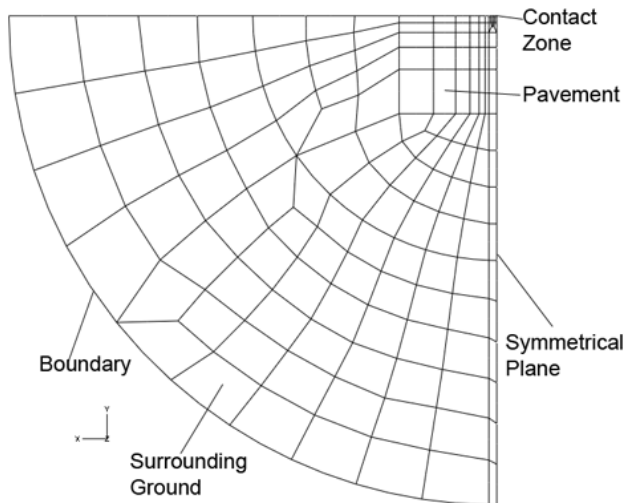


Figure 6-6 Mesh on Area 2 of asphalt concrete pavement model

6.3 Boundary Conditions

Table 6-2 presents the boundary conditions of the model. Area 1 is a symmetrical plane. Nodes at Area 2 and Area 5 are horizontally restrained. A viscous damping boundary is used at Area 4.

Table 6-2 Illustrations of boundary conditions as shown in Figure 6-3

Area	Boundary Condition
Area 1	Movement on z direction is restrained, x and y directions are free.
Area 2	Viscous damping boundary is applied.
Area 3	Same as Area 1
Area 4	A symmetrical boundary toward x-axis is applied.
Area 5	There are no boundary conditions (free surface).

Figure 6-7 shows the mesh at the boundary. 3 sets of VDBs have been applied on the boundary according the area size and related number of nodes. For the area of VDB-1 and VDB-3, the number of nodes is 630 and each node occupies 2493cm^2 on average. For the area of VDB-2, the number of nodes is 7023 and each node occupies 134 cm^2 on average. Table 6-3 gives dashpot coefficients used in VDBs.

Table 6-3 VDB configuration of asphalt concrete pavement model

	Dashpot Coefficient (N·s/m)	
	Primary (c_p)	Secondary (c_s)
VDB-1	1.16×10^5	6.22×10^4
VDB-2	6.20×10^3	3.35×10^3
VDB-3	1.16×10^5	6.22×10^4

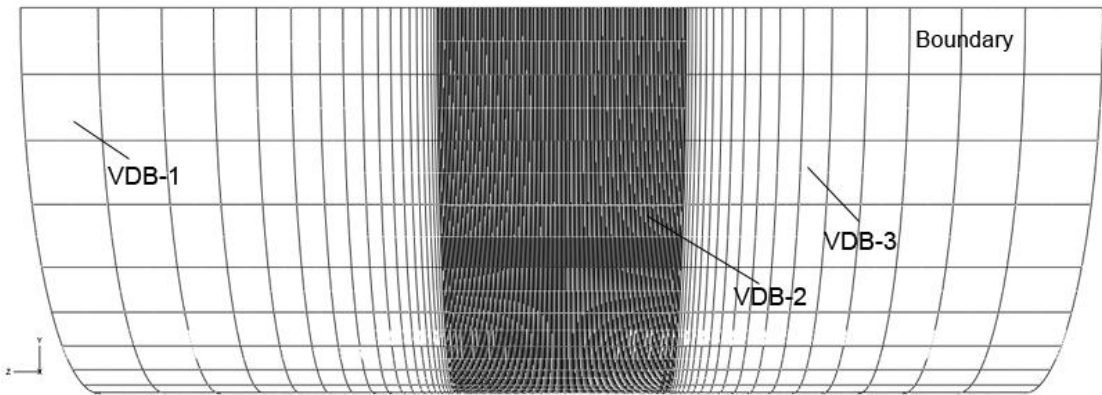


Figure 6-7 Mesh on Area 4 of asphalt concrete pavement model

6.4 Loading

According to the principles of the research, which are mentioned in Chapter 3.1.4, three load levels have been used for the analysis. The related dimensions of the tyre footprint can be found in the Table 3-2.

The longitudinal speed of the tyre has been varied as: 30, 50, 80, 100, 130, 160 and 190km/h. The speed levels cover a wide range of driving; city driving (30km/h), urban driving (50 to 100km/h), motorway driving (100 to 130km/h) and ultra-high speed driving (160 to 190km/h).

6.5 Solution Controls

Since the 3D model has numerous elements and nodes, thus, an abundance of variables have been generated in the numerical mode. To decrease the computational time required for the analyses, a quasi-Newton solution technique has been used in the simulation. A comparison at the model verification stage indicated that the quasi-Newton method gives the same results as the full Newton method, as regards on energy dissipation.

The parameters have been varied can be found as follows:

Table 6-4 Parameters has been varied for the asphalt pavement

Parameter	Value
Stiffness of asphalt (MPa)	1000, 3000, 5000, 7000, 9000, 11000
Speed (km/h)	30, 50, 80, 100, 130, 160, 190
Vertical load (kN)	40, 50, 60

6.6 Results

Results presented in this section include the deflections computed using BISAR, the maximum deflection retrieved from the FE model and pavement resistance of each FE simulation. Appendix E also includes 3 examples contour plots of vertical deflection under 3 different load positions.

6.6.1 Vertical deflection

A set of computations was carried out using BISAR to derive deflections at the surface of the pavement with varying top layer stiffness (1000 to 11000MPa) and vertical load (40, 50 and 60kN). The model used had the same configuration as the 3D model used in FE analyses, as shown in Table 6-1. Figure 6-8 shows vertical deflections calculated by BISAR. A logarithmic was deemed appropriate suit this generalised a near straight line relationship. Comparison between static analysis using BISAR and dynamic analysis using ABAQUS at 30km/h gives added confirmation to the FE computations.

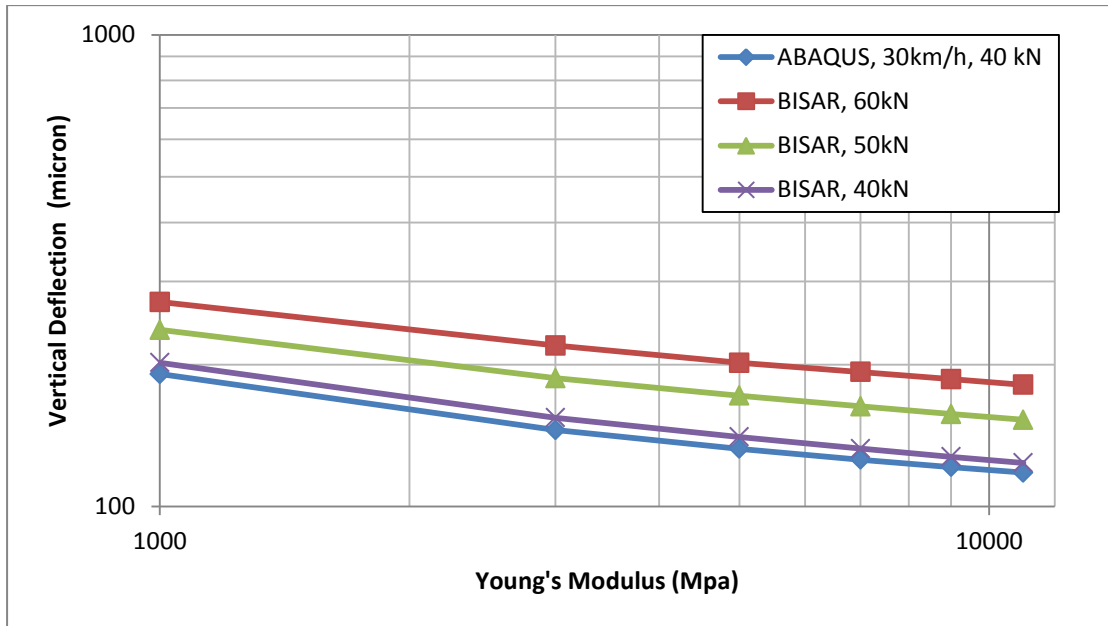


Figure 6-8 Deflection at P1, asphalt concrete pavement

Figure 6-9 shows the vertical deflections at the contact zone retrieved from the FE analyses when the vertical load of the tyre equals 40kN. The results when the vertical load equals 50 and 60kN can be found in Appendix B.2.

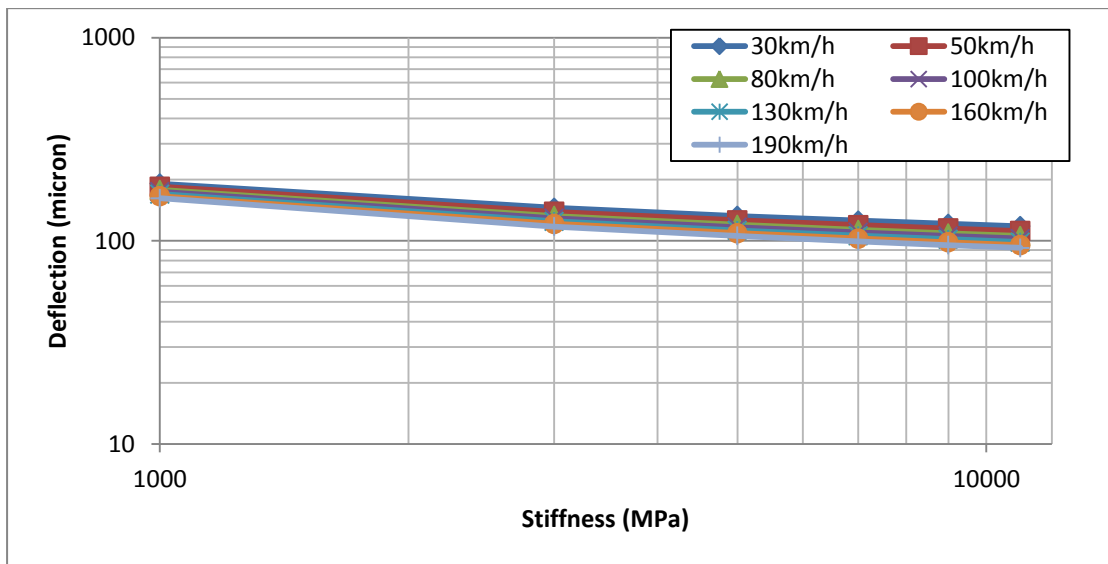


Figure 6-9 Deflection vs. stiffness, $L_v=40\text{kN}$, asphalt concrete

Firstly, the results imply that the influence of the stiffness of the asphalt layer on deflection follows a power law.

Secondly, the speed effect is minor in all cases. Results indicate that increasing speed by 10km/h leads to an average reduction of 1.61 microns of deflection at all speed levels when the load equals 40kN. The reduction 2.29 microns when the load is equal to 50kN and will be 2.59 microns when the load is 60kN.

Finally, the deflections retrieved from the FE analyses are similar to the results from the BISAR calculation. However the moving load acts on each element at the pavement surface over a relatively short time such that before the deflection can reach its maximum static value, the load had moved forward. Thus, the faster the speed, the shorter the action time, and a shorter action time leads to a smaller deflection. For instance, in the case when load=40kN and $E_1=1000\text{ MPa}$, BISAR shows the deflection equals 202 microns. The FE model with similar conditions shows the deflection is 191 microns at 30km/h, and it is 161 microns at 190km/h.

6.6.2 Speed influencing energy dissipation

Figure 6-10 shows results collected from the FE analysis where the vertical load equals 40kN. As can be seen, the curves plotted in the figure are approximately linear. The pavement resistance increases with increasing speed. It is also noted that the effect of speed is minor.

However when the influence of loading rate on asphalt modulus is taken into account, for example using the predictive equation given by Ullidtz (1979), it is found that pavement resistance is predicted to be almost independent of vehicle speed.

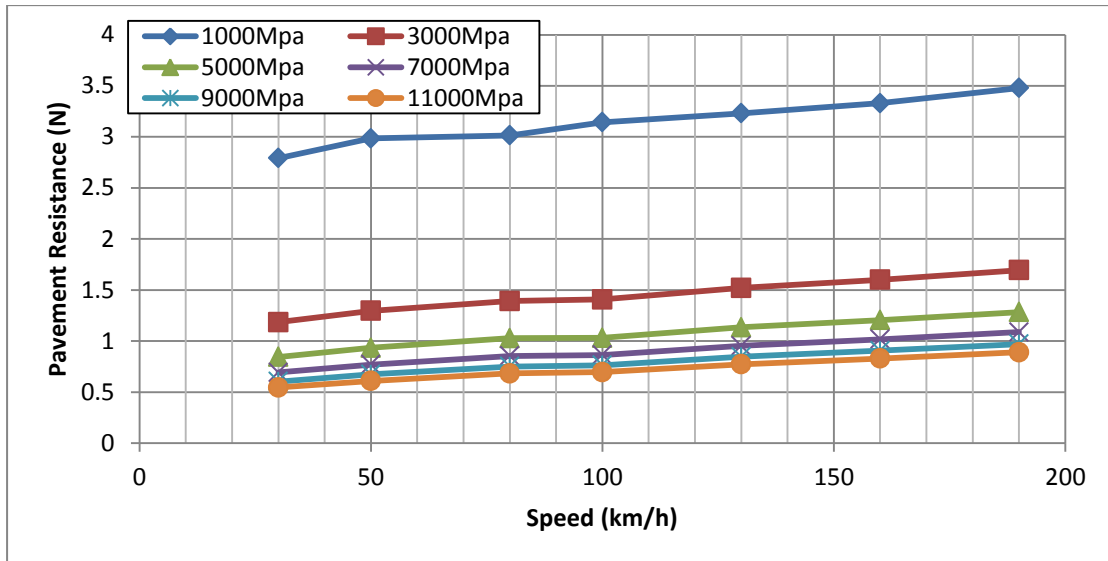


Figure 6-10 PR vs. speed, $L_v = 40\text{kN}$, asphalt concrete

For example, following the approximate formula given by Ullidtz (1979) as follows:

$$E = 1.157 \times 10^{-7} \times t^{-0.368} \times 2.718^{-PI} \times (SP - T)^{-5},$$

where: t is the load pulse duration,

PI is the Penetration Index of the bitumen,

SP is the softening point of the bitumen,

T is the temperature,

E is the stiffness of asphalt.

Thus, the ratio of the speed-influenced stiffnesses is:

$$n_s = \frac{E_2}{E_1} = \left(\frac{t_2}{t_1} \right)^{-0.368} = \left(\frac{v_2}{v_1} \right)^{-0.368}$$

where: v_1 and v_2 are velocities.

If the initial stiffness (E_1) is 3000MPa at 30km/h (v_1), and the speed was increased to 190km/h (v_2), the final stiffness (E_2) would become approximately 5917MPa. According to the data shown in Figure 6-10, the pavement resistance (PR) is 1.2N, when the speed is 190km/h and the stiffness is 6000MPa, which is the same as the pavement resistance when the speed is 30km/h and the stiffness is 3000MPa. Figure 6-11 shows the calibrated PRs according to the data collected whereas the vertical load equals 40kN. The calibrated PRs with other vertical loads (50kN and 60kN) can be found Figure 6-12 and Figure 6-13

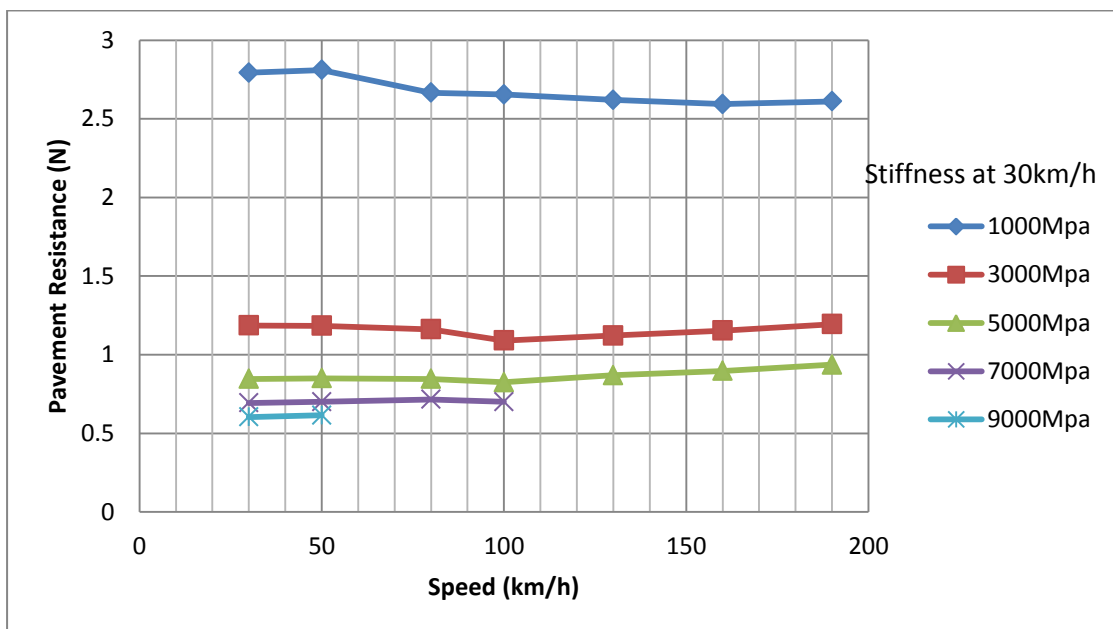


Figure 6-11 PRs with speed-influenced stiffnesses, $L_v=40\text{kN}$, asphalt concrete

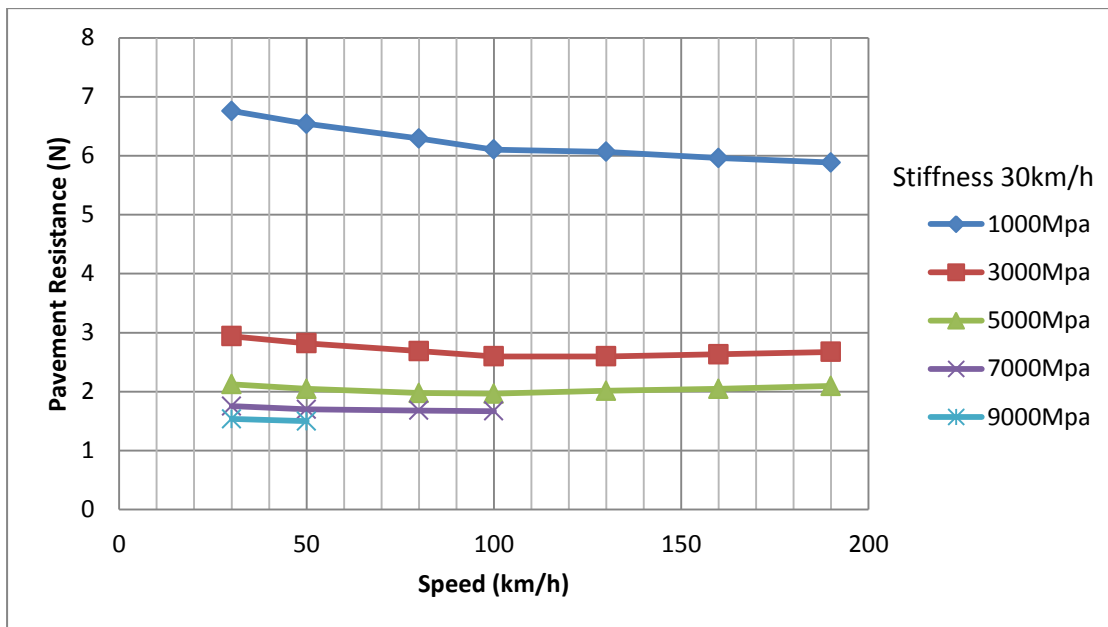


Figure 6-12 PRs with speed-influenced stiffnesses, $L_v=50\text{kN}$, asphalt concrete

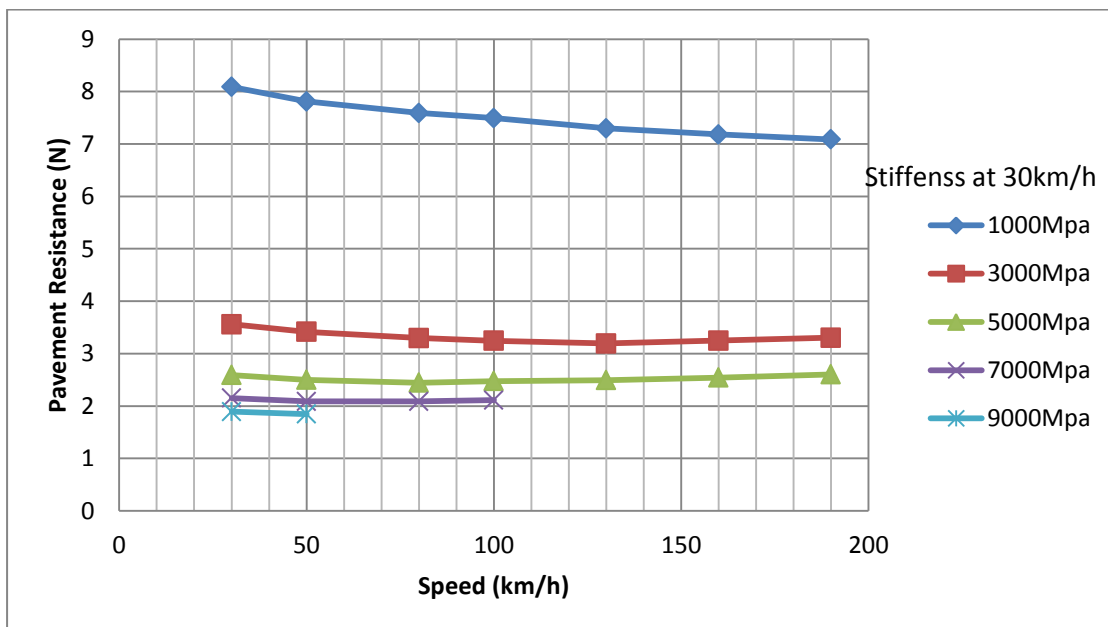


Figure 6-13 PRs with speed-influenced stiffnesses, $L_v=60\text{kN}$, asphalt concrete

6.6.3 Stiffness influencing energy dissipation

Figure 6-14 shows the influence of top layer stiffness on pavement resistance with varied speed when the load equals 40kN. Figure 6-15 and Figure 6-16 show similar results when the load equals 50 and 60kN.

The three figures indicate that stiffness has a significant effect on pavement resistance and energy dissipation. The pavement resistance reduces with increasing stiffness, i.e. a stiffer pavement saves energy. If the effect of speed is neglected, trend lines can be plotted as shown in the figures for each load case. Each trend line can be reduced to a numerical equation using a format such as $PR = aE^{-b}$, where PR is the pavement resistance, E is the Young's Modulus, a and b are constants. Equation 6-1 shows the results.

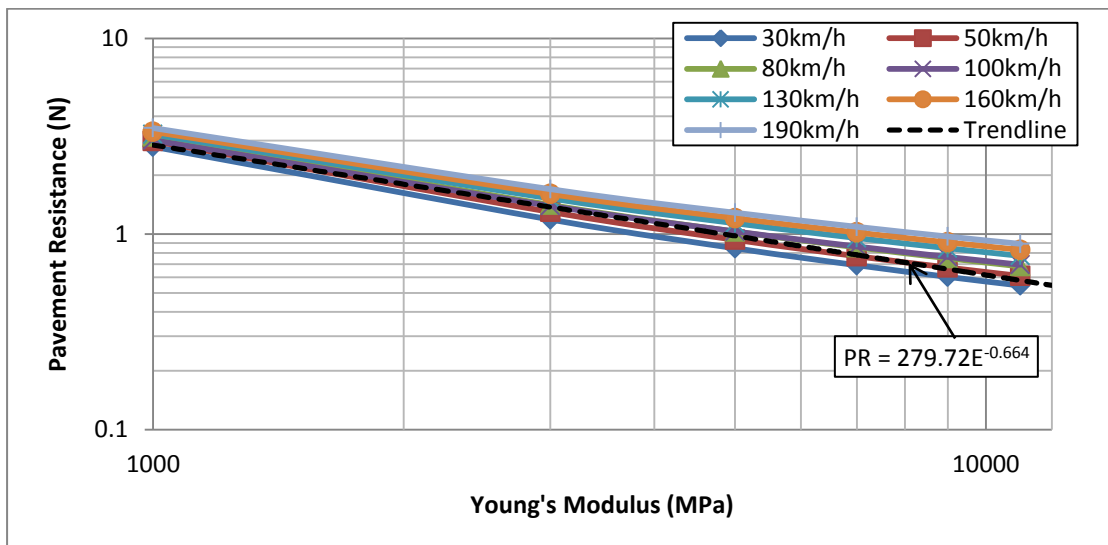


Figure 6-14 PR vs. stiffness, $L_v=40\text{kN}$, asphalt concrete

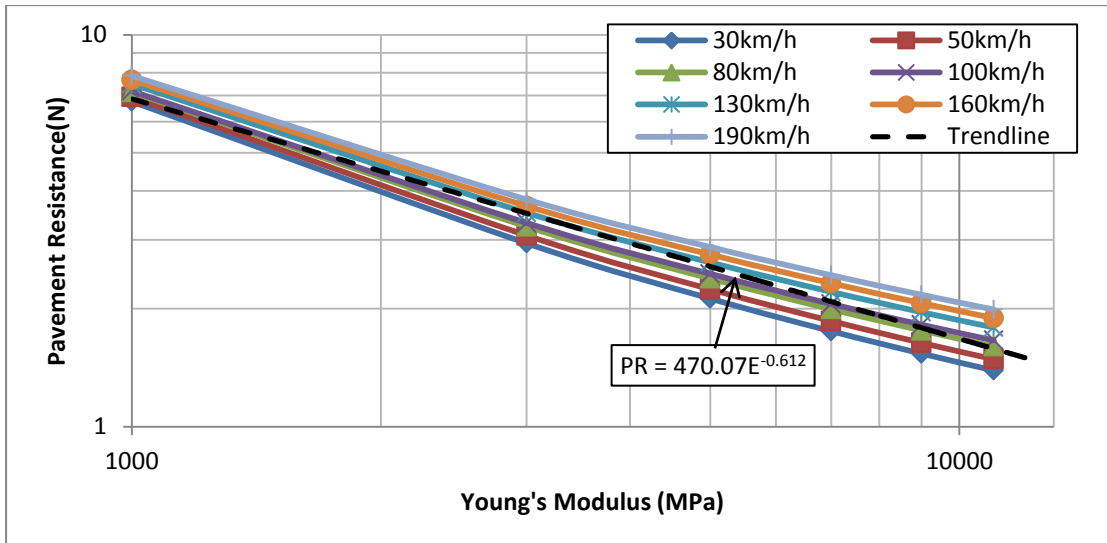


Figure 6-15 PR vs. stiffness, $L_v=50\text{kN}$, asphalt concrete

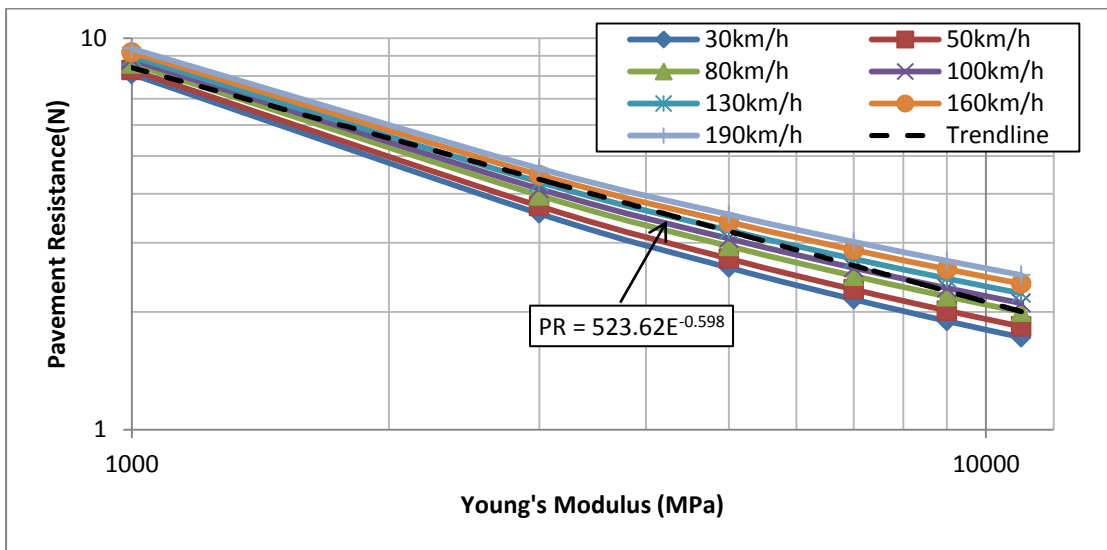


Figure 6-16 PR vs. stiffness, $L_v=60\text{kN}$, asphalt concrete

$$PR = 279.72E^{-0.664} \quad \text{when } L_v = 40\text{kN}$$

$$PR = 470.07E^{-0.612} \quad \text{when } L_v = 50\text{kN}$$

$$PR = 523.62E^{-0.598} \quad \text{when } L_v = 60\text{kN}$$

6-1

6.6.4 Load influencing energy dissipation

Figure 6-17 shows PRs obtained when the load equals 40, 50 and 60kN with varied speed assuming a stiffness of the top layer equal to 1000MPa. Figure 6-18 and Figure 6-19 also show similar results when stiffness is 5000MPa and 11000MPa. The results show that vertical load has an

obvious effect on the PR, and the effect can be expressed as a polynomial function.

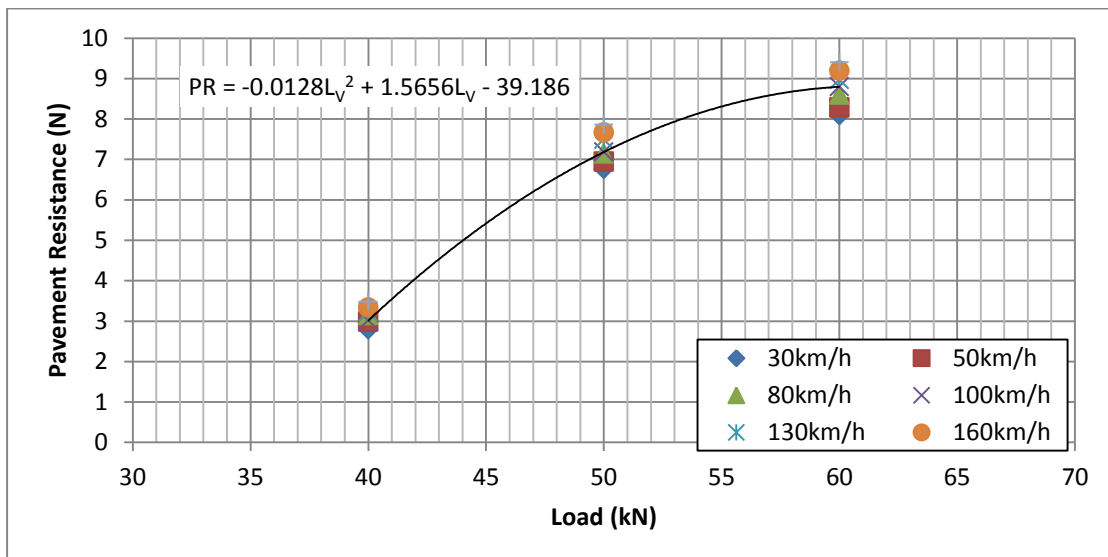


Figure 6-17 PR vs. Load, stiffness=1000MPa, asphalt concrete

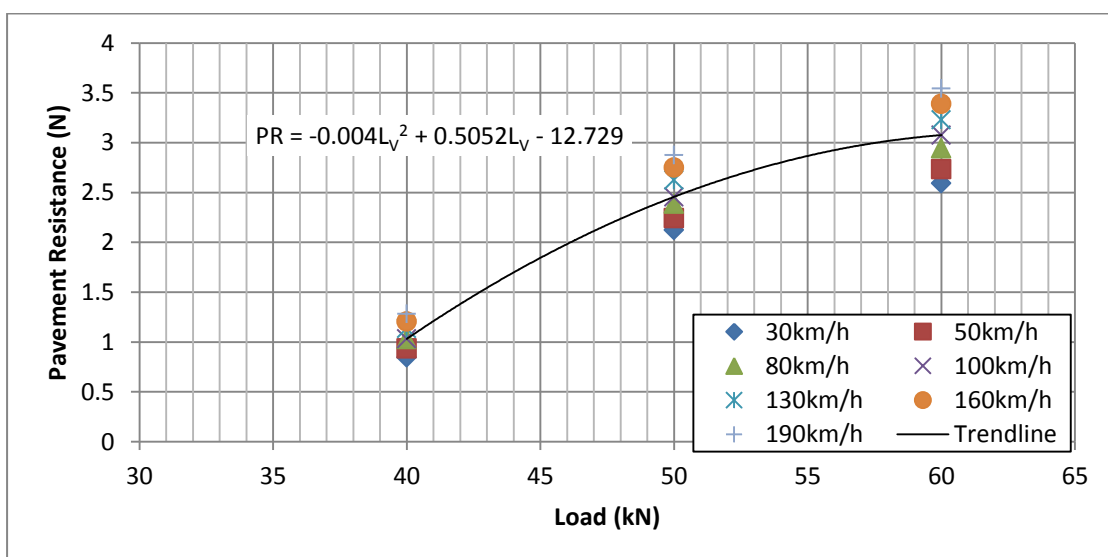


Figure 6-18 PR vs. Load, stiffness=5000MPa, asphalt concrete

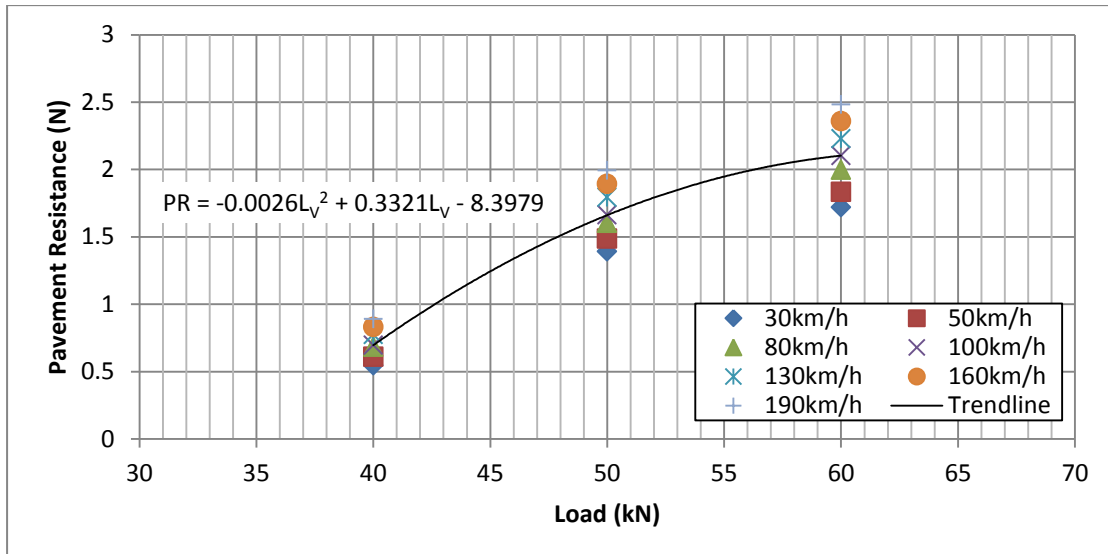


Figure 6-19 PR vs. Load, stiffness=11000MPa, asphalt concrete

6.7 Summary

The results of a series of linear elastic three-dimensional dynamic analyses to investigate the energy dissipated in pavement layers have been presented. The results show that:

- The influence of speed on PR is negligible once the effect of speed on asphalt modulus is included.
- The effect of pavement stiffness is significant and follows a power law. Results indicate that a stiffer pavement dissipates less energy than a low stiffness pavement. Comparing PR retrieved from the pavements with 11000MPa and 1000MPa top layer stiffness, the difference is not more than 10N.
- The results show that vertical load has an obvious effect on the PR, and the effect can be expressed as a polynomial function.

The results will be discussed further in Chapter 9.

Chapter 7

Low Quality Pavements

7.1 Introduction

There are large numbers of low quality pavements in urban road networks. Design standards and costs limit the quality of the pavements to a relatively low level. This chapter will present a set of FE analyses of low quality pavements in relation to energy consumption. The analyses focus on the vertical deflection at the tyre/pavement contact zone which is generated by a moving tyre load. A viscous damping boundary has been used in the analyses to simulate semi-infinite subgrade.

A 3D model has been used for the analyses. In order to exert load on the pavement surface accurately, the width of the contact zone has been generated according to the $\frac{1}{2}$ width of the tyre footprint.

The material properties of the pavement have also been used a BISAR calculation. This can be compared to FE modelling with similar stiffness properties. In the FE analyses material damping is also used to reduce oscillation and damp energy waves.

The results are presented in the form of energy dissipated per unit distance calculated by varying the vertical load, the top layer stiffness and the vehicle speed.

7.2 Model Definition

The analyses reported here are based on a 3D FE model. The pavement used for the analyses has 3 layers; a 150mm asphalt surface course (layer 1) 300mm aggregate base course (layer 2) and a subgrade (layer 3). The subgrade layer is combined into the surrounding ground, since the material properties are the same. Therefore, only surrounding ground with a 10m radius is created. The plot of the cross section can be found in Appendix C.

The load applied for the analysis is the same as in Chapter 6, the tyre inflation pressure (P_t) is a constant which is equal to 552kPa and the vertical load (L_v) is varied as 40, 50 and 60kN. Thus dimensions of the tyre footprint are given in Table 3.2.

Table 7-1 gives the material properties used for analyses. Young's modulus and Poisson's ratio are used to represent linear elastic behaviours; density is used as well to generate inertia force. Alpha damping is applied in the subgrade layer (surrounding ground) to damp energy waves.

Table 7-1 Material properties for low quality pavements

Layer	Name	Young's Modulus (MPa)	Poisson's Ratio	Density (kg/m ³)	Damping	
					Alpha (s)	Beta (1/s)
1	Asphalt	E1	0.35	2400	0	0
2	Aggregate	200	0.35	2400	0	0
3	Subgrade	90	0.3	1800	100	0.02

In order to assess the influence of pavement stiffness on energy dissipation, Young's modulus (E_1) of the asphalt in layer 1 has been varied as 500, 1000, 1500, 2000, 2500 MPa. A small modulus represents a situation in which the pavement is under a high ambient temperature or has been damaged. A high modulus means that the structural quality of the pavement is at an acceptable level.

The start condition for each simulation is that a static load has been applied to the start point of the 6m contact zone. Then, the load patch is time-stepped moving forwards, generating pressure waves. For the FE analyses, the load patch has been transformed to a set of vertical pressures as introduced in Chapter 3. The load levels and the dimensions of the footprint have been given in Table 3-2.

The parameters have been varied are follows:

Table 7-2 Parameters have been varied for the low quality pavement

Parameter	Value
Stiffness of asphalt (MPa)	500, 1000, 1500, 2000, 2500
Speed (km/h)	30, 50, 80, 100, 160
Vertical load (kN)	40, 50, 60

The viscous damping boundary is used as the boundary condition for the analyses. The dashpot coefficient of every single VDB is controlled by the related boundary area and stiffness of the material composing surrounding ground or subgrade. In order to retrieve accurate values of the dashpot coefficient, 3 sets of VDBs have been applied on the boundary, as shown

in Figure 7-1. VDB-1 is located in the area with a fine mesh. VDB-2 and VDB-3 are built on the area with a coarse mesh.

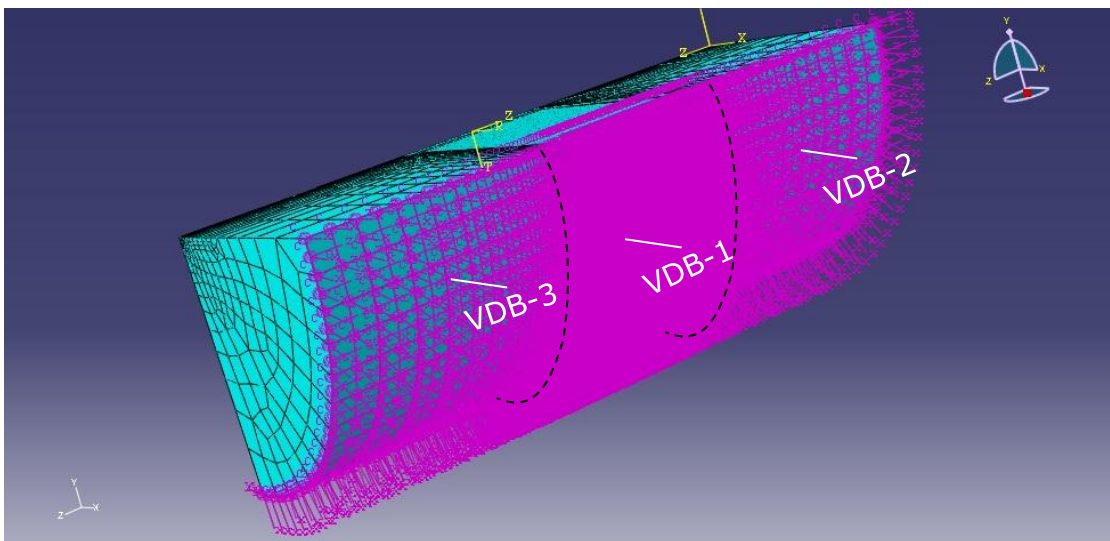


Figure 7-1 VDBs on pavement boundary

Since material comprising the surrounding ground is homogeneous, the stiffness used to calculate the dashpot coefficient of every VDB is the same; the dashpot coefficient therefore only varies with the area associated to VDB node relates to.

For VDB-1, since the nodes are uniformly distributed, the area used to calculate the dashpot coefficient equals the total area divided by the number of nodes.

Table 7-3 shows VDB configurations used for the analyses, which are calculated by using Equations 2-14 and 2-15.

Table 7-3 VDB configuration for low quality pavement

Load (kN)	Set	Nodes	Area (m ²)	Dashpot Coefficient (N·s/m)	
				Primary (c_p)	Secondary (c_s)
40	VDB-1	8227	94	5.34×10^3	2.86×10^3
	VDB-2	738	157	9.94×10^4	5.31×10^4
	VDB-3	738	157	9.94×10^4	5.31×10^4
50	VDB-1	8227	94	5.34×10^3	2.86×10^3
	VDB-2	765	157	9.59×10^4	5.13×10^4
	VDB-3	765	157	9.59×10^4	5.13×10^4
60	VDB-1	8227	94	5.34×10^3	2.86×10^3
	VDB-2	765	157	9.59×10^4	5.13×10^4
	VDB-3	765	157	9.59×10^4	5.13×10^4

7.3 Results

7.3.1 Vertical deflections

Example contour plots are shown in Appendix E, where it is observed that the zone effected by the load is much smaller for these types of pavement compared to those in Chapters 5 and 6 due to much reduced pavement stiffness.

In order to assess the solutions given by the FE analyses and evaluate the characteristics of each model, a BISAR calculation has been applied to calculate the static vertical deflection of the pavement.

The parameters used for the BISAR calculations are the same as for the FE analyses. The loads used for the calculation have the same levels as in the FE analyses; the pressure is kept as a constant 552kPa and vertical load varied as 40, 50 and 60kN. The Young's modulus of each pavement layer

used can be found in Table 7-1. The Young's modulus (E_1) used for layer 1 has also been varied in the same manner in BISA and FE.

The results from the BISAR calculation are the vertical deflections under the load at the centre of the area of the applied pressure. Thus, the deflections represent the characteristic stiffness of the pavement.

Figure 7-2 shows deflections retrieved from the BISAR calculations. The relationship between deflection and the stiffness E_1 follows a power law. The maximum deflection 899.7 microns was calculated under the maximum load 60kN and the lowest stiffness 500MPa. The minimum deflection was 441.1 microns, with a load of 40kN and the stiffness of 2500MPa. A stiffness increase from 500MPa to 2500MPa brings a decrease in deflection of about 34% when the load is 40kN and 30% when the load is 60kN.

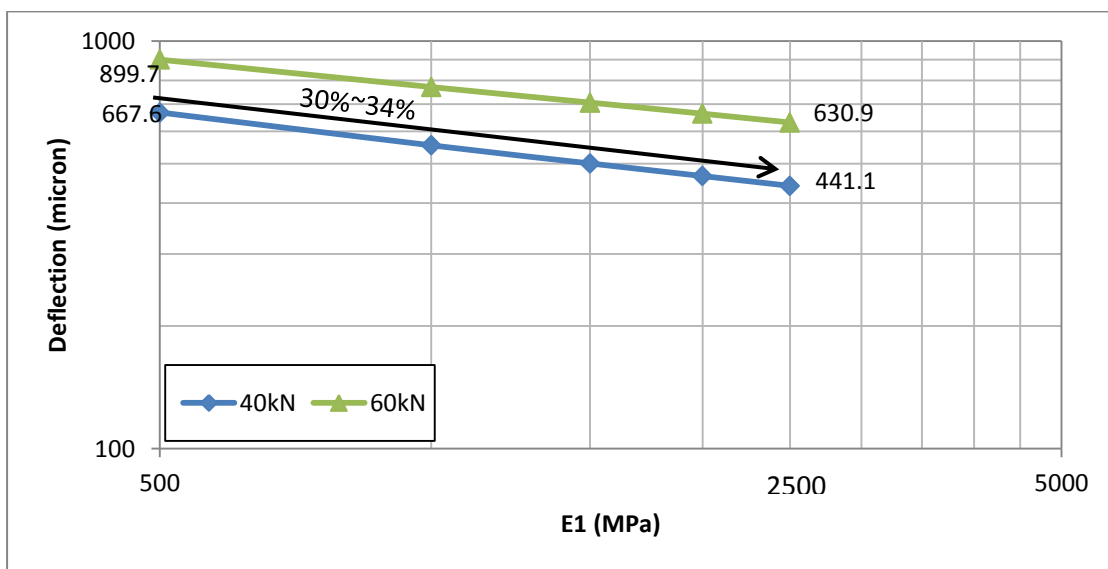


Figure 7-2 Deflection vs. upper layer stiffness, BISAR

Results from the FE analyses, as shown in Figure 7-3, show that the maximum deflection is 895.4 microns at a speed of 30km/h. It is similar

to the BISAR result. The minimum deflection retrieved with a load of 40kN and a stiffness of 2500MPa is 424.2 microns. This is similar to the BISAR result as well. As the stiffness increases from 500MPa to 2500MPa this brings a decrease in deflection of about 33% with a load of 40kN and 29% with a load of 60kN.

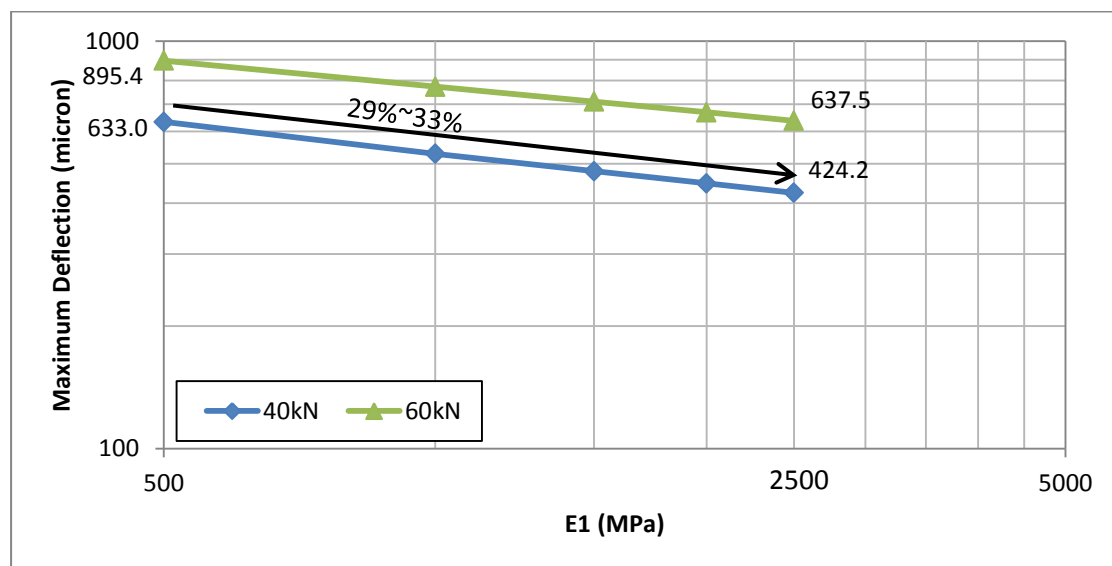


Figure 7-3 Maximum deflection vs. upper layer stiffness, 30km/h, FE analyses

Results estimated from the FE analyses as speed increases to 160km/h, as shown in Figure 7-4, show that deflection readings decrease by 23% when the load is 40kN and 20% when the load is 60kN. A stiffness increase from 500MPa to 2500MPa brings a decrease of deflection by about 34% when the load is 40kN and 28% when the load is 60kN.

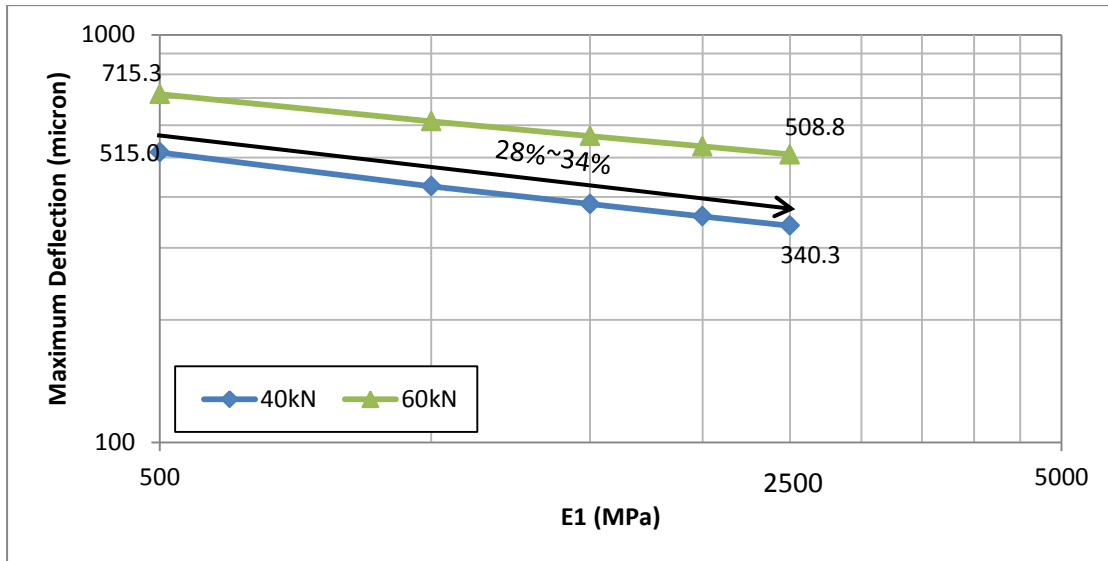


Figure 7-4 Maximum deflection vs. upper layer stiffness, 160km/h, FE analyses

Comparison of the results indicates that the influence of dynamic calculation on the maximum deflection is varied as speed changing. The deflections from the simulations when the speed was 30km/h are similar to that from BISAR calculation. The deflections from the simulations when the speed was 160km/h are smaller than that from BISAR calculation. Thus, a significant influence of speed on maximum deflection can be found; the maximum deflection on pavement surface decreases as the speed of tyre increases.

7.3.2 Stiffness influencing energy dissipation

In order to assess the influence of pavement stiffness on energy dissipation, the calculated pavement resistance (PR) for each simulation has been plotted against the Young's modulus of layer 1 (E1) with varied speed levels.

Figure 7-5 shows the PR-E1 curves when the vertical load $L_v=40\text{kN}$. An obvious relationship between E1 and PR can be seen in the figure. The P_R decreases with E1 increases, which means that a stiffer pavement absorbs

less energy. With a speed of 160km/h, the PR=16N when E1=500MPa, and the PR=7N when E1=2500MPa, which theoretically means the energy dissipation can decrease by 56% with an increase in upper layer stiffness of 80%. If the speed is 30km/h, when the upper layer stiffness increases by 80%, the energy dissipation decreases by 59%.

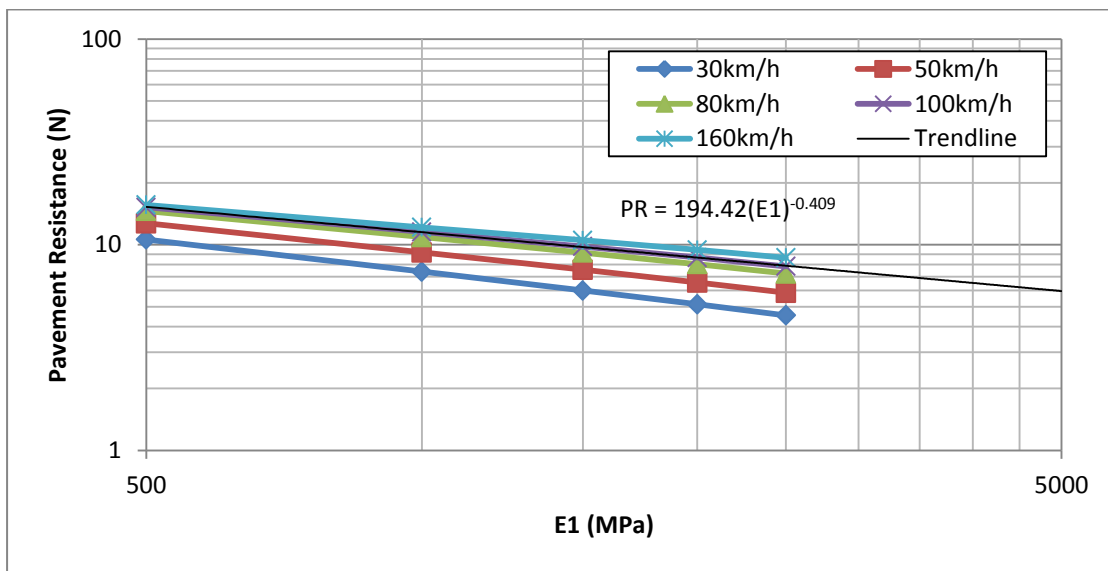


Figure 7-5 PR vs. E1 when $L_v = 40kN$

The relationship between pavement resistance and top layer stiffness when vertical load equals 50 and 60kN can be found in Appendix B.4.

7.3.3 Speed influencing energy dissipation

It is found that speed has a relatively significant influence on pavement resistance, especially within the range between 30 to 100km/h, as shown in Figure 7-6. With E1=500MPa, when the speed increases from 30km/h to 100km/h, the pavement resistance increases by 5N. It is also found that the increment becomes relatively small, when the speed increases from 100km/h to 160km/h. However, the effect of loading rate on asphalt stiffness modulus (e.g. using the parameters in Ullidtz, 1979) will reduce

the slope of the line in Figure 7-6, typically leading to an approximate 50% reduction in pavement resistance. By using the method mentioned in Section 6.6.2 the calibrated pavement resistances can be found in Figure 7-7.

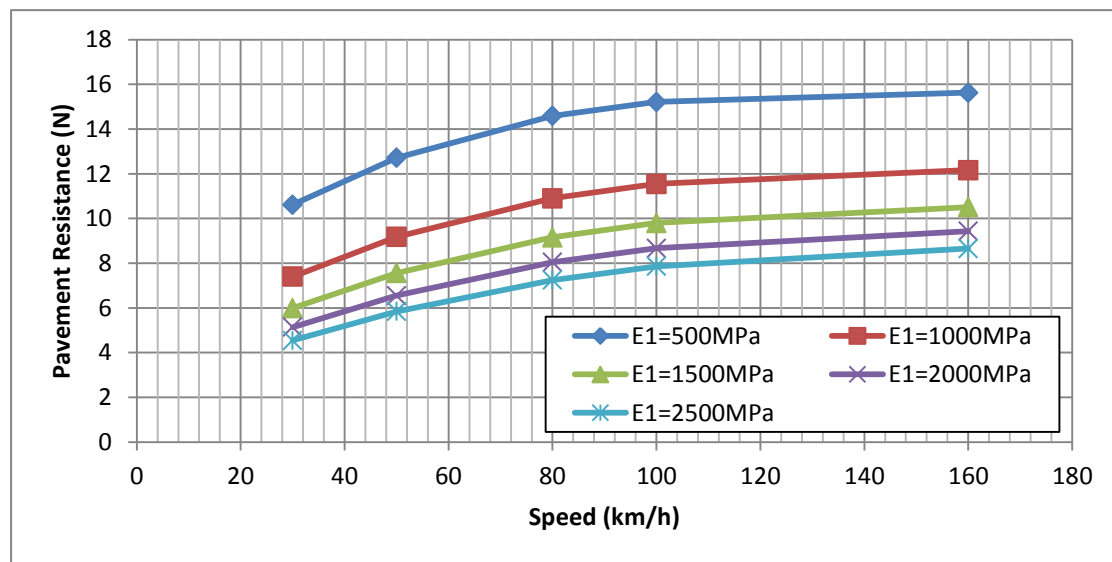


Figure 7-6 PR vs. speed when $L_v = 40\text{kN}$

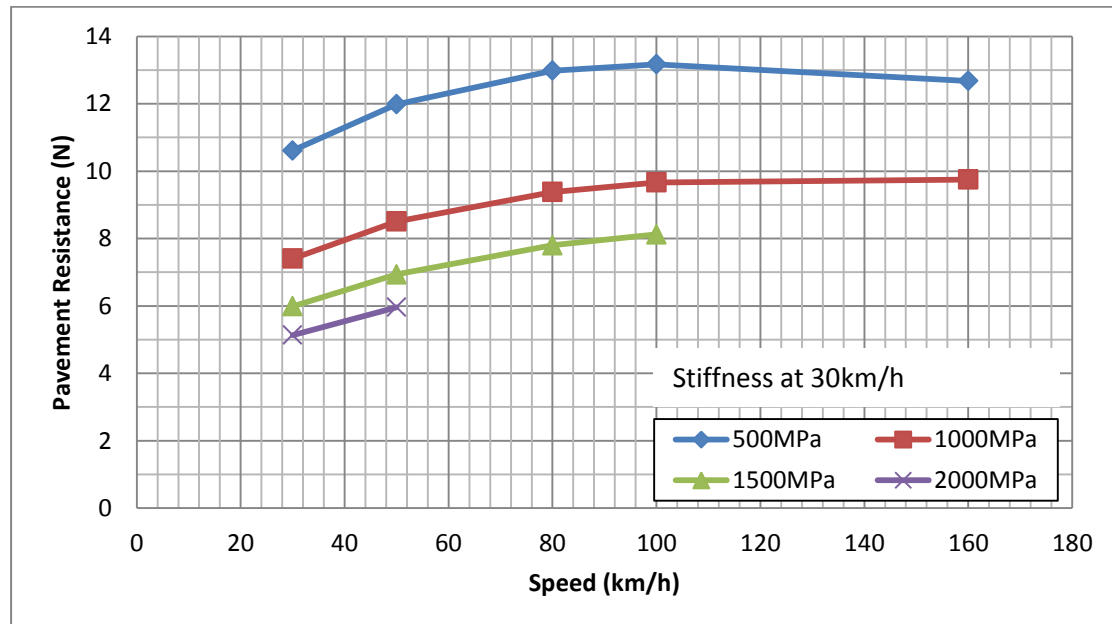


Figure 7-7 PRs with speed-influenced stiffnesses, $L_v=40\text{kN}$

The relationship between the speed and pavement resistance is nonlinear. Similar relationships also can be found when load equals 50kN and 60kN, as shown in Appendix B.1.

7.3.4 Load influencing energy dissipation

The results plotted in Figure 7-8 are pavement resistance against vertical load. A linear relationship can be found in all cases. A change in pavement resistance of 13N was found when vertical load increased from 40kN to 60kN, at a speed of 30km/h. This means that every 1kN additional vertical load yields 0.6555N pavement resistance. Trend lines 'linear (30km/h)' and 'linear (160km/h)' give the numerical relationship.

For the HGV mentioned in Section 3.1.4, an additional 13kJ/km would be consumed when the vehicle is loaded by 20 tonnes of goods when the speed is 30km/h, compared to the unloaded case.

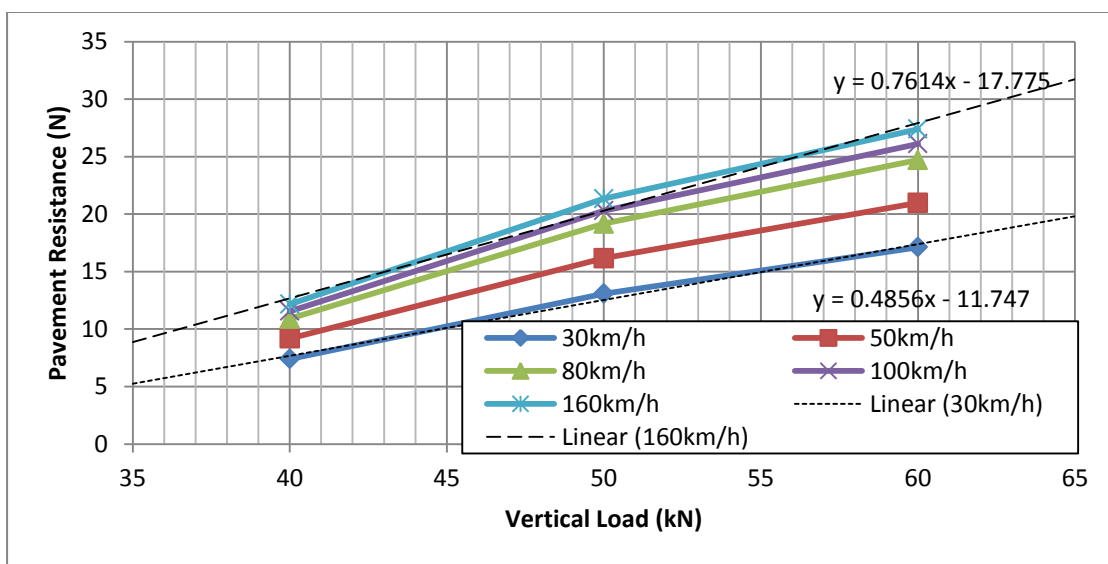


Figure 7-8 PR vs. L_v when $E_1=500\text{MPa}$

The plotted data of pavement resistance against vertical load where the upper layer stiffness is varied in the range between of 1000MPa to

2500MPa can be found in Appendix B.3. The results also reflect similar linear relationships between the pavement resistance and vertical load.

7.4 Summary

The comparison of vertical deflections between BISAR calculation and the FE analyses indicates that speed has a significant influence on vertical deflection. Deflections obtained from the FE analyses are similar to BISAR results when the speed is relatively slow (30km/h).

From the results, and from inspection of Figure 7-4, it may be seen that there is an obvious relationship between stiffness and deflection. This can be found in Figure 7-7 and Figure 7-8. The pavement with a high stiffness upper layer always has low deflection.

The relationship between the upper layer stiffness and pavement resistance follows a power law. A pavement with a stiffer top layer consumes less energy. If the stiffness of the top layer increases from 500MPa to 2500MPs, this results in a reduction of 41% to 61% in energy dissipation as the speed ranges from 30km/h to 160km/h.

The influence of speed on pavement resistance is nonlinear. It is that found an increment of 1.5 to 2.5N of pavement resistance accrues when speed in increased from 30km/h to 100km/h. When the speed is over 100km the increment becomes relatively small once the effect of speed on asphalt stiffness is taken into account.

The vertical load influence affects pavement resistance linearly. Pavements absorb more energy under a high vertical load. Results imply

that a heavily loaded 40ton HGV will consume 13kJ additional energy compared to the normally loaded case.

The results will be discussed further in Chapter 9.

Chapter 8

Concrete Pavements

8.1 Problem description

In order to compare the energy dissipated due to pavement stiffness between rigid and flexible pavements, a 3D model of a section of concrete pavement will be presented in this chapter. This is an extension of the energy consumption analyses reported in Chapter 6.

8.2 Model Definition

Dimensions of the model are the same as for the model used in Chapter 6. It consists of a 26m length of layered pavement and a 10m radius of the surrounding ground, in order to simulate the case of a pavement laid over a semi-infinite space. This is a compromise arrangement to allow sufficient space to absorb energy due to subgrade soil hysteresis and avoid dangers of interference from reflected waves while keeping the element number to a reasonable value. A 6m length contact zone transmits the load that comes from the rolling wheel. Since only vertical load is applied and this load distributes symmetrically on the contact patch, the model has been considered to be symmetrical to save calculation time.

A typical pavement structure has been used, which consists of a concrete layer of 300mm, 150mm of lean concrete base and 300mm of aggregate subbase. The subgrade can be considered as part of the surrounding ground with a 10m radius.

Table 8-1 shows the material properties used in the model. In order to assess the influence of pavement stiffness, Young's modulus of layer 1 has been varied as 15, 20, 25, 30, 35, 40GPa. A typical lean concrete base has been assumed, with 10GPa Young's modulus and 0.2 Poisson's ratio. An aggregate subbase has been used as well, with 150MPa Young's modulus and 0.35 of Poisson's Ratio. A material with 90MPa Young's Modulus and 0.3 Poisson's ratio is used for infinite media, which means the subgrade and surrounding ground.

Table 8-1 Material configurations of the concrete pavement model

layer	Name	Thickness (m)	Young's Modulus (MPa)	Poisson's Ratio	Density (kg/m ³)	Damping	
						Alpha (s)	Beta (1/s)
1	Concrete	0.3	E1	0.35	2400	0	0
2	Lean Concrete	0.15	10000	0.2	2400	0	0
3	Aggregate	0.3	150	0.35	2000	0	0
4	Subgrade	infinite	90	0.3	1800	100	0.02

8.3 Loading

Results retrieved from simulations presented in Chapter 6 and 7 indicate that the relationship between pavement resistance and vertical load is approximately linear. Therefore, only one load level has been used in the concrete pavement simulation, in order to reduce the total simulation time. Thus, the load level used for the analyses is 40kN. This load level is equivalent to the load exerted on a single tyre which comes from a typical 40 tonnes 5-axle HGV. The inflation pressure of a tyre is 552kPa. Therefore, by using the method mentioned in Section 2.5.3, the

tyre/pavement contact area is rectangular with a length of 324.4mm and a width of 223.4mm. The width of the contact zone is 111.7mm since the model is symmetrical.

8.4 Boundary Conditions

These are the same as for models used in prior tests. VDBs have been located in 3 sections of the surrounding ground. By using the method mentioned in Chapter 3, for VDB1 or VDB3, the primary dashpot coefficient equals 1.87×10^5 ; the secondary dashpot coefficient equals 1.00×10^5 . For VDB2, the primary dashpot coefficient equals 1.01×10^4 and the secondary dashpot coefficient is 5.39×10^3 .

8.5 Parameters

The parameters have been varied can be found as follows:

Table 8-2 Parameters have been varied for the concrete pavement

Parameter	Value
Stiffness of concrete (GPa)	15, 20, 25, 30, 35, 40
Speed (km/h)	30, 50, 80, 100, 130, 160, 190

8.6 Results

Example contour plots of vertical deflection are given in Appendix E. Figure 8-1 shows the relationship between pavement resistance and E_1 , the stiffness of the concrete layer. The relationship in each case is exceptional. Trend lines 1 and 2 have been plotted to predict the

pavement resistance in the range of E1 between 10 to 80GPa. For the case when speed equals 30km/h the relationship is:

$$PR = 1.3986(E1)^{-0.505} \quad 8-1$$

When the speed equals 190km/h the relationship is:

$$PR = 2.102(E1)^{-0.439} \quad 8-2$$

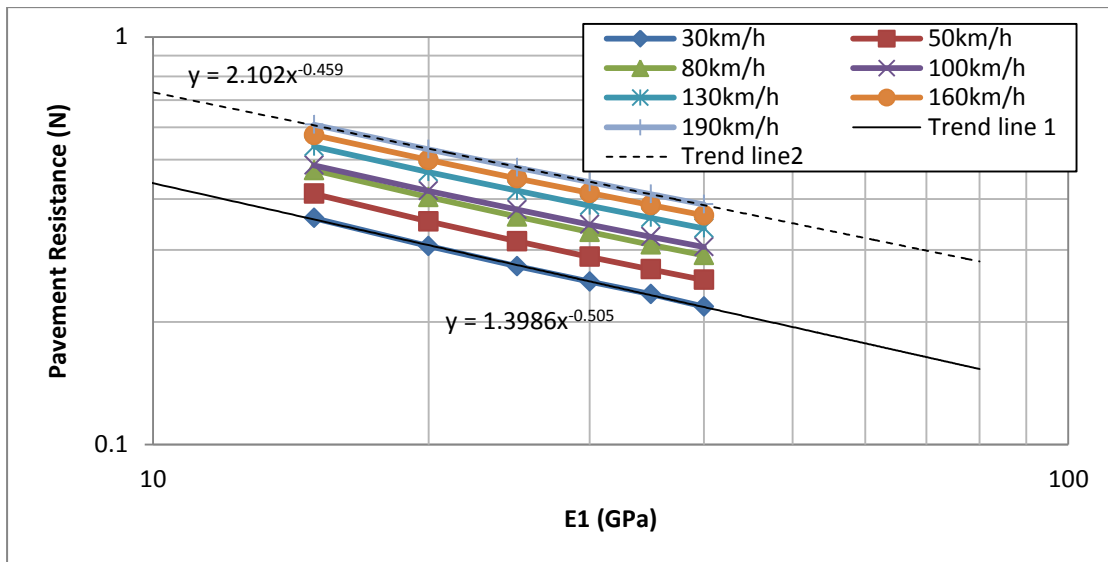


Figure 8-1 Pavement resistance vs. top layer stiffness, concrete pavement

By using Equation 8-1 and 8-2, a prediction of pavement resistance increase vs. stiffness increasing rate can be plotted, as show in Figure 8-2. $P_{R,50}$ is the pavement resistance when $E1=15\text{GPa}$. ΔP_R is the difference in pavement resistance between $P_{R,50}$ and the PR results at other stiffnesses. $\Delta E1$ equals the current stiffness less 15GPa. It can be estimated that if the stiffness increases 100%, from 15GPa to 30GPa, the pavement resistance will approximately reduce by 28%.

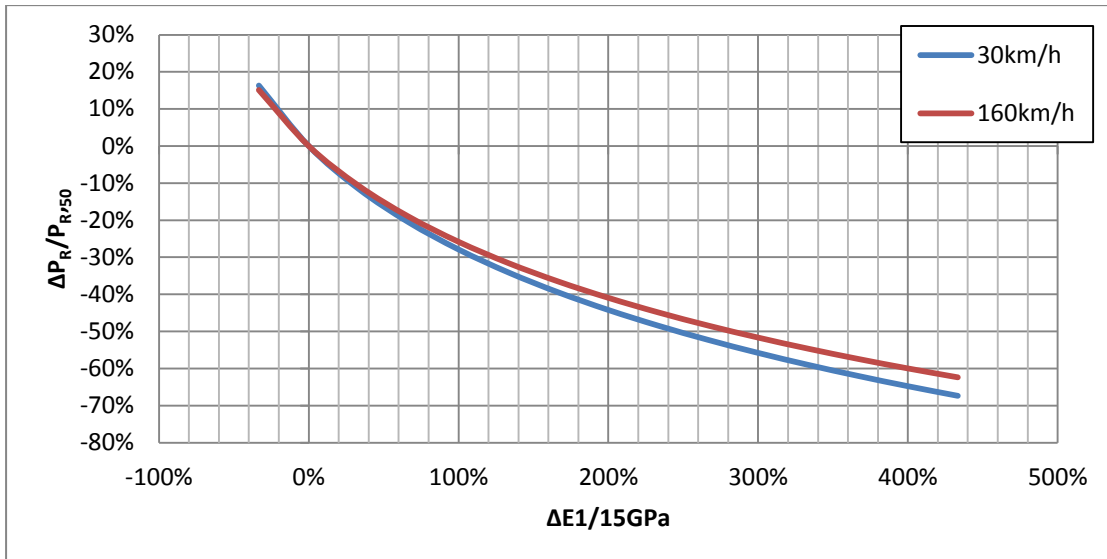


Figure 8-2 PR increment vs. E1 increment

Figure 8-3 shows the influence of speed on pavement stiffness. Two trend lines have been drawn based on the cases where E_1 equals 15GPa and 40GPa. Both of them indicate that the relationship between pavement resistance and speed (v) is linear. Furthermore, trend lines and results also show that the effect of speed is secondary. For a pavement with $E_1=15\text{GPa}$ as speed increases from 30km/h to 190km/h, the pavement resistance increases by 0.25N.

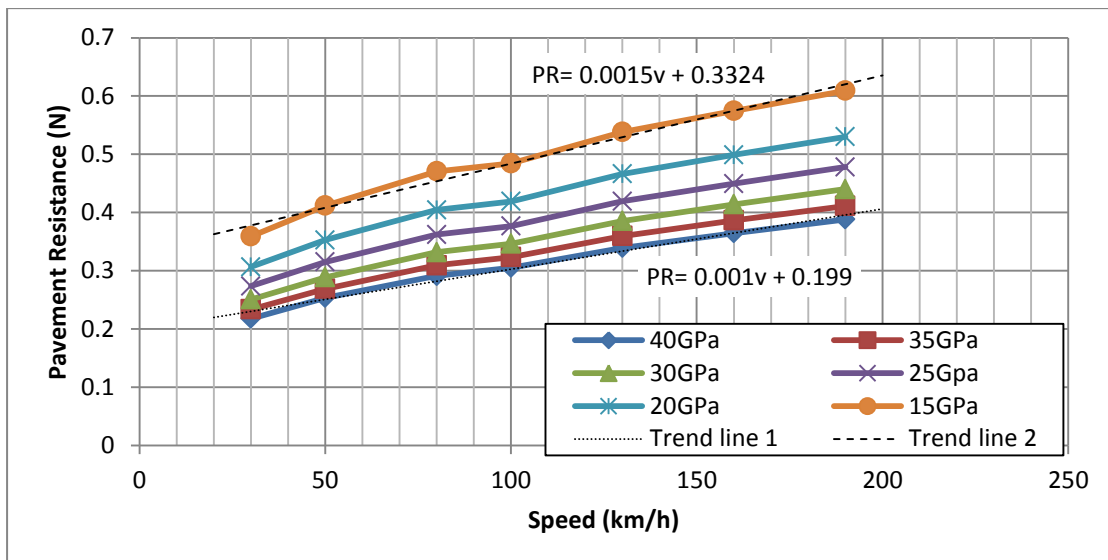


Figure 8-3 Pavement resistance vs. speed, concrete pavement

For a typical 40ton HGV, driven at a constant speed of 100km/h (62mph) on a concrete pavement, which has a structure as shown in Table 8-1 and $E_1=15\text{GPa}$, the pavement resistance is 0.484N per wheel. Thus the HGV consumes 4840J of energy to overcome the resistance generated by pavement stiffness, during a 1km journey. If the speed reduces to 80km/h, which all other factors remains equals, pavement resistance will be 0.471N, which means the reduction of speed brings a saving of 130J per kilometre. In order to achieve the same value of energy saving, keeping the speed at 100km/h, E_1 would have to be increased to 16.2GPa, an increment of about 8%. Thus, this example shows that the stiffness is a major factor influencing pavement resistance.

8.7 Summary

This chapter has presented FE analyses of a concrete pavement model. It was again found that pavement stiffness is a major factor influencing energy dissipation. When the stiffness increases, pavement resistance

decreases. The relationship between upper layer stiffness and pavement resistance follows a power law.

The influence of speed on energy consumption is significant but it is also limited. For a pavement with a 15GPa upper layer as speed increases from 30km/h to 190km/h, the pavement resistance increases by 0.25J/m.

The results will be discussed further in Chapter 9.

Chapter 9

Discussion of Results

9.1 Discussion of TRL measurements

According to the linear trend line plotted in Figure 5-10 and results retrieved from the FE analysis (Table 5-10), a comparison of pavement resistance and vehicle fuel economy can be found in Table 9-1. It is worth noting that the deflections (78 and 102 microns) were the average deflections calculated by FE analyses. The values of pavement stiffness can be found in Table 5-7 and Table 5-8.

Table 9-1 Comparison of FE and fuel economy

Research	Pavement	Deflection (micron)	Fuel Economy (L/100km)	PR per tyre (kJ/100km)	Pavement Related Fuel usage (L/100km)
TRL	Rigid	78	57		
TRL	Flexible	102	72		
FE	Rigid	78		61	0.03
FE	Flexible	102		79	0.05

The pavement related fuel usage is calculated using the pavement resistance in Table 9-1. In accordance with the conditions of the TRL experiment mentioned in Section 5, it is worth to make some assumptions as follows:

- The vehicle is a 5-axle tractor trailer, which has 10 tyres,

- The engine of the vehicle is a diesel engine,
- The speed of the vehicle is 80km/h,
- The engine efficiency of the vehicle is 40%,
- The energy density (energy per unit volume) of diesel is 44.8MJ/L,

Since engine efficiency varies with engine rotation speed, a vehicle driving at 80km/h requires a higher frequency of engine rotation. Thus, a 'typical' value of engine efficiency, 40%, has been used.

Following these assumptions, the energy generated by the engine is 18MJ/L. By using the pavement resistance values in Table 9-1, every tyre consumes 0.003L of diesel to overcome the pavement resistance per 100km for the rigid pavement. For the flexible pavement, the tyre needs 0.005L fuel per 100km journey. Since the vehicle has 10 tyres, the pavement related fuel consumption is 0.03L/100km for the rigid pavement and 0.05L/100km for the flexible pavement.

The results indicate that the fuel consumed for overcoming pavement resistance is a very small part of total vehicle fuel consumption; only about 0.05% for the rigid pavement and 0.07% for the flexible pavement. It also means that the direct influence of pavement stiffness on fuel consumption is relatively small.

It also indicates that stiffer pavements generate less resistance than flexible pavements; an increase of 24 microns in vertical deflection yields a corresponding 0.02L/100km increase in fuel consumption to overcome pavement resistance for a 5-axle tractor trailer.

9.2 Discussion of pavement stiffness

In order to investigate the influence of pavement stiffness on energy dissipation, some results calculated from the FE analysis mentioned in Chapters 6, 7 and 8 have been plotted in Figure 9-1. The PR values have been retrieved from the FE analyses of the three pavements (concrete, asphalt and low quality pavements) for the case with a speed of 100km/h and a vertical load (L_v) of 40kN. The stiffnesses and thicknesses of the three pavements have been listed in the Table 9-2.

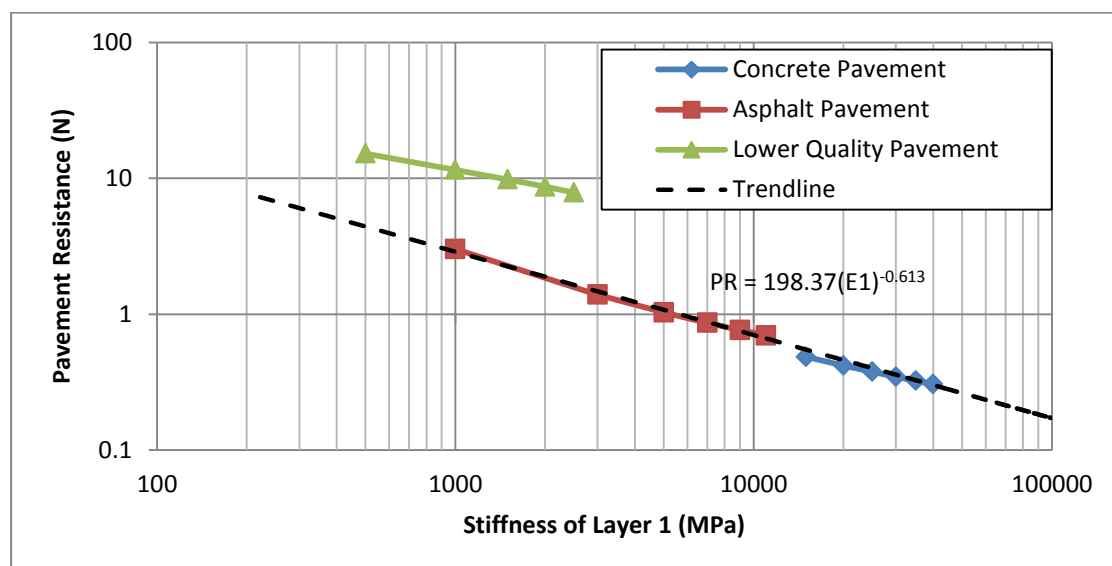


Figure 9-1 Pavement stiffness vs. pavement resistance

Table 9-2 Comparison of Young's modulus and layer thickness

Layer	AP		CP		LQP	
	E (MPa)	Thickness (mm)	E (MPa)	Thickness (mm)	E (MPa)	Thickness (mm)
1	1000 to 11000	140	15000 to 40000	300	500 to 2500	150
2	7000	200	10000	150	200	300
3	2400	300	150	300	90	Infinite
4	90	Infinite	90	Infinite	None	None

Note: CP is concrete pavement, AP is asphalt pavement, LQP, is lower quality pavement and E is Young's modulus.

A trend line based on the results from the FE analyses of asphalt pavement has been plotted in the diagram to show the relationship between pavement stiffness and fuel consumption (pavement resistance). Since the lower quality pavement has a relatively lower stiffness on layer 2 (base layer), the related PR values are higher than the values predicted by the trend line. The trend line shows similar values to the results from the calculations of concrete pavement, and this can logically be explained by the fact that in these examples both the concrete and asphalt pavements have similarly high base layer stiffnesses.

Depending on the value of stiffness, the trend line has been divided to three sections. Table 9-3 shows the ranges of the sections and related values of fuel economy. The results of fuel usage are again based the assumption that the energy density of diesel would be 44.8MJ/L and the engine efficiency of the vehicle would be 40%. It also assumes that the vehicle is a "typical" 40-tonne 5-axle HGV.

Table 9-3 Pavement resistance and fuel economy

Section	Stiffness (MPa)	PR for single tyre (kJ/100km)	Fuel usage (ml/100km)
1	<3000	>147	>81
2	3000 to 15000	55 to 147	30 to 81
3	>15000	<55	<30

The fuel usage induced by pavement stiffness has a relatively small change, in section 3, when the pavement stiffness is more than 15000MPa. Thus, for concrete pavement, when the stiffness is larger than 15000MPa, the savings in fuel caused by stiffness increase is insignificant, i.e. it is not worth increasing pavement stiffness to achieve a limited benefit of fuel saving when the stiffness is larger than 15000MPa. Nevertheless, compared to the asphalt pavement and lower quality pavement, fuel saving can be achieved when driving on rigid pavements.

In section 2, when the stiffness is between 3000 and 15000MPa, the savings of fuel caused by stiffness increase is more significant, but it is relatively small. A 13000MPa increase of pavement stiffness yields 0.012L/100km decreased fuel usage. Therefore, for asphalt pavements, the benefit of fuel saving induced by stiffness increase is limited.

Section 3 shows an obvious benefit of fuel saving when the stiffness increases from 500MPa to 3000MPa and this yields an increased fuel economy of 163ml/100km. Therefore, for low quality pavements, the benefit of fuel saving induced by stiffness increase is obvious and significant.

9.3 Discussion of vehicle speed

A diagram to show the relationship between PR and vehicle speed with three typical pavements is plotted in Figure 9-2; a concrete pavement with a 40GPa concrete layer, an asphalt pavement with a 3GPa asphalt layer at 30km/h and a minor road with a 1GPa asphalt layer at 30km/h. The data used for the diagram was collected from the results of previous FE analysis when vertical load equals 40kN.

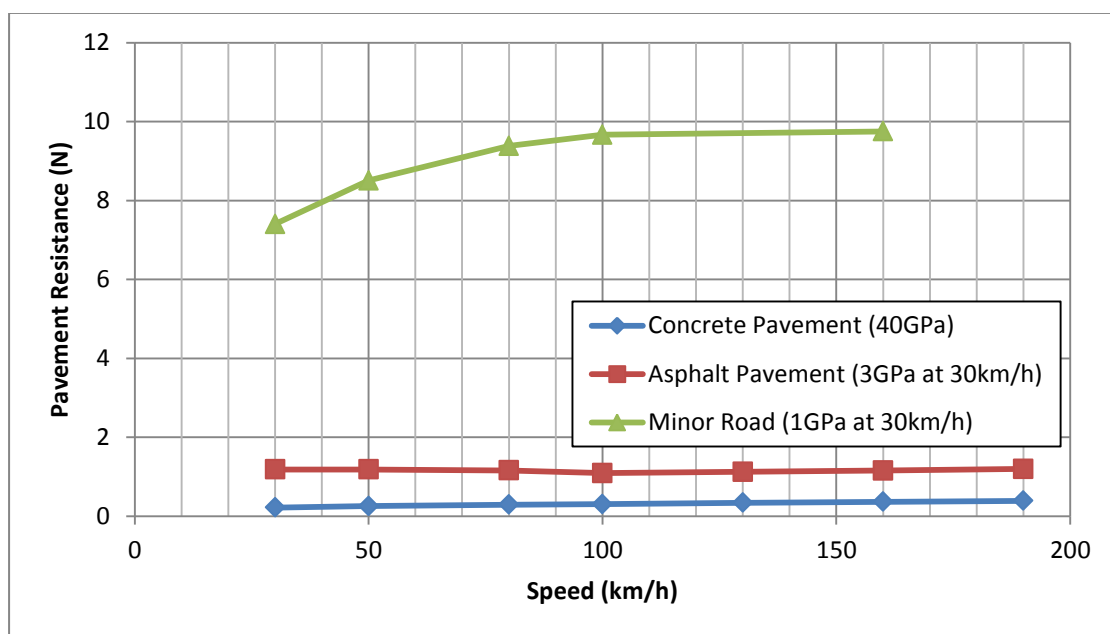


Figure 9-2 Pavement resistance vs. speed, typical pavement stiffness

In order to show the related fuel usage induced by pavement stiffness, a conversion was applied, which is based on the method mentioned in Chapter 9.1; the energy density of diesel is 44.8MJ/L and the engine efficiency is 40%, the vehicle has 10 wheels. The results can be found in Figure 9-3.

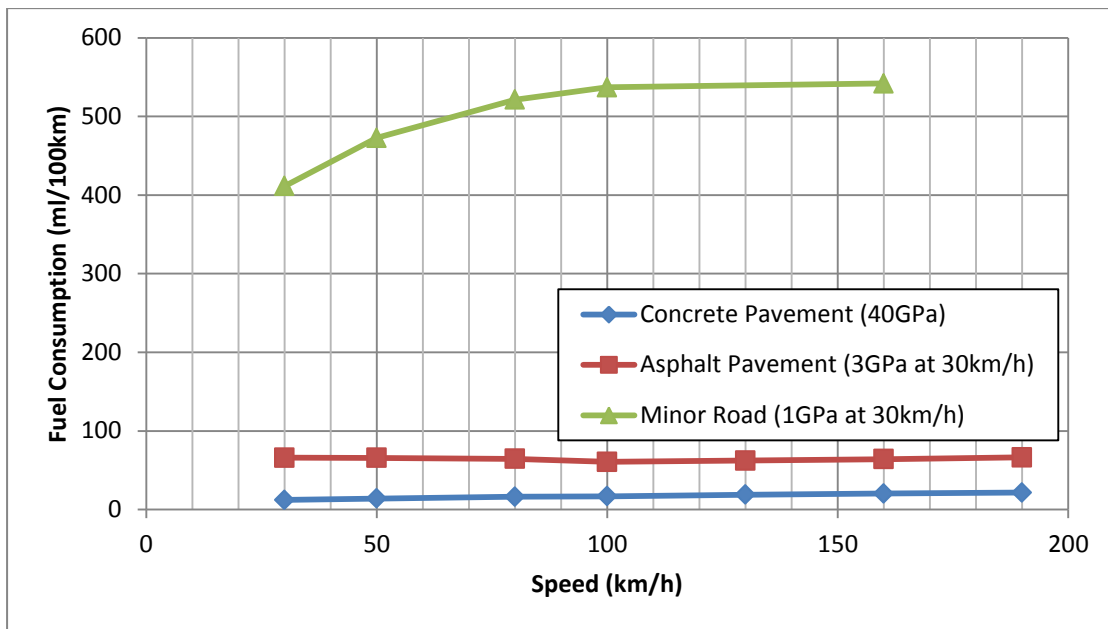


Figure 9-3 Pavement stiffness related fuel consumption

For the concrete and asphalt pavements, the influence of speed on fuel usage induced by pavement stiffness is relatively insignificant. The average fuel usage is 17ml/100km for the concrete pavement. For the vehicle driving on the asphalt pavement, the fuel used to overcome pavement resistance is 64ml/100km. A HGV fuel consumption measurement conducted by A1 Paper Plc. (2006) indicated that the average fuel consumption of a typical HGV was 19L/100km between 2004 and 2005. Therefore, for an HGV, the fuel used to overcome the pavement stiffness can almost be ignored.

The case of a minor road shows a significant influence of speed on pavement resistance. In other words the vehicle needs more fuel to overcome pavement resistance when it is driven at a higher speed, and the increase is significant.

9.4 Discussion of embedded energy

Embedded energy and carbon life cycle analysis are acknowledged as being of paramount interest in ensuring that engineering construction is as environmentally friendly as possible. In the case of a highway the bulk usage of materials is considerable, resulting in high costs, high embedded energy – particularly where bitumen or cement is involved – and consequently large carbon footprints.

In order to illustrate a simplified comparison between material embedded energy and vehicle fuel energy, Table 9-4 and Table 9-5 present material embedded energy estimates for two typical heavy duty pavements, based on the values given in Thom (2008) which were derived from Stripple (2001).

It might be assumed for example that a further 100mm of asphalt overlay will be required on the asphalt pavement over the course of a 40-year life while there is no such demand on the concrete pavement, in which case the material embedded energy demand for the asphalt pavement has to be increased to 2347MJ/m, only marginally lower than that for concrete pavement. Overall therefore there appears to be a difference (917MJ/m) in total material embedded energy between the asphalt and concrete options.

Chapter 9 Discussion of Results

Table 9-4 Embedded energy of asphalt pavement

Layer	Material	Density (kg/m3)	Width (m)	Thickness (m)	Embedded Energy (MJ/T)	Energy (MJ/m)
Asphalt	Asphalt	2400	4	0.24	700	1613
Base	Crushed Rock	2400	4	0.20	20	38
Subbase	Gravel	2000	4	0.30	10	24
Overlay*	Asphalt	2400	4	0.1	700	672
Total						2347

Note*: 100mm of asphalt overlay to asphalt pavement during 40-year life

Table 9-5 Embedded energy of concrete pavement

Layer	Material	Density (kg/m3)	Width (m)	Thickness (m)	Embedded Energy (MJ/T)	Energy (MJ/m)
Concrete	Concrete	2400	4	0.3	900	2592
Lean Concrete	Lean Concrete	2400	4	0.15	450	648
Aggregate	Gravel	2000	4	0.3	10	24
Total						3264

By way of comparison, consider the fuel energy expended in a heavily trafficked lane of a busy highway. The traffic flow may be more than 3000 HGVs per day. By using the predicted energy loss at 100km/h (1.090J/m for asphalt pavement, 0.305J/m for concrete pavement), as shown in Figure 9-2, the pavement-related energy consumption during a 40-year life is plotted in Figure 9-4. In all cases the load exerted on the single tyre

was transmitted from a 40-tonne 5-axle HGV driving at 100km/h, i.e. the vehicle has 10 wheels. The tyre pressure was kept constant at 552kPa.

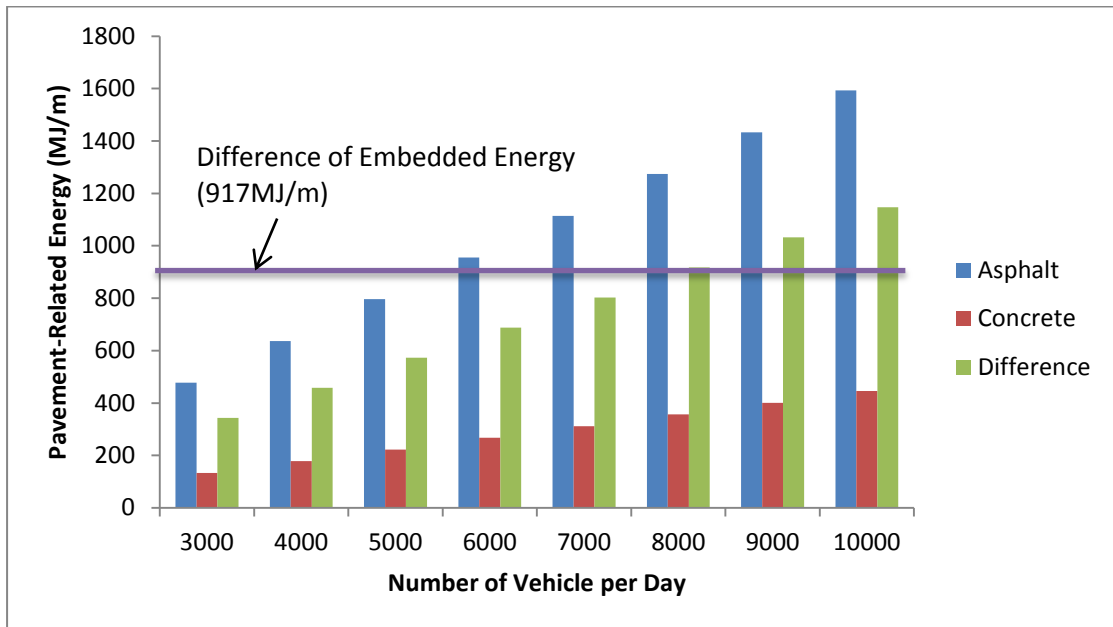


Figure 9-4 Pavement-related energy of pavements during 40-year life

The key point to note from Figure 9-4 is that it is worth investing some embedded energy to cut down pavement-related energy consumption so long as that the number of HGV is more than 8000 per day.

Chapter 10

Conclusions and Recommendation

A model has been developed and substantially validated that calculates the energy dissipated within a pavement due to surface deflection under the passage of a moving wheel. Results from this model indicate only minor effects on energy loss from vehicle speed. The effect of load level was more significant, as expected. However the effect of upper pavement layer stiffness was of most significance, with a factor of around 3 to 4 between pavements with stiffnesses representing asphalt and concrete surfaces, the range of factors reflecting the range of possible asphalt temperatures and therefore stiffnesses.

Results also indicate that, for concrete pavement, it is not worth increasing pavement stiffness so as to achieve a small benefit of fuel saving when the stiffness is larger than 15GPa; for asphalt pavement, the benefit of fuel saving induced by stiffness increase is also limited; but for low quality pavement, the benefit of fuel saving induced by stiffness increase is obvious and significant.

In the context of embedded energy in pavement construction this difference is significant and suggests that a concrete surface generates a lower energy demand over a full pavement life cycle for heavily trafficked roads. It is worth investing some embedded energy to cut down pavement-related energy consumption so long as that the number of HGV is more than 8000 per day.

The work has given considerable insight into the influence of pavement stiffness on fuel consumption, and also considered the effects of vehicle speed and vertical load conducted at tyre. However there is still some works which be undertaken in the future:

- The effect related to pavement layer thickness was not observed in this research. The stiffness influenced by layer thickness can be observed in the future work.
- The load applied onto pavement surface was a set of vertical time interval pressures. The lateral load between tyre and pavement has been neglected in this research. Thus, a simulation of a full 3D tyre rolling onto a section of pavement could be conducted.
- The materials used for this research were assumed to be linear elastic. The energy dissipation of nonlinear material is not fully understood. A nonlinear model could be built in further work. Based on this, the energy consumption of a section pavement under repeated load can be conducted.

Reference

- A1 Paper Plc. (2006). *Small Fleet Performance Management Tool (SFPMT) helps A1 Paper improve efficient.* Department for Transport.
- ABAQUS Theory Manual.* (2001). Pawtucket.
- Akcelik, R., Bayley, C., Bower, D. P., & Briggs, D. C. (1983, October). A hierarchy of vehicle fuel consumption models. *Traffic Engineering and Control*, pp. 491-496.
- Ang-Olson, J., & Schroer, W. (2002). Energy efficiency strategies for freight trucking: Potential impact on fuel use and greenhouse gas emissions. *Transportation Research Record* (1815), 11-18.
- Ardekani, S., & Sumitsawan, P. (2010). *Effect of Pavement Type on Fuel Consumption and Emissions in City Driving.* Arlington: RMC Research & Education Foundation.
- Bang, J. R. (1990). Reduction in Automobile Fuel Consumption. *OECD/IEA Informal Expert Panel on Low Consumption Low Emission Automobile, Proceedings of an Expert Panel, Rome*, 14-15.
- Bamberger, R. (2005). *Automobile and Light Truck Fuel Economy: The CAFE Standards.* CRS Issue Brief for Congress.
- Benbow, E., Iaquinta, J., Lodge, R., & Wright, A. (2007). *Investigation of the Effects of Pavement Stiffness of Fuel Consumption.* TRL Limited.
- Bendtsen, H. (2004). *Rolling resistance, fuel consumption - a literature review.* Road Directorate, danish Road Institute.

- British Standards Institution (2006a). Environmental Management: Life Cycle Assessment – Principles and Frameworks. BSI, London. ISO14040.
- British Standards Institution (2006b). Environmental Management: Life Cycle Assessment – Requirements and Guidelines. BSI, London. ISO14044.
- British Standards Institution (2008). Specification for the assessment of life cycle greenhouse gas emissions of goods and services. BSI, London. PAS 2050:2008.
- Casadei, A., & Broda, R. (2007). *Impact of Vehicle Weight Reduction on Fuel Economy for Various Vehicle Architectures*. Conducted by Ricardo Inc.
- Cenek, P., Jamieson, N., & Ball, G. (1996). Effect of pavement deflection on rolling resistance of commercial vehicle tyres. *Third International Symposium on Pavement Surface Characteristics*. Christchurch, New Zealand.
- Clark, S. (1971). *Reproduced with permission from Mechanics of Pneumatic Tires*. Monograph 122: National Bureau of Standards.
- De Beer, M., Fisher, M., C., & Kannemeyer, L. (2004). Towards the application of Stress-In-Motion (SIM) results in pavement design and infrastructure protection. *Eight (8th) International Symposium on Heavy Vehicles, Weights and Dimensions.*, (pp. 14-18). Misty Hills Conference Centre, Muldersdrift, Gauteng, South Africa.
- Descornet, G. (1990). Road-Surface Influence on Tire Rolling Resistance. In W. E. Meyer, & J. Reichert, *Surface Characteristics of Roadways*:

- International Research and Technologies, ASTM STP 1031* (pp. 401-415). Philadelphia: American Society for Testing and Materials.
- Descornet, G. (1990). Road-Surface Influence on Tire Rolling Resistance. *Surface Characteristics of Roadways: International Research and Technologies, ASTM STP 1031*, 401-415.
- Design Manual for Raod and Bridges HD 26/06.* (2006). The Highway Agency.
- DeRaad, L. (1977). The influence of Road Surface Texture on Tire Rolling Resistance. *Special Publication P-74* (Tire Tolling Losses and Fuel Economy- An R&D Planning Workshop).
- Everall, P. F. (1968). *The effect of road and traffic conditions on fuel consumption.* Road Research Laboratory, Crowthorne: Ministry of Transport Road Research Laboratory Report LR 226.
- Ejsmont, J. A. (1990). Tire/road noise and rolling resistance – is there a trade-off? *International Tire/road Noise Conference. INTROC 90.*, (pp. 8-10). Gothenburg, Sweden.
- Fueleconomy.gov. (2010). *2010 Toyota Prius.* Retrieved 2 8, 2010 from Fueleconomy.gov: <http://www.fueleconomy.gov/feg/bestworst.shtml>
- FuelEconomy.gov. (2009). *Advanced Technologies & Energy Efficiency.* Retrieved 7 22, 2009 from www.fueleconomy.gov: <http://www.fueleconomy.gov/feg/atv.shtml>

- FPMS. (2008). *Fugro PMS - Structural Testing*. Retrieved 2010 from Fugro PMS (previously Pavement Management Services):
http://www.pavement.com.au/Structural_Testing.html
- Gyenes, L., & Mitchell, C. G. (1994). The effect of Vehicle-Road Interaction Fuel Consumption. In B. T. Kulakowski, *Vehicle-Road Interaction.ASTM SPT 1225*. (pp. 225-239). Philadelphia: American Society for Testing and Materials.
- Huang, Y. H. (2004). *Pavement Analysis and Design* (2nd Edition ed.). Kentucky, USA: Pearson Education Inc.
- Huang, Y., Bird, R., and Heldrich, O. (2009). Development of a life cycle assessment tool for construction and maintenance of asphalt pavements. *Journal of Cleaner Production*, Volume 17, Issue 2, pages 283-296. Elsevier.
- Hucho, W. H. (1987). *Aerodynamics of Road Vehicle: From Fluid Dynamics to Vehicle Engineering*. Cambridge: University Press.
- Herndon, R. (1990). *Engineering and Design Settlement Analyses*. U.S. Army Corps of Engineers, Department of the Army. Washington, DC: Depart of the Army.
- HRB. (1972). 'Synthesis 14: Skid Resistance'. Transportation Research Board, National Cooperative Highway Research Program. Washington,D.C: National Research Council.
- Jiang, T., & Zhang, X. (2004). Dynamic analysis of elastic half space problems by using FEM with visocous boundary element. 25 (4), 535-540.

- Kuo, C.-M., & Chou, F.-J. (2004). Development of 3-D Finite Element Model for Flexible Pavements. *Journal of the Chinese Institute of Engineers*, 27 (5), 707-717.
- Kim, J.-M., & Kim, S. (2008). Fast spectral analysis of an axisymmetric layered structure. *Mechanics Research Communications*, 35 (4), 222-228.
- Lysmer, J., & Kuhlemeyer, R. L. (1969). Finite dynamic model for infinite media. *Journal of the Engineering Mechanics, ASCE*, 95 (4), 859-877.
- Langanier, R., & Lucas, J. (1990). The Influence of Pavement Evenness and Macrotexture on Fuel Consumption. In W. E. Meyer, & J. Reichert (Ed.), *ASTM Committee E17 on Pavement Management Technologies, Permanent International Association of Road Congresses. ASTM STP 1301*, pp. 454-459. Philadelphia: American society for Testing and Materials.
- Langdon, M. G. (1984). Factors in road design which affect car fuel consumption. *Traffice Engineering and Control*, Printerhall Ltd., London.
- Lei, W., & Wei, D. (2005). Spring-viscous boundary in finite element analyses for infinite media. *Earthquake Engineering and Engineering Vibration*, 25 (3), 110-114.
- Maddock, I. (1979). *Road vehicle and engine design : short and medium term energy considerations*. London: Road Vehicle and Engine Design Working Group.
- Martin, D., & Shock, R. (1980). *Energy use and energy efficiency in UK transport up to the year 2010*. Energy Technology Support Group, Department of Energy. London: Her Majesty's Stationery Office: Energy Technology Support Group, Harwell.

- McCallen, R., McBride, D., Rutledge, W., Browand, F., Leonard, A., & Ross, J. (1998). *A Multi-Year Program Plan for the Aerodynamic Design of Heavy Vehicles.* Lawrence Livermore National Laboratory, Sandia National Laboratories, University of Southern California.
- McKeown, A. (2002). *Influence of Pavement Construction on Vehicle Fuel Economy.* TRL Limited.
- Meyer, M. D., Watson, L., & Skinner, R. (2006). *Tires and passenger Vehicle Fuel Economy.* TRANSPORTATION RESEARCH BOARD. National Research Council of the National Academies.
- Miege, A. J., & Popov, A. A. (2005). Truck tyre modelling for rolling resistance calculations under a dynamic vertical load. *Journal of Automobile Engineering*, 441-456.
- Nokian Tyres plc. (1999). *European Tyre School.* Retrieved 11 14, 2008 from Tampere University of Technology: <http://www.tut.fi/plastics/tyreschool/index.html>
- NRC. (1992). *Automotive Fuel Economy: How Far Should We Go?* Washington, D.C.: National Academy Press.
- Papagiannakis, A., & Masad, E. (2008). *Pavement Design and Materials.* New Jersey: John Wiley & Sons, Inc.
- PCA. (1984). *Thickness Design for Concrete Highway and Street Pavements.* Portland Cement Association.
- PCA. (1966). *Thickness Design for Concrete Pavements.* Portland Cement Association.

- PIARC. (2009). *Terminology*. Retrieved 3 2, 2010 from World Road Association: <http://termino.piarc.org/term.php?tm=1041>
- Plessis, H. W., Viser, A. T., & Curtayne, P. C. (1990). Fuel consumption of Vehicles as Affected by Road-Surface Characteristics. In W. E. Meyer, & J. Reichert, *Surface Characteristics of Roadways: International Research and Technologies, ASTM STP 1031* (pp. 480-496). Philadelphia: American Society for Testing and Materials.
- Plotkin, S. (1991). Improving Automobile Fuel Economy: New Standards, New approaches. *Office of Technology Assessment, US Congress*. Washington D.C.: US Government Printing Office.
- Popov, A. A., Cole, D. J., Cebon, D., & Winkler, C. B. (2002). Laboratory Measurement of Rolling Resistance in Truck Tyres under Dynamic Vertical Load. *Automobile Engineering , 217 Part D*, 1017-1079.
- Sweatman, P. (1983). A study of dynamic wheel forces in axle group suspensions of heavy vehicles. *Special report 27*, 56.
- Sandberg, U. (1997). *Influence of Road Surface Texture on Traffic Characteristics Related to Environment, Economy and Safety*. Swedish National Road and Transport Research Institute.
- Rahnama, M., & Krawinkler, H. (1993). *Effects of Soft Soil and Hysteresis Model on Seismic Demands*. Stanford, CA, US: The John A. Blume Earthquake Engineering Center, Department of Civil and Environmental Engineering, Stanford University.

- Redsell, M., Lucas, G., & Ashford, N. J. (1988). *Comparison of no-road fuel consumption for diesel and petrol car*. Department of Transport. Crowthorne: Transport and Road Research Laboratory.
- RMA. (2005). *Factbook 2005: U.S. Tire shipment Activity Report for Statistical Year 2004*. Washington D.C.: Rubber Manufacturers Association.
- Ross, M. (2004). Modeling Methods for Silent Boundaries in Infinite Media. *Fluid-Structure Interation. ASEN 5519-006* .
- Sandberg, U. S. (1990). Road macro- and megatexture influence on fuel consumption. In W. E. Meyer, & J. Reichert (Ed.), *STM Committee E17 on Pavement Management Technologies, Permanent International Association of Road Congresses. ASTM STP 1301*, pp. 460-479. Philadelphia: American Society for Testing and Materials.
- Schuring, D. J., & Redfield, J. S. (1982). Effect of tire rolling loss on fuel consumption of trucks. *SAE Transactions 821267* , 4086-4096.
- (2008). *Specification for the assessment of life cycle greenhouse gas emissions of goods and services*. British Standards Institution. London: BSI.
- Stripple, H. (2001). *Life cycle assessment of road - a pilot study for inventory analysis* (Second Edition ed.). Swedish Environmental Research Institutue (IVL).
- Taylor, G., & Patten, J. (2000). *Effect of Pavement Surface Type on Fuel Consumption. Phase 2 : Seasonal Tests*. Centre for Transportation Technology.

- Taylor, G., & Patten, J. (2006). *Effects of Pavement Structure on Vehicle Fuel Consumption – Phase III*. Ottawa: Centre for Surface Transportation Technology (CSTT), National Research Council of Canada (NRC).
- Thom, N. (2008). *Principles of pavement engineering*. London: Thomas Telford Publishing Ltd.
- Toyota. (2010). *Prius Specification*. Retrieved 2 9, 2010 from Toyota: http://www.toyota.co.uk/cgi-bin/toyota/bv/generic_editorial.jsp?deepLink=PS3_Specification_new&nodiv=TRUE&fullwidth=TRUE&edname=specSheet_PS3&carModel=Prius&imgName=/bv/specSheet_images/Next_Prius_Hatchback_5_Door.jpg&zone=Zone%20NG%20Prius&navRoot=toyota
- TRRL. (1980). *Fuel consumption of diesel and petrol cars*. Transport and Road Research Laboratory, Department of Transport. Crowthorne: Department of the Environment.
- Ullidtz, P. (1979). A fundamental method for the prediction of roughness, rutting and cracking in asphalt pavements. *Proceedings of the Association of Asphalt Paving Technologists*, 48, 557-586.
- Watson, H. C., Milkins, E. E., & Marshall, G. A. (1980). A simplified method for quantifying fuel consumption of vehicles in urban traffic. *The Journal of the Society of Automotive Engineers - Australasia*, 6-13.
- Wayman, M, Sciavi-Mellor, I, and Cordell, B. (2009). Protocol for the calculation of life cycle greenhouse gases generated by asphalt as used in highways. TRL. Available at: www.sustainabilityofhighways.org.uk accessed 29th October 2009.

- Week, R. (1981). *Fuel consumption of a diesel and a petrol car.* Deparment of the Environment Department of Transport. Crowthorne: Transport and Road Research Laboratory.
- Wikipedia. (2006). *Fuel economy in automobiles.* Retrieved 01 01, 2010 from Wikipedia:
http://en.wikipedia.org/wiki/Fuel_economy_in_automobiles
- Wikipedia. (2010). *Gasoline.* Retrieved 2 3, 2010 from Wikipedia:
<http://en.wikipedia.org/wiki/Petrol>
- Wong, J. Y. (2001). *Ground Vehicles, 3rd Edition.* Ottawa, Cananda: John Wiley & Sons, Inc.
- Zaniewski, P. E., & Jhon, P. (1989). *Effect of Pavement Surface Type on Fuel Consumption.* Portland Cement Associationng.

Appendix A. Plotted data of FE analyses

A.1 Static pressure on axisymmetric model

Following the model design policy in Chapter 3, with respect to the efficiency of calculation, appropriate dimensions are required for the 3D model. Therefore, the radius of the cross section has been designed and tested using the FE method. The aim of the test is to find a suitable size for the radius of the surrounding ground.

In the test a load pulse was applied on an axisymmetric subgrade. Data were collected during the loading period and for another 10 subsequently; this allows enough time for the observation of the model. In order to build a far boundary, a 20-meter radius has been applied. Thus, sufficient data can be collected.

Figure A-1 shows the model used for the test. It is an axisymmetric model with a fan cross section. The symmetrical axis is parallel to the y-axis. In terms of FE analysis, a far boundary has been applied, in which all freedom degrees of the nodes on the boundary were fixed. The Young's modulus of the material is 90MPa. The Poisson's ratio is 0.35. The density of the material is 1800kg/m³. A pulse pressure of 850kPa (Figure A-2) has been conducted vertically centred on Point A (Node A) of the model with a contact radius of 0.15m.

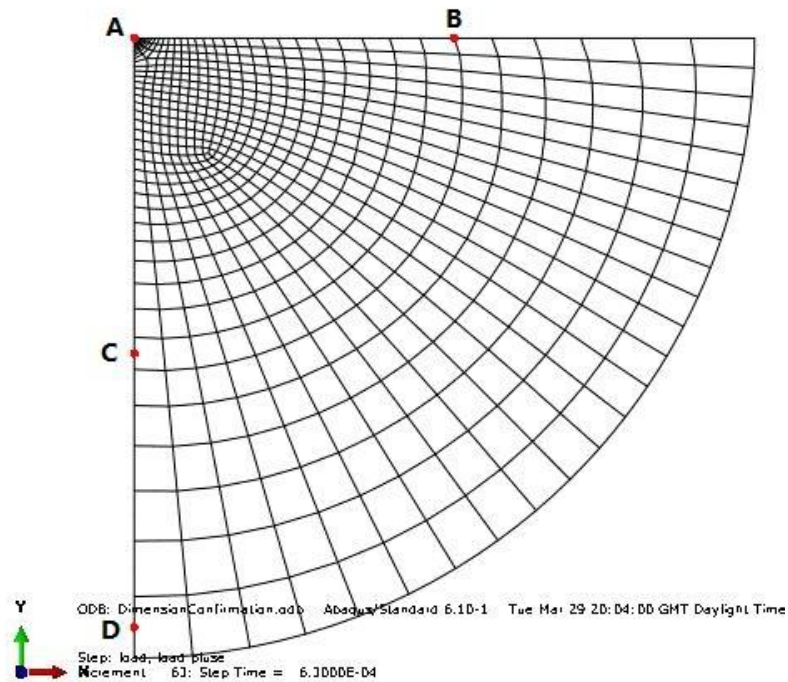


Figure A-1 Vertical Deflection of static simulation

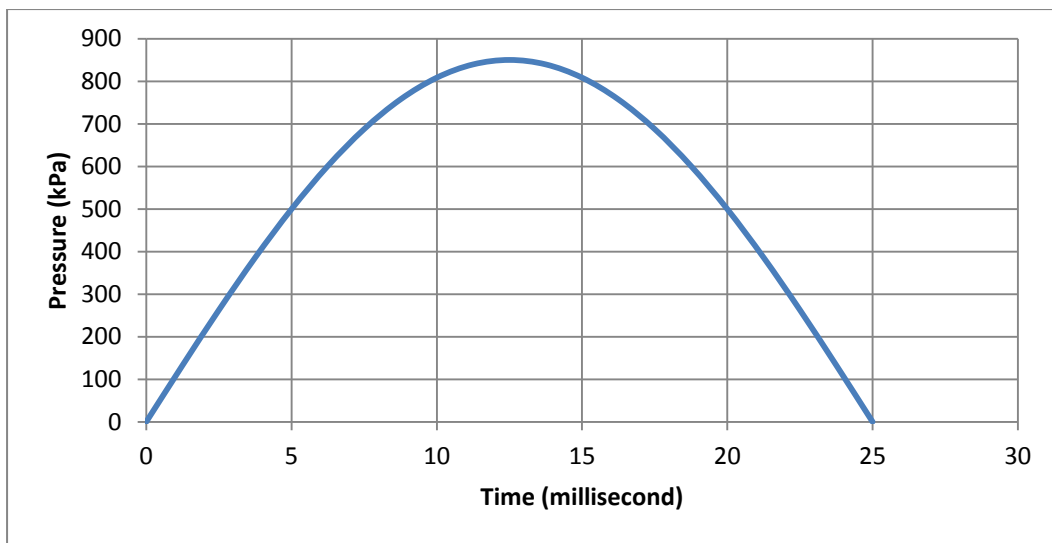


Figure A-2 Load pulse

The results collected from the test are displacement magnitude (δ_m) and velocity magnitude (v_m), which is derived using the following equations:

$$\delta_m = \sqrt{(\delta_x)^2 + (\delta_y)^2}$$

$$v_m = \sqrt{(v_x)^2 + (v_y)^2}$$

where:

δ_x and δ_y are deflections in the x and y directions

v_x and v_y are velocities in the x and y directions

Since model is axisymmetric, the deflection and velocity in the z direction do not need to be considered.

Figure A-3 and Figure A-4 show the results retrieved from the selected nodes. It is clear that, the deflections and velocities of Nodes C, D and B are very small. It is not necessary to take account of the deflections and velocities of these nodes. Therefore, a radius of 10m (that of Nodes B and C) is to be determined sufficient to obtain satisfying results.

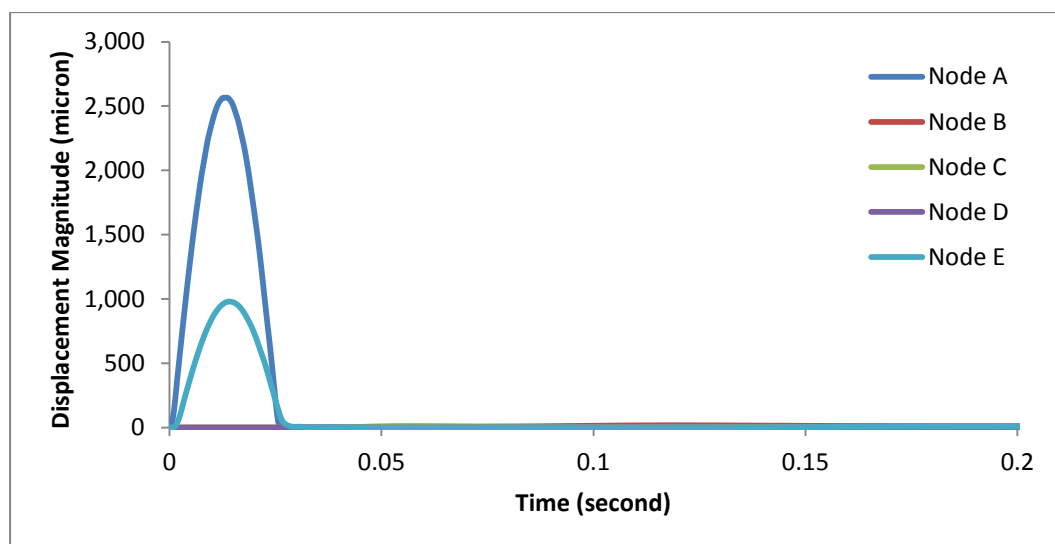


Figure A-3 Deflections magnitudes of collected nodes

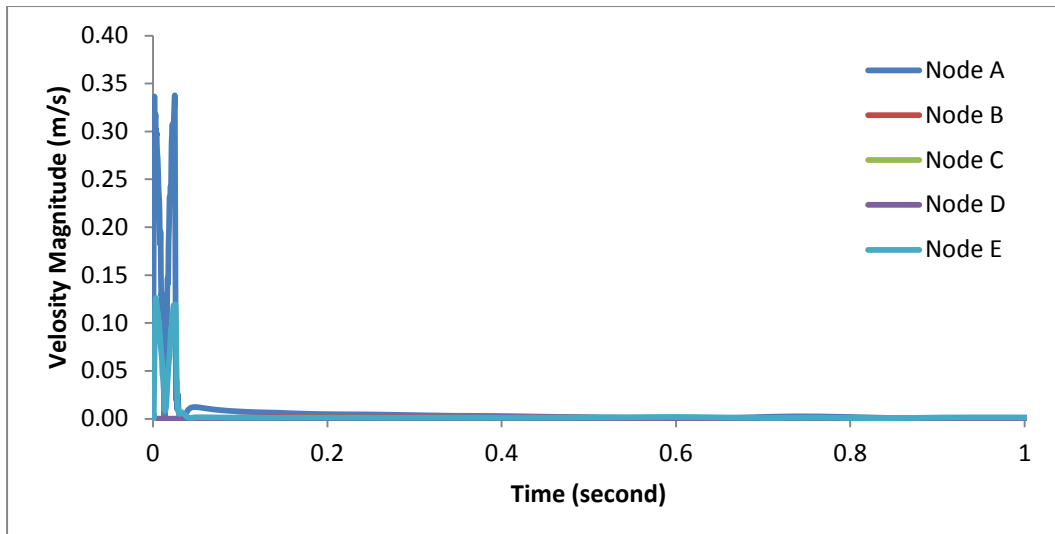


Figure A-4 Velocity magnitudes of collected nodes

A.2 Dynamic pressure on axisymmetric model

In order to assess the influence of dynamic load, a time-dependent pressure generated by FWD has been applied on the model. The peak value of the pressure is 850kPa and the effect duration is approximate 30ms, as shown in Figure A-5.

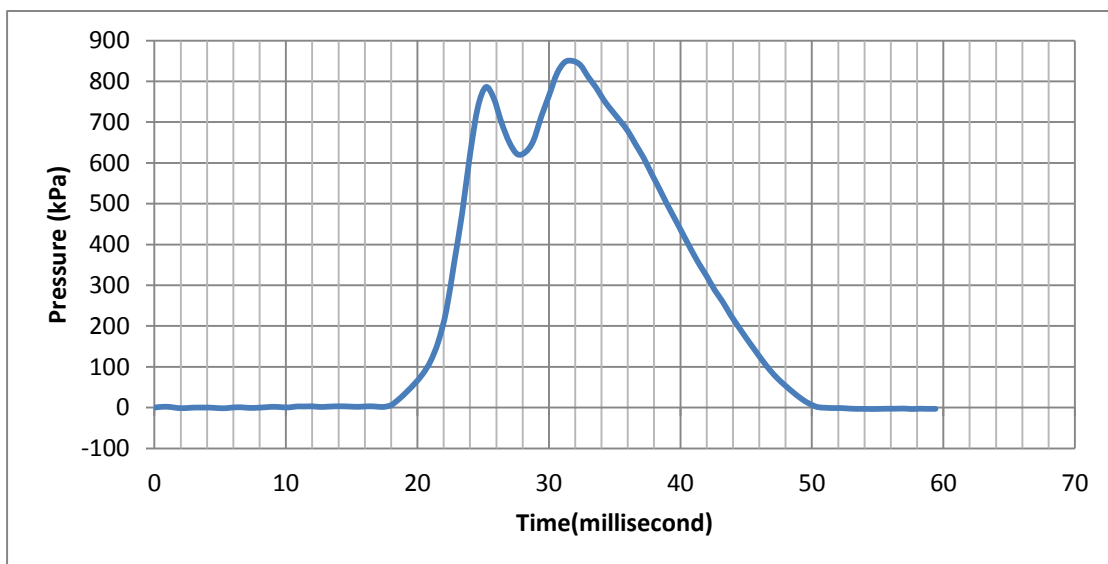


Figure A-5 FWD pressure, peak=850kPa

The material used for the dynamical simulation is same as the static simulation. In addition to that, a 100 alpha damping and 0.015 beta damping has also apply for the dynamic simulation.

Figure A-6 shows vertical deflections retrieved from the model with time increasing. Each colours plotted in a figure represent a value of deflection at a specified time. The represented value is varied with time changing. These figures show that deflection is increased with time increasing from 31 to 126ms. After that, it is decreased with time increasing. Figure A-6(d) states that the deflection waves have not reach the boundary at 10m. Thus, no wave is reflected at the boundary.

Results of the simulation also indicates that the model with 10m of radius is enough for a dynamic simulation when the pressure is smaller than 850kPa or the corresponding loading force is smaller than 60kN. For a rolling wheel simulation, the waves might reach the boundary due to the consequence of a moving pressure. But the effect of the waves on boundary should be limited.

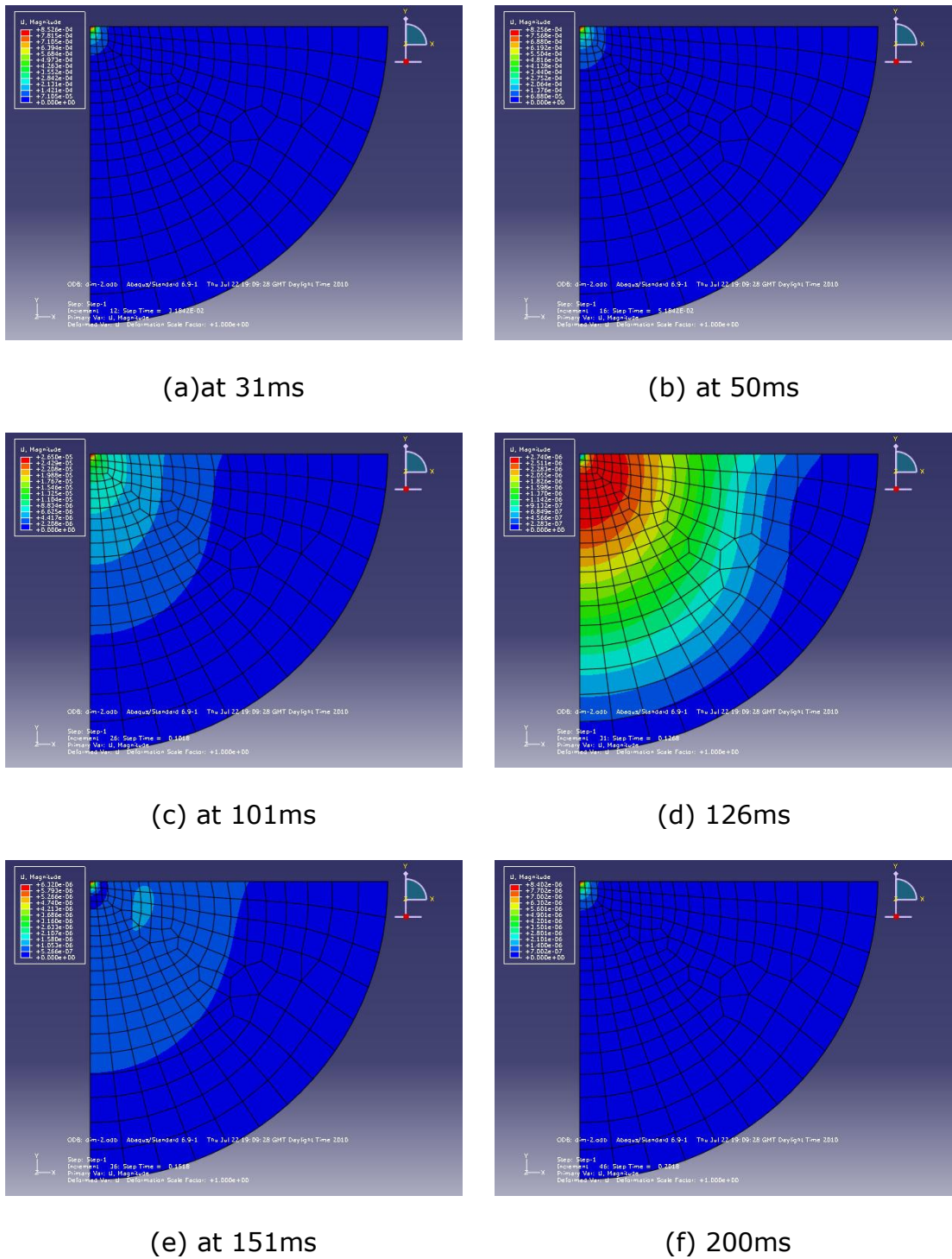


Figure A-6 Vertical deflection against time

A.3 Deflection-time traces of FWD-FE confirmation tests

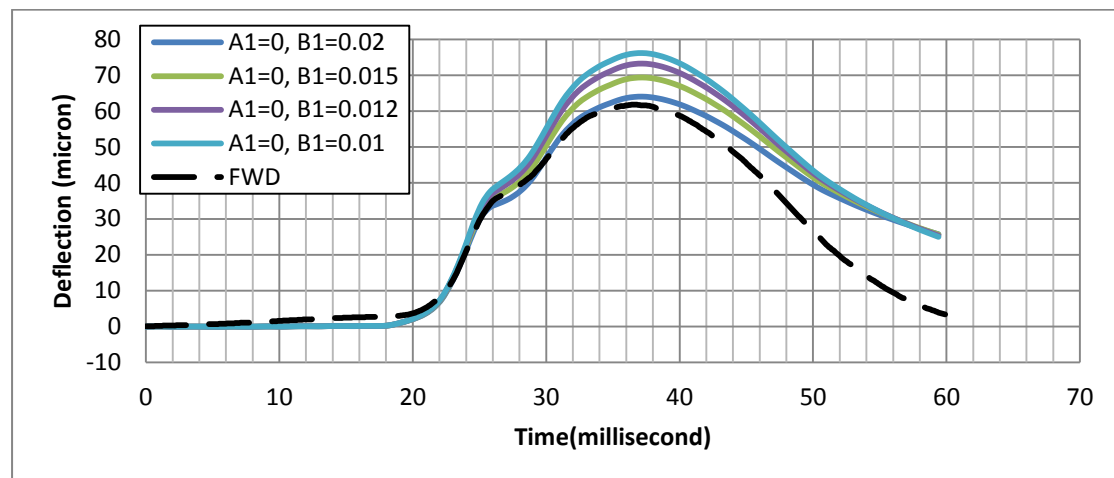


Figure A-7 Deflection-time traces when $A1=0$

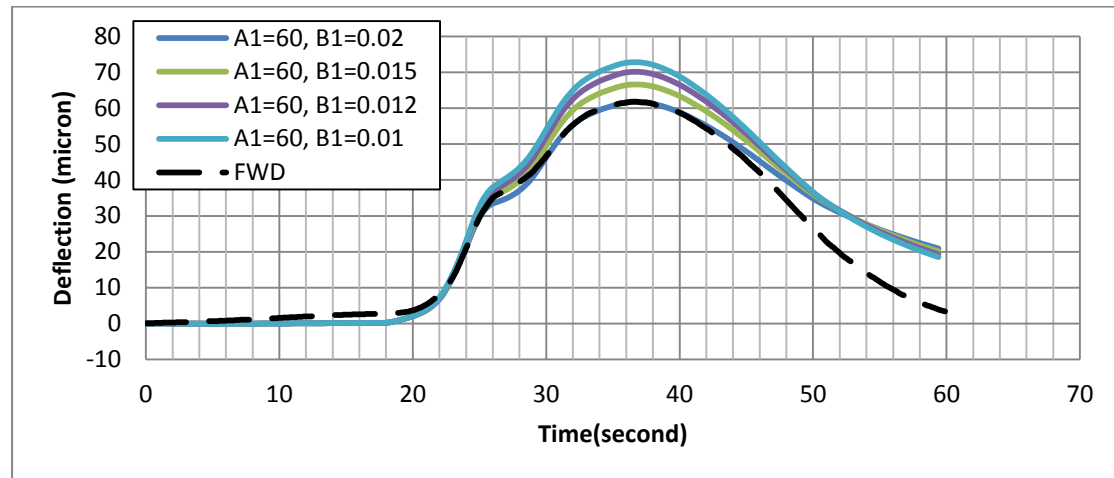


Figure A-8 Deflection-time traces when $A1=60$

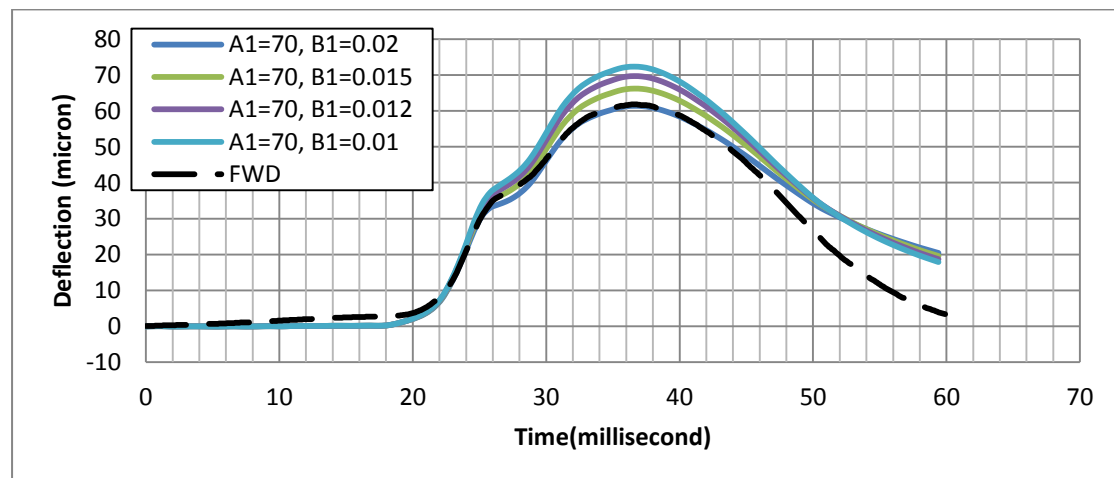


Figure A-9 Deflection-time traces when $A1=70$

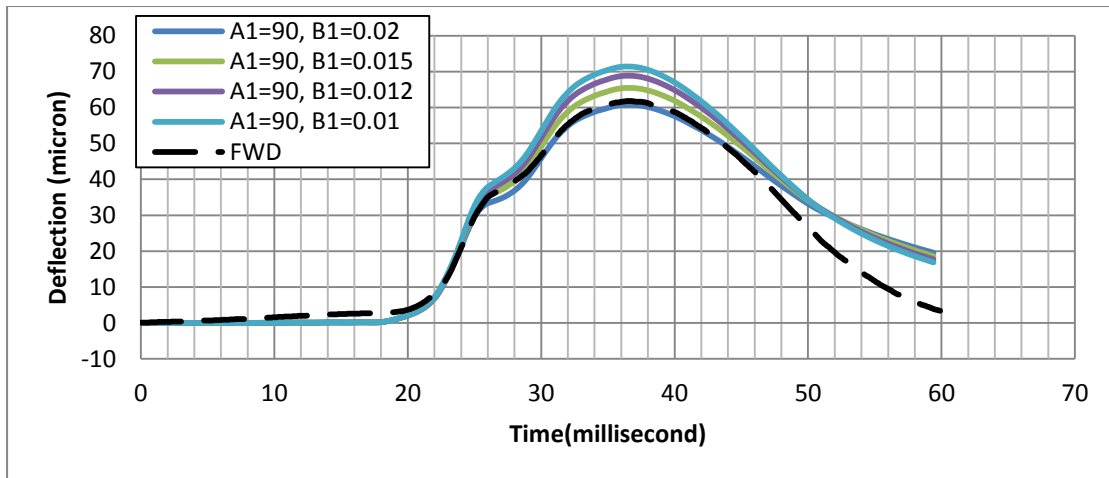


Figure A-10 Deflection-time traces when $A1=90$

A.4 Hysteresis curves of FWD-FE confirmation tests

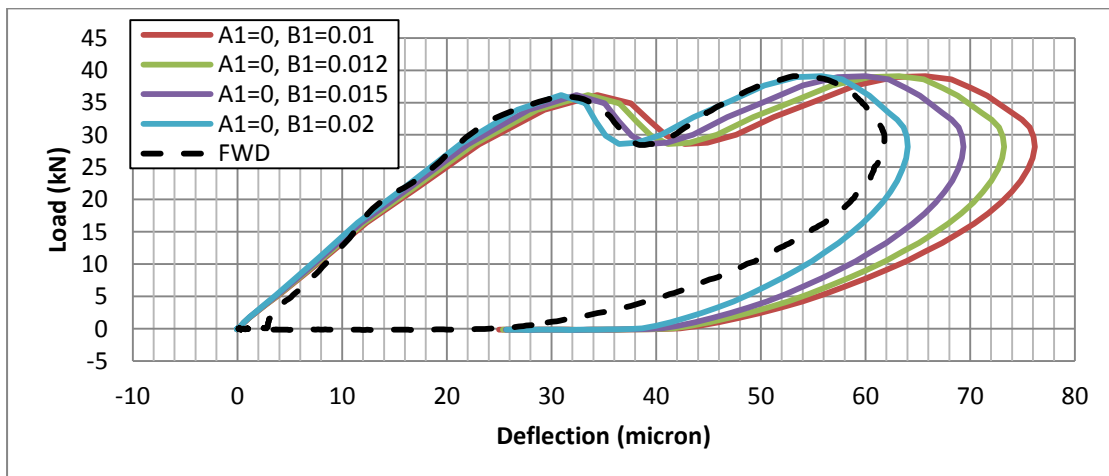


Figure A-11 Load vs. deflection when $A1=0$

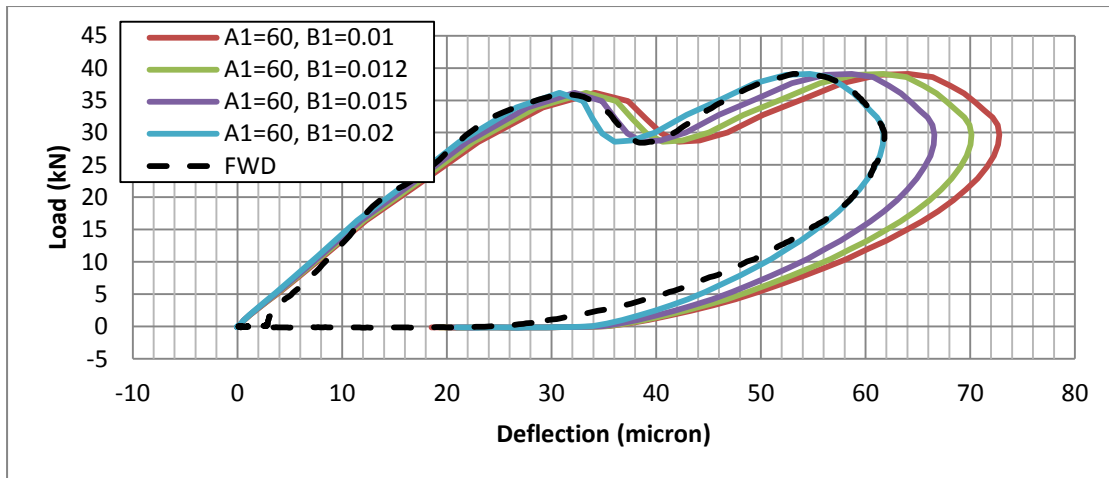


Figure A-12 Load vs. deflection when A1=60

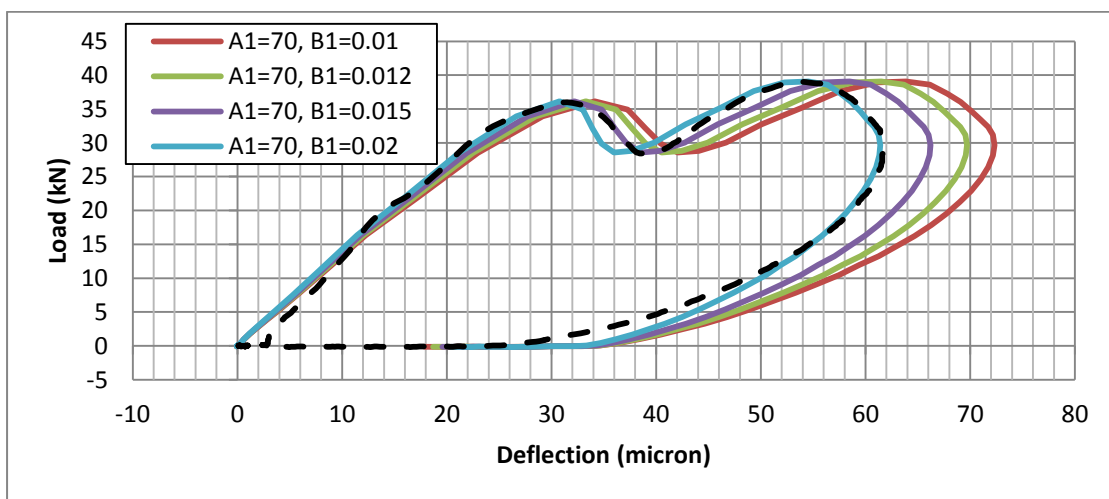


Figure A-13 Load vs. deflection when A1=70

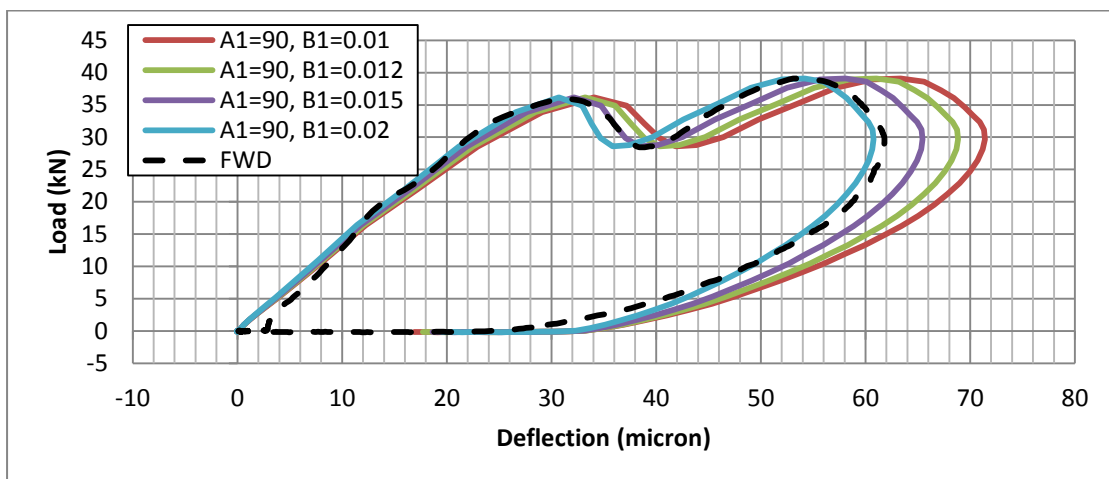


Figure A-14 Load vs. deflection when A1=90

Appendix B. Plotted data of FE analyses

B.1 Speed influencing pavement resistance

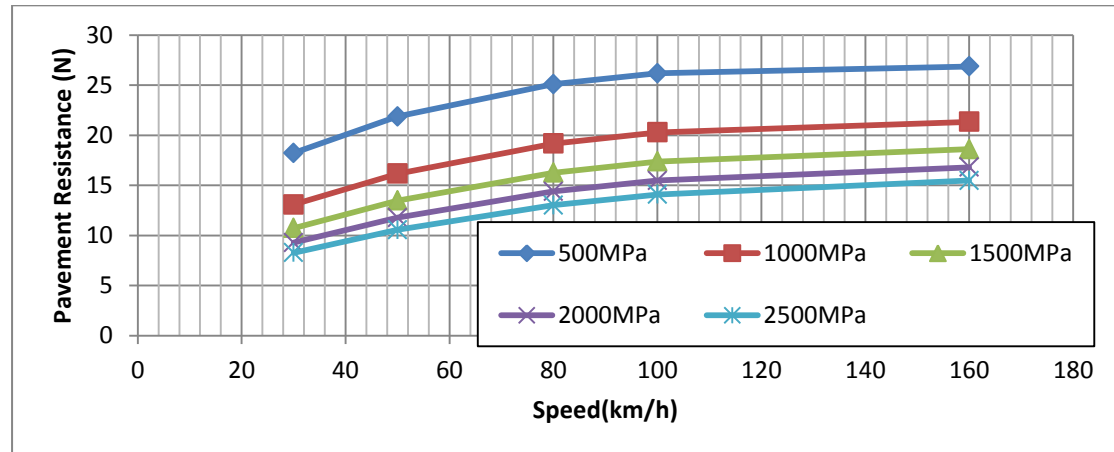


Figure B-1 PR vs. speed when $L_v = 50kN$, low quality pavement

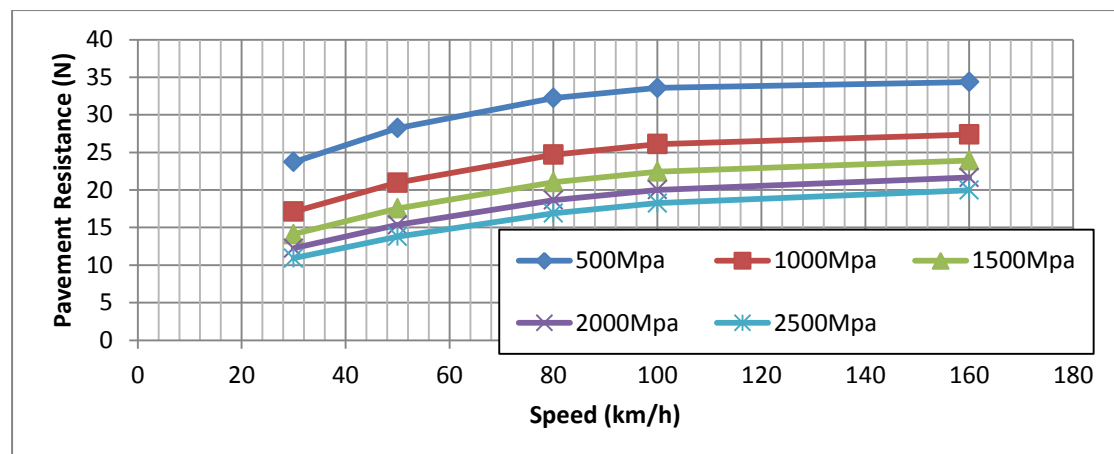


Figure B-2 PR vs. speed when $L_v = 60kN$, low quality pavement

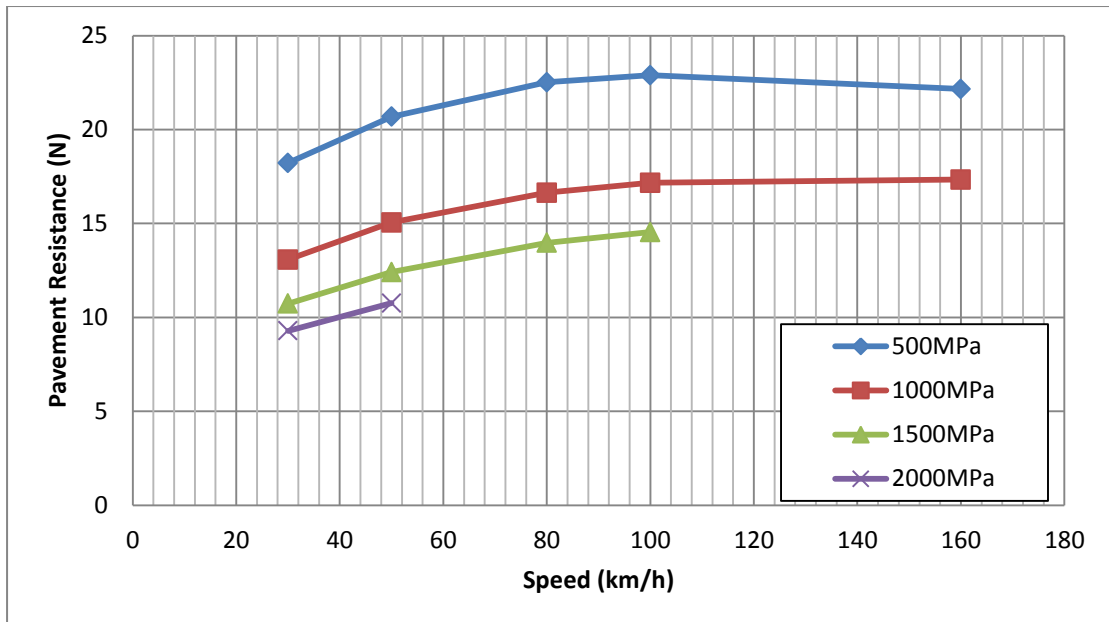


Figure B-3 Calibrated PR vs. speed when $L_v = 50kN$, low quality pavement

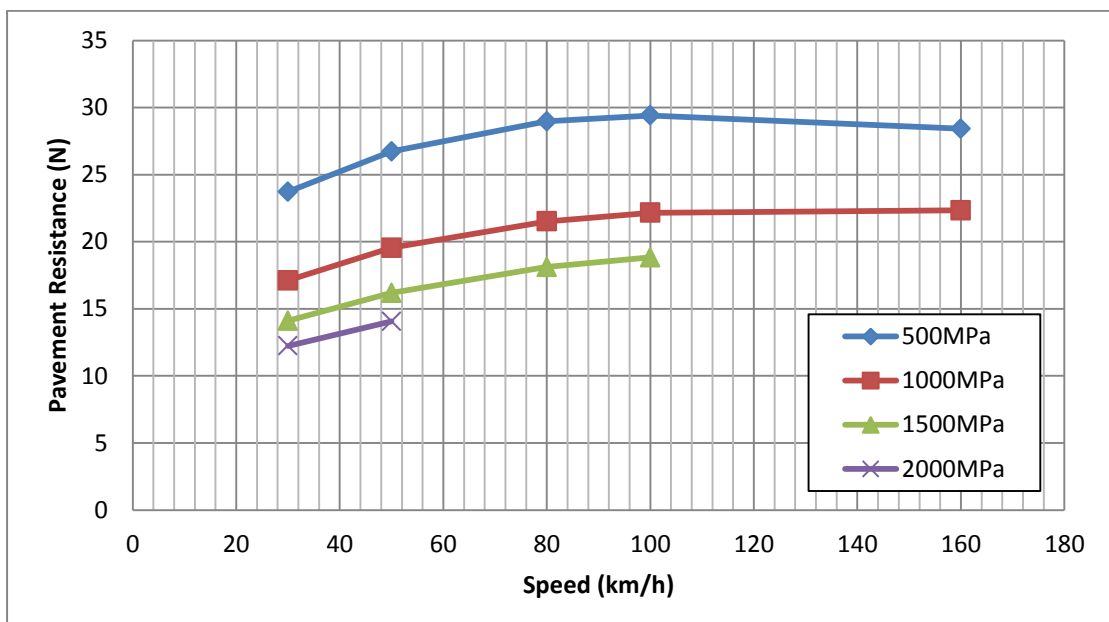


Figure B-4 Calibrated PR vs. speed when $L_v = 60kN$, low quality pavement

B.2 Speed influencing maximum deflection

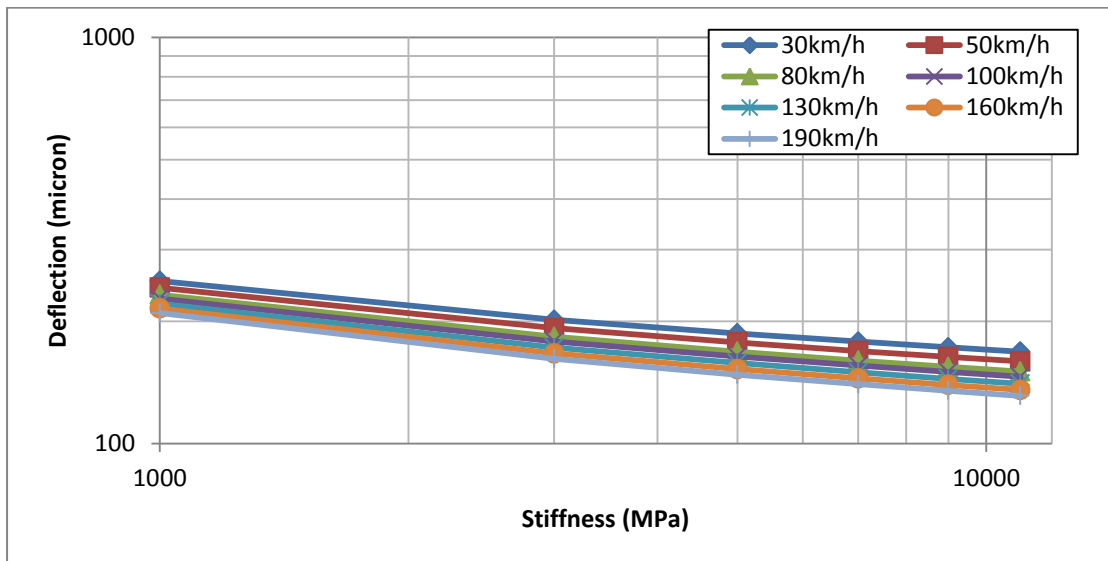


Figure B-5 Deflection vs. stiffness, $L_v=50\text{kN}$, asphalt concrete

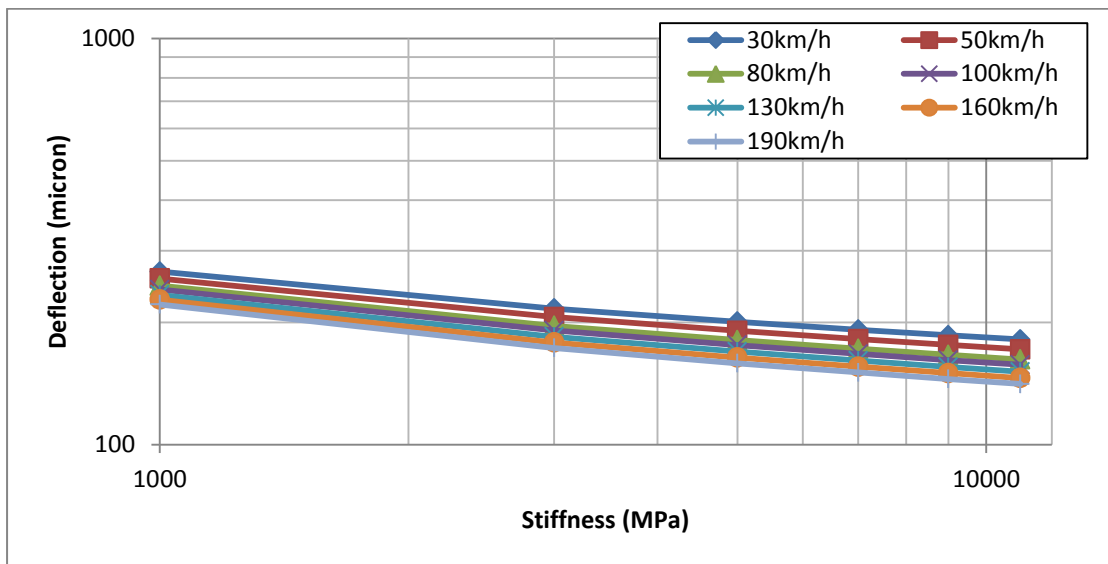


Figure B-6 Deflection vs. stiffness, $L_v=60\text{kN}$, asphalt concrete

B.3 Vertical load influencing pavement resistance

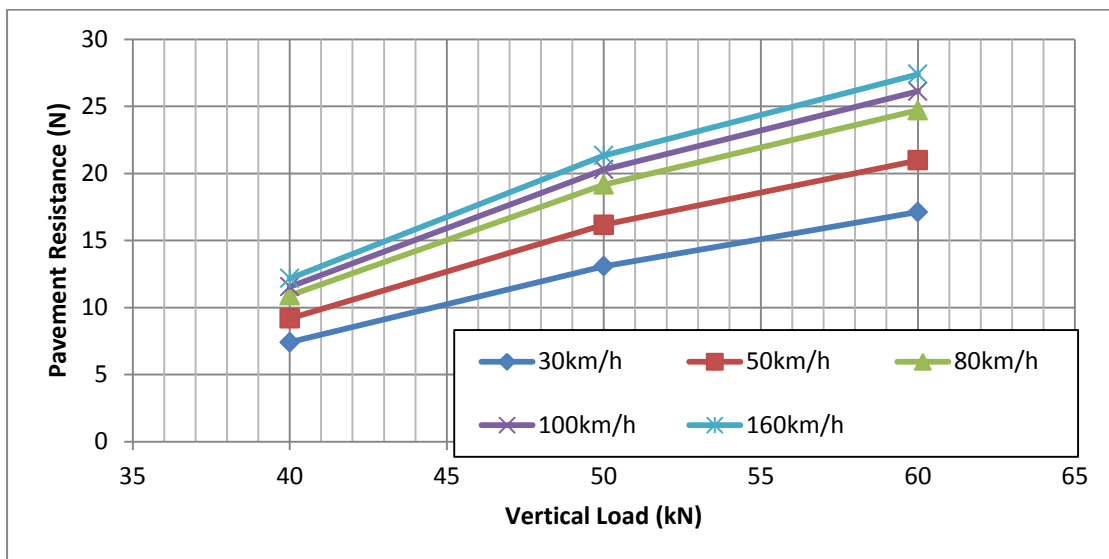


Figure B-7 PR vs. L_v when $E_1=1000\text{MPa}$, low quality pavement

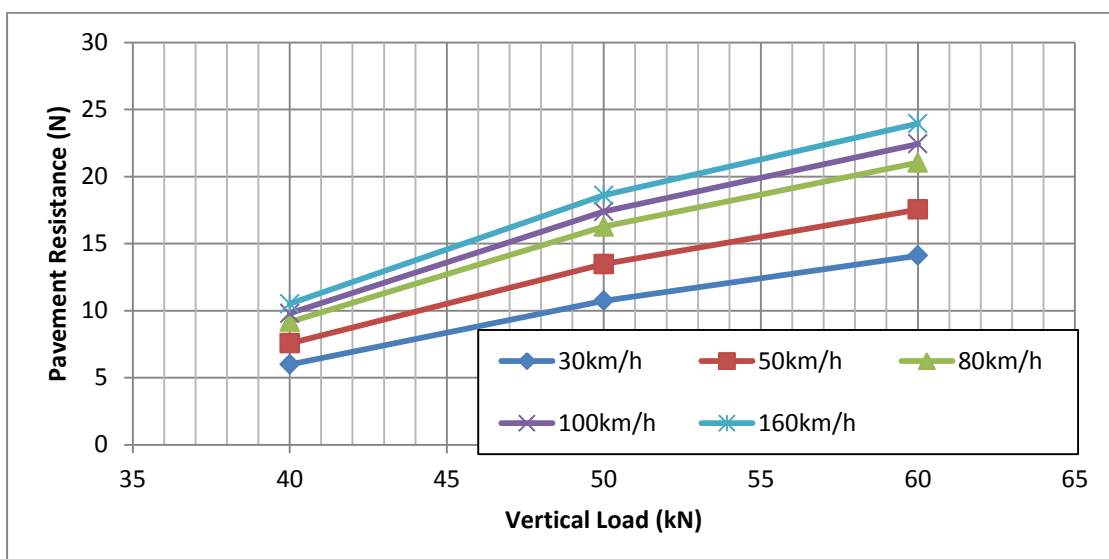


Figure B-8 PR vs. L_v when $E_1=1500\text{MPa}$, low quality pavement

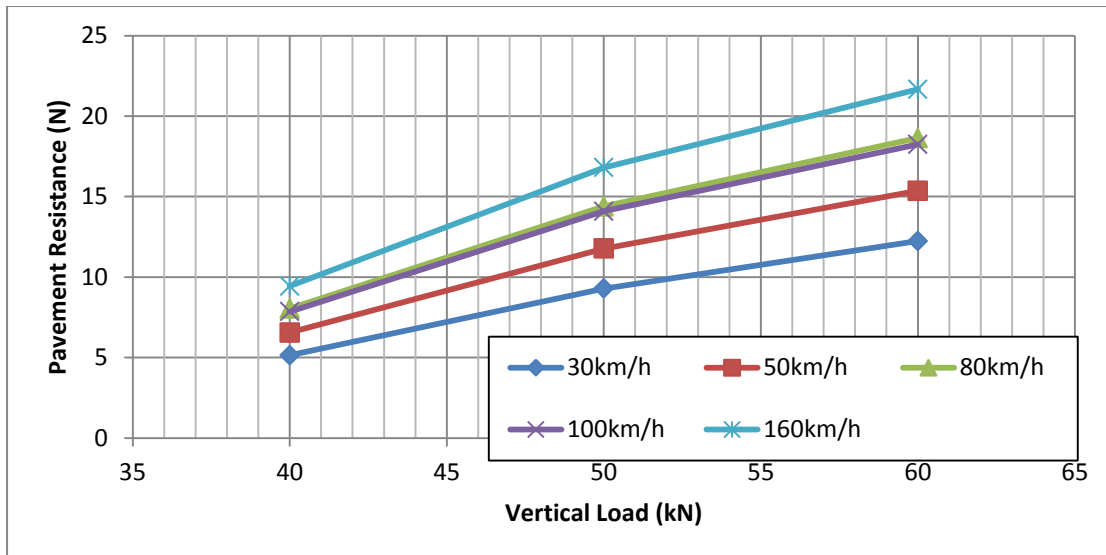


Figure B-9 PR vs. L_v when $E_1=2000\text{MPa}$, low quality pavement

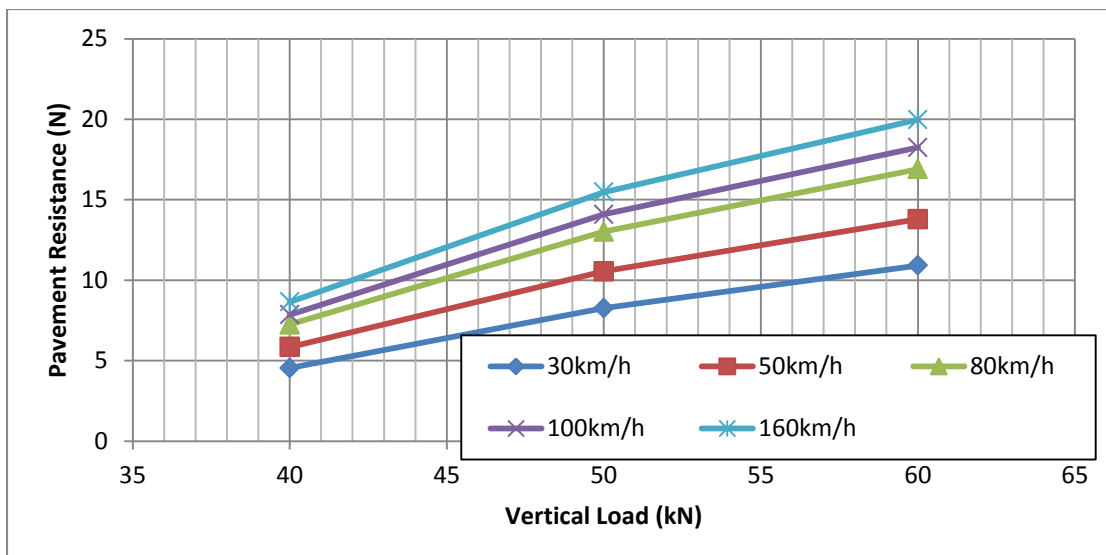


Figure B-10 PR vs. L_v when $E_1=2500\text{MPa}$, low quality pavement

B.4 Stiffness influencing pavement resistance

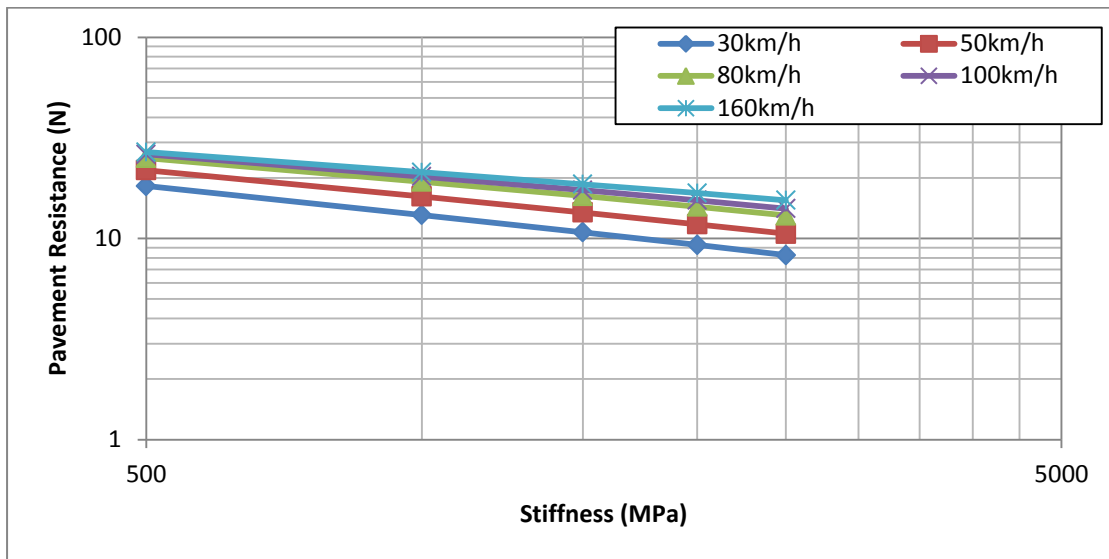


Figure B-11 PR vs. E1 when $L_v = 50kN$, low quality pavement

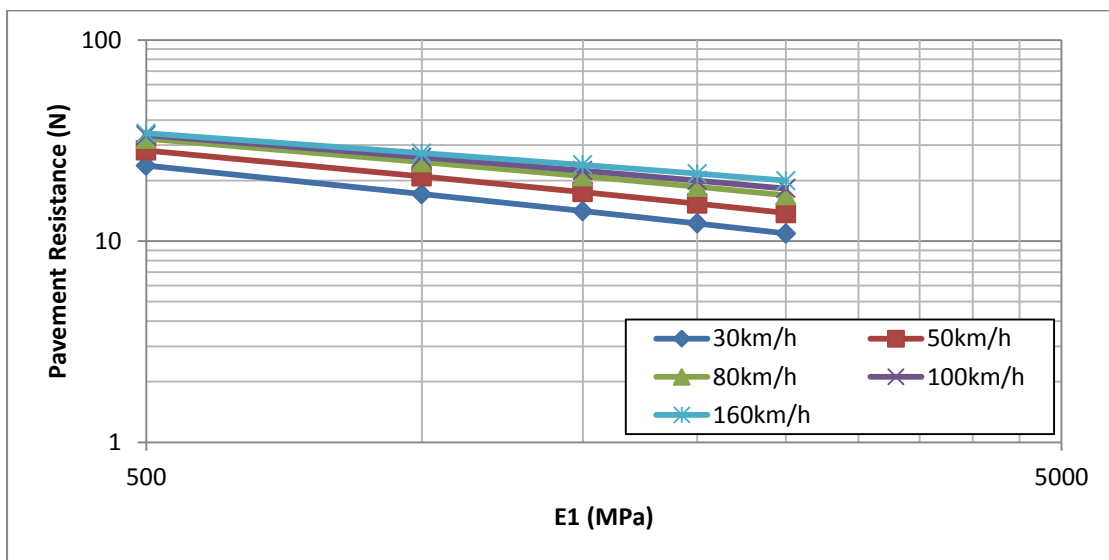


Figure B-12 PR vs. E1 when $L_v=60kN$, low quality pavement

Appendix C. Model dimensions

C.1 Cross section

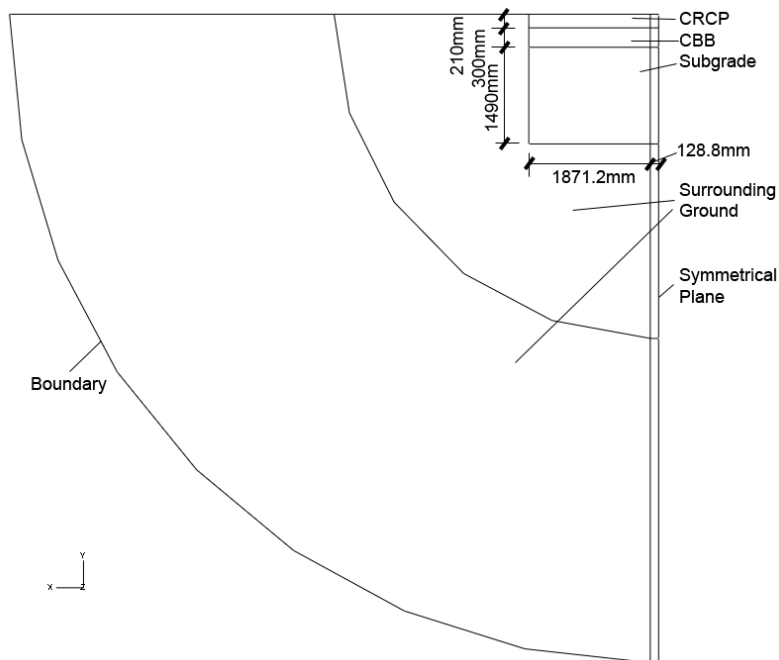


Figure C-1 Profile of the model used for the rigid pavement

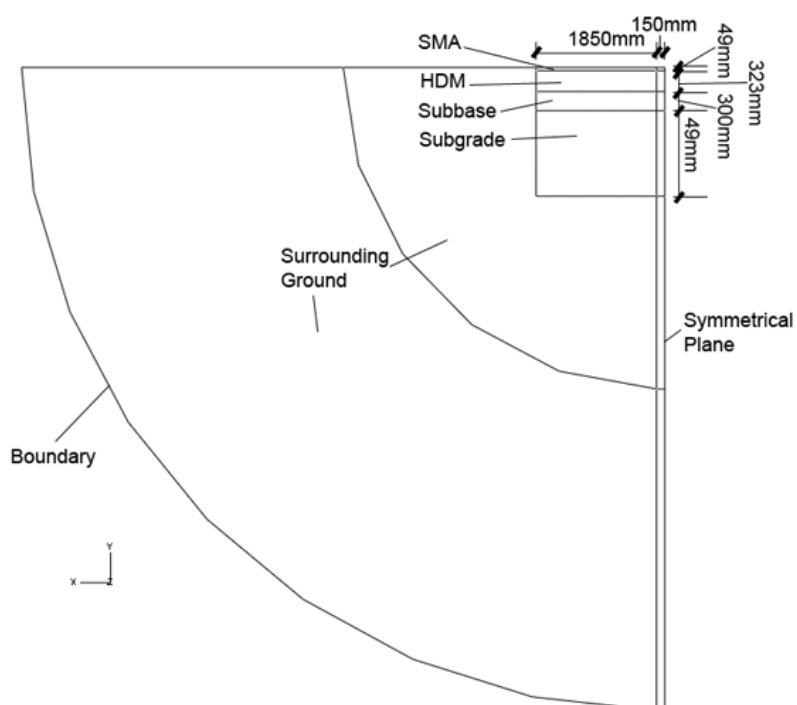


Figure C-2 Profile of the model used for the fully flexible pavement

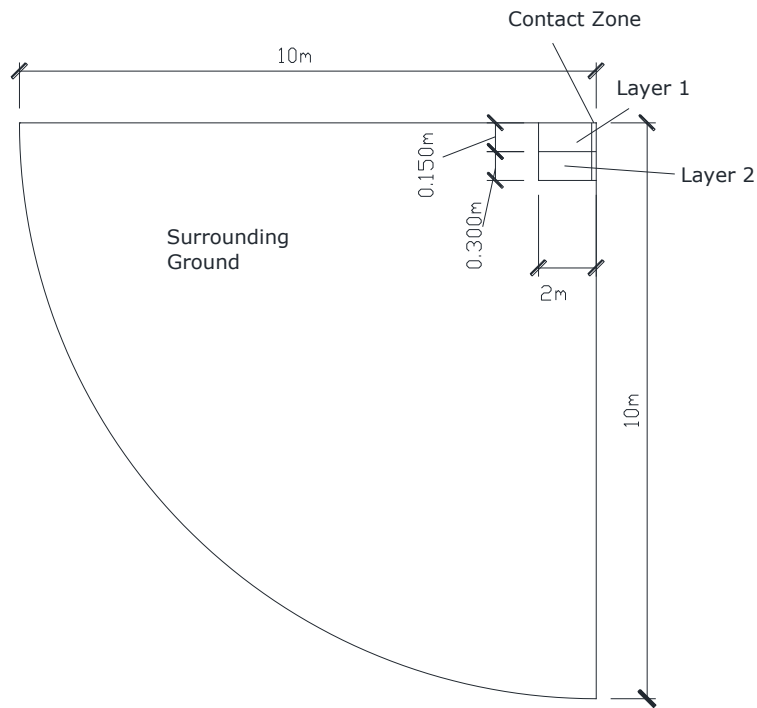


Figure C-3 Profile of the mode used for the low quality pavement

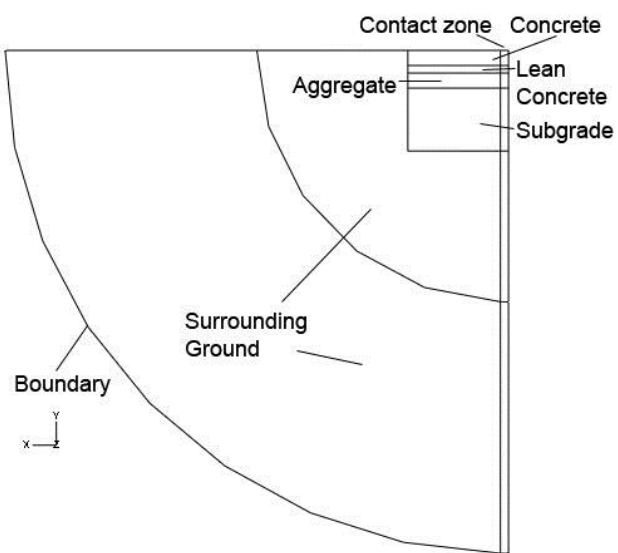


Figure C-4 Profile of the mode used for the concrete pavement

C.2 Dimension of the 3D models

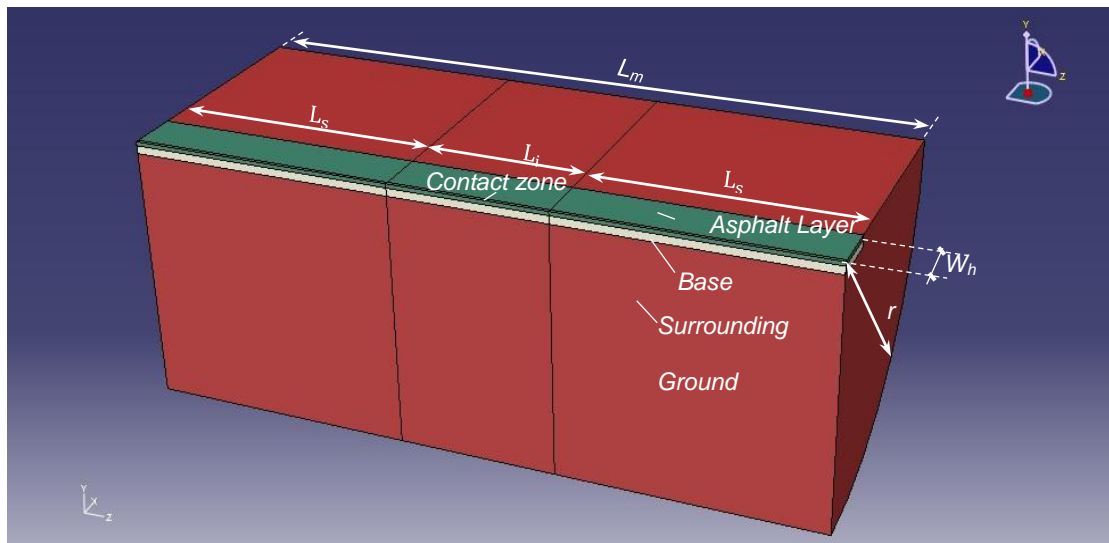


Figure C-5 Dimensions of the model for low quality pavement

Appendix D. Infinite Element Boundary

In order to test the possibility of using infinite elements as a boundary to the pavement subgrade, a symmetrical 3D FE model with an infinite element boundary has been built. A time-interval moving pressure has been applied onto a contact patch, which is located at the centre of the model. The vertical deflections were collected from 5 selected nodes. Results showed that an obvious permanent vertical deflection was still present after the load had been removed.

The 3D model shown in Figure D-1 has been designed and built in ABAQUS CAE using C3D8R finite elements and CIN3D8 infinite elements to measure the vertical deflections of nodes A, B, C, D and E under a time-interval moving load. The detailed locations of the nodes can be found in Table D-1. The model with a length of 17.5m and a radius of 10m is a combination of pavement layers and the surrounding ground. The pavement consists of 3 layers and a subgrade. The surrounding ground has been built around the pavement. The material property of the surrounding ground is consistent with the subgrade of the pavement. The detailed material properties of the pavement and surrounding ground are shown in Table D-2.

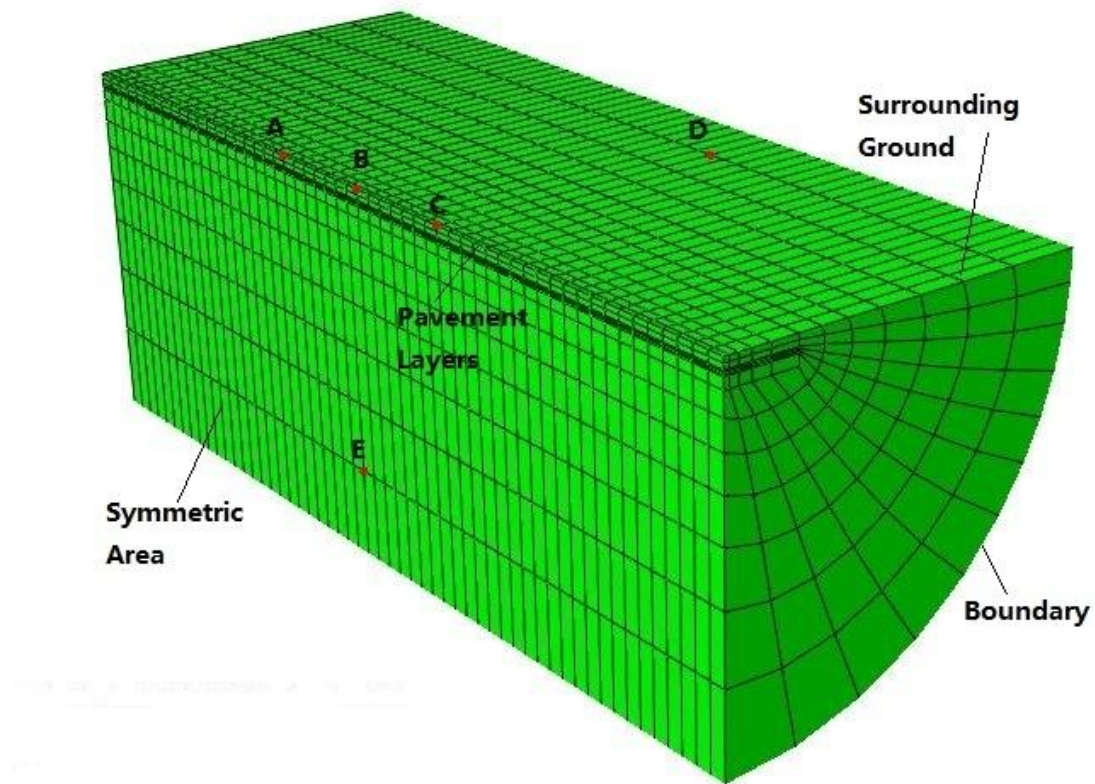


Figure D-1 View of the 3D model with a boundary of infinite element

Table D-1 Locations of nodes

Node	X	Y	Z
A	0	0	10
B	0	0	13.5
C	0	0	17
D	8.2	0	17
E	0	-7.8	13

Table D-2 Material properties of pavement layers and surrounding ground

Layer	Young's Modulus (MPa)	Poisson's Ratio	Density (kg/m ³)	Depth (mm)
1	40,000	0.2	2400	300
2	10,000	0.2	2400	150
3	150	0.35	2000	300
Subgrade or Surrounding Ground	90	0.3	1800	-

A time-interval moving pressure, which was introduced in Section 3.3.2, has been applied to the contact patch (width 0.5m and length 7.5m) as shown in Figure D-2. Each single stress of the time-interval moving press is 552kPa and the contact area is a 0.3m-by-0.5m rectangle. The horizontal velocity of the stress is 100km/h.

Three calculation steps have been designed. The first one is a static step, which allows the pressure to be applied onto the pavement for 10 seconds. The second step is a dynamic step for the simulation of time-interval moving stress. The third step is also dynamic to simulate the situation when the load has been removed, and lasts 5 seconds.

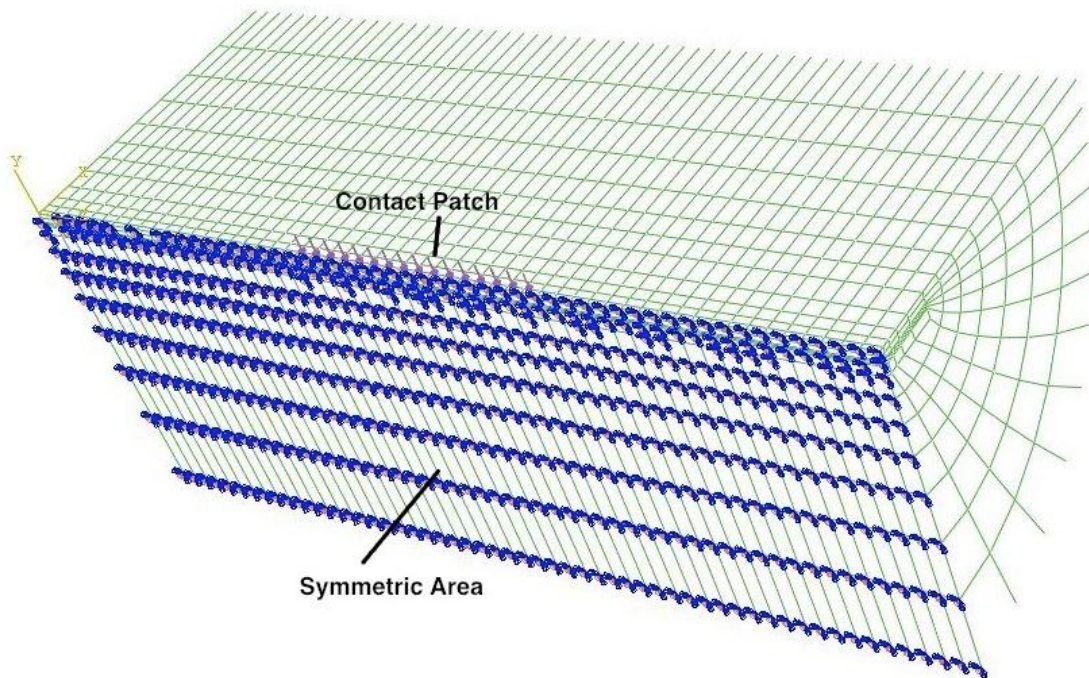


Figure D-2 Contact area and symmetrical boundary

The infinite elements, CIN3D8, have been designed and built on the boundary, as shown in Figure D-3. In order to test two possible boundary conditions, the nodes that located at the outside have been set as fixed or free.

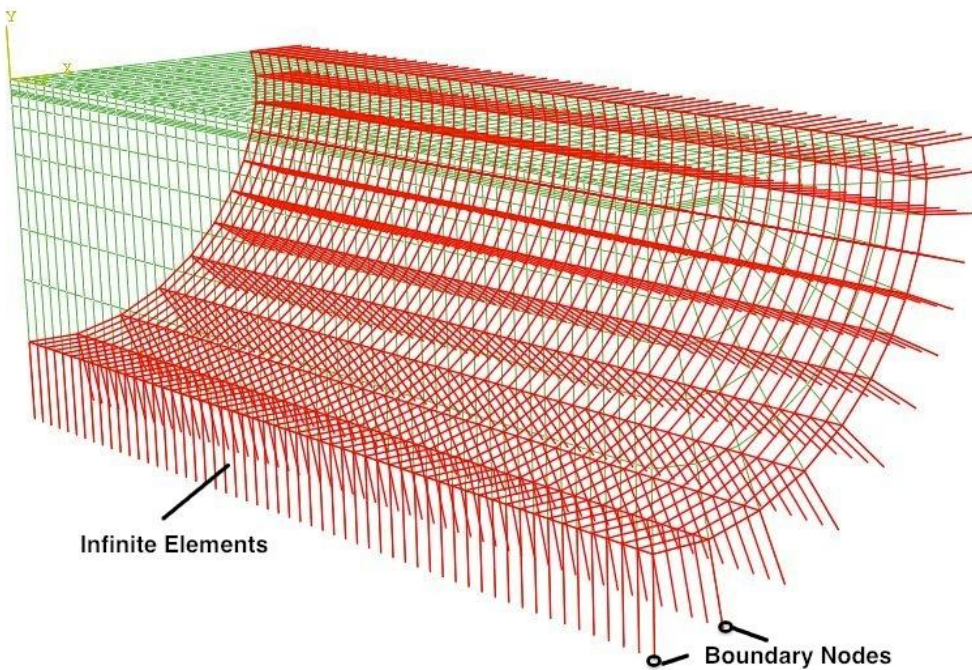
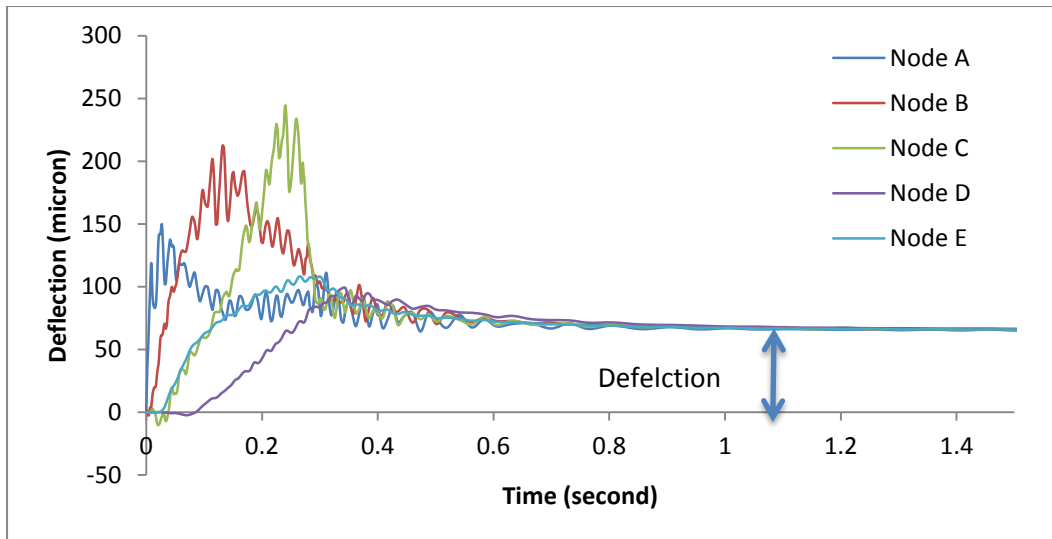
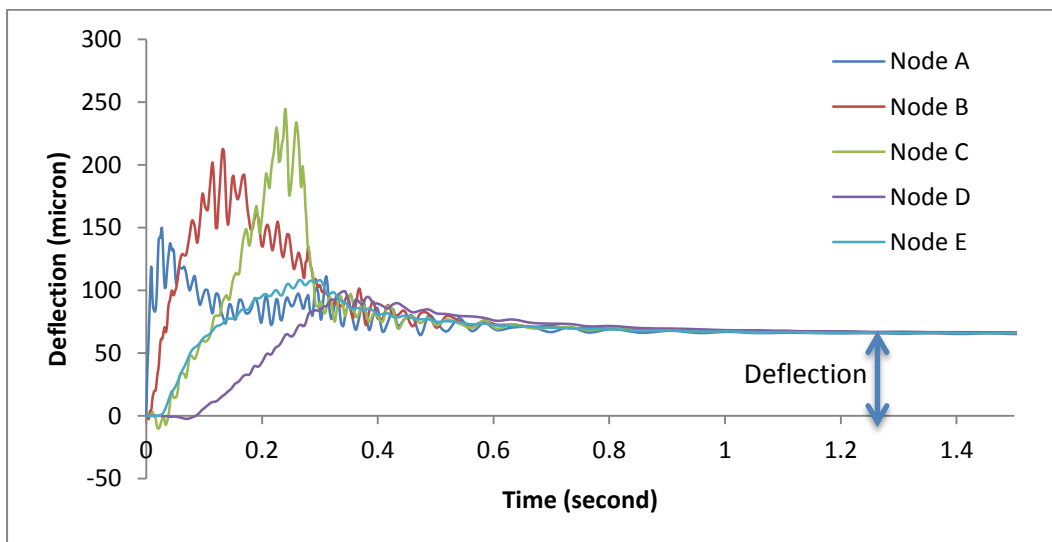


Figure D-3 Boundary of infinite element

The vertical deflections collected during calculation step 2 and step 3 have been plotted, as shown in Figure D-4 and Figure D-5. A significant residual deflection can be found from all of the selected nodes in both cases (fixed or free boundary nodes). The results indicate that the nodes of the model did not rebound to the original positions when the time-interval moving stress has been removed. Thus, infinite elements are shown to be inappropriate for the calculation of energy consumption in the pavement.

**Figure D-4 Vertical Deflection (free boundary nodes)****Figure D-5 Vertical deflections (fixed boundary nodes)**

Appendix E. Contour Plots

Some typical contour plots of vertical deflection have been given in this section.

Table E-1 Parameters of models

Figure	Model	Material Properties					
E-1	Asphalt Pavement			Layer	Young's Modulus (MPa)	Poisson's Ratio	Density (kg/m ³)
				Asphalt	7000	0.35	2400
				Base	7000	0.35	2400
				Subbase	2400	0.25	2000
				Subgrade	90	0.3	1800
				Surrounding ground	90	0.3	1800
E-2	Low Quality Pavement	Layer	Name	Young's Modulus (MPa)	Poisson's Ratio	Density (kg/m ³)	
		1	Asphalt	1000	0.35	2400	
		2	Aggregate	200	0.35	2400	
		3	Subgrade	90	0.3	1800	
E-3	Concrete Pavement	layer	Name	Young's Modulus (MPa)	Poisson's Ratio	Density (kg/m ³)	
		1	Concrete	20000	0.35	2400	
		2	Lean Concrete	10000	0.2	2400	
		3	Aggregate	150	0.35	2000	
		4	Subgrade	90	0.3	1800	
E-4	TRL Rigid Pavement	See Table 5-7					

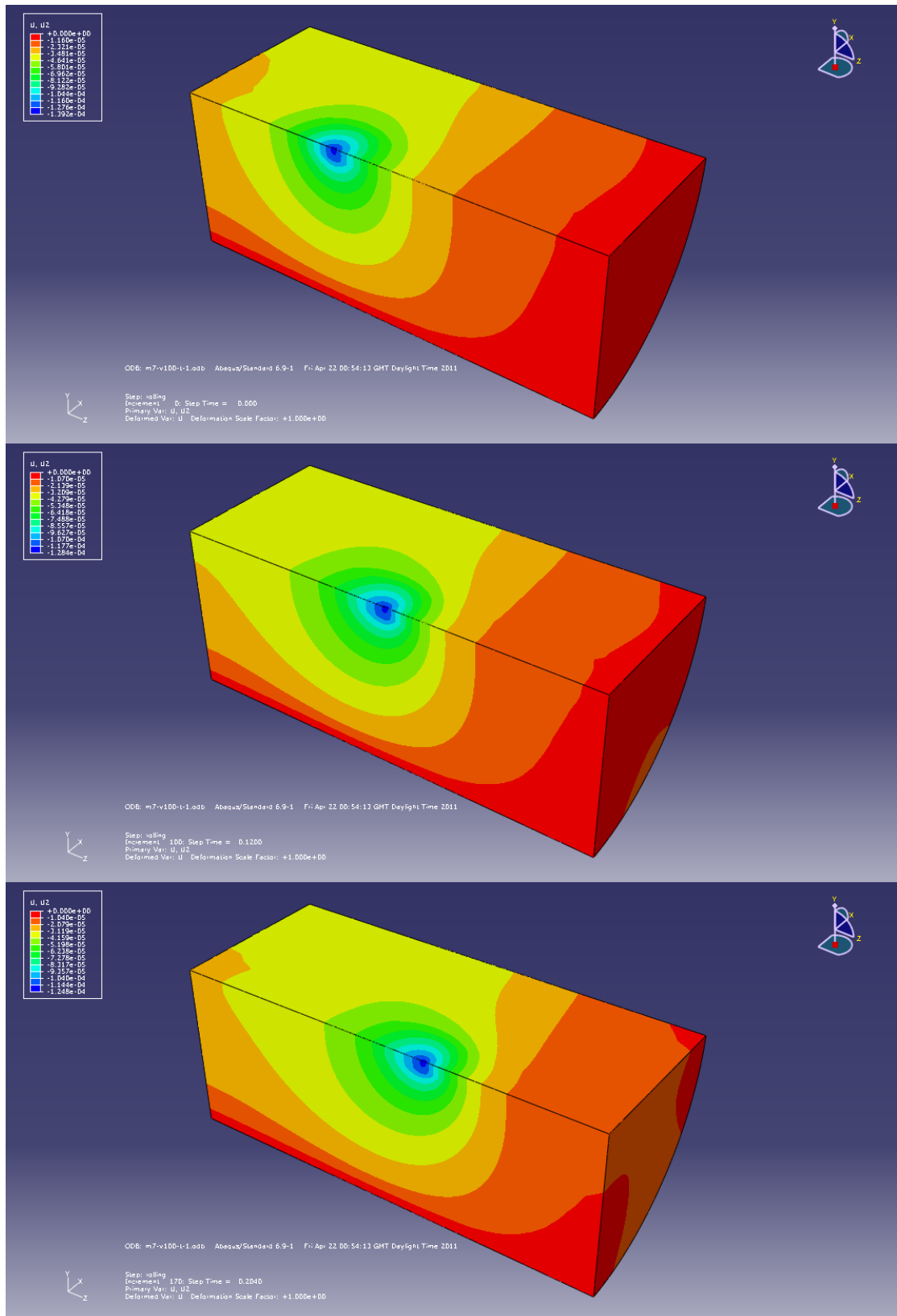


Figure E-1 Contour plots of the asphalt pavement

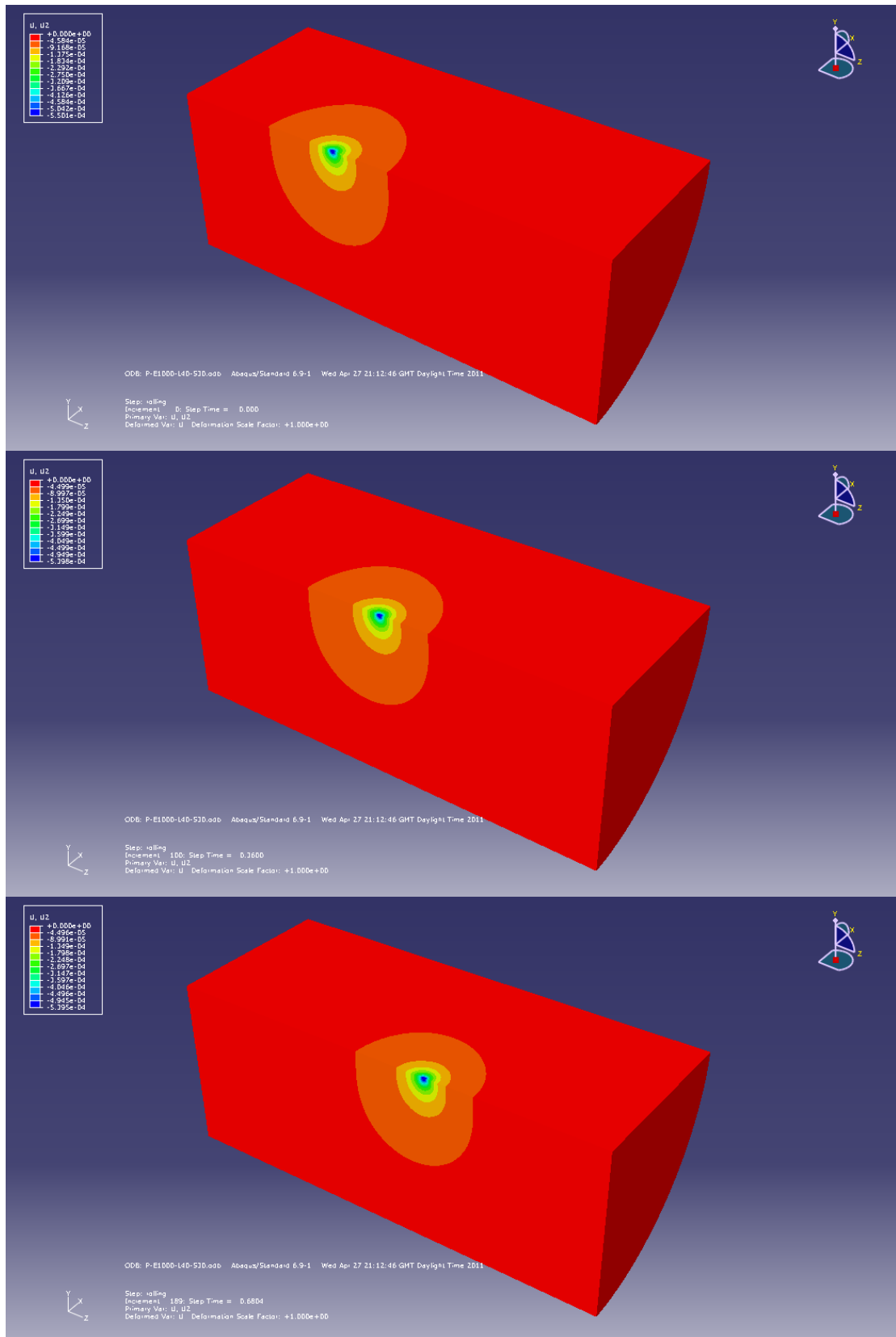


Figure E-2 Contour plots of the low quality pavement

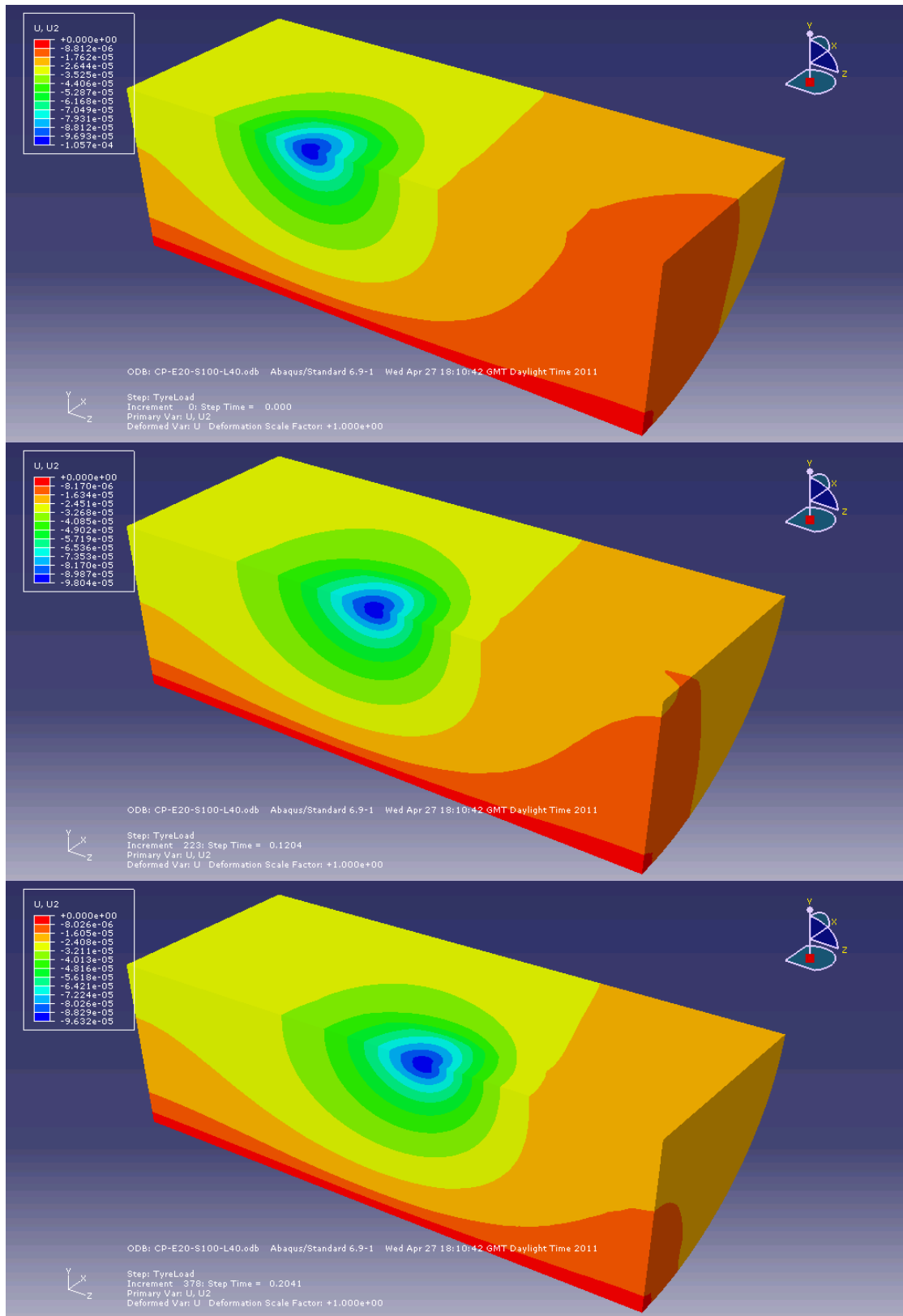


Figure E-3 Contour plots of the concrete pavement

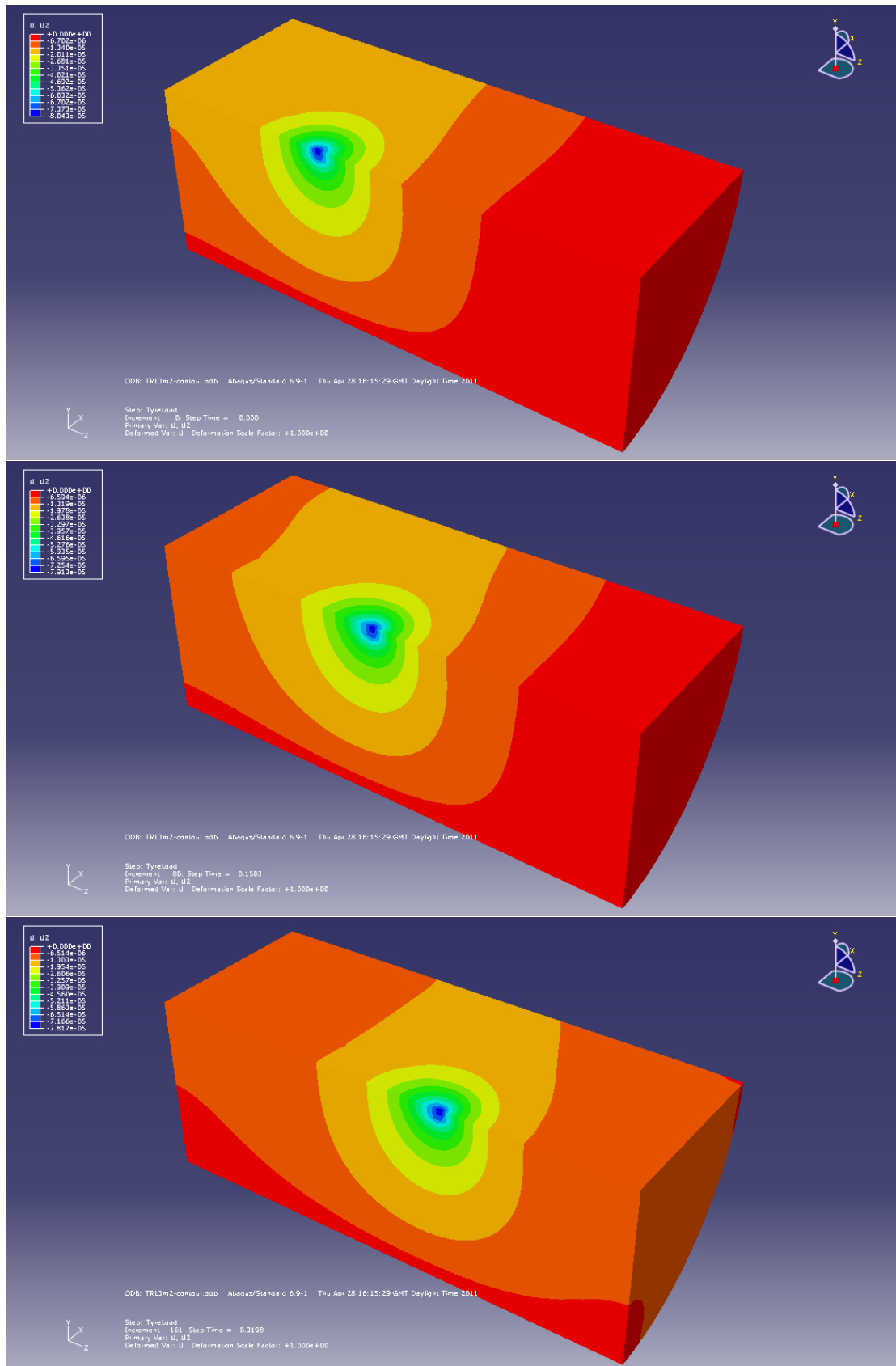


Figure E-4 Contour plots of the TRL rigid pavement